PN-AAZ-651

6.599

HIGH-RESOLUTION SEDIMENTOLOGY AND PALEOCLIMATOLOGY OF LAKE TURKANA, KENYA

John D. Halfman

Dept of Geology

Duke Marine Laboratory

Duke University

1987

Rec'd in SCI: MAR 24 1988

Copyright by

John David Halfman

1987

HIGH-RESOLUTION SEDIMENTOLOGY AND PALEOCLIMATOLOGY

OF

LAKE TURKANA, KENYA

John David Halfman

Department of Geology
Duke University

Date: 20 October 1987

Approved:

Thomas C. Johnson, Supervisor

Dissertation submitted in partial fulfillment of
the requirements for the degree of Doctor
of Philosophy in the Department of
Geology in the Graduate School
of Duke University

1987

ABSTRACT

(Geology)

HIGH-RESOLUTION SEDIMENTOLOGY AND PALEOCLIMATOLOGY

OF

LAKE TURKANA, KENYA

John David Halfman

Department of Geology
Duke University

Date: 20 October 1987

Approved:

Thomas C. Johnson, Supervisor

An abstract of a dissertation submitted in partial fulfillment of the requirements for the degree of Doctor of Philosophy in the Department of Geology in the Graduate School of Duke University

1987

ABSTRACT

The purpose of this study is to investigate the high-resolution sedimentology of Lake Turkana in order to obtain a detailed paleoclimatic record of the basin. The large, alkaline, closed-basin lake is situated in an arid environment in northwestern Kenya.

Piston cores were analyzed for down-core trends of lithology, porosity, grain size and clay mineralogy. Other parameters included total organic carbon and nitrogen, diatom assemblages, biogenic silica, and carbonate content, plus oxygen and carbon stable isotopes and trace element geochemistry of the carbonate fraction. A series of successive laminations were also analyzed.

The Omo River dominates the hydrological budget and the sedimentology of the lake. The carbonate fraction consists of authigenic, low-Mg calcite in the micrite fraction and ostracod tests. The down-core trends in bulk carbonate reveal a correlative, intra-basin variability, which is modulated by a variable influx of detrital material. The north basin stratigraphy suggests that episodes of low Omo River flow existed from 1,000 to 1,500 and 2,100 to 4,000 yr BP, which follows the pattern inferred from other east African lakes.

The sediments are faintly laminated, containing couplets of alternating light and dark layers. The only parameter that consistently changes between laminae is carbonate content, with more carbonate in the light laminations. Each light/dark couplet represents about 4 years, on

the average, based on the interpolated linear sedimentation rate from five radiocarbon dates in core 8P. The sediments are believed to respond to an average 4-year variation in the mean Omo River discharge, which may correspond to the El Nino / Southern Oscillation Event.

Down-core profiles of both couplet thickness and carbonate content reveal a consistent paleohydrologic record that was analyzed for periodicity. Numerous and consistent periodicities above the 95% confidence level occur in the data sets. These are approximately 275, 200, 165, and 100 radiocarbon years long. The thickness data provide finer time resolution than the carbonate data, and reveal additional cycles at 78, 44, 31, 25, and possibly 20 years. The record of inferred fluctuation in Ethiopian monsoon is unique for the length of time covered, the high degree of temporal resolution and the geographic location.

ACKNOWLEDGEMENTS

There are numerous people and institutions who have assisted in the preparation of this dissertation. Without their help this work would have been impossible.

I would like to thank the captain and crew of the M/V Halcyon; Dr. Guy Lister and Kurt Ghilardi at ETH, Zurich; Jim McGill, Charles Gove and other memebers of Project PROBE's field team at Lake Turkana; the Kenyan Department of Fisheries; and Richard Leakey, Director of the National Museum of Kenya for extending their assistance in collecting the sediment cores and high-resolution seismic profiles. Dr. Richard Barber provided valuable discussions on El Nino. Dr. William Showers provided the stable isotope measurements. Dr. Thure Cerling provided the pore water and lake water geochemistry data. Dr. Donald Van Nieuwenhuise provided ostracod identifications. Dr. Richard Strelitz provided computer and mathematical expertise. Sue Book typed an earlier version of the dissertation. I would like to thank various high school, undergraduate and graduate students who provided various data sets, including Amy Gillespie, Karla Hahn, M. Bishop, Lisa Lynch, Patrick Ng'ang'a, Terri King, and all the other students who helped my graduate career.

I thank Project PROBE under the direction of Dr. Bruce Rosendahl for funding the field work and other aspects of my research, at times under stressful conditions. At the time of the Turkana program, Project PROBE was funded by Amoco, Arco, Conoco, ESSO, Marathon, Mobil, Pecten,

Pennzoil, and Shell International Oil Companies, and by the World Bank. Two research grants to Thomas C. Johnson provided additional financial support for laboratory analyses from the American Chemical Society # PRF-17428-AC2 and the Agency for International Development # DPE-5542-G-SS-00. The Graduate School of Duke University provided conference travel funds to present a portion of this dissertation at the XII International Congress of the International Union for Quaternary Research.

I also thank the members of my committee, Dr. Daniel Livingstone, Dr. Bruce Corliss, Dr. Paul Baker, Dr. Bruce Rosendahl, and Dr. Thomas C. Johnson, who provided invaluable discussion at a moments notice.

Finally, I would like to thank my advisor, Dr. Thomas C. Johnson, for his constant help and discussions on a daily basis through my entire graduate career.

I dedicate this dissertation to my

family:

Barbara

&

Samuel Otto

TABLE OF CONTENTS

	Page
Abstract	iii
Acknowledgements	v
Dedication	vii
Table of Contents	viii
List of Figures	x
Introduction	1
Laminations in Sediments	1
Paleoclimatology at Different Scales of Time	4
Lake Turkana	12
Geological Setting	15
Climatic Setting	23
Former Lake Levels and Past Climates	27
Modern Limnology	32
Modern Lake Sediments	34
Methods	36
Field Methods	36
Laboratory Methods	40
Results	51
High-Resolution Seismic Profiles	51
Geochronology	58
Sediment Analyses	61
Discussion	91
Total Organic Carbon	91

TABLE OF CONTENTS

Page

Carbonate 95

Origin of Laminations and their Climatic Significance 108

High-Resolution Paleoclimatology 116

Conclusions 128

References 131

Appendix 148

LIST OF FIGURES

Figure	Description	Page
1.	Map of central Africa showing location of Lake Turkana ...	13
2.	Bathymetric map of Lake Turkana	14
3.	Topographic map of East Africa	16
4.	Generalized stratigraphic column of the Turkana region ...	17
5.	Generalized geologic map of the Turkana region	19
6.	Structural configuration of Lake Turkana	21
7.	Examples of multichannel seismic lines	22
8.	Generalized surface circulation and rain belts for Africa .	25
9.	Fluctuations in the level of Lake Turkana, previous work .	28
10.	Histograms of temporal variations in lake level	30
11.	High-resolution survey trackline map	37
12.	Bathymetric map of Lake Turkana with core sites	39
13.	Summary diagram of the high-resolution seismic profiles ..	52
14.	A comparison of 1-kHz and 28-kHz seismic profiles	53
15.	Examples of Type I, II and III 1-kHz seismic profiles	54
16.	Regional distribution of the three profile types	56
17.	Radiometric age versus depth in the cores	59
18.	Generalized core stratigraphy from visual descriptions ...	62
19.	Porosity profiles	64
20.	Diatom relative abundance profiles	67
21.	Biogenic silica profiles	68
22.	Grain size profiles	70

LIST OF FIGURES

Figure	Description	Page
23.	Total organic carbon profiles	71
24.	Total organic carbon versus biogenic silica values	73
25.	Carbon to nitrogen profiles	75
26.	Carbonate profiles	76
27.	Carbonate values versus distance from Omo River	78
28.	Smoothed carbonate profiles, cores LT84-7P, 8P and 10P	80
29.	Trace element geochemistry profiles	82
30.	Stable isotope profiles	84
31.	Lamination thickness profiles	87
32.	Lamination geochemical profiles	89
33.	SEM photographs of the fine fraction of the sediment	97
34.	Pore water geochemistry profiles	101
35.	Carbonate values versus age	102
36.	Carbonate versus biogenic silica and oxygen isotope values	105
37.	El Nino / Southern Oscillation global correlations	112
38.	Annual rainfall for Jima and Addis Ababa, Ethiopia	114
39.	Carbonate and lamination thickness profiles for LT84-8P	118
40.	Power spectra from time-series analysis of LT84-8P records	121
41.	Power spectra from other records in Lake Turkana	124

INTRODUCTION

The purpose of this study is to investigate the high-resolution stratigraphy of recent sediments in Lake Turkana, Kenya, in order to obtain a detailed paleoclimatic record of the region. The focus is on two specific problems. The first is to determine the processes that form the laminations found in the bottom sediments. The second is to determine the nature of lacustrine and climatic change at Lake Turkana, with emphasis on relatively short-term (i.e. decade to century) variability during the last few millennia.

Laminations in Sediments

Laminated sediments are found throughout the geological record and in vastly different environments. A lamina is the thinnest recognizable layer of original deposition that is different from other layers by color, composition, or particle size. In the strictest sense, lamina is a sedimentary bed less than 1 cm thick. This discussion will loosely refer to all thin (arbitrary thickness) layers as laminations, and concentrate on deposits formed in lacustrine environments.

Anderson (1986) states that virtually all fine-grained sediment would be seasonally laminated if left in an undisturbed condition after deposition. Unfortunately, very little is known about seasonal sedimentation. However, preservation is an indispensable factor for the formation of laminations. The sediment surface must not be disturbed by water movements (e.g., waves, currents, dewatering), gas bubbling, bioturbation, slumping or surface creep (Renberg and Segerstrom, 1981).

In a review of basin characteristics where laminated sediments are found, an ideal basin is flat-bottomed, deep, and anoxic at depth, to escape the previously outlined destructive processes (O'Sullivan, 1983). These ideal characteristics are not mandatory, however, and rare occurrences of laminated sediments are found in basins with intense water circulation and oxygenated bottom waters (O'Sullivan, 1983; Cohen, 1984).

A variable supply of different sediment fractions over time is also required in the formation of laminated sediments (reviewed by O'Sullivan, 1983). Four major types of laminations are common, although other types do exist. Calcareous laminations can form in lakes with high bicarbonate concentrations. The surface water chemistry shifts towards super-saturation with respect to calcite either by increasing the water temperature or increasing algal productivity (Kelts and Hsu, 1978). Ferrogenic laminations can form in soft water lakes due to variations in redox conditions and consequent changes in the solubility of iron and manganese through cyclic hypolimnion anoxia and oxygenation (Anthony, 1977). Biogenic laminations are formed by temporal changes in prominent fluxes of diatoms or other biogenic remains (Simola, 1977). In the preceding three cases, a lamina is produced by internal lake processes, yielding autochthonous lamina. Allochthonous (clastic) matter also can form lamina (e.g., glacial varves; de Geer, 1912) by various temporal combinations of circulation patterns and variable sediment influx (Sturm, 1979).

Annual climatic change is a dominant cyclic perturbation that can stimulate the formation of two or more seasonal lamina. An underlying

assumption is that the sedimentation rate i sufficiently large to resolve seasonal events in the sediment record, which is true for most lacustrine basins. The terms annual laminations or (non-glacial) varves are used to denote the recognizable, annual groups of laminations. Unfortunately, both terms have semantic shortcomings but are widely used in the literature. The distinguishing features that identify individual members of annual laminations may also fluctuate through larger groups of laminations (Anderson, 1964; Anderson and Kirland, 1969; Smith, 1978; Williams and Sonett, 1985; Anderson, 1986). This suggests that there are cycles within cycles, and only the resolution of the sediments limits their detection.

The chronologic control provided by annual laminations provides a powerful basis for calibration of other dating techniques (Stuiver, 1971; Appleby and Oldfield, 1978), deciphering paleoclimates (Dean et al., 1984), and determining the impact of man on the environment (Renberg and Segerstrom, 1981; Simola, 1983). Several studies suggest that the thickness of annual couplets is sensitive to climatic variability (Bradley, 1929; Anderson and Koopmans, 1963; Kempe and Degens, 1978; Williams and Sonnet, 1985; Fisher, 1986). Time-series analysis of thickness results has been used to indicate periodicities of about 5, 11, and possibly 50 years from the lacustrine Green River Formation (Bradley, 1929; Crowley et al., 1986) and about 11, 22, 145, 290 and possibly 90 years from the varved Elatina Formation (Williams, 1981).

The large, deep lakes of eastern Africa contain laminated sediments. Lakes Kivu and Idi Amin Dada (formerly Lake Edward) have carbonate

laminae (Hecky and Degens, 1973; Stoffers and Hecky, 1978). Diatomaceous laminae are found in Lakes Malawi, Tanganyika and Kivu (cited in Richardson and Richardson, 1972). Lake Malawi contains clastic and perhaps other types of laminae as well (Crossley and Owen, 1987; Pilskaln, pers. commun.). However, knowledge of the detailed structure of these laminations and their formational processes is incomplete (O'Sullivan, 1983).

The laminations in Lake Turkana sediment also are not well understood. They exist throughout the lake except in mottled or sandy nearshore sediments, despite well oxygenated bottom waters. The benthic standing crop, which could potentially homogenize the sediments, consists primarily of epibenthic detritovores that decline precipitously from nearshore to offshore environments, presumably due to the parallel decline in edible detritus (Cohen, 1984). Thus bioturbation does not keep up with sedimentation. The laminations are approximately 0.1 to 2 cm thick and consist of light and dark couplets. Yuretich (1979) reported that the lighter layers are possibly finer-grained and less calcareous than the darker layers and were suspected to result from the seasonal flooding of the Omo River. The dark layer was interpreted to represent the rapidly settled flocculent material, which compacts before the light-colored clays reach the lake floor.

Paleoclimatology at Different Scales of Time

The geologic record provides direct evidence for major variations in the Earth's climate since its formation, even though the majority of rocks formed during Earth's history have subsequently been eroded

(Crowley, 1983). Interpretation of the record indicates that climatic variability occurs over a broad range of time scales. Transitions between non-glacial and glacial states (eg., from non-glacial Miocene to glacial Pleistocene epochs) is observed on time scales of 10^6 to 10^8 years, primarily due to paleogeographic factors (e.g., continental drift). Cyclic depositional processes recorded in oceanic sediments and sedimentary rocks on time scales of 10^4 to 10^5 years are frequently attributed to Milankovitch orbital perturbations (e.g., Hays et al., 1976; Imbrie et al., 1984, and other papers in Berger et al., 1984; Fisher, 1986; Dean and Gardner, 1986, and other papers edited by Arthur and Garrison, 1986; Schwarzacher, 1987). Milankovitch-scale periodicities also may influence the hydrology and depositional sequences in ancient lakes (Kutzbach and Street-Perrott, 1985; Olsen, 1986). A major obstacle for assessing the significance of cycles recorded in sediments and sedimentary rocks is precisely determining the cycle's period (Arthur and Garrison, 1986; Fisher, 1986).

The resolution of climatic history on a scale of less than 10^3 years is difficult in oceanic sediments and sedimentary rocks. The resolution is limited by sedimentation rates, typically below 10^{-3} cm/yr, and biological mixing of at least the upper 10 cm of sediment, which effectively smooths the record of paleoclimatic change. A few exceptions occur in isolated basins with faster sedimentation rates and anaerobic bottom environments (e.g., Santa Barbara Basin, California). Annual to millennial climate cycles are inferred from other paleoclimatic records including instrumental and historical data, tree rings, ice cores, glacial movements, and lake sediments (Morner and

Karlen, 1984). Paleoclimatic reconstructions for given geographical regions are augmented through a combination of these techniques.

Instrumental and historical records are a direct link to the present and past climates. The time resolution of instrumental records is unsurpassed (10^{-4} years). Unfortunately, the duration of the records is on the order of 10 to 10^2 years, and the station locations are skewed towards heavily populated land areas. Climatic information from oceanic areas (ship logs) is just now being analyzed for paleoclimatic trends (Folland et al., 1984; Jones et al., 1986). The network of stations combined with satellite information has provided a truly global picture of weather phenomena for the past 20 years. Historical records, observations of weather phenomena in written records and observations of weather-dependent natural phenomena extend further back in time than instrumental records, but the information may be discontinuous, unreliable, and may lack the potential for quantitative interpretations (Bradley, 1985).

Instrumental and historical records do provide isolated glimpses into the past and are extremely helpful in the interpretation and calibration of proxy data. The records are too short for statistical analysis of climatic variability on a century or longer time scale. Studies have shown quasi-periodic fluctuations, that may lack rigorous statistical basis, of about 3, 11, 22, 35, 80, 100, 200, 380 and 2,000 years (Lamb, 1977).

The consensus of historical records from the Sahel and other African regions, extending back for 5 centuries, indicate wetter conditions between the 16th and 18th centuries, then a marked trend towards

increased aridity to the present day (Nicholson, 1978). The desiccation trend is interrupted with a period of increased rainfall in the late 19th century. Some of this information was compiled from river discharge data. For example, the height of the Nile River is very important to the success of the season's crop. Consequently, it has been sporadically recorded since 3,100 BC and almost continuously recorded on the Rauda nilometer near Cairo since 622 AD, except for two brief interruptions due to political instability. The level is interpreted as a barometer of climatic change for the White and Blue Nile drainage basins (Reihl and Meitin, 1979; Hassan, 1981; Flohn and Burkhurdt, 1985). Relatively lower flood levels occurred from about 600 to 1,400 AD and higher flood levels from about 800 BC to 600 AD and 1,500 to 1,900 AD. Time-series analysis of the flood data reveals significant periods at 18.4 and 77 years (Hameed, 1984). An inferred Senegal River discharge record reveals fluctuations on a 31 year average (Faure and Gac, 1981).

Variations in the widths of annual growth rings and possibly stable isotope ratios of tree cellulose of many species of trees found in temperate and sub-polar climates can be successfully used as proxy records reflecting past moisture and temperature conditions (Stockton et al. 1985; Stuiver and Braziunas, 1987). The records are precisely dated (annual rings), but most are relatively short (10^2 years) in contrast to other proxy records. Paleoclimatic information is obtained through mathematical calibration of the tree rings for a given site to nearby instrumental records, then the calibration is applied to the remaining tree-ring record. An approximate 22 year drought rhythm is revealed by

time-series analysis from western and central plains sites in N. America (Mitchell et al., 1979; Meko et al., 1985). The records are too short to reveal significant periodicities longer than 50 years. A dense grid of sites, such as in southwestern N. America, was manipulated with transfer functions to generate time-slice maps of pressure, precipitation and temperature (Fritts et al., 1979). In Africa, dendrochronological analysis has been limited to the extreme northern and southern parts of the continent (Stockton et al., 1985; G. Jacoby, pers. commun.).

Vertical ice cores from ice sheets provide very long (about 10^5 years), high-resolution (about 0.1 m/yr), stratigraphic records of paleoclimate (Bradley, 1985). The technique is limited by the distribution of suitable ice, and the determination of the non-linear, age-versus-depth relationship, especially at depths corresponding to ages greater than 10^4 years ago. For example, the age-depth profile for the Camp Century, Greenland ice core underwent several revisions in the last few decades (Dansgaard et al., 1982). Paleoclimatology has profited from the interpretation of oxygen isotope and conductivity profiles of the ice (Dansgaard et al., 1971), along with the analysis of air bubbles (Neftel et al., 1982) and microparticles (Thompson and Mosley-Thompson, 1981) trapped in the ice lattice. Records from the last millennium reveal historic volcanic activity (Hammer et al., 1980; Legrand and Delmas, 1987), anthropogenic increase of CO_2 (Neftel et al., 1982), variations in δC-13 of the entrapped CO_2 (Freidli et al., 1986) and prominent cyclicities in the δO-18 record and inferred past climates on the order of 78, 181 and possibly 350 years (Dansgaard et al., 1971;

Johnsen et al., 1970).

In the tropics, ice cores have been successfully recovered from the Quelecaya Ice Cap in the Andes of southern Peru (Thompson et al., 1985, 1986). The 1,500 year record suggests that relatively drier periods occurred between 1,720 and 1,860, 1,250 and 1,310, and 570 and 610 AD and relatively wetter periods between 1,500 and 1,720 AD. The record also reveals decreased temperatures over the ice cap that may temporally correspond to the Little Ice Age. Fluctuations in the spatial distribution and extent of tropical glaciers has provided discontinuous climatological interpretations that are consistent with other long term (10^4 year) climatic patterns (Hastenrath, 1985). A more continuous record of glacial activity and inferred regional precipitation was interpreted from lake sediments on Mt. Kenya (Karlen, 1985). It suggests more intense precipitation from 3.2 to 2.9, 2.3 to 1.7 kyr BP and 600 to 50 yr BP, with superimposed shorter fluctuations.

The sedimentary record of some large lakes is potentially the most detailed record of past climates available for the past few million years (Livingstone, 1975; Livingstone, 1981; Johnson, 1984). The areal distribution of lakes is skewed towards areas scoured by the Pleistocene ice sheets. Lakes are abundant in these areas, yet the oldest sediments date since the retreat of the last ice sheet (about 10^4 years). Lakes are less common beyond the maximum extent of the former ice sheets, especially between the latitudes of 20° and 40°, but some have existed for millions of years. Sampling resolution is about 10 years or less because sedimentation rates are typically 10^{-3} m/yr, and the biological mixed layer is typically less than 5 cm, or is absent in lakes with

anoxic bottom waters (Johnson, 1984).

The age-depth relationship for lake sediments may be difficult to determine. Annual laminations provide the most precise method of dating sediments. Otherwise, chronologies from radionuclides (e.g. C-14 and Pb-210 chronologies, Krishnaswami and Lal, 1978), secular paleomagnetics (Johnson and Fields, 1984), tephrochronologies (Degens et al., 1973) and other stratigraphic techniques (e.g., pollen profiles, Kemp et al., 1978) are used to date the sediments. The age-depth relationship may deviate from a linear trend due to compaction, variable sediment input and other processes.

The paleoclimatic signal in lacustrine basins is inferred from a large number of parameters. Examples from African basins are pollen records (Kendall, 1969; Livingstone, 1975; Hamilton, 1982), diatom records (Gasse, 1980; Owen et al., 1982; Stager, 1982), molluscs and other biological records (Palmer, 1976; Williamson, 1978) sediment lithology and mineralogy (Richardson and Richardson, 1972; Stoffers and Hecky, 1978; Stoffers and Singer, 1979; Talbot and Kelts, 1986), grain size (Karlen, 1985), stable isotope analysis (Abell, 1982), and the dating of former, exposed deposits (Butzer et al., 1972; Street and Grove, 1979). Most of the major East African basins have been investigated by a limited number of parameters with varying degrees of temporal control.

Paleolimnological investigations must consider the regional variability within lakes of surface sediment composition and core stratigraphy (Lerman, 1978; Hakanson and Jansson, 1983; Johnson, 1984). This heterogenous mosaic of surface sediments and stratigraphy requires

that the sedimentary processes within a basin be examined in detail before any paleolimnologic interpretations of one or more cores are made (Johnson, 1984).

LAKE TURKANA

Lake Turkana (formerly Lake Rudolf) is the largest body of water within the eastern branch of the East African Rift System (Fig. 1). It is located in the desolate Northern Frontier District of Kenya with its northern shoreline in Ethiopia near the Sudanese border. It was the last of the large African lakes to be discovered by Europeans, when Teleki and von Hohnel visited it in 1888 (von Hohnel, 1894). The remoteness of the lake resulted in geological and limnological research being limited to only a few expeditions in the first half of the 20th century (Cambridge Expedition, 1932-1933, Fuchs, 1934, 1935, 1939; Arambourg, 1933, 1935, 1944, 1948). Since then, research activity has grown due to the discovery of the extensive vertebrate fauna, including hominid fossils, in the exposed Cenozoic deposits within the basin. Geological studies focused on the stratigraphy and environmental setting of these deposits (Coppens et al. 1976; Leakey, 1976; Bishop, 1978). Research within the lake proper started just during the last decade and includes the modern sedimentology (Yuretich, 1979), limnology (Hopson, 1982) and benthic ecology (Cohen, 1982) of the lake.

Lake Turkana is presently a closed basin lake (Fig. 2). The elongate lake has a surface area of approximately 7500 km^2, with a length and mean width of 260 km and 30 km, respectively (based on data collected during the early 1970's, Ferguson and Harbott, 1982). The lake is divided into two major basins, north and south, with a bathymetric high between them, lakeward of the Turkwel and Kerio Rivers. The north and south basins have maximum depths of just over 80 m and 115

Fig. 1. Map of central Africa showing the location of Lake Turkana, Omo River, the rift systems (stippled areas), and other lakes, rivers, and cities mentioned in text.

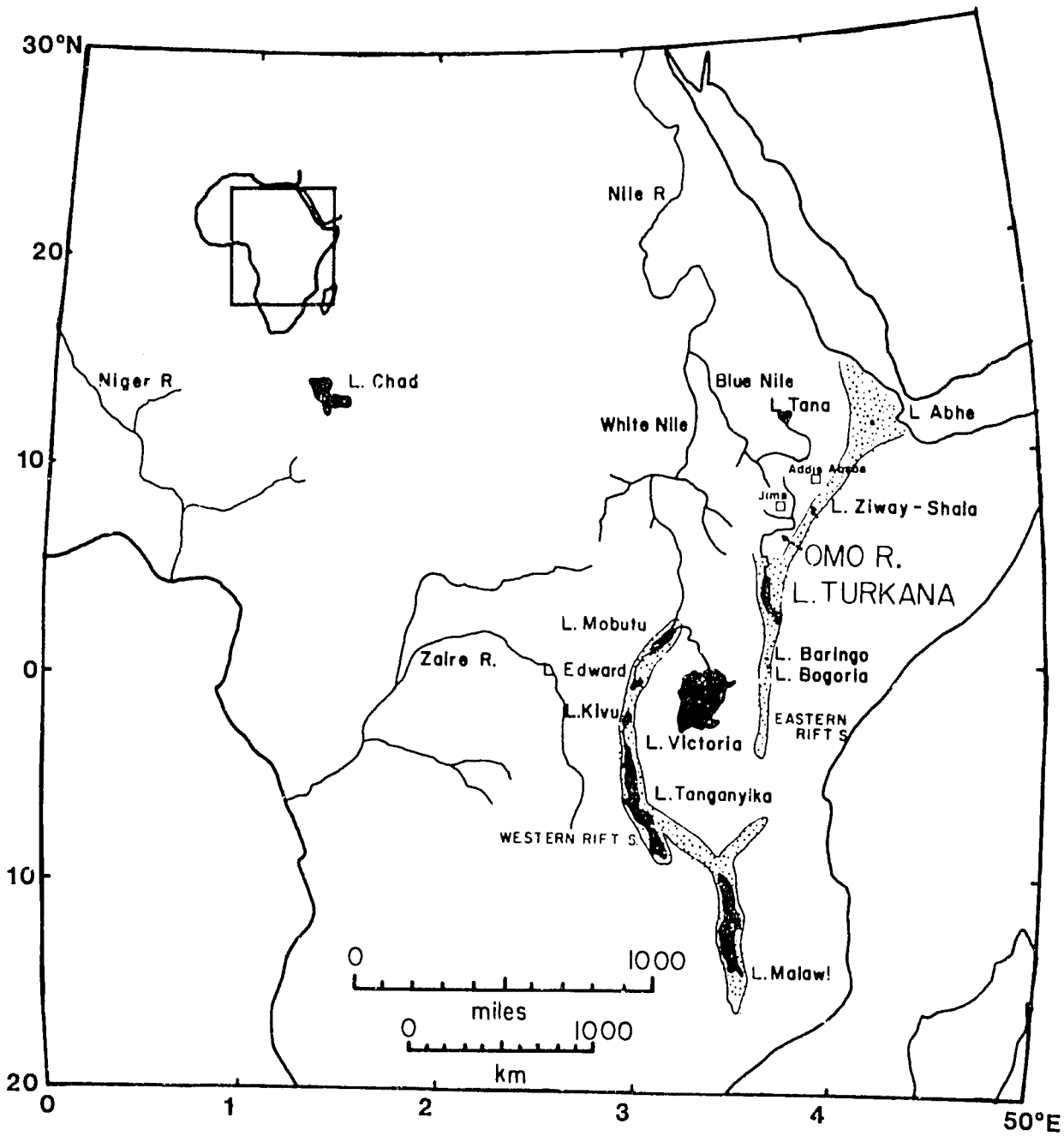
30°N
20
10
0
10
20
0
1
2
3
4
50°E
Nile R
Niger R
L. Chad
Blue Nile
L. Tana
L. Abhe
White Nile
Addis Ababa
Jima
L. Ziway - Shala
OMO R.
L. TURKANA
L. Mobutu
Zaire R.
Edward
L. Baringo
L. Bogoria
L. Kivu
L. Victoria
EASTERN RIFT S.
L. Tanganyika
WESTERN RIFT S.
L. Malawi
0
1000
miles
0
1000
km

13a

Fig. 2. Bathymetric map of Lake Turkana. The North basin extends from Eliye Springs to the Omo River, the South basin is approximated by the 40 m contour surrounding South Island, and the Central basin is between the preceeding basins. Ferguson's Gulf (FG) is located on the west-central portion of the lake. Soundings are based on a speed of sound of 1,463 m/s (800 fm/s) (modified from Johnson et al., 1987).

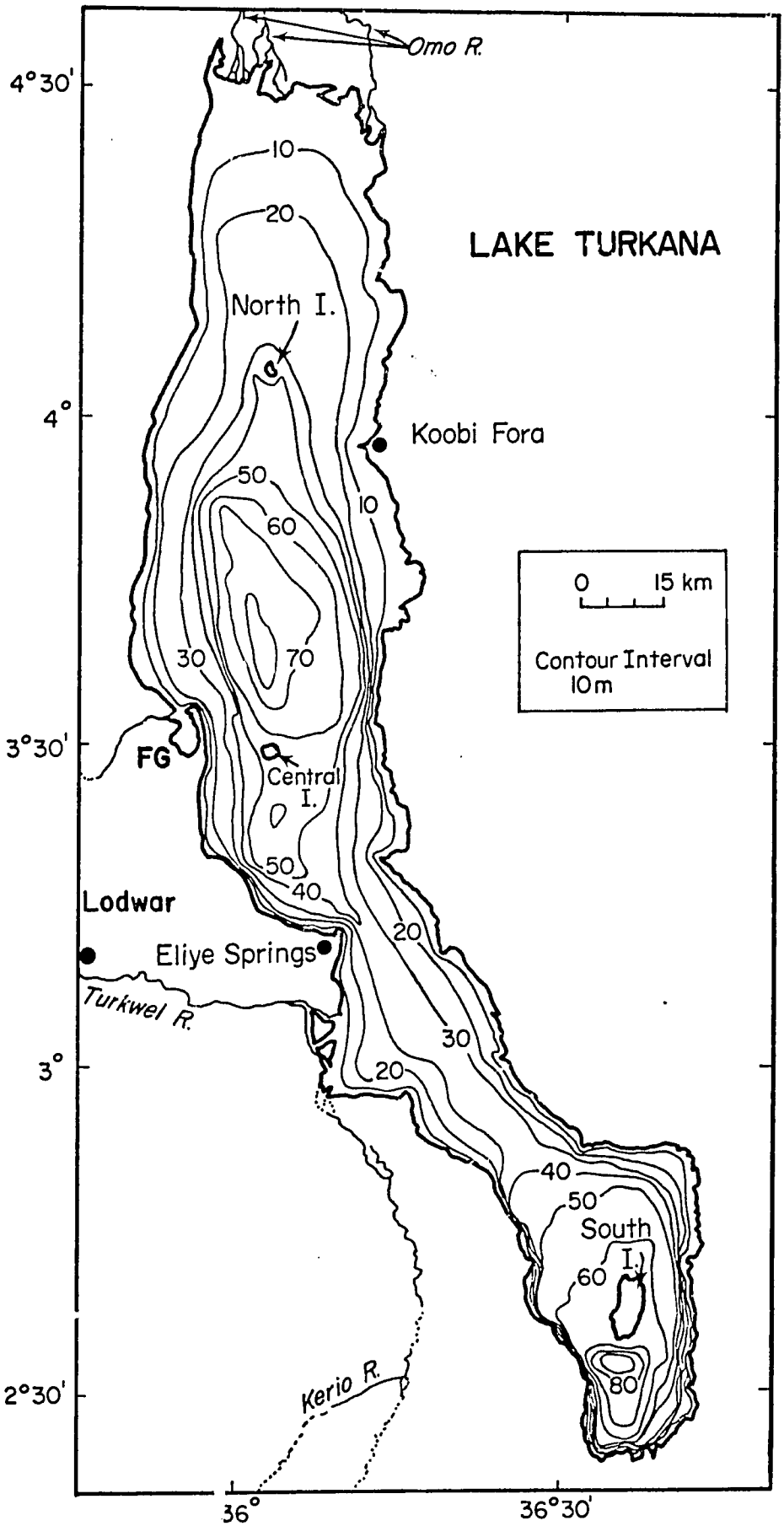
LAKE TURKANA
Omo R.
4°30'
4°
3°30'
3°
2°30'
36°
36°30'
North I.
Koobi Fora
Central I.
South I.
FG
Lodwar
Eliye Springs
Turkwel R.
Kerio R.
0 15 km
Contour Interval 10m
10
20
30
40
50
60
70
80

14a

m, respectively. The lake's mean depth of 31 m is anomalously shallow for a large rift-valley lake, where depths can reach 1,700 m (Herdendorf, 1982).

Geological Setting

Lake Turkana lies within the north-central portion of the Turkana Depression, between the Kenyan and Ethiopian topographic domes (Fig. 3). The elongate zone is approximately 400 km long, with a variable width of approximately 200 km across the northern tip of the lake and about 50 km at the southern end near Lake Baringo (Baker et al., 1972; Gabriel and Aronson, 1987). Along with the adjacent and more prominent Kenyan Rift farther south, these structures delineate the Eastern Branch of the East African Rift System. More conspicuous rifts continue to the north of Lake Turkana, slightly offset toward the east (Stephanie and Ethiopian Rifts). The exact boundaries of individual zones are poorly constrained because their surface manifestations are obscured by voluminous volcanic cover (Baker et al., 1972, Rosendahl, 1987). The Mozambique Fold Belt of metasediments and igneous rocks (Precambrian to Lower Paleozoic age) is the foundation for most of the Eastern Branch (Baker et al., 1972).

The Turkana basin may be one of the oldest existing lake basins in the world. The oldest exposed sediments discovered in the basin are the Turkana Grits (Murray-Hughes, 1933) (Fig. 4). The immature, coarse-grained, arkosic, mostly fluvial and alluvial sediments lie unconformably over basement (Williamson et al., 1986). Williamson (1986) divides the Turkana Grits into the Sera Iltomia of late Mesozoic age and Kajong Formations of mid-Miocene age on the basis of lithology,

Fig. 3. Topographic map of East Africa revealing the Ethiopian Plateau (Dome) and the Kenyan Dome to the north and south of Lake Turkana, respectively. The Eastern Branch of the East African Rift System strikes south from Lake Turkana. The Ethiopian Rift strikes northeast from the lake. Contour interval is 1000 m, with elevations greater than 2000 m highlighted (vertical lines).

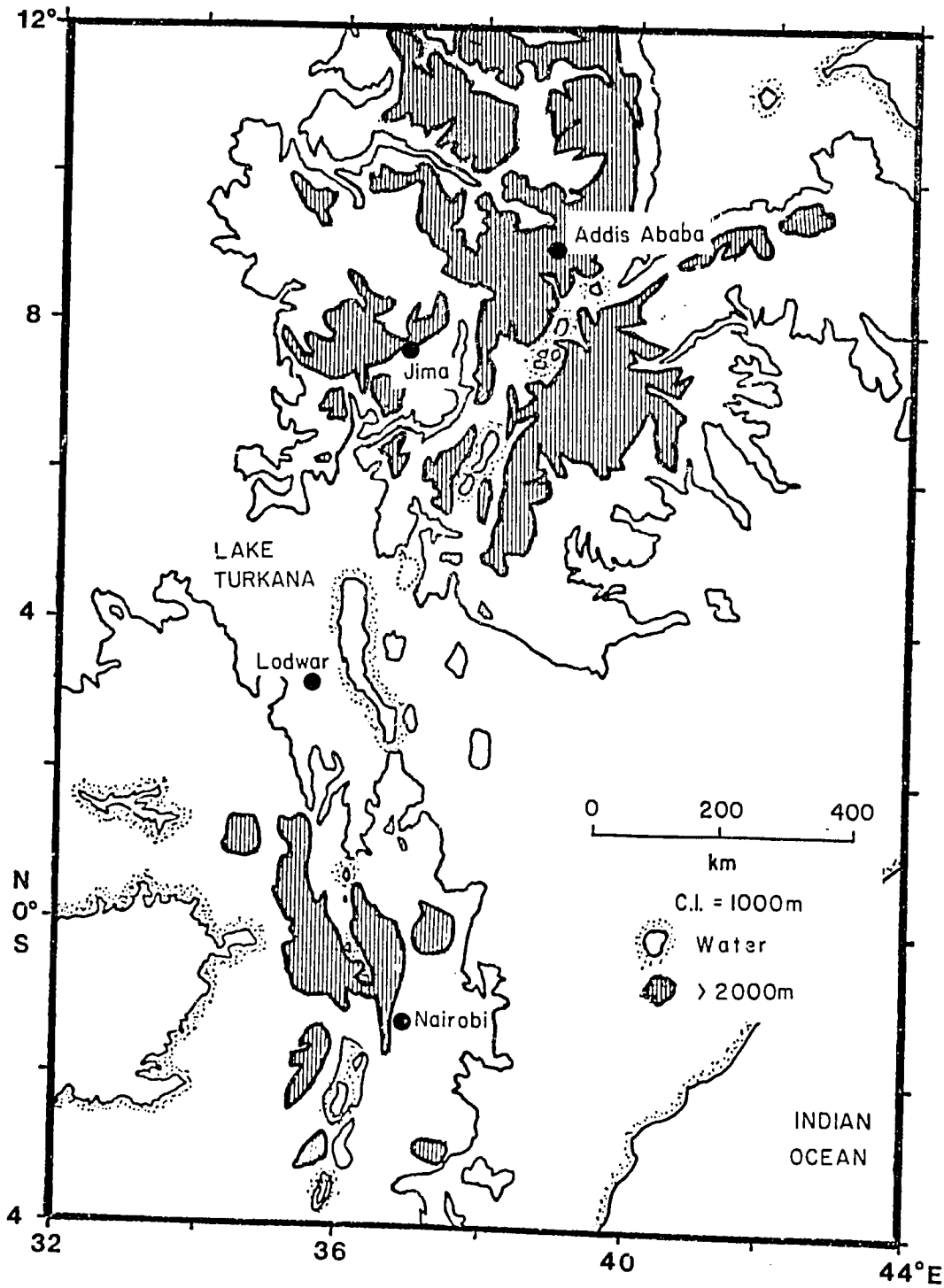
12°
8
4
N
0°
S
4
32
36
40
44°E
Addis Ababa
Jima
LAKE
TURKANA
Lodwar
Nairobi
0
200
400
km
C.I. = 1000m
Water
> 2000m
INDIAN
OCEAN

16a.

Fig. 4. Generalized stratigraphic column of the Turkana region (modified from Dunkelman, 1986).

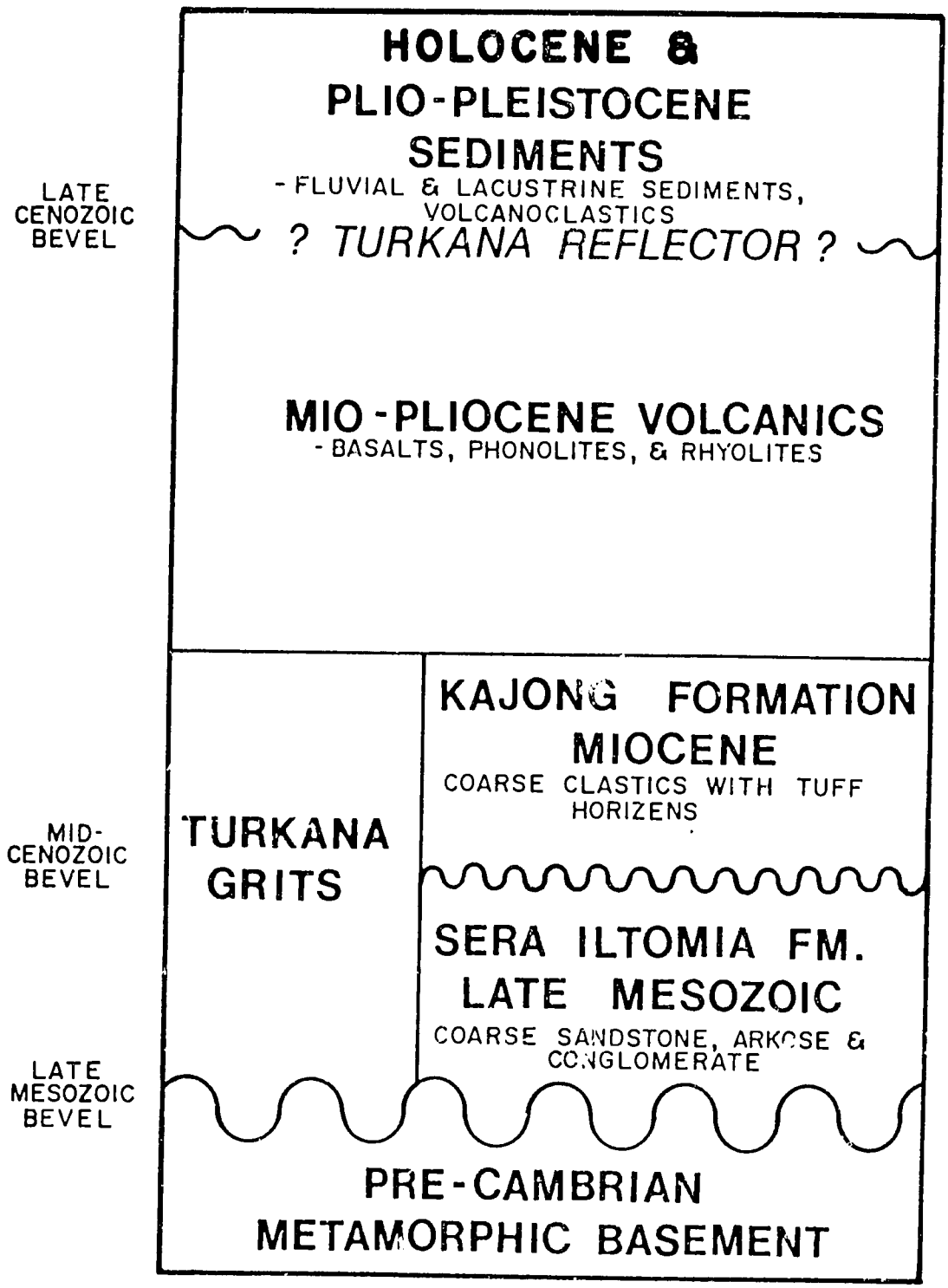
HOLOCENE &
PLIO-PLEISTOCENE
SEDIMENTS
- FLUVIAL & LACUSTRINE SEDIMENTS,
VOLCANOCLASTICS
LATE
CENOZOIC
BEVEL
? TURKANA REFLECTOR ?
MIO-PLIOCENE VOLCANICS
- BASALTS, PHONOLITES, & RHYOLITES
KAJONG FORMATION
MIOCENE
COARSE CLASTICS WITH TUFF
HORIZENS
MID-
CENOZOIC
BEVEL
TURKANA
GRITS
SERA ILTOMIA FM.
LATE MESOZOIC
COARSE SANDSTONE, ARKOSE &
CONGLOMERATE
LATE
MESOZOIC
BEVEL
PRE-CAMBRIAN
METAMORPHIC BASEMENT

structure, and paleontology. The lower formation marks the onset of rifting with supposedly east-west trending transform faults. The onset of major tectonic activity isassociated with north-south trending normal faults and voluminous volcanics (mainly basalts), which are stratigraphically conformable with the Kajong Formation, and are found throughout the Eastern Branch (Baker et al., 1972). Radiometric ages of the mid- to late-Cenozoic volcanics cluster around the mid-Pliocene, although some dates are reported from latest-Oligocene to early-Pleistocene (Williamson, 1986). Jurassic-age sediments filling the Anzu trough, which trends northwest from the Kenyan coast to the active rift zone, have not been found in the Turkana Basin (Reeves et al., 1987).

The formation of the rift zone has provided an effective trap for water and water-lain sediments since the Pliocene. Discontinuous pockets of Plio-Pleistocene sediments and volcanics lie unconformably above the mid-Cenozoic deposits (Baker et al., 1972) (Fig. 5). Their lithology, stratigraphy and depositional environment have been extensively studied at a few paleontological and anthropological sites along the shores of Lake Turkana. Examples include the Koobi Fora Formation along the northeastern shore, the Shungura Formation in the lower Omo Valley, the Lothagam Formation located between the Turkwel and Kerio Rivers and recently described deposits along the northwest shore (Leakey, 1970; Butzer, 1971a; Behrensmeyer, 1976; Brown et al., 1985; Leakey and Walker, 1985).

The youngest series of exposed deposits span the late-Pleistocene through the mid-Holocene. The Kibish Formation in the Omo Valley and the Galena Boi Beds near Koobi Fora are the most extensive lacustrine

Fig. 5. Generalized geologic map of the Turkana drainage basin. Alluvium includes Plio-Pleistocene and younger sediments (from Yuretich and Cerling, 1983).

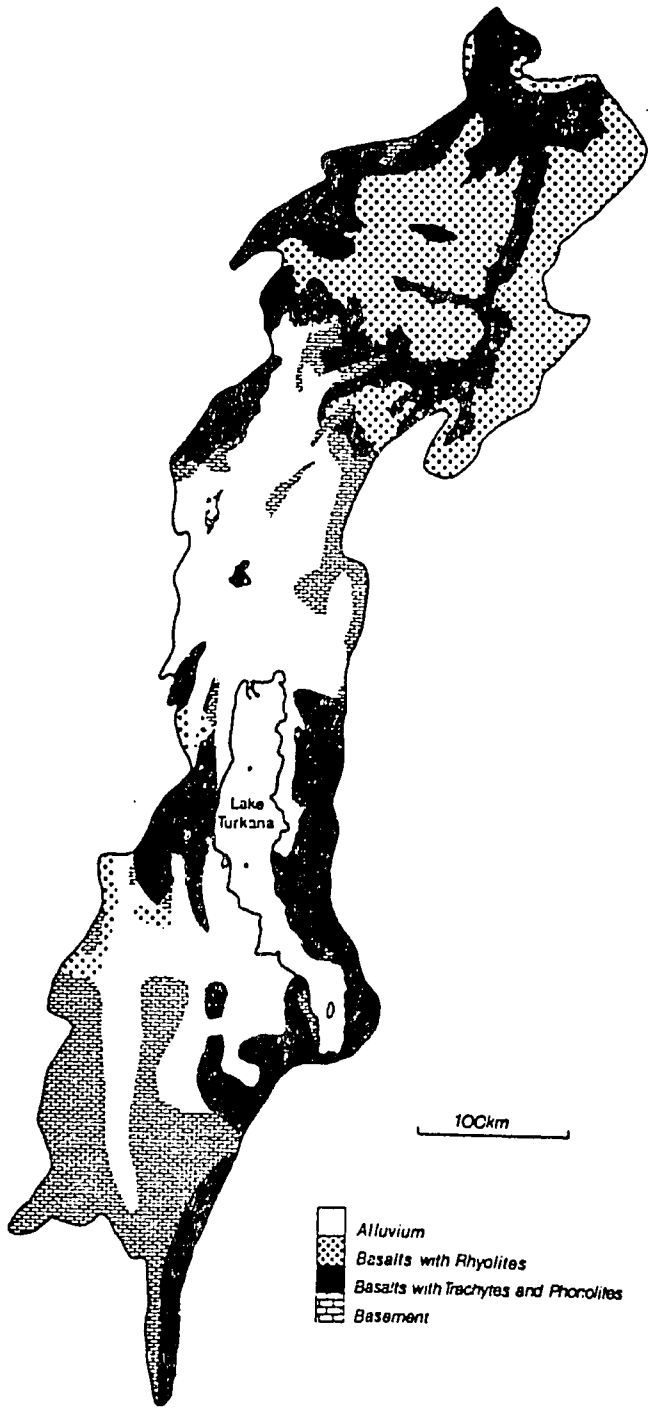
Lake
Turkana
100km
Alluvium
Basalts with Rhyolites
Basalts with Trachytes and Phonolites
Basement

and marginal lacustrine sequences described to date (Butzer, 1976; Owen et al., 1982). Additional early Holocene deposits are located on the western and southern shores of the lake (Cohen, 1981). The more recent volcaniclastics and volcanic flows have occurred primarily from isolated centers (Truckle, 1976; Curtis, 1987). The last major eruption occurred at the south end of the lake during the Teleki and von Hohnel expedition in 1888, and all three volcanic islands show evidence for recent volcanism and hydrothermal activity (Curtis and Karson, 1984; Curtis, 1987).

The surface manifestation of the Turkana Rift Zone is not as pronounced as the neighboring Ethiopian and Kenyan Rifts. Multichannel seismic profiles obtained by Project PROBE show, however, that more than 3 km of sediment underlie the lake floor and infill a deep rift structure (Dunkelman, 1986). Using the nomenclature of Rosendahl (1987), six fundamental, half-graben units with alternating polarities occur along the strike of the lake (Dunkelman, 1986) (Figs. 6 and 7). Turkana is similar in the style of rifting as other lakes investigated by Project PROBE (Reynolds, 1984; Burgess, 1985; Sander, 1986; Rosendahl et al., 1986; Rosendahl, 1987; Specht, 1987). The major difference is that half-graben units in Lake Turkana are about one-third the size of similar units from Lake Tanganyika, and contain considerable volcanic and magmatic material.

A deep, high-amplitude, reflector that marks acoustic basement is seen throughout most of the lake. Dunkelman (1986) believes that it corresponds to the erosional bevel between the mid-Cenozoic volcanics and the Plio-Pleistocene fluvial, lacustrine and volcaniclastic

Fig. 6. Structural configuration of Lake Turkana and identification of half-gragen units revealed from the multichannel seismic profiles (from Dunkelman, 1986). Contours indicate depth to acoustic basement in two-way travel time. The three, thick, roughly east-west lines represent locations for multichannel lines 302, 330 and 342 shown in Fig. 7.

STRUCTURE CONTOUR MAP OF ACOUSTIC BASEMENT

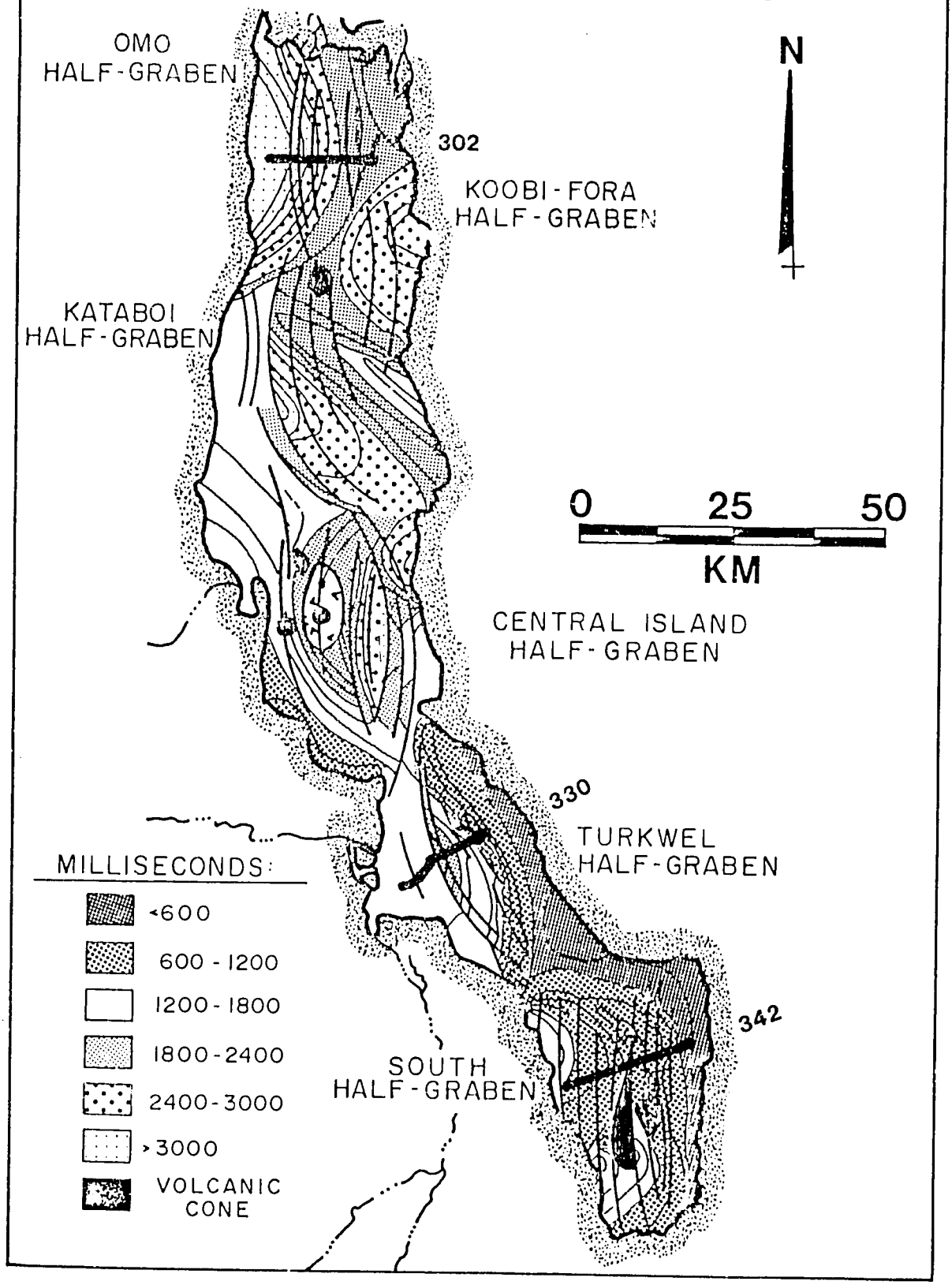

21v.

Fig. 7. Multichannel seismic lines (stacked and migrated sections, V.E. = 2.5:1) number 302 (above), 330 (middle) and 342 (below). The geologic interpretation is presented below each seismic line. Several unconformities (solid horizontal lines) and major faults (vertical lines) are shown which occurred druing the past few million years (from Dunkelman, 1986). See Fig. 6 for line locations.

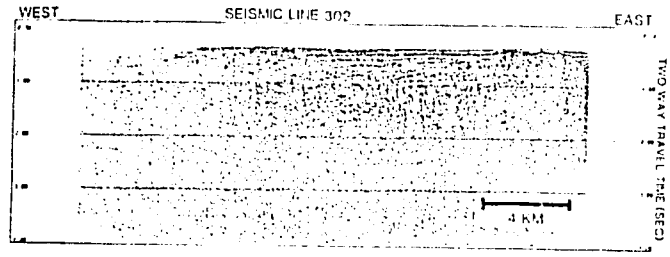
WEST
SEISMIC LINE 302
EAST
TWO WAY TRAVEL TIME (SEC)
4 KM

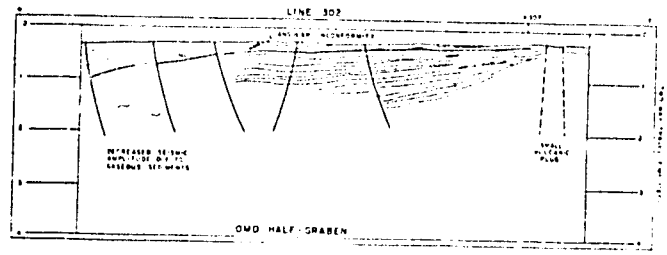
LINE 302
OMO HALF-GRABEN

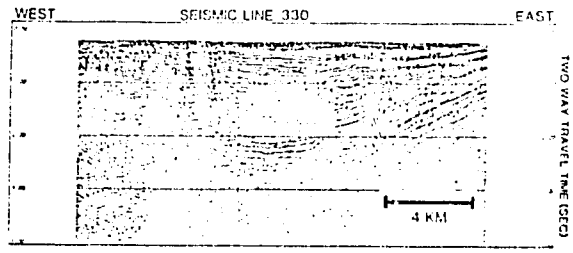
WEST
SEISMIC LINE 330
EAST
TWO WAY TRAVEL TIME (SEC)
4 KM

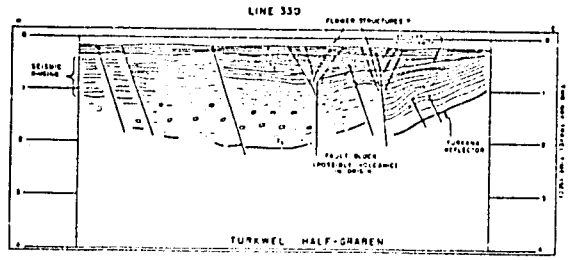
LINE 330
TURKWEL HALF-GRABEN

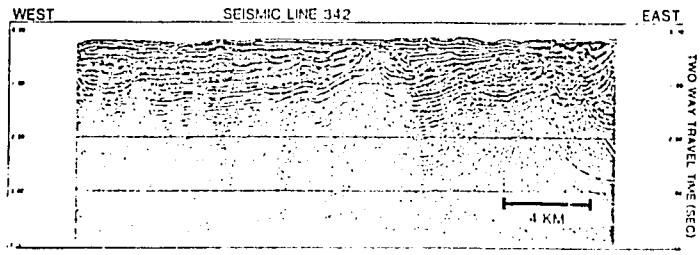
WEST
SEISMIC LINE 342
EAST
TWO WAY TRAVEL TIME (SEC)
4 KM

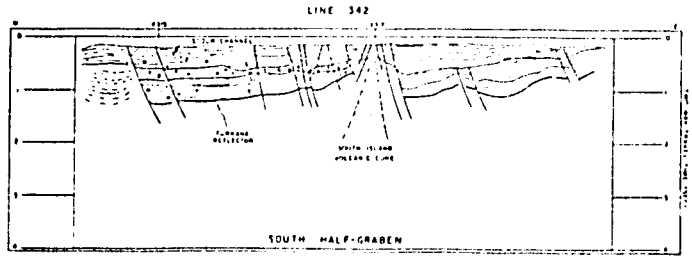
LINE 342
SOUTH HALF-GRABEN

deposits. Sediment thicknesses above acoustic basement often exceed two seconds of two-way travel time and thicken northward. The maximum thickness is in excess of 3.5 seconds of two-way travel time (at least 2.5 and possibly 4 km of section). The northern depositional basin is presently bathymetrically contiguous, although four half-graben (structural) units underlie it, suggesting that the clastic deposition from the Omo River masks the earlier structural controls on deposition. Three to four major angular unconformities are identified within each depositional basin (Dunkelman, 1986). The exposed Koobi Fora Formation has at least three major hiatuses of approximately 0.5 to 0.7 Ma duration (McDougall, 1985). The acoustic character of the seismic sections suggests that lithologies in the lake are similar to the exposed Plio-Pleistocene deposits (Dunkelman, 1986). Unfortunately, structural highs between basins preclude lake-wide correlation of the seismic sections and the absence of well data precludes correlation to the exposed Plio-Pleistocene deposits.

Climatic Setting

Tropical rainfall is generated by convection, and zones of convection are generated by circulation patterns. Assuming the Earth is uniformly covered with water and the axial tilt is 0°, then a simplified Hadley circulation generates a band of convergence (Inter Tropical Convergence Zone, ITCZ) near the equator. A band of divergence (surface high pressure) occurs at 30° N and S. Reinstating the Earth's axial tilt, the thermal equator, which corresponds to the zone of maximum solar radiation, follows the seasonal progression of the sun. The

result is seasonal rainfall in the tropics for any one location. Biannual rainy seasons occur near the equator, diminish to an annual rainy season away from the equator, and ultimately reduce to desert conditions at approximately 30°N and S. The rainfall in the tropics is more intense, of shorter duration, and with stronger localization than temperate latitudes, due to convectional lifting of warm and very moist air (Nieuwolt, 1977).

Tropical climatology actually is much more complex than the preceding simple model due to the irregular distribution of continents, oceans, mountain systems, and other local factors. African climatology follows the general model, with the ITCZ lagging the sun by about one month (Nieuwolt, 1977) (Fig. 8). The longitudinal alignment of the mountains, rift system, and coastline in eastern Africa, in contrast to western Africa, probably influences the drier conditions and larger displacement of the ITCZ in the east relative to the west.

Lake Turkana and the southern drainage basin is in an arid climate. Annual rainfall for Lodwar (30 km west of the lake) averages 155 mm/yr (East African Meteorological Dept., 1975) and is only 40 mm/yr less than a 2 1/2 year temporary record obtained at the lakeshore at Ferguson's Gulf (Ferguson and Harbott, 1982). Rainfall data are not available for the southern basin, but desert vegetation suggests minimal rainfall. The seasonal variation in rainfall for the region is minimal. Intense and short-lived thunderstorms dominate the precipitation, which may be less frequent from October to March (Beadle, 1981; Ferguson and Harbott, 1982).

Mean annual rainfall increases from just north of the lake to

Fig. 8. The generalized surface circulation and rain belts (ITCZ) in January and July for Africa (adapted from Nieuwolt, 1977). The stippled area receives over 50 mm of rain during the summer rains. The dotted line represents the approximate position of the ITCZ.

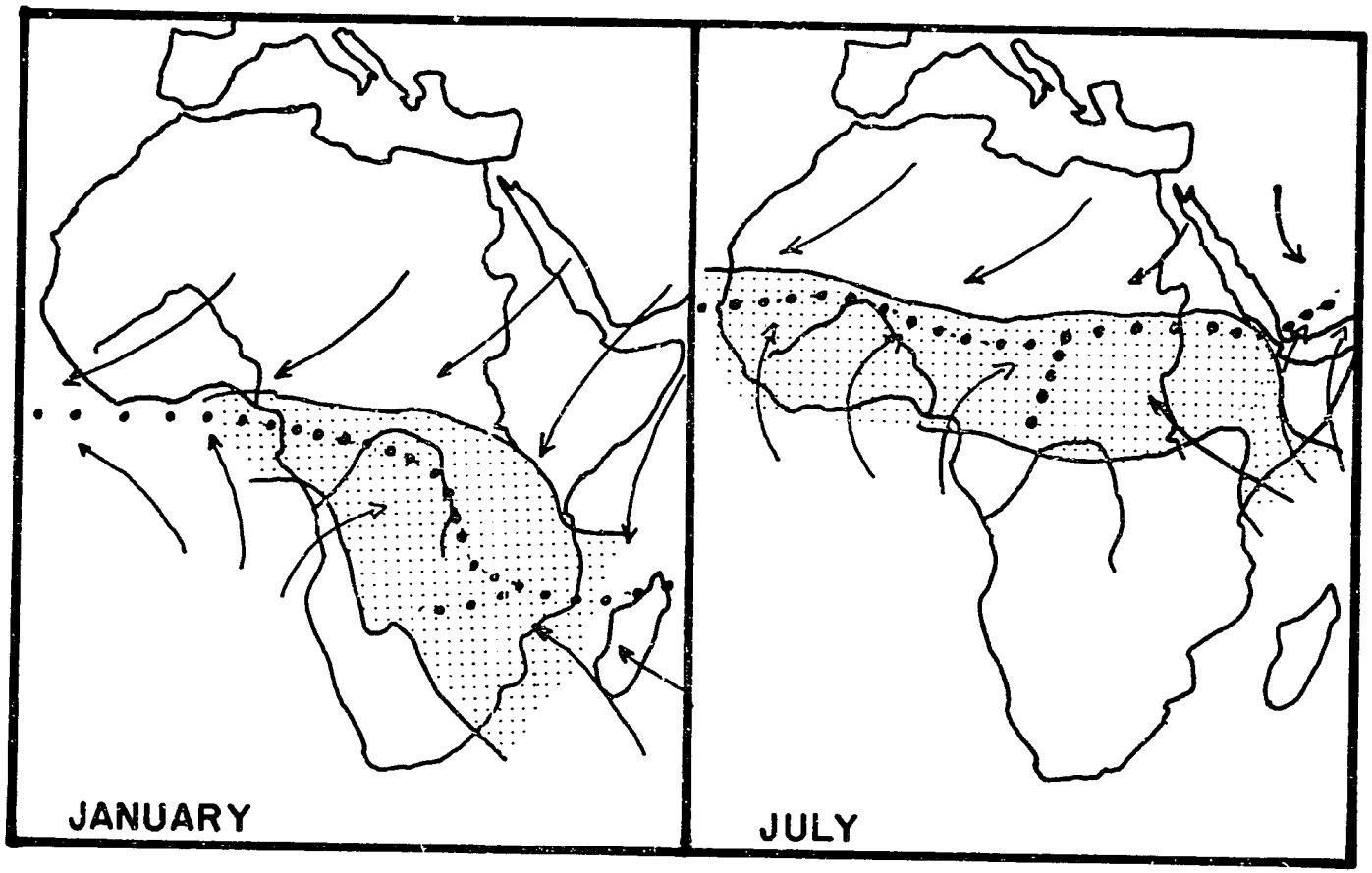
JANUARY
JULY

regions farther north, especially at elevations above 1,000 m in the Ethiopian Plateau, with values from 300 mm/yr to 2,000 mm/yr, respectively. The orographic effect of the plateau creates an "island" of increased precipitation by extending the mid-year rains, compared to adjacent low-lying areas. Mean annual rainfall for regions just south of the lake's drainage basin, including the Kenyan Dome, is typically 1000 mm and is unequally divided into two seasons. The anomalous lack of rainfall at Lake Turkana and other parts of northern Kenya and eastern Ethiopia is caused by widespread divergence of the southwest monsoon to the north of the equator due to, in part, the orographic influence of the Ethiopian and Kenyan Plateaus, and the north/south alignment of the eastern coastline of Africa (Nieuwolt, 1977).

Strong southeasterly winds dominate the climate at Lake Turkana. Daily mean wind speeds up to 840 km/24 hrs (25 km/hr) were recorded, and averaged 300 km/24 hrs (14.5 km/hr) during a period of 2 1/2 years (Ferguson and Harbott, 1982). Daily runs are misleading because the winds are diurnal, typically exceeding 80 km/hr during the early morning hours and calm in the afternoon. The winds are slightly stronger and more persistent in direction at the southern end of the lake. The seasonal pattern of winds shows only a slight tendency to be more intense and more consistent in direction during October to March. The factors controlling the winds are unknown but probably involve the interaction between locally generated thermal winds and the trade winds (Griffiths, 1972). A sharp decline in wind velocity during a solar eclipse (June 30, 1973) suggests that the winds are thermally driven (Ferguson and Harbott, 1982).

Air temperatures reveal minimal seasonal fluctuations and are typically dominated by larger diurnal than annual temperature ranges in the tropics (Nieuwolt, 1977). They are very uniform at Lake Turkana. The mean minimums and maximums range from 26° to 32°C, respectively. The coolest and warmest months occur from July to August and December to May, respectively. Rainfall is the factor that has the greatest effect on air temperature, by reducing temperature during rainstorms (Ferguson and Harbott, 1982). Climates near other large African lakes, compared to Lake Turkana, show more seasonality in precipitation, wind speed and direction, and occasionally temperature (Beadle, 1981).

Former Lake Levels and Past Climates

Lake Turkana responds dramatically to changes in climate. The lake level fluctuates up to 1 meter annually by seasonal flooding and evaporation. Since the early 1970's a pier was left stranded, and since 1984, Ferguson's Gulf has dried up (R. Leakey, pers. commun.) (Fig. 2). The recent desiccation is probably in response to the severe droughts in Ethiopia. The level varied by 20 m between 1896 and 1970 (Fig. 9), with a net drop of 15 m, based on sedimentary, photographic and written evidence (Butzer, 1971b). Historical fluctuations of other lake levels throughout East Africa reveal a parallel decline in lake levels since the end of the 19th century. This desiccation is substantiated by river discharge and other records, and suggests a regional decline in precipitation (Nicholson, 1978; Vincent et al., 1979).

Exposed beach ridges and littoral deposits occur throughout the basin as high as 80 m above the lake's surface (Butzer et al., 1972).

Fig. 9. Fluctuations in lake level of Lake Turkana inferred from sedimentary, photographic, and written evidence: Lake level for the last century (above) relative to 1970 (from Butzer, 1971) and for the Holocene (below) relative to 1976 (from Owen et al., 1982). Lake level dropped about 1 meter between 1970 and 1976 (Ferguson and Harbott, 1982).

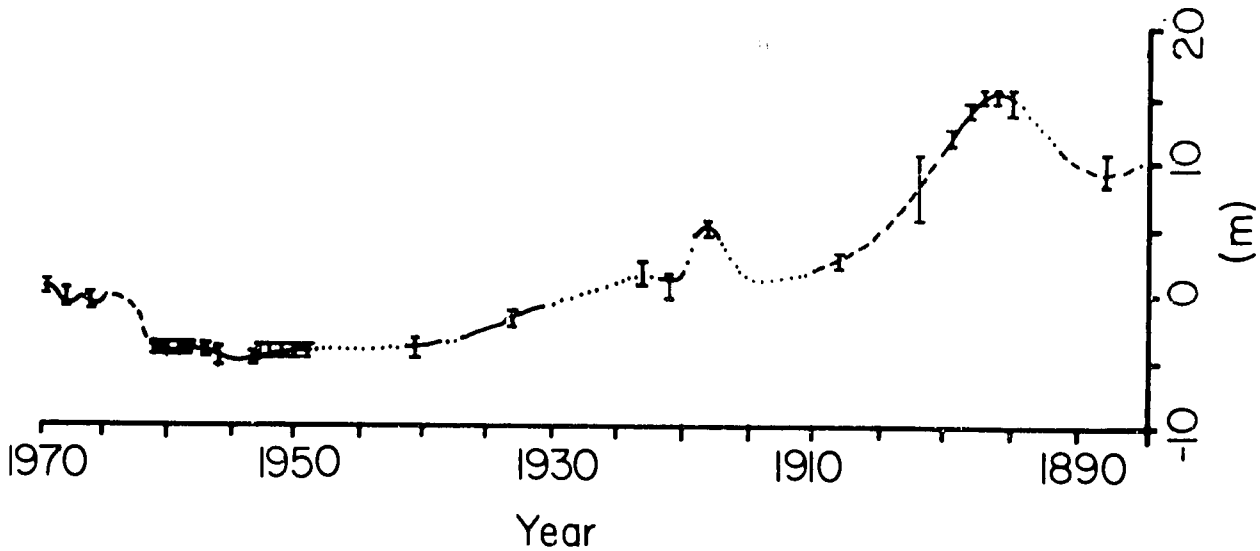
1970
1950
1930
1910
1890
Year
-10
0
10
20
(m)

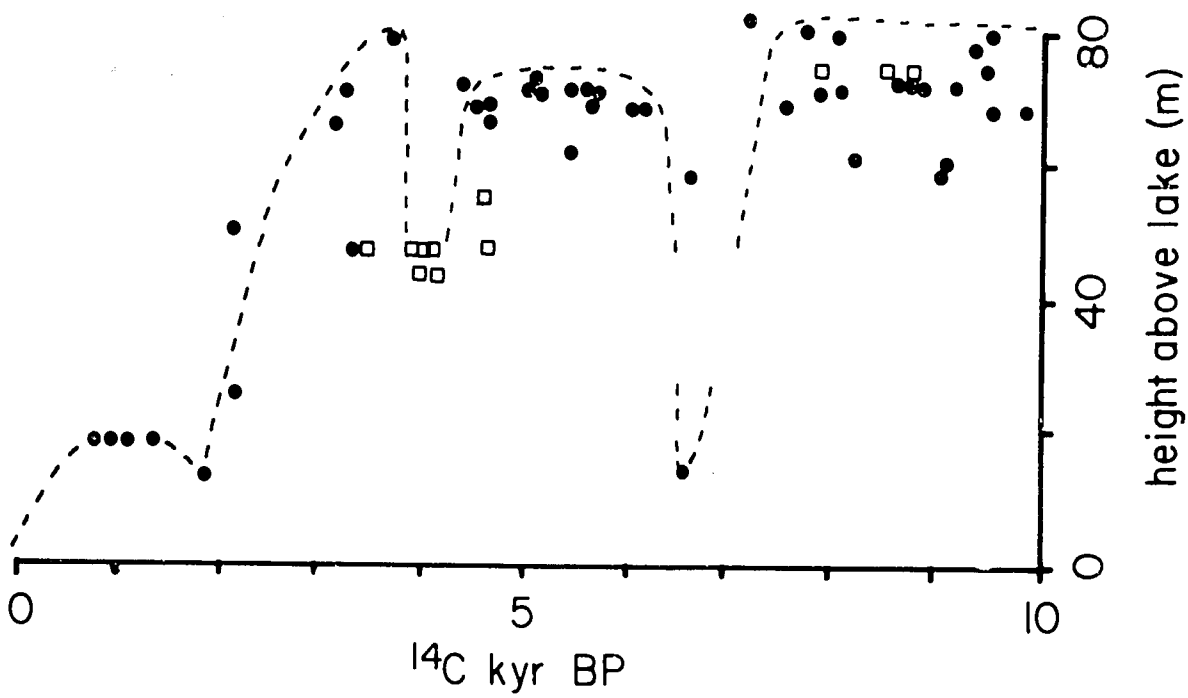
0
5
10
14C kyr BP
0
40
80
height above lake (m)

28a

At this level, the enlarged surface area is estimated to have been between 22,000 and 24,000 km^2 (Cohen, 1981; Ferguson and Harbott, 1982). The pluvial lake overflowed into the Nile River through the Pibor-Sobat River system. Holocene deposits reflecting high stands of lake level have been radiocarbon-dated from 10.0 to 7.5 Ka; 6.0 to 4.2 Ka; and less reliably from 3.8 to 3.2 Ka (Livingstone and Kendall, 1969; Butzer, 1980; Owen et al., 1982), although very little is known about the paleoclimatic record for the last few millennia (Fig. 9).

Lacustrine deposits of Plio-Pleistocene age are also exposed up to 80 m above the lake floor, suggesting that lake level was at a similar height at several times in the late Cenozoic. An important climatic shift at about 1.8 Ma reduced the effective precipitation for Lake Turkana and much of East Africa (Hay, 1976; Cerling, 1979; Bonnefille, 1976; Abell, 1982). Since then, the lake has probably fluctuated between open and closed conditions (Cohen, 1981). The lake level also might be influenced by past changes in Omo River drainage (Cerling, 1986), and by tectonics (Vondra and Bowen, 1978). The latter probably requires on the order of 10^5 years to alter lake level to a similar magnitude accomplished by climatic change in less than 10^2 years (Cerling, 1986).

The majority of lakes in East Africa and the rest of the tropics experienced a synchronous increase in lake level during the late Pleistocene and early Holocene (Butzer et al., 1972; Street and Grove, 1976, 1979; Street-Perrott and Roberts, 1983; Street-Perrott and Harrison, 1984, 1985) (Fig. 10). The data base represents a compilation of approximately 200 lakes that were closed at some time in the last

Fig. 10. Histograms showing the temporal variations in lake level for lakes in the northern extratropical lakes (above) and global intratropical lakes (below) (from Street-Perrott and Harrison, 1984). The three lake level states are high (across-hatch), intermediate (diagonal) and low (blank).

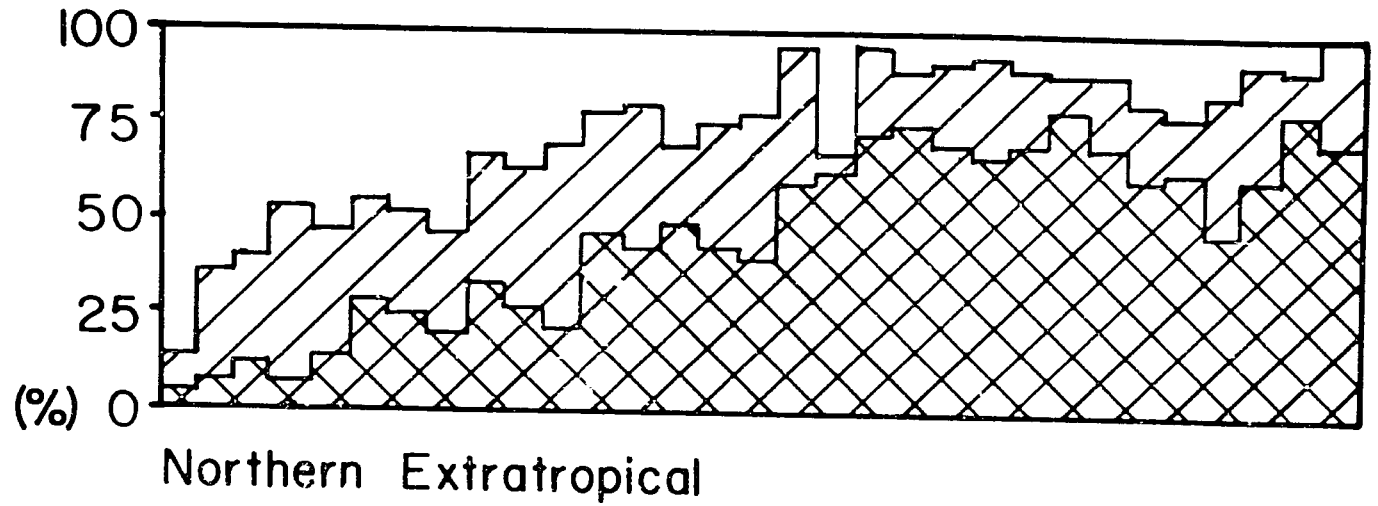
100
75
50
25
(%) 0
Northern Extratropical

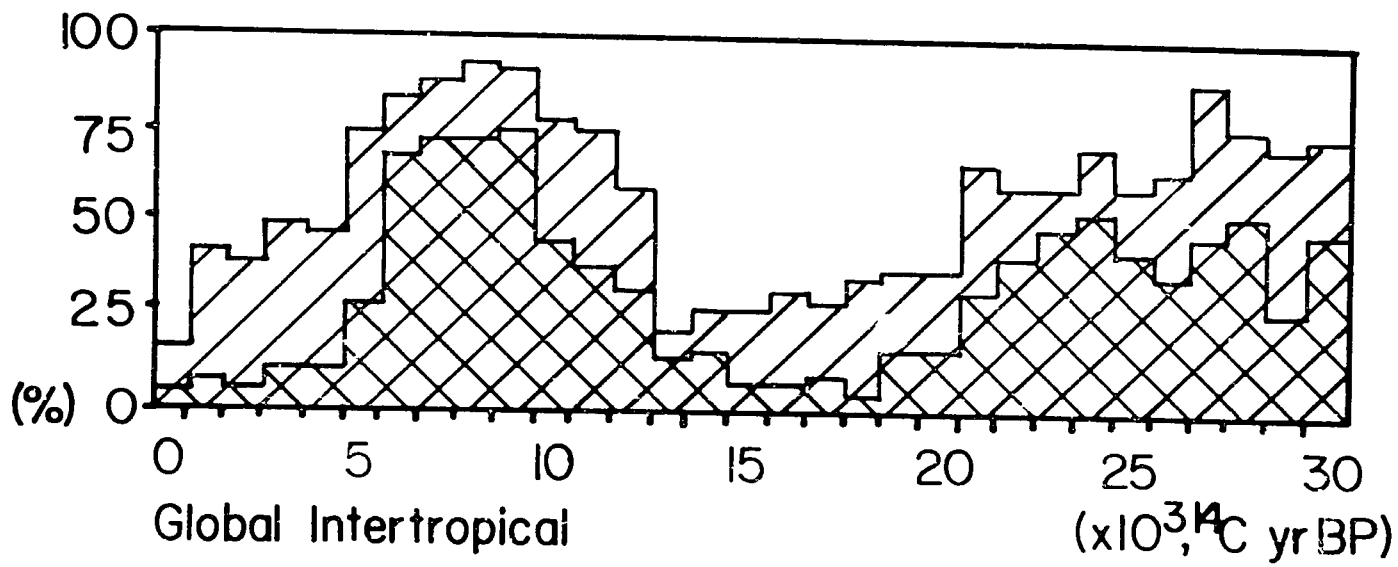
100
75
50
25
(%) 0
0
5
10
15
20
25
30
Global Intertropical
(x10³, ¹⁴C yr BP)

30,000 years. The lake levels were inferred from radiocarbon-dated horizons of former stands of lake-level and paleo-lake level stratigraphies (see earlier section), grouped into 1,000 year increments. The last major pluvial phase has been radiocarbon dated to start at 12 Ka, culminate around 9 Ka and abruptly terminate at 5 Ka. Extensive aridity dominated the tropics during and just after the northern hemisphere glacial maximum from 20 to 13 Ka. Correlative evidence for a dry glacial maximum and a moist early Holocene comes from the Nile Valley (Adamson et al., 1980; Williams and Adamson, 1982), tropical glaciers (Hastenrath, 1985), oceanic sediments off western Africa (Sarnthein and Diester-Haass, 1977; Maley, 1982; Stein and Sarnthein, 1984; Pokras and Mix, 1987) and other records throughout the tropics (Williams, 1975). The intertropical pluvial and desiccation periods indicate a regional climatic change that is consistent with the record at Lake Turkana (except for the reported 3.8 to 3.2 Ka high-stand) (Fig. 10).

Atmospheric general-circulation models for the past 15,000 years in 3,000 year increments reveal that increased precipitation culminated at 9 to 6 Ka (Kutzbach and Street-Perrott, 1985). The monsoon intensity is responding to Milankovitch orbital forcing of incoming solar radiation (Kutzbach, 1981; Kutzbach and Guetter, 1984). A latest-Pleistocene and early-Holocene episode of increased upwelling and inferred increased monsoonal activity also was interpreted from sediment cores off Saudi Arabia (Van Campo et al., 1982; Prell, 1984; Prell and Van Campo, 1986). Sapropels in the Eastern Mediterranean, which are interpreted to reflect African pluvial phases, also occur when orbital parameters are aligned

so that solar insolation is above a threshold value over the middle latitudes (Rossignol-Strick, 1983, 1985).

Modern Limnology

The tropical temperature regime is, in general, conducive to prolonged lake stratification. Diurnal and seasonal temperature changes are usually insufficient to induce convectional mixing. Warm water undergoes a larger density change for a given difference in temperature than colder water, and this contributes to a more stable density stratification in tropical lakes. The stability of stratification can be greatly increased by relatively high concentrations of dissolved salts in the hypolimnion. Deep water stirring by winds opposes the tendency for stratification (Beadle, 1981).

Lake Turkana is well mixed by the strong southeasterly winds. The intense mixing of the water column combined with the shallow depth is reflected in the nearly uniform temperature, oxygen and conductivity profiles with depth in the lake. The profiles reveal minimal stratification, with water temperatures (average 25° to 26° C) varying less than 2°C and oxygen concentrations above 70% saturation throughout the water column (Ferguson and Harbott, 1982). Thermal stratification may occur during calm afternoons only to be destroyed by the nightly winds. Wave mixing depths are estimated at over 30 m (Cohen, 1984).

The hydrology of the closed-basin lake is dominated by the perennial Omo River, which drains the Ethiopian Highlands approximately 500 km to the north. Careful monitoring of the inflow during 1973 and 1974 indicated that the Omo River provides 88% of the fluvial inflow to the

lake (Ferguson and Harbott, 1982). The annual flooding of the Omo raises lake level by 0.5 to 1 m. The intermittent Turkwel and Kerio Rivers contribute most of the remaining fluvial input by draining the region to the west and south. The remaining ephemeral springs and streams and direct rainfall are insignificant to the water budget. Subterranean inflow and outflow is postulated not to exist, because chemical mass balance arguments showed that the accumulation of dissolved ions is taking place at expected rates (Yuretich and Cerling, 1983).

The lake is moderately saline (2.4 $^{o}/oo$) and alkaline (pH = 9.2). The principal ions are Na^+ (33 mmoles/l), HCO_3^- (19.5 meq/l), and Cl^- (12 mmoles/l). The secondary ions are K^+ (0.5 mmoles/l), Ca^{+2} (0.1 mmoles/l), Mg^{+2} (0.1 mmoles/l), SO_4^{-2} (0.4 mmoles/l), F^- (0.5 mmoles/l) and SiO_2 (0.3 mmoles/l). The weighted average fluvial concentrations are pH (7.1), alkalinity (1.4 meq/l), Na^+ (0.6 mmoles/l), K^+ (0.1 mmoles/l), Ca^{+2} (0.3 mmoles/l), Mg^{+2} (0.2 mmoles/l) and Cl^- (0.1 mmoles/l) (see Yuretich and Cerling, 1983, for details). A chemical mass-balance approach suggests that Ca^{+2} is precipitated as calcite; Mg^{+2} is probably incorporated into smectite; K^+ may be used in illite regradation; some Na^+ is removed as an exchangable cation; and Cl^- is conservative (Yuretich and Cerling, 1983; Yuretich, 1986). The current concentration of Cl^- indicates about 4,000 years of evaporitic concentration (Cerling, 1986).

The open-water algae are dominated by Cyanophyta (blue-greens), especially Microcystis species, with Chlorophyta (greens) and Bacillariophyta (diatoms) contributing equally to the remainder (Harbott, 1982). The temporal and spatial distribution of algae is

influenced by the Omo River (Harbott, 1982). The highest open-water biomass and productivity were found in the north end of the lake, peaking during Omo River floods. Harbott (1982) presumed that the Omo River supplied usable nitrogen, which is otherwise limiting to algal growth. Net productivity measurements range from 0.2 to 6.2 $gC/m^2/day$, based on only 13 measurements (Harbott, 1982). The average value is approximately 1 $gC/m^2/day$, which is similar to values reported from other African lakes (Beadle, 1981). Nearshore algal biomass, especially in protected bays and inlets (e.g., Ferguson's Gulf), is higher than all but one open-water site (Harbott, 1982). The algal community supports 48 species of fish, of which 30 are characteristically Sudanian species and the remainder are clearly descendants of Sudanian species (Hopson and Hopson, 1982). The common lineage suggests that Lake Turkana and the Nile were connected during the past.

Modern Lake Sediments

The profundal sediments are laminated muds, averaging 71% clay (Yuretich, 1979, 1986). The mineralogy and chemical composition of the sediments vary systematically from north to south. The north and Turkwel basins are dominated by detrital sediments derived from the Omo River and the Turkwel and Kerio River System, respectively. The sediments in the south basin are coarser grained due to a greater abundance of biogenic components, presumably due to decreased detrital input.

The nearshore sediments divide into major substrate classes that reflect the wave energy of the environment (Cohen, 1982; Cohen et al.,

1986). The western shore is dominated by intense wave activity and displays erosional, rocky headlands with occasional gravel substrates in the south and sandy silt substrates farther north. Protected embayments, especially along the eastern shore, contain silty muds. Limited marshland substrates of vegetated, organic-rich sediments occur in the Omo delta and to a lesser extent the Turkwel and Kerio deltas and Allia Bay where wave activity is minimal.

Very few sedimentation rates have been reported for the modern sediments and most only as personal communications. Sedimentation rates of about 0.20 $g/cm^2/yr$ were obtained by C. Barton using Pb-210 methods and are similar to rates estimated from his paleomagnetic stratigraphies (Barton, pers. commun. in Cerling, 1986; Barton et al., 1987). Crude sediment traps, deployed near North Island, provided average sedimentation rates of 0.46 $g/cm^2/yr$ (Ferguson and Harbott, 1982). The preceding mass sedimentation rates can be converted to linear sedimentation rates of 0.40 and 1.0 cm/yr, respectively, assuming a sediment porosity of 0.8 and particle density of 2.7 g/cm^3. Yuretich (1979) estimated an average sedimentation rate of 0.1 cm/yr for the basin based on calcium removal from the lake water. The Galena Boi beds have a maximum sedimentation rate of 0.3 cm/yr, based on tentative biostratigraphic correlations (Owen et al., 1982). If the laminations are annual couplets, then sedimentation rates are between 0.2 cm/yr and 4 cm/yr. Thus, the range of sedimentation rate estimates extends from 0.1 to 4.0 cm/yr, but still remains to be well documented. Large lake level fluctuations and fast sedimentation rates makes Lake Turkana an excellent site for high-resolution paleoclimatic study.

METHODS

Field Methods

The shipboard methods employed were twofold; normal incidence seismic reflection profiling and sediment coring. The seismic profiling was used to conduct a reconnaissance survey of the upper 50 m of sediment. High-resolution seismic profiles have provided important insight into the modern sedimentary processes in lakes (e.g., Johnson, 1980; Johnson et al., 1984) and the marine environment (e.g., Damuth, 1980).

High-resolution seismic profiles were obtained along 770 km of trackline using a Ferranti-O.R.E. Geopulse System (Fig. 11). The transducer catamaran was towed at a speed of 5 to 6 knots. The power output was set at 280 joules. The incoming data were filtered in the range of 0.5 to 5 kHz and displayed on an EPC 3200 graphic recorder. This system will hereafter be referred to as the 1 kHz system.

Echo sounding profiles were obtained on Duke University's multichannel seismic vessel, R/V NYANJA, using a Furuno Model FE-814 profiler (Fig. 11). The depth finder operates on a frequency of 28 kHz, has a hull mounted transducer, and displays lake-floor morphology on a graphic recorder. Most of these profiles were obtained along 900 km of multichannel seismic lines at a speed of 2 knots.

Navigation was by radar and satellite systems. Radar fixes supplemented the satellite navigation at the ship speeds used for multichannel seismic data acquisition. Radar fixes every 15 minutes were supplemented by satellite fixes whenever possible at 1 kHz data

Fig. 11. High-resolution seismic survey trackline map.

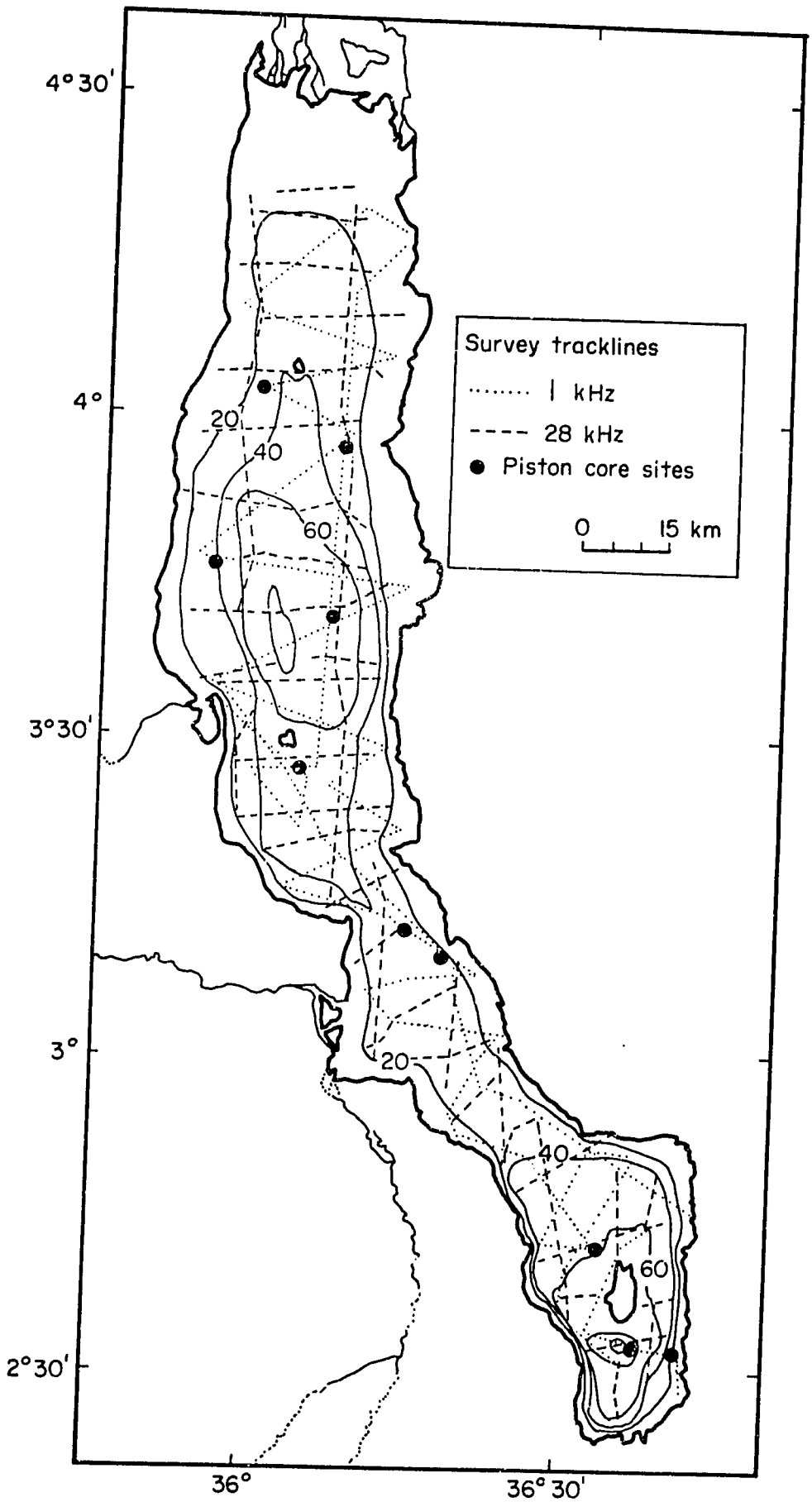
4°30'
4°
3°30'
3°
2°30'
36°
36°30'
20
40
60
20
40
60
Survey tracklines
1 kHz
28 kHz
Piston core sites
0
15 km

31a.

acquisition speeds.

A bathymetric chart was constructed from the echosounding records assuming a speed of sound of 1463 m/sec (800 fm/sec) (Fig. 12).

Sediment sampling was by gravity and piston (Kullenburg) corers (Fig. 12) (Appendix A). Two gravity cores (giant gravity corer designed by Oregon State University) 15 cm in diameter and approximately 1 m long were obtained. The extremely fluid nature of Lake Turkana's upper sediments resulted in very poor gravity core recovery. Subsequent routine gravity coring was abandoned in favor of piston coring.

Piston coring was done with an ETH corer in cooperation with Dr. Guy Lister, Geologisches Institut, ETH-Zentrum, Zurich. The ETH corer (Kelts et al., 1984) is designed to recover cores slightly less than 6 cm in diameter, inside a PVC liner, and to be modular for simple transport and operation. The piston coring objectives were to provide lake-wide coverage and to core major seismic reflectors. Individual core sites were selected with the aid of the 1 kHz system. Each core was cut into 1 m lengths, capped and sealed immediately after recovery. The cores were subsequently flown from Lake Turkana to either the Duke Marine Lab at Beaufort, NC, or to ETH, Zurich. Ten piston cores were collected, each approximately 11 meters long, except for core LT84 - 3P, which was 4 meters long. Five cores (LT84 - 1P, 2P & PG, 4P, 7P, 8P) are at Beaufort, NC, and the remaining cores (LT84 - 3P, 5P, 6P, 9P, 10P) are at Zurich.

Fig. 12. Map of bathymetry, piston (P) and gravity (G) core sites.

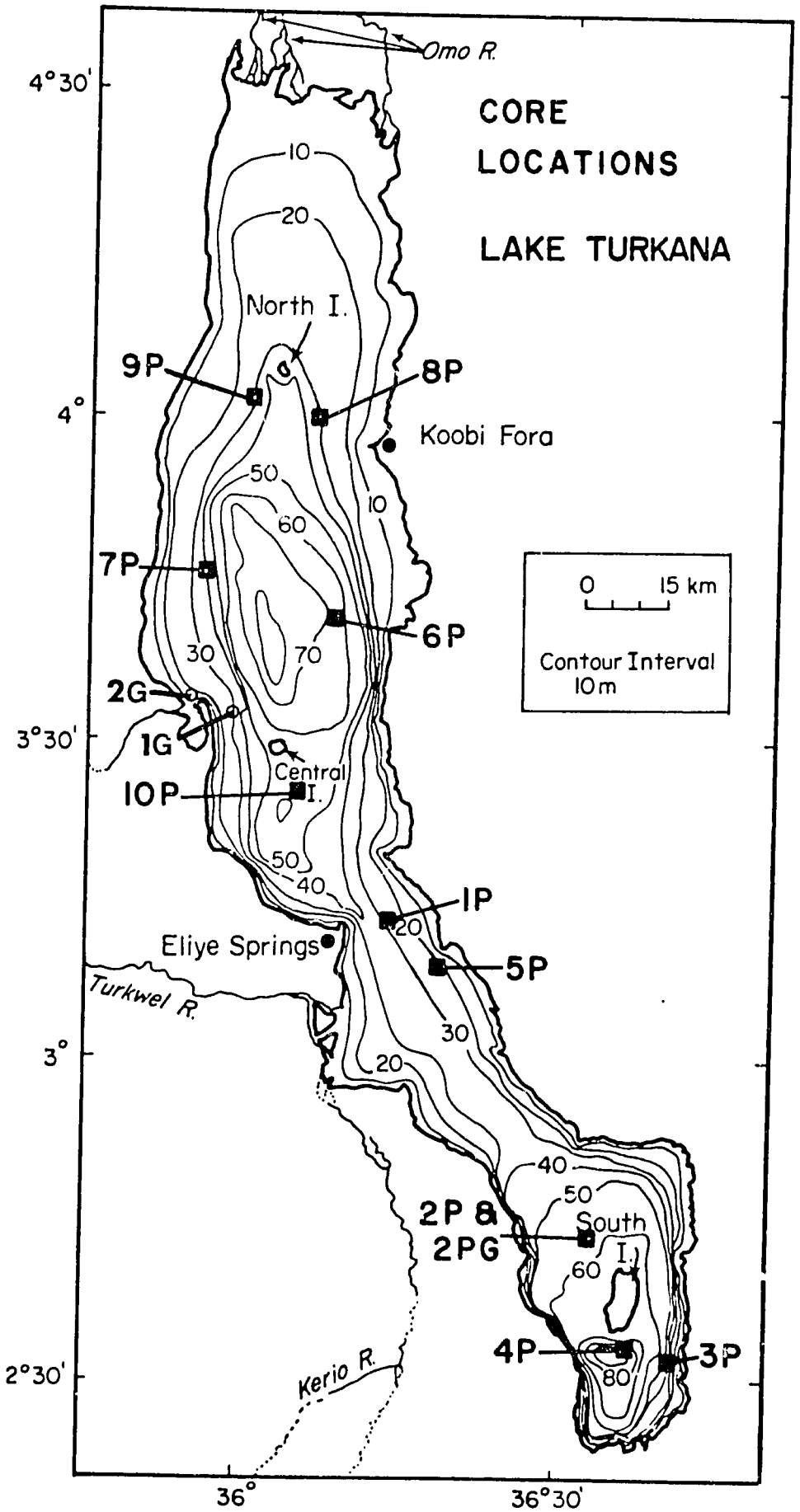
CORE
LOCATIONS
LAKE TURKANA
Omo R.
4°30'
4°
3°30'
3°
2°30'
36°
36°30'
North I.
9P
8P
Koobi Fora
7P
6P
2G
1G
Central I.
10P
1P
5P
Eliye Springs
Turkwel R.
2P &
2PG
South I.
4P
3P
Kerio R.
0 15 km
Contour Interval 10m
10
20
30
40
50
60
70
80

Laboratory Methods

The sediments were analyzed for down-core trends to understand the factors controlling deposition through time. The analyses included geochronology, routine sediment description, porosity, diatom genus relative abundances, biogenic silica, grain size, total organic carbon, total carbonate, trace element and stable isotope composition of carbonates, and clay mineralogy. On a smaller scale, the laminations were described in detail and their thicknesses determined. In addition, 56 successive laminae from approximately 35 to 100 cm of core LT84-8P were subsampled and analyzed to investigate their origin.

Geochronology

Carbon-14 dating of sediment samples was performed commercially by Beta Analytic, Inc., Coral Gables, FL. Each sample consisted of 20 to 30 cm of core, which was freeze-dried before shipping to Beta. The carbon from the carbonate fraction was utilized for dating. The dates are reported as radiocarbon years before 1950 A.D. The half-life of radiocarbon was taken as 5568 years. The errors represent 1 standard deviation of the measured activity, and accumulate from the random nature of the radioactive disintegration process when counting the modern standard, background and sample. No correction was made for DeVries effect, reservoir effect or isotopic fractionation in nature.

Lead-210 analysis of the freeze-dried, bulk sediment was performed by Dr. D. DeMaster at the NCSU geochronology laboratory. The Pb-210 activity was measured by alpha counting its daughter Po-210. A Po-208 spike was used to monitor chemical yield. The activities of the samples

were reported as disintegrations/minute/gram dry sediment (dpm/g).

Core Description and Sampling

The cores were split longitudinally, photographed, and described visually and with smear slides. One half was designated as the working half, and the other the archive half. The Duke University Marine Lab core curation procedures were modified from Mountain (1973). Sediment subsamples of approximately 4 g wet weight were immediately taken from approximately every 25 cm down core, weighed and frozen for porosity and other analyses. Sediment samples from core LT84-3P were not analyzed because the core was just recently split and the samples were not yet received from Zurich.

Porosity

The porosity (the ratio of volume of pore space to total volume) of a sediment sample can be estimated from water content measurements. The following assumptions are made. The density of water and the sediment are 1 and 2.65 g/cc, respectively, and the water originally filled all of the non-sediment spaces. The sample is weighed wet (Wwet), freeze-dried, and weighed dry (Wdry). The porosity is calculated by the formula:

$$\text{Porosity} = (W_{wet} - W_{dry})/1 \;/\; [(W_{wet} - W_{dry})/1 + (W_{dry})/2.65]$$

where: Wwet = weight of the wet sediment sample (g),
Wdry = weight of the dry sediment sample (g).

Diatoms

The relative abundance of diatom species was determined by Karla

Hahn, as an undergraduate independent study project at Duke University Marine Lab during the Spring of 1986. Smear slides were made every 25 cm down cores LT84 - 2P and 4P. The other cores lacked sufficient diatoms for analysis. The slides were viewed at 100x power using an Olympus Model BH-2 polarizing light microscope. Diatom valves were counted by identifiable species until 400 valves had been counted. Species identification was verified by Mr. Kurt Haberyan, Dept. of Zoology, Duke University. Percent frequency of occurrence was calculated by sample for each species.

Biogenic Silica

The percent biogenic silica of a sediment sample was determined by a wet-chemical extraction method modified from DeMaster (1979) and developed and described by Lynch (1986). The technique also incorporates grain-size analysis of the non-biogenic, carbonate-free, silt-sized fraction of the sample by an electronic grain size analyzer. Lynch (1986) found that this digestion technique completely dissolved the biogenic silica without significant alteration to the detrital sediment.

The sampling resolution was at least 1 sample / meter of core except for cores LT84-4P and 9P, where it was less than 1 sample / 2 meters of core. No samples were taken from core LT84-6P. A known weight (approximately 0.3 g) of dry sediment (Wdry) was acidified with 25% acetic acid in a preweighed centrifuge bottle (Wbot) to dissolve the carbonates. The sample was centrifuged at 2000 rpm for 30 minutes to decant the liquid. The bottle was then weighed (Wrinse). The sample

was digested in 200 ml of 5% sodium carbonate solution for 2 hours to determine and dissolve the biogenic silica. An aliquot of 1 ml was withdrawn from the digestion, and diluted to 100 ml with distilled water, at 15, 30, 60, 90, and 120 minutes into the digestion. The silica concentration of the extracted dilutions was determined by a colorimetric method (Strickland and Parsons, 1968) using a Technicon Auto Analyzer. The percent biogenic silica was calculated using the formula:

$$\%Silica = [VNa \times (Wrinse - Wbot) \times MSiO2 \times Siconc]/[Wdry \times 10000]$$

where: VNa = Volume of Sodium carbonate for digestion (ml),
Wrinse = weight of centrifuge bottle, after acetic acid rinse,
Wbot = weight of centrifuge bottle (g),
Siconc = concentration of biogenic silica (micro-molar),
Wdry = weight of dry sediment used for analysis,
MSiO2 = molecular weight of SiO2 (60.09).

Grain Size

Grain size of the detrital silt fraction, that remained after the silica digestion, was performed by the following method. The sodium carbonate was removed by centrifuging at 2000 rpm for 30 minutes and decanting the liquid prior to grain size analysis. The organic matter was removed from the sample by adding 10 ml of 30% hydrogen peroxide. The coarse sediment was removed by sieving at 62 microns. The clay fraction was removed by repeated centrifuging at 500 rpm for 3.5 minutes, and decanting the non-sedimented slurry until the decant liquid was clear. The remaining silt-size fraction was stored in a 1% sodium chloride solution until analysis by an Elzone Model 80 XY particle analyzer, manufactured by Particle Data, Inc. Detailed instructions on the calibration and operation of the Elzone are found in Halfman (1982).

The silt-sized fraction was disaggregated with a sonic dismembrator, and shaken by hand for 1 minute to homogenize the sample. Immediately afterwards, a 1 ml aliquot was extracted and dispersed in 200 ml of clean electrolyte (1% sodium chloride solution). Each analysis counted 20,000 particles with a 190 microns diameter orifice. Each sample was analyzed in duplicate. If the median grain size of the duplicate run was not within 3 channels of the original run, then the sample was analyzed again. The count for each respective channel was summed from all the analyses of the sample and stored on floppy disk with the interfaced IBM-PC for later retrieval and statistical analysis. The statistics were calculated by moments assuming spherical particles. The Elzone status parameters used in this study were:

Current = 5.5,
Gain = 1.5,
Diameter of Channel 1 = 5.85 microns,
True log scale = 10.647,
Orifice = 190 microns,
Total counts / sample = 20 000.

Total Organic Carbon and Nitrogen

Total organic carbon (TOC) and total organic nitrogen (TON) content of 2 to 4 sediment samples / meter of core were determined by CHN analyzer using procedures of Hedges and Stern (1984). The hydrogen was not determined because the samples absorbed an unknown quantity of water prior to analysis. A known weight (Wo) of sediment (50 -100 mg) was acidified with 2 ml of 1 M carbon-free hydrochloric acid to remove non-organic carbon (carbonate). The acidified sample was dried overnight, allowed to equilibrate with room moisture and reweighed (Wf). Two homogenized samples were weighed (between 5.7 and 6.2 mg) in tin boats

on a CAHN electrobalance (CAHNwt). These subsamples were analyzed for elemental carbon and nitrogen using a Carlo Erba Model 1106 CHN Analyzer. Standard curves relating weight of carbon and nitrogen to the results of the analyzer were generated using an acetanilide standard. The percent TOC was calculated using the formula:

$$\% \text{ TOC} = 100 \times (\text{mgC})(\text{Wf}) / [(\text{CAHNwt})(\text{Wo})]$$

where: mgC = mg of C determined from the C standard curve,
CAHNwt = mg of sample weighed on the CAHN electrobalance,
Wo = sample weight before acidification,
Wf = sample weight just after acidification.

The percent TON was calculated in a similar manner. Substitute mg of nitrogen, as calculated from the nitrogen standard curve, instead of mg of carbon into the % TOC formula. The percent TON formula is:

$$\% \text{ TON} = 100 \times (\text{mgN})(\text{Wf}) / [(\text{CAHNwt})(\text{Wo})]$$

where: mgN = mg of N determined from the N standard curve,
CAHNwt = mg of sample weighed on the CAHN electrobalance,
Wo = sample weight before acidification,
Wf = sample weight just after acidification.

The C/N ratio by weight was calculated using the formula:

$$\text{C/N ratio} = \% \text{ TOC} / \% \text{ TON}.$$

Carbonate

The carbonate content of 3 to 4 sediment samples / meter of core plus 10 samples / meter of core for cores LT84-7P, 8P, 10P was determined by a rapid vacuum-gasometric technique (Jones and Kaiters, 1983). Preweighed (approximately 0.5 g), freeze-dried, powdered sediment and 3 ml of 85% phosphoric acid were placed in separate chambers of a reaction bomb. The bomb was evacuated to a known pressure (Pi). The sample was reacted with the acid for 1.5 hours with periodic

agitation every 20 minutes. The sample was placed in a water bath of known temperature during the last 15 minutes . The final pressure (Pf) was measured. The change in pressure (Pf - Pi) is proportional to the amount of carbonate in the sample. A standard curve calibrating the change in pressure to milligrams of carbonate in a sample was generated for each bomb using known weights of pure calcium carbonate. The procedure assumed the sample did not contain dolomite, which is substantiated by other analyses. The carbonate percentage was calculated using the formula:

$$\% \text{ Carbonate} = 100 \times [(Pf - Pi)(Tcorr) - b] / [(m)(Wdry)]$$

where: Pf = the finale pressure after digestion,
Pi = the initial pressure before reaction,
Tcorr = [1 + (25.0 - Temperature water bath, ^{o}C) / 298.15],
b = the y-intercept of the standard curve,
m = the slope of the standard curve,
Wdry = weight of dry sediment reacted in the bomb (g).

Trace Element and Stable Isotope Analysis of Carbonates

Molar ratios of strontium to calcium (Sr/Ca) and magnesium to calcium (Mg/Ca) and oxygen and carbon stable isotope analyses were determined on species-specific ostracod samples and on fine-grained (<44 microns), organic-free carbonate in the sediment. Samples from about 1 meter intervals down cores LT84-2P and 7P were prepared in an identical fashion for both analyses. Sample preparation included the following.

The organic matter was digested by adding a few ml of hydrogen peroxide to approximately 15 g (wet weight) of sediment dispersed in 250 ml of distilled water. The rate of the reaction was increased by warming the slurry on a hot plate. After the digestion, the peroxide was removed by centrifuging at 2000 rpm for 30 minutes and decanting the

liquid. The sample was dispersed in approximately 200 ml of 2.5 g/l calgon solution by a wrist action shaker (at least 1 hour). Then, the coarse fraction was separated from the fines by sieving at 150 microns. The coarse fraction was gently washed with at least 200 ml of distilled water and dried overnight at 70°C. Adult and juvenile forms of Sclerocypris clavata were picked from the coarse fraction for separate analyses. The picked tests were lightly crushed just prior to elemental and isotopic analysis.

Calgon was decanted from the fine fraction (< 150 microns) after centrifuging at 2000 rpm for 30 minutes. The fine fraction was dispersed in 100 ml of distilled water by a wrist action shaker (at least 1 hour). The sediment finer than 44 microns was isolated by sieving. The sample was rinsed by dispersing the sample in 200 ml of distilled water, centrifuging at 2000 rpm for 30 minutes and decanting the liquid for 3 repetitions. The sample was subsequently freeze-dried and stored for elemental and isotopic analysis. The carbonate in the fine fraction will hereafter be referred to as micrite.

Elemental analysis was preformed on a Perkin-Elmers Model 5000 Atomic Absorption Spectrophotometer (AA). Appropriate dilutions were made to insure the concentrations measured were within the linear response for the specific element. The AA response was calibrated using 5 standards diluted from commercial stock (1000 ppm) solutions. The ostracods were reacted in 1 ml of 1 M hydrochloric acid for at least 15 minutes. The sample was well shaken, and a 0.2 ml aliquot was added to 1.0 ml of distilled water for Mg analysis, a 0.1 ml aliquot was added to 5.0 ml of distilled water for Ca analysis. The remaining sample was

used for Sr analysis. The micrite was reacted with constant agitation in 10 ml of 1 M hydrochloric acid for at least 30 minutes. The remaining slurry was centrifuged at 2000 rpm for 30 minutes. Approximately 2 ml of the solution was used for Sr analysis. An 0.1 ml aliquot was added to 20 ml of distilled water for both Ca and Mg analyses. The concentration (moles/l) of an element from a sample is calculated using the formula:

$$\text{Element (M)} = [(\text{Xconc})(\text{Tvol} + \text{Dvol})]/[1000(\text{Mwt})(\text{Tvol})]$$

where: Xconc = concentration determined by the AA of element (mg/l) in the diluted sample,
Tvol = volume of aliquot transferred for dilution,
Dvol = volume of distilled water the aliquot is added to,
Mwt = molecular weight of the element.

Isotopic analyses were performed by Dr. William Showers at North Carolina State University Stable Isotope Lab. A sample was reacted with 5 ml of 100% orthophosphoric acid at 50°C. The evolved carbon dioxide was cleaned of water vapor in a alcohol/slush trap, and sealed in a break seal container. The Finnegan MAT 251 mass spectrometer was used for isotopic analysis. The results are reported relative to PDB isotopic standard.

Scanning Electron Microscopy

A scanning electron microscope (Joel JSM-T20) located at the Zoology Dept. of Duke University was used to identify the constituents of the fine grain sediment. Sediment was scraped from individual laminae, and allowed to dry on a glass slide for 10 minutes. Two-sided adhesive tape was fixed onto SEM stubs. Each stub was subsequently pressed onto the dry sediment. The stubs were desiccated overnight to remove all traces

of moisture. The sample was sputter-coated for 4 minutes and then ready for SEM analysis.

Lamination Description

In addition to visual and smear slide descriptions of individual laminae, the sediment from Lake Turkana was X-rayed in the hope that the laminations may be more clearly depicted as in the case of other studies (Edmondson and Allison, 1970; Johnson et al., 1984). X-radiography did not increase the resolution of individual lamina, however.

Lamination Thickness

Lamination thicknesses were measured in two cores. The other cores lacked continuous and long sections of distinct laminae. The archive half of core LT84-8P was uniformly scraped and left exposed to oxidize with the air for about 20 minutes. The laminations became more distinct with mild oxidation. A reference string was stretched down the middle of the core, parallel to a aluminum core holder. A strip of paper, with a straight line down the middle, was laid parallel to the string. A mark was made at all junctions of lamination boundaries and the string. These marks were transferred to the strip of paper using a T-square against the aluminum core holder. The relative color (light vs dark) of each laminae was noted. The distances between lamination boundaries were digitized and converted to millimeters. The digitizer accuracy is +/- 0.03 mm.

The other core, LT84-9P, is stored in Zurich. Instead of using the core, a 4x5" negative, taken by a large format camera, was enlarged and

printed at approximately full scale. This photograph was used in a similar manner as the core above. A meter scale in the photograph was used to convert the digitized measurements to millimeters. The distortion due to enlarging the negative was determined to be negligible by measuring the meter scale at numerous locations. The down-core thickness data is reported as the thickness of successive light/dark couplets. The horizontal gaps in the core that lacked sediment were not included in the thickness data because they assumably are the result of gas expansion during core recovery.

Lamination Geochemical Analyses

Bulk carbonate, biogenic silica, grain size and total organic carbon analyses were performed on the subsamples of successive laminae. The methods are the same as described above.

Clay Mineralogy

X-ray diffraction analyses of the bulk sediment were determined by Michelle Bishop as a graduate independent study project at Duke University, Dept. of Geology, Spring, 1986. Samples from at least 2 sets of adjacent laminae were analyzed from cores LT84-1P, 4P and 8P. The samples were ground to a fine powder, smeared onto a glass slide, and dried on a hot plate. The Phillips X-ray diffraction unit uses copper K-alpha radiation. The sample was scanned from 2 to 50 degrees of 2 theta, at a rate of 1 degree/minute. Mineralogy and relative abundances were determined using standard reference guides and total peak height proportions with standard corrections for crystallinity.

RESULTS

High-Resolution Seismic Profiles

The interpretations from the high-resolution, 1-kHz and 28-kHz, seismic profiles are published (Johnson et al., 1987). A review of their interpretations is presented below (Fig. 13).

The 1-kHz and 28-kHz seismic profiles revealed sub-bottom reflectors as much as 60 m below the lake floor, assuming that the velocity of sound through the upper sediments was 1463 m/sec (Fig. 14). The spacing of reflectors over a given depth interval was greater for the 1-kHz records than the 28-kHz records, as expected. The 1-kHz records, however, revealed greater contrast in reflector amplitude than the echo-soundings.

The survey indicates that the basin is filling with sediments in a simple, ponding, style. Only limited evidence exists for sediment erosion and redistribution by bottom currents. This is in contrast to what is seen in other large lakes (Johnson, 1984). The result is surprising, due to the strong southeasterly winds that dominate the climate at Lake Turkana. Either these winds do not generate a consistent circulation pattern that might generate erosional bedforms, or sediment influx overwhelms any redistribution of sediments by current activity.

The seismic profiles could be categorized into three major types based on the character of the sub-bottom reflectors (Fig. 15). Type I profiles have a diffuse and prolonged surface reflection with no sub-bottom reflectors. Type II profiles have weak or discontinuous sub-

Fig. 13. A summary diagram relating the deep structure of the Turkana Basin (above) (from Dunkelman, 1986) and the high-resolution features (below) (from Johnson et al., 1987).

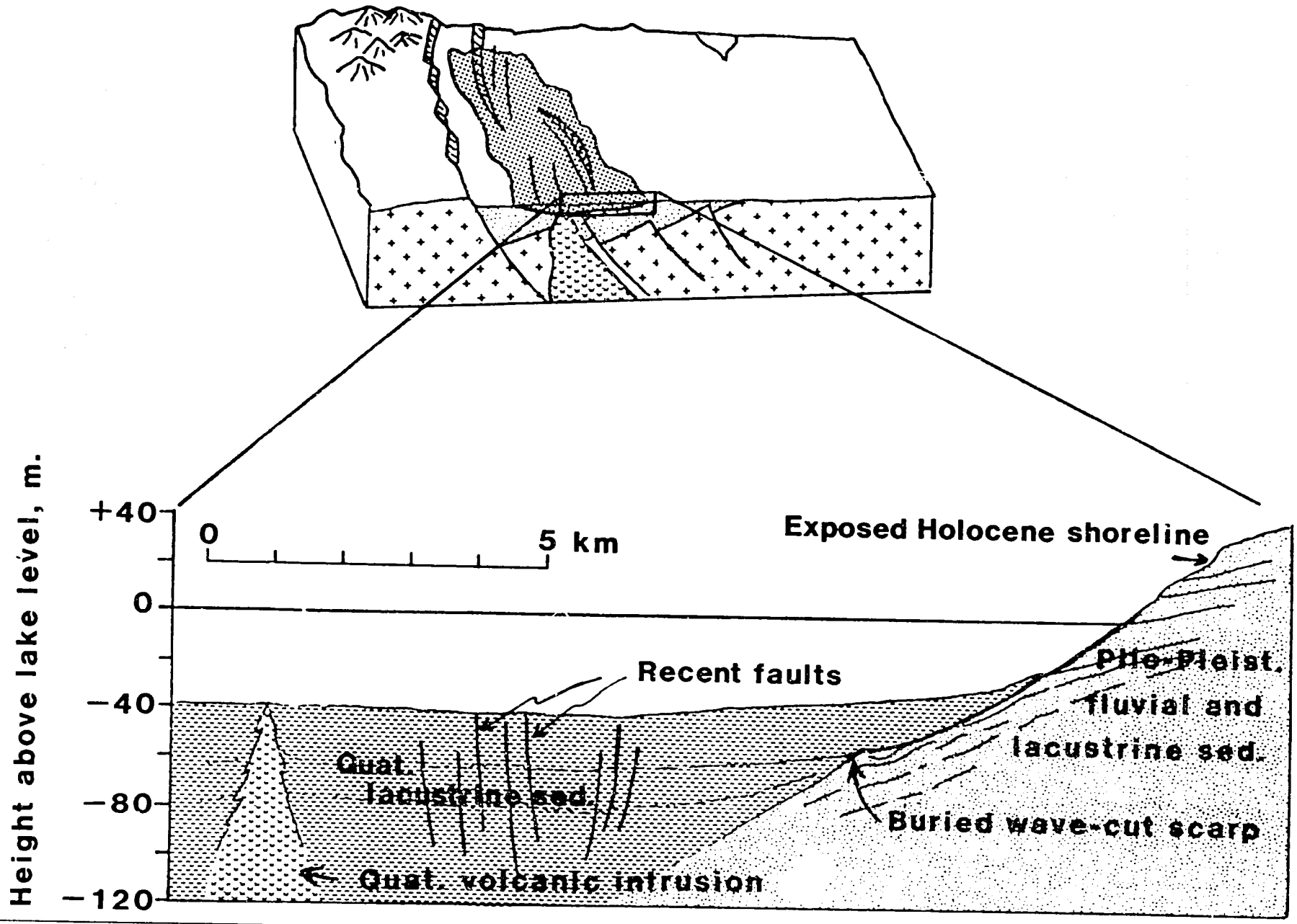
Height above lake level, m.
+40
0
−40
−80
−120
0
5 km
Exposed Holocene shoreline
Recent faults
Pliо-Pleist.
fluvial and
lacustrine sed.
Quat.
lacustrine sed.
Buried wave-cut scarp
Quat. volcanic intrusion

52a

Fig. 14. A comparison of 1-kHz profile (above) and the 28-kHz profile (below) from the same area. Note how the 1-kHz profile reveals the deeper structure and the 28-kHz profile shows more stratification in the upper horizons (from Johnson et al., 1987).

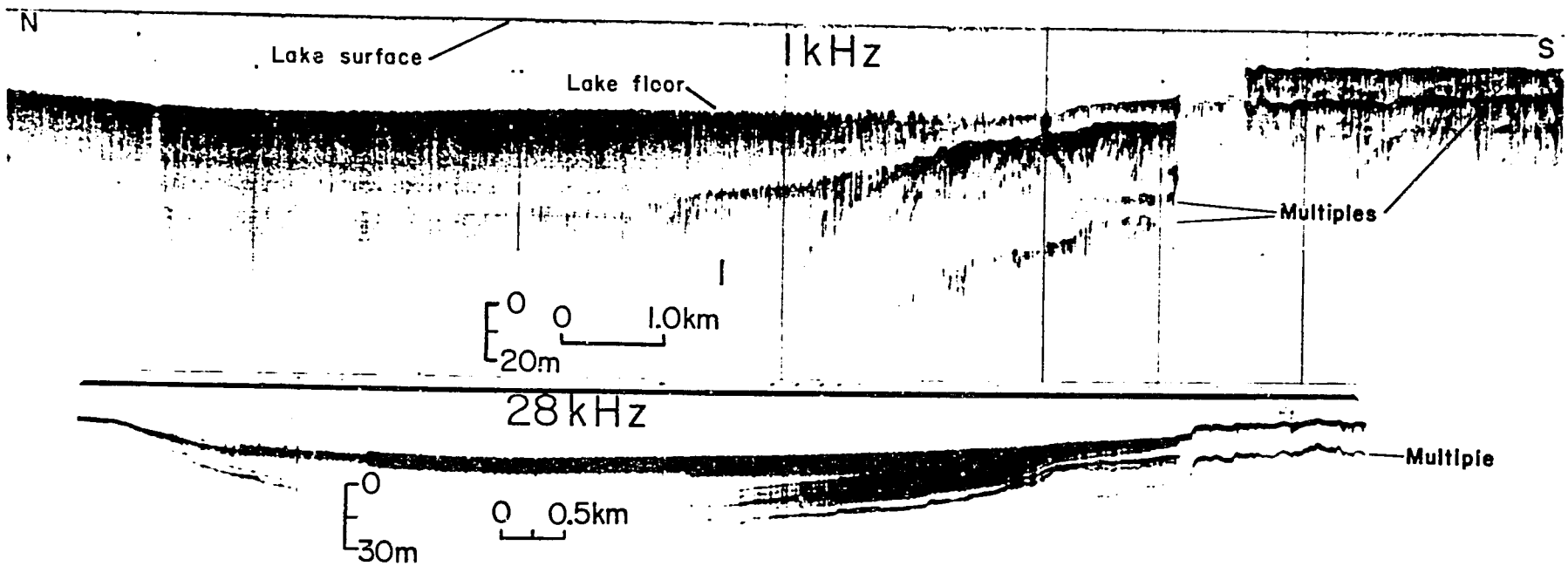
N
S
Lake surface
Lake floor
1kHz
Multiples
0
0
1.0km
20m
28kHz
Multiple
0
0
0.5km
30m

Fig. 15. Examples of the three major types of 1-kHz profiles from Lake Turkana. LS = Lake Surface, LF = Lake Floor (from Johnson et al., 1987).

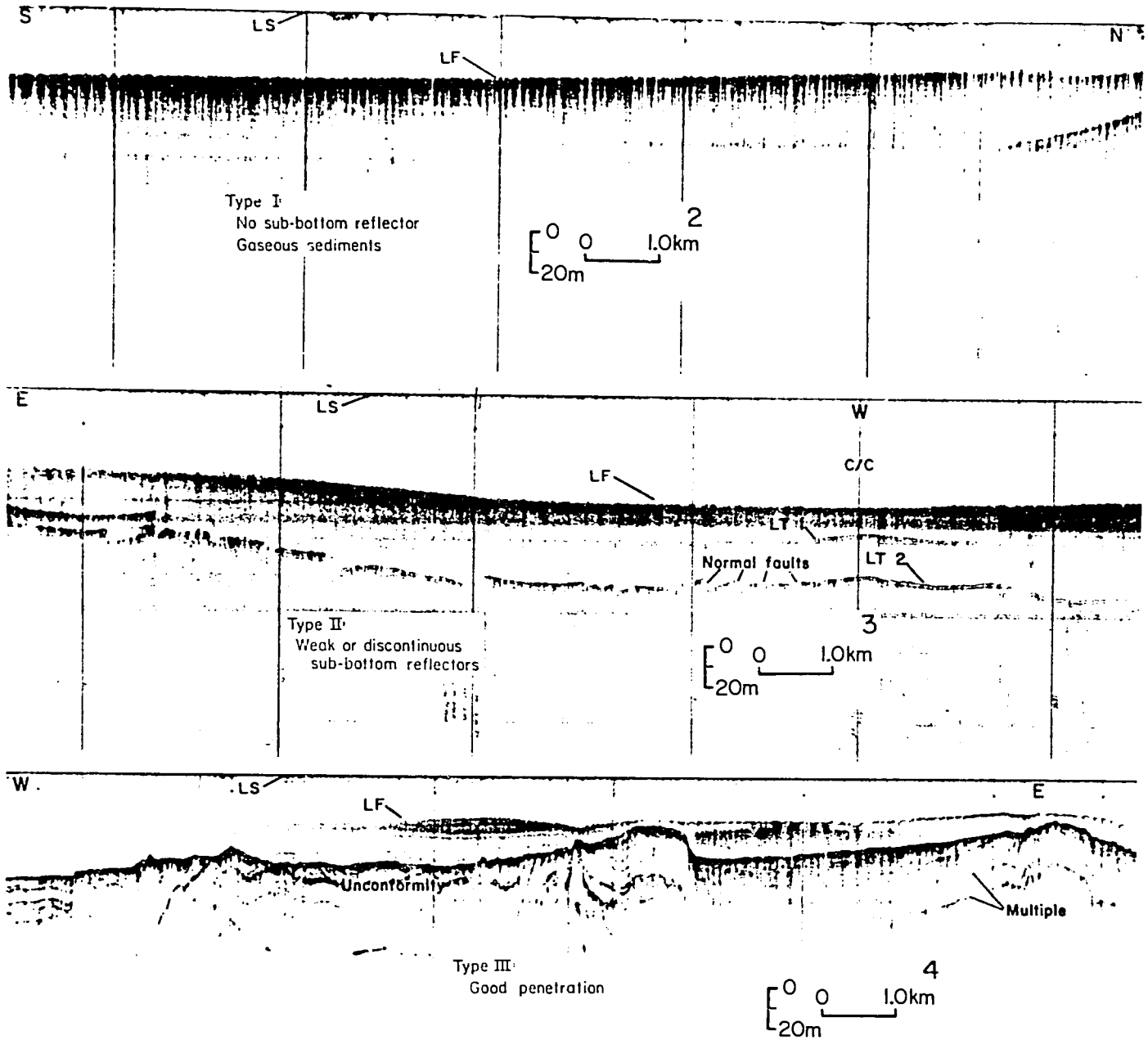
S
N
LS
LF
Type I
No sub-bottom reflector
Gaseous sediments
2
0
0
1.0km
20m
E
W
C/C
LS
LF
LT
LT 2
Normal faults
Type II
Weak or discontinuous
sub-bottom reflectors
3
0
0
1.0km
20m
W
E
LS
LF
Unconformity
Multiple
Type III
Good penetration
4
0
0
1.0km
20m

5b2

bottom reflectors. Type III profiles are typically well defined with multiple sub-bottom reflectors. The transition between various types is usually abrupt and occasionally evanescent.

The diffuse nature of the surface reflector of Type I profiles and the weak or discontinuous nature of the sub-bottom reflectors of Type II profiles compared to Type III profiles are interpreted to reflect higher concentrations of gas in t sediments resulting in the diffuse records. Various other lines of evidence support this interpretation. The piston cores contained noticeable gas content when they were collected. Sub-millimeter-sized bubbles from an odorless gas developed in the sediment just after the cores were split. Carbon isotope measurements of the dissolved, inorganic carbon in the pore water of the sediment from cores LT84-2P and 7P yield increasing values of δC-13 down core, from 0 to +12 $^{o}/oo$ (PDB), and the alkalinity of the pore water increases with depth. Both trends indicate that methanogenesis is occurring in the upper sediments (Irwin et al., 1977; Cerling et al., 1985; Talbot and Kelts, 1986). The distribution of Type I reflectors is restricted to deep-water environments and proximity to major rivers, where relative sedimentation rates are assumed to be higher than the rest of the lake due to sediment focusing and high sediment loading (Fig. 16).

Type III profiles provide strong evidence for a major lowstand of lake level during the last few millennia. These profiles are usually found in water depths shallower than 35 m. A hard reflector seen in the profiles marks a major angular unconformity, and is present at a number of locations. The acoustic character of the reflector is representative of a coarse-grained erosional lag deposit or beach-rock. Beach-rock is

Fig. 16. The regional distribution of the three profile types in Lake Turkana (from Johnson et al., 1987).

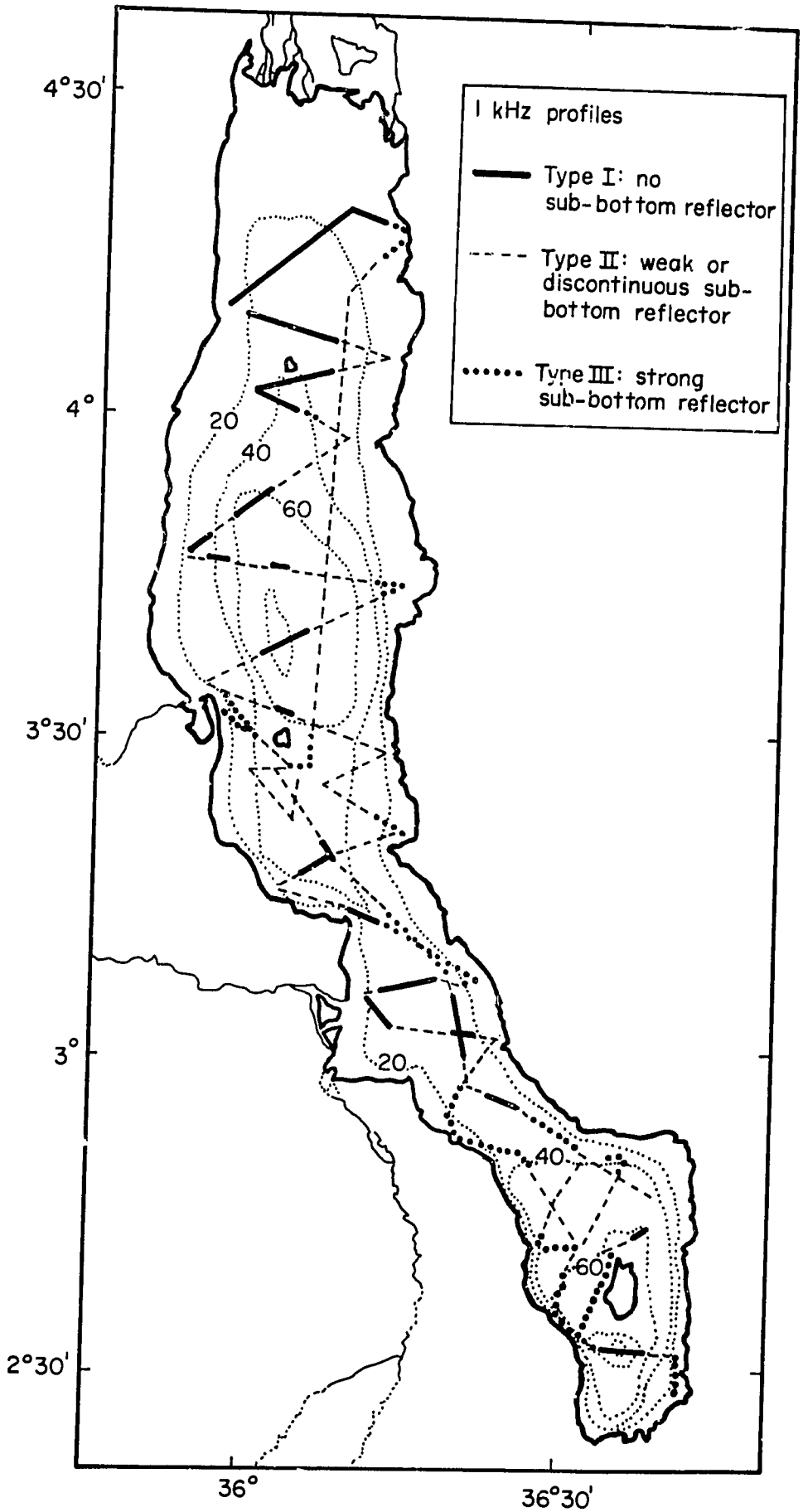
1 kHz profiles
Type I: no sub-bottom reflector
Type II: weak or discontinuous sub-bottom reflector
Type III: strong sub-bottom reflector
4°30'
4°
3°30'
3°
2°30'
36°
36°30'
20
40
60
20
40
60

46a

currently forming at a few locations along the present shoreline. The hard reflector can be traced lakeward on two profiles to a depth of 57 and 63 m below the present lake surface, before it weakens significantly. Sedimentary structures interpreted as wave cut scarps and onlapping sequences are found at depths of 50 and 65 m, and 63 and 72 m, respectively.

The hard reflector can be traced lakeward into two diffuse sub-bottom reflectors seen in most Type II profiles. The sediments corresponding to these reflectors might contain higher concentrations of sand or carbonate which would be deposited during low stands of the lake. Alternatively, the reflectors may represent volcanic ash deposits. The previous evidence suggests, however, that lake level was 50 to 60 m lower than the present day. A crude estimate on the occurrence of this lowstand is calculated from sediment thicknesses above the reflector and estimated sedimentation rates. The most recent lowstand occurred roughly 10,000 years ago, which corresponds to the termination of the East African glacial maximum desiccation period.

Multiple unconformities are identified in the deep-penetrating multichannel seismic lines and are traced across individual basins within the lake (Fig. 7) (Dunkelman, 1986). These profiles suggest that the lake has been substantially reduced in size on a number of occasions. In conclusion, extreme lowstands of lake level, and possibly complete desiccation of the lake, have occurred in the past, and are probably the result of major climatic changes.

High-angle growth faults and localized volcanism also influence the recent sediments. High-angle growth faults have vertically offset the

recent sediments and are characteristic of an extensional regime. A "spruce-tree" structure is seen on the 1 kHz profiles south of Central Island that is interpreted as multiple intrusive/extrusive events of volcanic or hydrothermal deposits.

Geochronology

Radiocarbon dating of the bulk carbonate fraction from various depth intervals of four cores resulted in good determinations of sedimentation rates in two of them despite some problems (Fig. 17) (Appendix B). Eight of the 15 radiocarbon dates yield ages between 850 and 3,840 yr BP. In addition, a core-top sample from LT84-8P yields an age younger than 1950 AD, due to the presence of nuclear bomb radioactivity. The ages of these samples increase with depth down-core. The age-versus-depth relationship for these samples reveals a strong correlation for both core LT84-2P ($r^2 = 0.99$) and LT84-8P ($r^2 = 0.96$). The precision of the dates is not optimal, primarily because of small carbon yields from the samples (Beta Analytic, pers. commun.).

The remaining six ages are younger than 1950 AD (modern) or very close to 1950 AD. A number of observations suggest that these modern or close to modern ages are unreliable. These ages are reported from sediments below 6 meters in cores LT84-4P and 7P and below 4 meters in core LT84-8P. The modern ages at these depths imply that sedimentation rates are over 10 cm/yr which is at least an order of magnitude larger than sedimentation rates previously reported for the basin. Modern or close to modern ages are reported for two samples at mid-depth in core LT84-8P. These ages are completely inconsistent with the linear depth

Fig. 17. Radiometric dating of the sediments. Radiocarbon age vs. depth down cores LT84-2P (top left) and 8P (top right). Lead-210 activities vs. depth down core LT84-2PG (bottom right). Horizontal error bar represents 1 standard deviation, and vertical error bar represents depth interval. Map insert shows core locations.

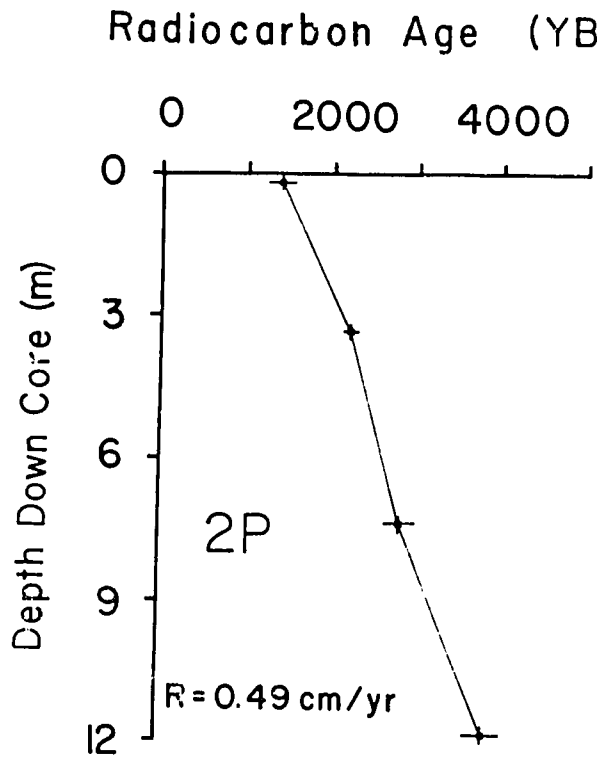
Radiocarbon Age (YBP)
0
2000
4000
Depth Down Core (m)
0
3
6
9
12
2P
R = 0.49 cm/yr

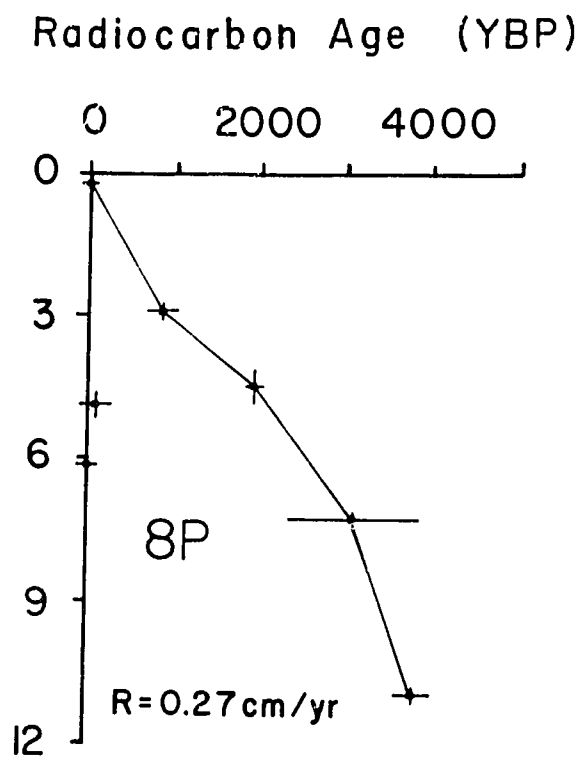
Radiocarbon Age (YBP)
0
2000
4000
0
3
6
9
12
8P
R = 0.27 cm/yr

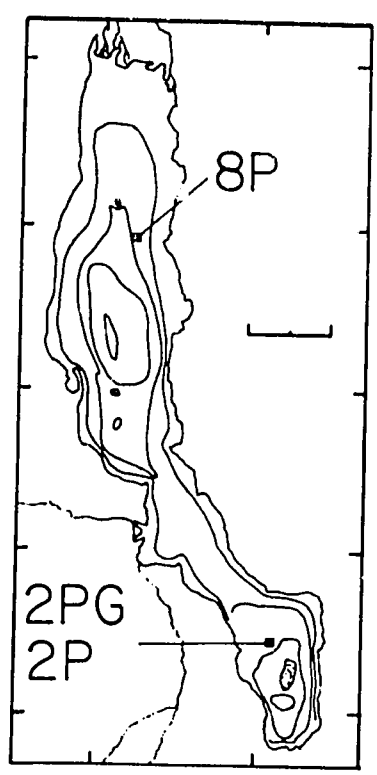
8P
2PG
2P

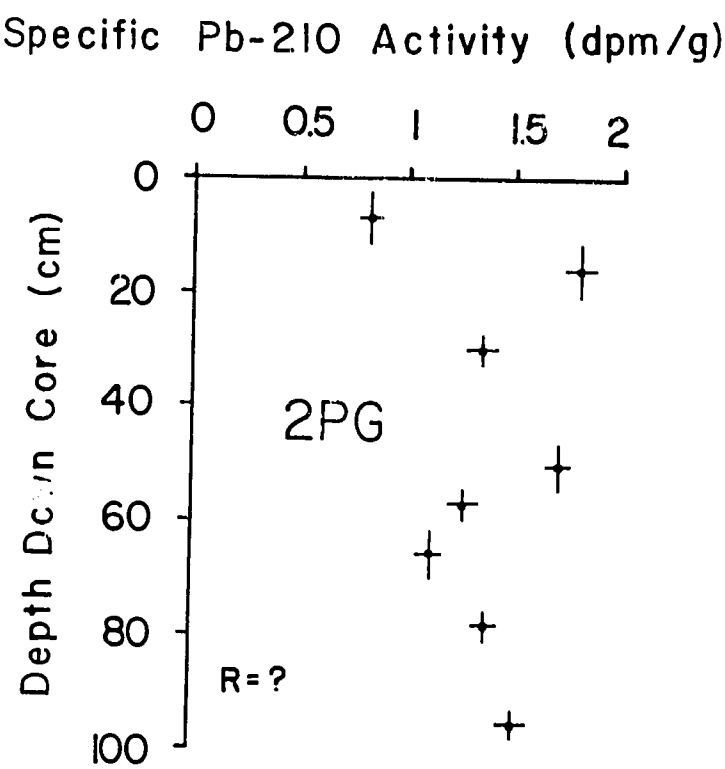
Specific Pb-210 Activity (dpm/g)
0
0.5
1
1.5
2
Depth Down Core (cm)
0
20
40
60
80
100
2PG
R = ?

59a

versus age trend from the other dates in this core. No explanation can account for modern carbon infiltrating 10 meters of LT84-7P and yet only the mid-depth of 8P. A similar situation exists between LT84-2P and 4P in the south basin. The pore water geochemistry profiles do not reveal anomalous results that would suggest differential horizontal influx of modern carbon (Cerling, unpublished data). All of the anomalous dates are from samples sent in the second of three shipments to Beta Analytic (Beta # 18356-18361; see Appendix B). Subsequent dating of a sample from just above an anomalously modern date in LT84-8P yielded 1,930 yr BP, consistent with the original linear depth versus age trend. Apparently, the second shipment of samples sent to Beta Analytic was exposed to modern carbon that was assimilated into the carbonate fraction, or an error was consistently made in their analysis. Ignoring the questionable dates, the average linear sedimentation rates for cores LT84-2P and 8P are 0.49 and 0.27 cm/yr, respectively. The sedimentation rates are consistent with previously reported values for the basin and, in fact, constitute the most reliable rates presently available for Lake Turkana.

The radiocarbon ages were not corrected for reservoir effect, isotopic fractionation, or DeVries effect (the variation in the natural concentration of radioactive CO_2 with time). The reservoir effect probably is negligible because there is no major source of detrital carbonate in the drainage basin (Cerling, pers. commun.), and the LT84-8P core-top sample yielded a modern age. The isotopic fractionation effect is estimated to be nearly constant throughout the core because the δC-13 values reveal minimal variability down-core. If the dates are

corrected for the presently accepted DeVries effect (Klein et al., 1982), then the sedimentation rates change from 0.27 to 0.24 cm/yr and from 0.49 to 0.40 in cores LT84-8P and 2P, respectively.

Pb-210 activities are constant and less than 2 dpm/g from the core-tops of LT84-1P, 2P, 2PG, 4P, 7P and 8P, and eight down-core samples from 2PG (Fig. 17) (Appendix B). These results suggest that all cores overpenetrated the lake floor and that the activities measured represent supported Pb-210 activities. A sedimentation rate cannot be calculated for LT84-2PG, and consequently additional samples were not analyzed.

Sediment Description

Visual description and smear-slide analysis of the sediment reveals that the sediment is predominantly faintly laminated clays (Fig. 18). The color of the sediment just after splitting the core ranged from olive grey to dark olive green and has since oxidized to include tints of brown or tan. The clay and fine-silt fractions constitute approximately 85 to 95% of the sediment and consist primarily of clay minerals and microcrystalline carbonate grains with minor amounts of quartz and feldspar. The accessory sedimentary components include detrital grains (coarse silt to sand sized), volcanic debris and biogenic components. Diatoms dominate the biogenic fraction, and ostracods also are abundant in some cores.

The constituents of the sediments vary systematically from north to south. The relative abundance of biogenic components in the sediments increases from trace amounts to between 5 and 10% with distance from the Omo River. North basin clays contain rare, poorly preserved diatoms

Fig. 18. Generalized core stratigraphy from visual examination. The units are: distinct laminations (horizontal lines); faint laminations (broken horizontal lines); homogeneous lacustrine muds (blank); volcanic lenses (V); homogeneous lacustrine sands (dots).

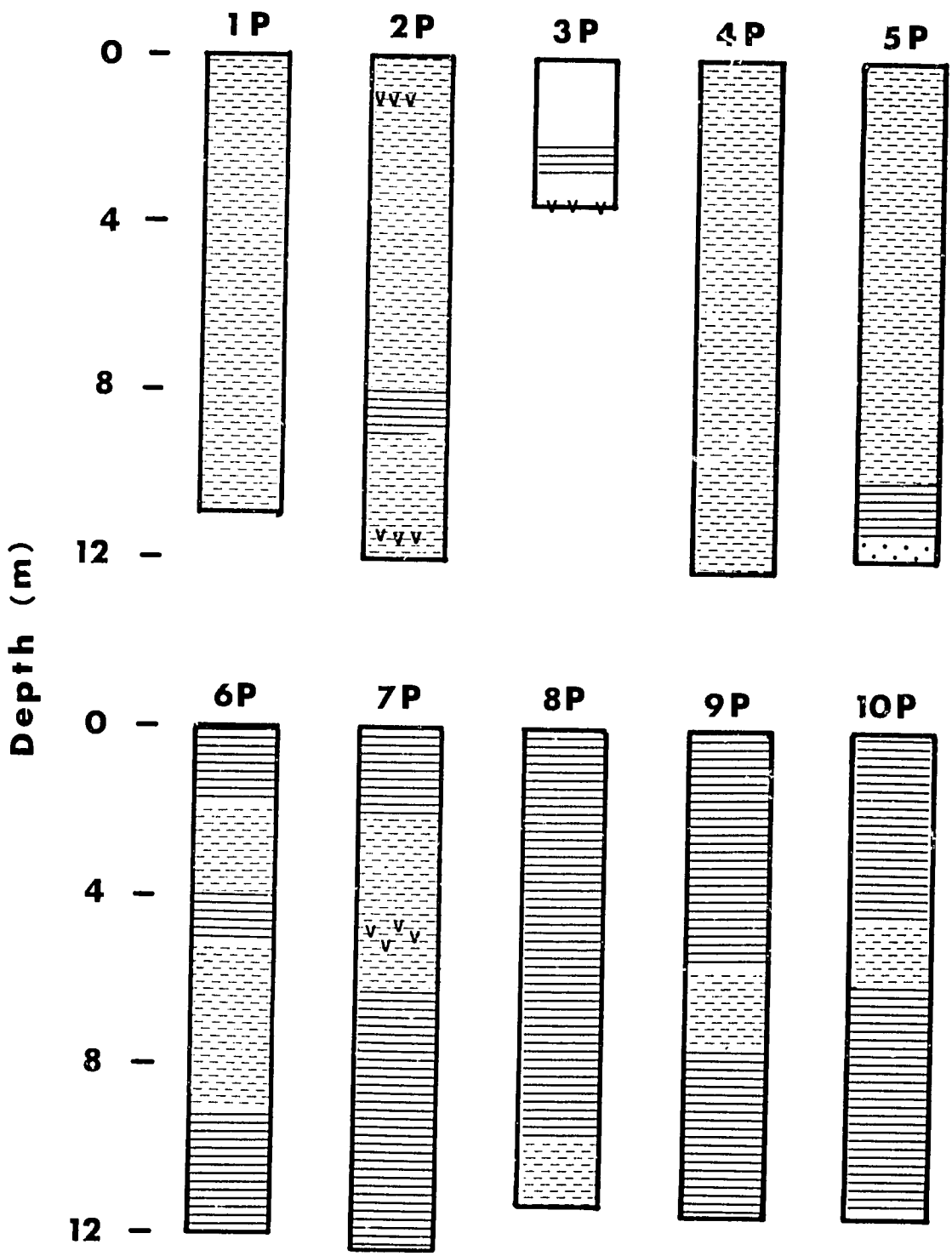

62a

whereas in the south basin, the sediments have well-preserved and relatively abundant diatoms and ostracods.

Most of the cores appear relatively uniform throughout their lengths. A few volcanic ash layers of black silt to sand-sized glass shards interrupt the lacustrine muds in two cores, LT84-2P and 7P. They are between 0.1 and 2 cm thick and probably represent localized ash deposits which have not proven useful for stratigraphic correlation for the cores in this study. Microscopic analysis reveals subtle changes in the lithology of LT84-1P where relatively more biogenic material is found in smear slides at and below 650 cm than above 450 cm.

The most conspicuous down-core changes are found in LT84-5P and 3P. The bottom 18 cm of core LT84-5P (1172-1190 cm) is relatively firmer and contains more sand than the overlying lacustrine muds. The sand concentration within the lower 18 cm of core increases towards the base of the core. Rip-up clasts of this basal unit are included in the overlying muds. The sedimentary evidence suggests that this basal unit represents an erosional unconformity. This core was located to recover the major erosional unconformity seen on the 1-kHz seismic profiles. The unit probably corresponds to the targeted seismic reflector. The objective of core LT84-3P was also to recover a seismic unconformity. Only 347 cm of sediment was recovered from this site. A pebbly unit was recovered in the nose of the corer which prevented full penetration of the core barrel.

Porosity

The porosity values from sediment samples average 0.91 (Fig. 19)

Fig. 19. Porosity of the sediment vs. depth down core. Map insert shows core locations. The mean value for each profile is indicated after the x.

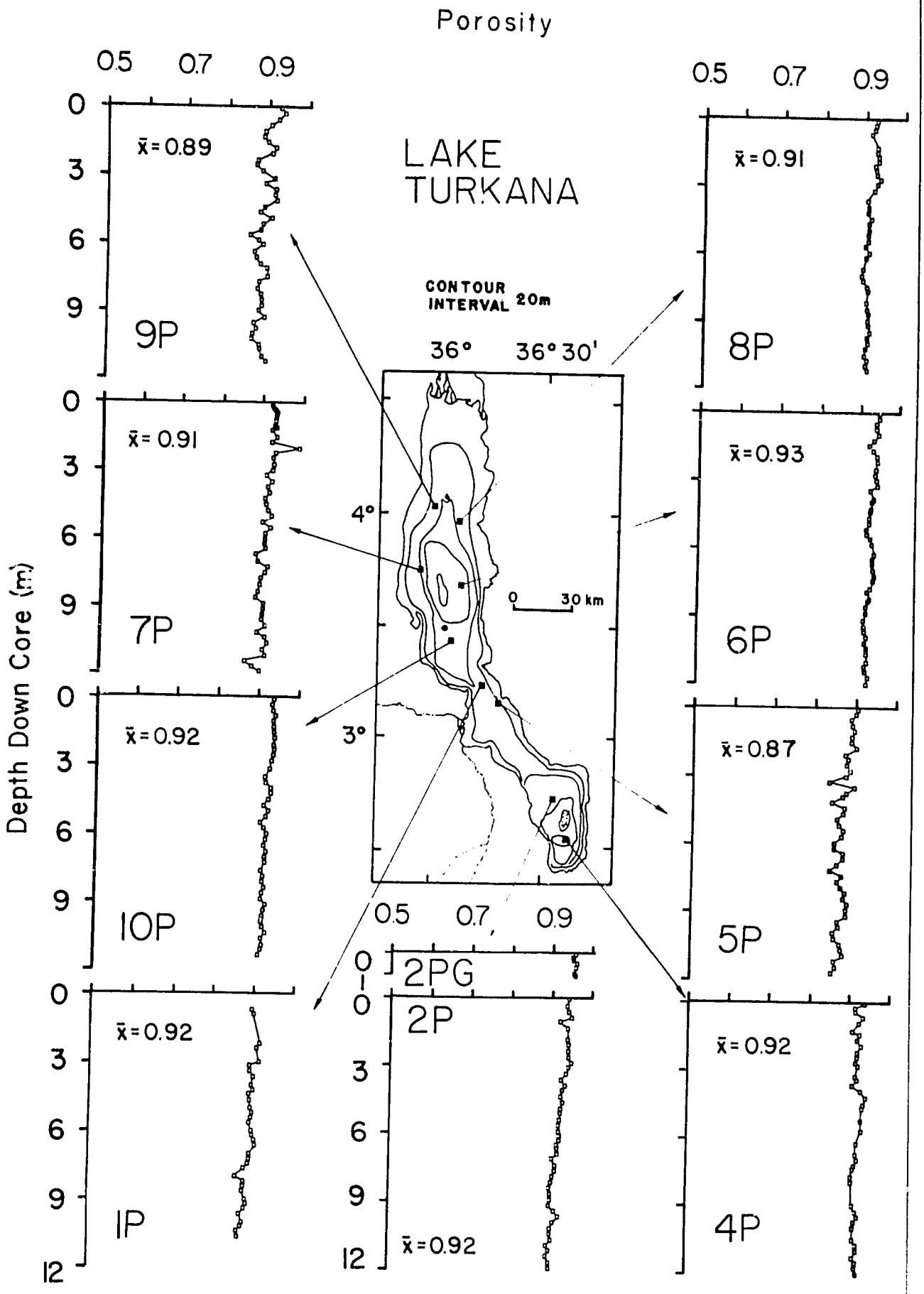
Porosity
0.5
0.7
0.9
Depth Down Core (m)
LAKE TURKANA
CONTOUR INTERVAL 20m
36°
36° 30'
4°
3°
0
30 km
x̄ = 0.89
9P
x̄ = 0.91
8P
x̄ = 0.91
7P
x̄ = 0.93
6P
x̄ = 0.92
10P
x̄ = 0.87
5P
x̄ = 0.92
1P
2PG
2P
x̄ = 0.92
x̄ = 0.92
4P

(Appendix C). Mean values for the cores range from 0.87 (LT84-5P) to 0.93 (LT84-6P) and individual measurements between 0.84 and 0.99. The error is assumed $\pm$ 0.01 and depends primarily on the accuracy of sample weight.

The porosity values are high throughout the lake. The high porosities facilitated penetration of the 28-kHz echo sounder, and frustrated our recovery of the giant gravity cores. The mean core porosity values weakly correlate to water depth of the core site (r^2 = 0.58). The major exception is LT84-4P, which has unusually low porosity for the depth from which it was recovered. The weak correlation may be attributed to sediment focusing by faster sedimentation and corresponding higher porosities in the deeper portions of the lake. Porosity values decrease down-core with minor fluctuations about the trend except for LT84-4P which is constant down-core. The decrease is presumably due to sediment compaction. Minor down-core fluctuations of porosity may yield the sub-bottom reflectors seen on the 28-kHz echo soundings but not observed on the 1-kHz profiles, although the resulting change in sediment density is minimal. The porosity values from LT84-2PG are higher than the top few meters of the corresponding piston core LT84-2P. The discrepancy suggests that the piston core over-penetrated the sediment-water interface by at least 1 meter.

Diatoms

Analysis of smear slides for identification and assemblage analysis of diatoms was hampered by poor preservation and low concentrations in all cores except LT84-2P and 4P. The diatom concentration is

significantly higher in 2P than 4P. The assemblage is dominated by varying proportions of Surirella species, Stephanodiscus astrea, Melosira nyassensis, and Thalassiosira rudolfi (Fig. 20) (Appendix D). Species of Anomoeoneis, Rhopalodia, Gomphocymbella, Cocconeis and Cymbella occur in trace amounts.

The diatom assemblages of the two cores reveal significant yet opposite down-core trends. The top 750 cm of core LT84-2P is dominated by Surirella and Thalassiosira. Melosira dominates the assemblage below 750 cm. Core LT84-4P is dominated by Surirella, with Thalassiosira also abundant below 800 cm. Both cores contain variable percentages of Stephanodiscus throughout their length, although the relative percentage is lower in core LT84-4P than 2P.

Biogenic Silica

Biogenic silica values from sediment samples average 2.1% of the dry weight (Fig. 21) (Appendix E). Mean values for the cores range from 1.6 (LT84-8P) to 3.4% (LT84-2P), and individual analyses between 0.6 and 7.4%. The average deviation from the mean of all replicate analyses is 0.2. Microscopic analysis of the residue after biogenic silica digestion revealed only trace amounts of fragmented and dissolved diatom valves (mostly Melosira species) in the more concentrated samples.

Biogenic silica values are uniformly low throughout the lake, although slightly higher values occur in the south basin and site LT84-9P. Down-core profiles of biogenic silica values are generally uniform and lack significant deviations from the mean. The lower section of LT84-5P reveals gradually decreasing biogenic silica values from 2.0% at

Fig. 20. Relative abundance of three genera of diatoms: Melosira, Surirella and Thalassiosira vs. depth down cores LT84-2P (left) and 4P (right). A profile of interpreted paleo-salinity vs. depth down core is shown to the right of the diatom profiles for each core. The paleosalinity interpretation is based on ecological data for the genera Melosira and Thalassiosira. Increasing conductivity (salinity) is towards the right.

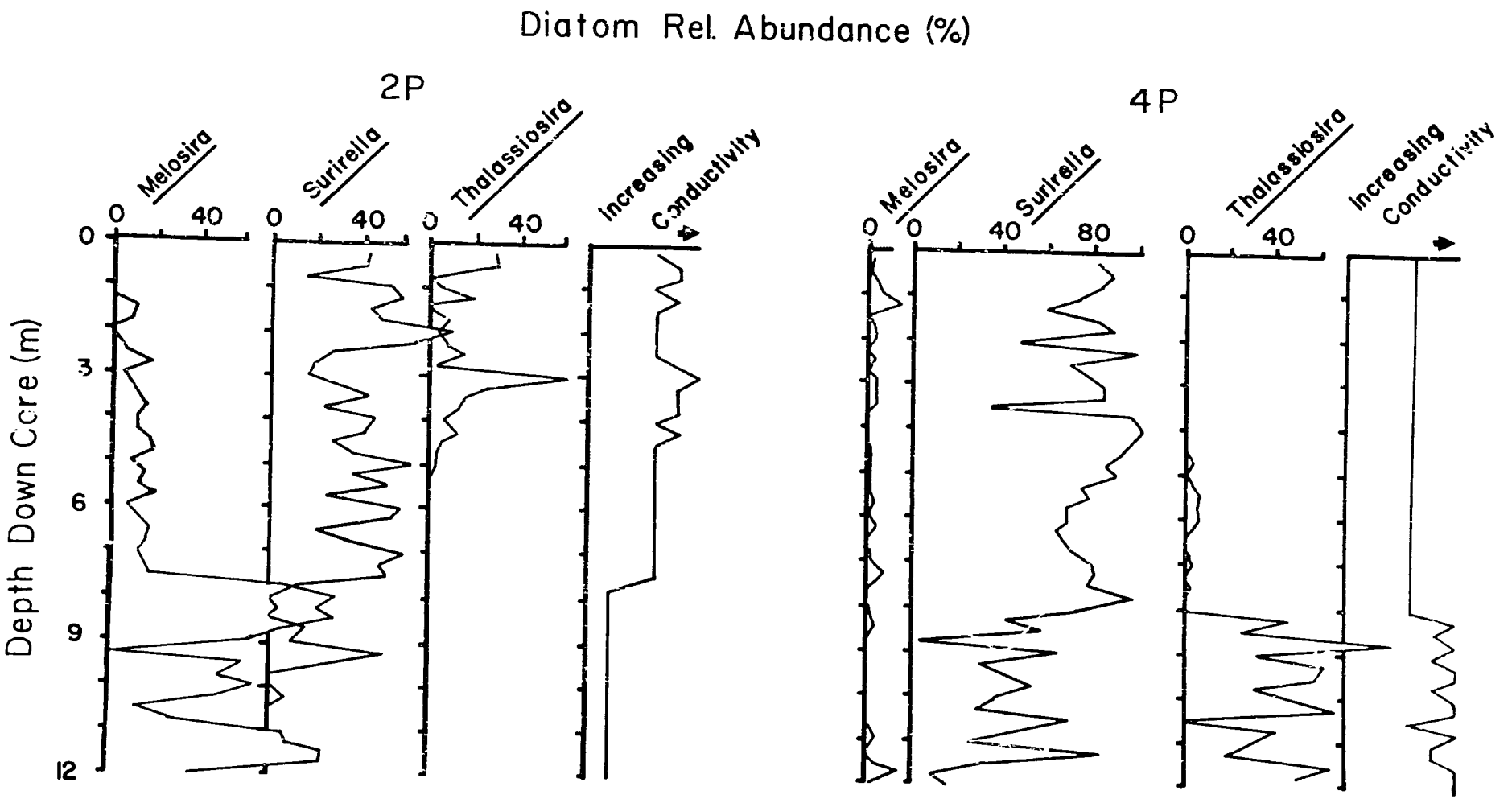
Diatom Rel. Abundance (%)
2P
4P
Melosira
Surirella
Thalassiosira
Increasing Conductivity
Depth Down Core (m)
0
3
6
9
12
0
40
80

(7b)

Fig. 21. Weight percent biogenic Silica (SiO_2) of the dry sediment vs. depth down core. A number of depths have duplicate analyses. The line connects the average of all analyses at a given depth. Map insert shows core locations. The mean value for each profile is indicated after the x.

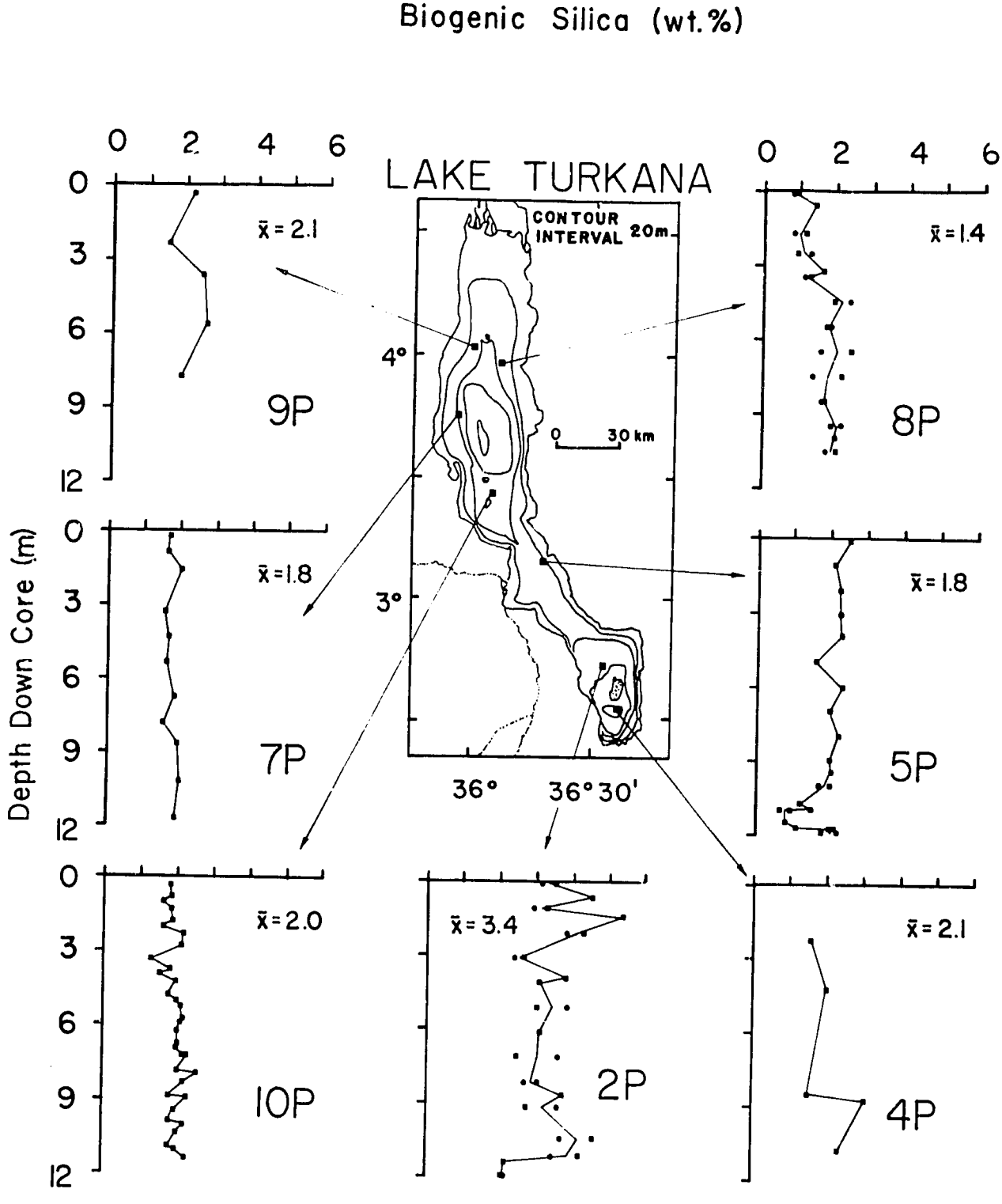
Biogenic Silica (wt.%)
LAKE TURKANA
CONTOUR INTERVAL 20m
0 30 km
4°
3°
36°
36°30'
Depth Down Core (m)
0 2 4 6
0 3 6 9 12
x̄ = 2.1
9P
x̄ = 1.4
8P
x̄ = 1.8
7P
x̄ = 1.8
5P
x̄ = 2.0
10P
x̄ = 3.4
2P
x̄ = 2.1
4P

Ba

996 cm down to 0.8% at 1143 cm only to increase again to approximately 2% below the unconformity.

Grain Size

The median grain size of the detrital, silt fraction is variable throughout the lake (Fig. 22) (Appendix F). Mean values for the cores range from 13.7 (LT84-7P) to 17.4 microns (LT84-10P), and individual analyses between 11.9 and 22.4 microns. The average deviation from the mean of all replicate analyses is 0.2. The average median grain size from each core does not correlate to water depth of the core site, location of the core, or other parameters.

The down-core profiles of median grain size are uniform except for cores LT84-5P and 10P. The grain size profile from LT84-5P reveals steadily decreasing values from 20 to 14 microns from 0 to 995 cm. Relatively coarser grain sizes (16 to 19 microns) occur down core from 995 cm, except for the samples at 1146 and 1170 cm. The profile from LT84-10P reveals a noisy signal with depth, with fluctuations between 14 and 22 microns between each sample.

Total Organic Carbon and Nitrogen

Total organic carbon values (TOC) from sediment samples average 0.93% of the dry weight (Fig. 23) (Appendix G). Mean values for the cores range from 0.77 (LT84-1P and 8P) to 1.31% (LT84-4P), and individual analyses between 0.41 and 4.31%. The average deviation from the mean of all replicate analyses is 0.02.

The south basin cores, LT84-2P and 4P, contain significantly more

Fig. 22. Median grain size of the detrital silt-sized fraction of the sediment vs. depth down core. A number of depths have duplicate analyses. The line connects the average of all analyses at a given depth.

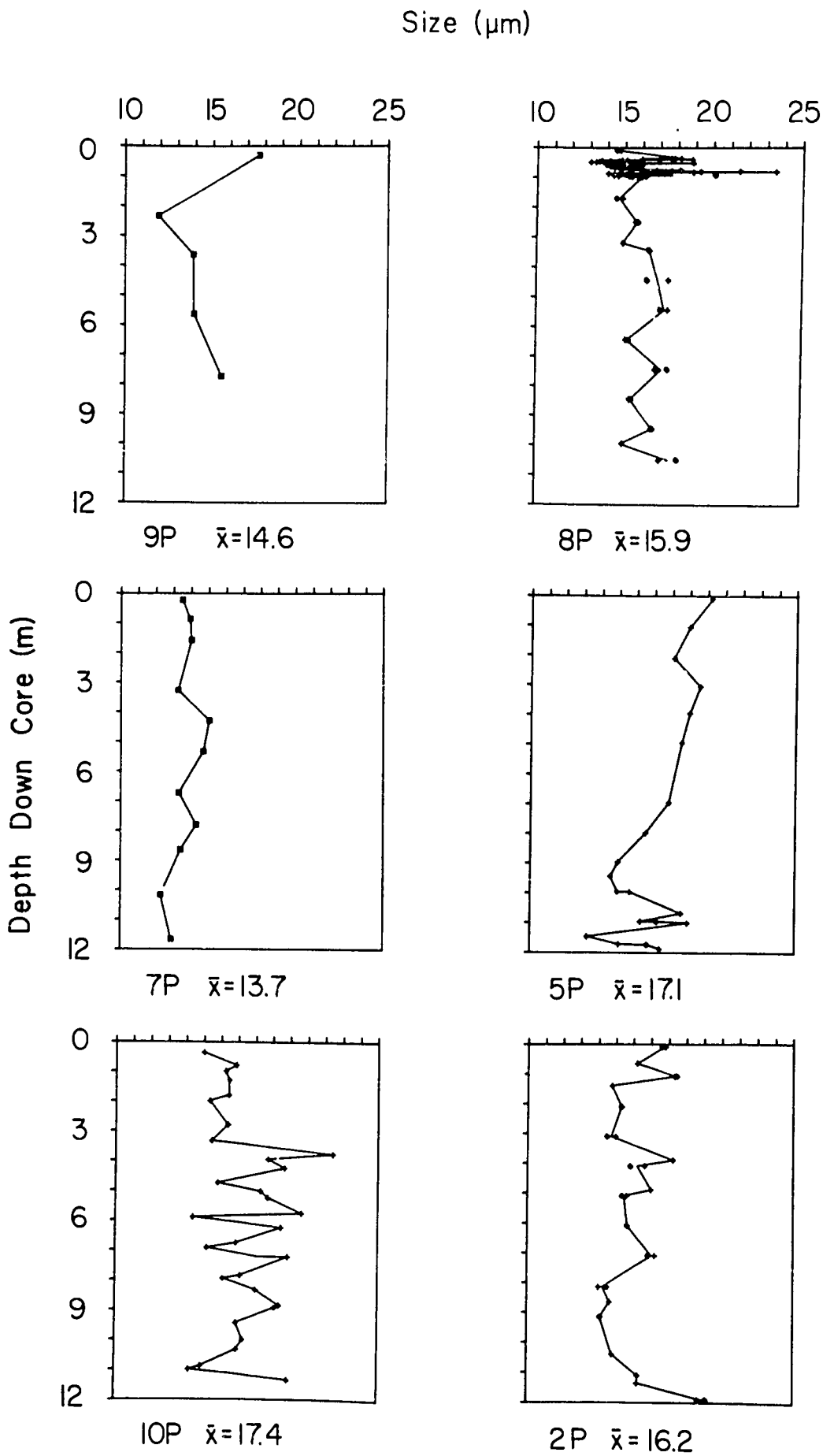
Size (μm)
10
15
20
25
Depth Down Core (m)
0
3
6
9
12
9P x̄=14.6
8P x̄=15.9
7P x̄=13.7
5P x̄=17.1
10P x̄=17.4
2P x̄=16.2

Fig. 23. Weight percent total organic carbon (C) of the dry sediment vs. depth down core. Note scale change for LT84-5P profile. Duplicate analyses are plotted with a line connecting their averages at a given depth. Map insert shows core locations. The mean value for each profile is indicated after the x.

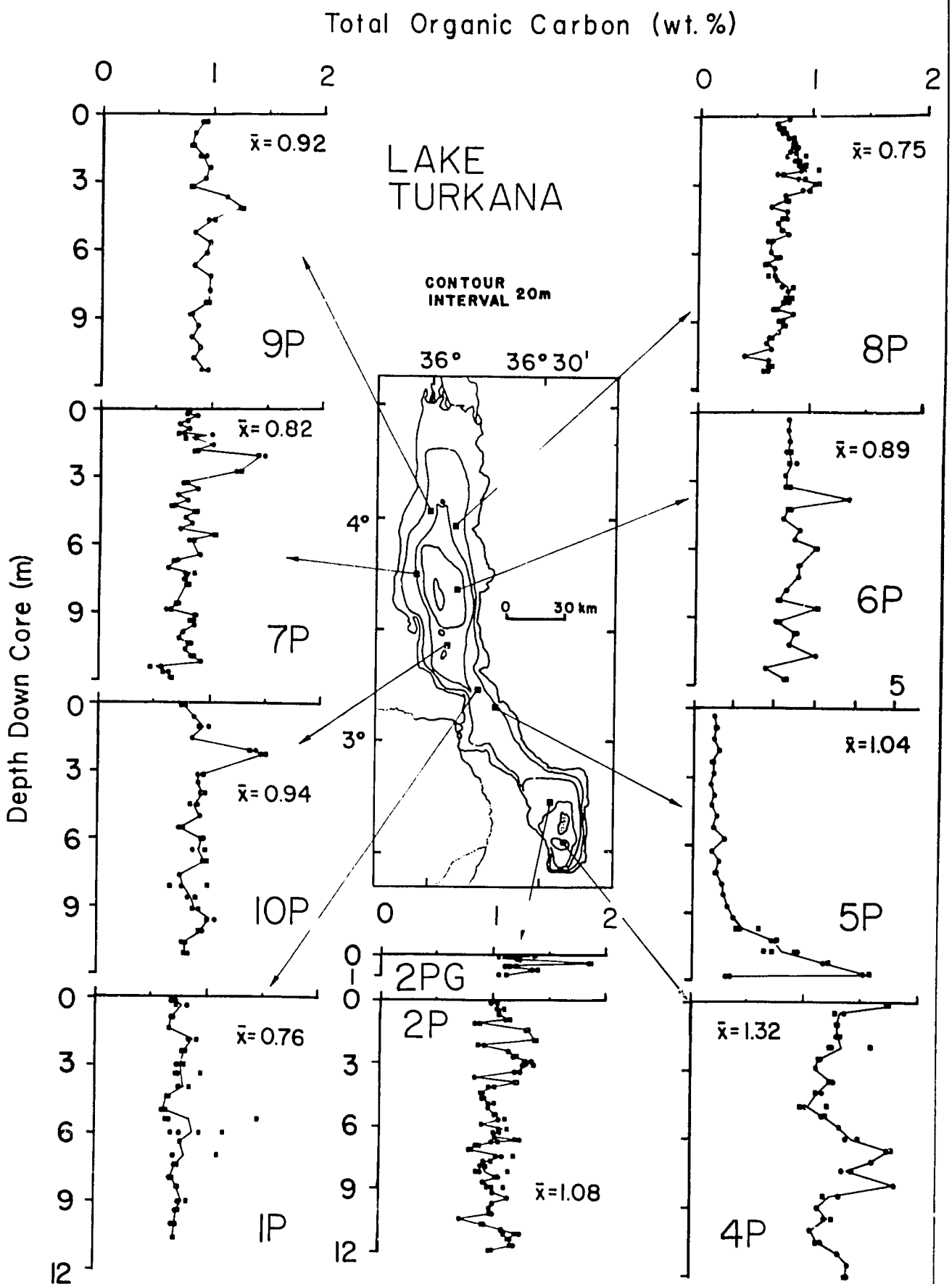
Total Organic Carbon (wt. %)
Depth Down Core (m)
LAKE TURKANA
CONTOUR INTERVAL 20m
36°
36° 30'
4°
3°
0 30 km
9P
x̄ = 0.92
8P
x̄ = 0.75
7P
x̄ = 0.82
6P
x̄ = 0.89
10P
x̄ = 0.94
5P
x̄ = 1.04
1P
x̄ = 0.76
2PG
2P
x̄ = 1.08
4P
x̄ = 1.32

91a

TOC than the other cores. Cores LT84-9P and 10P contain the highest mean values among the cores from the north basin, and are located at opposite ends of the basin. The mean TOC value for cores LT84-1P and 5P would be similar and low, if the samples within the lower 3 meters of core 5P were excluded from the average.

The down-core trend in TOC is noisy. Cores LT84-2P, 7P, 8P, 9P and possibly 6P, show relatively high TOC values near 3m ($\pm$ 1 m) down-core. Higher TOC values are located at 8 m down core LT84-4P. A gradual decrease in TOC content is revealed in the down-core profiles from cores LT84-2P, 7P and 8P, although the high TOC values near 3 m depth of the respective cores might cause the apparent decrease in TOC. The highest TOC values are revealed in the down-core trend from core LT84-5P. TOC content averages about 0.7% down to 920 cm, steadily increases from 1.0 to 4.3% between 920 and 1170 cm, and sharply decreases to below 1% at 1180 cm. The sharp decline brackets the lithologic erosional unconformity.

Mean values for the cores may correlate (r^2 = 0.79) to the mean biogenic silica value but only if cores 4P and 5P are excluded from the correlation (Fig. 24). Core LT84-5P fits the linear trend if the values from 1000 cm to the erosional unconformity (1172 cm) are ignored. In this interval, the TOC and biogenic silica values trend in opposite directions, TOC increasing and biogenic silica decreasing from the mean core value. Core LT84-4P does not fit the correlation. The TOC profile trends opposite to the biogenic silica profile in the upper 3 m of core LT84-8P. Profiles of TOC and biogenic silica may correlate in core LT84-2P.

Fig. 24. Weight percent biogenic Silica (SiO_2) vs. weight percent total organic carbon (C). Each point represents the mean value from each core and is identified by core number.

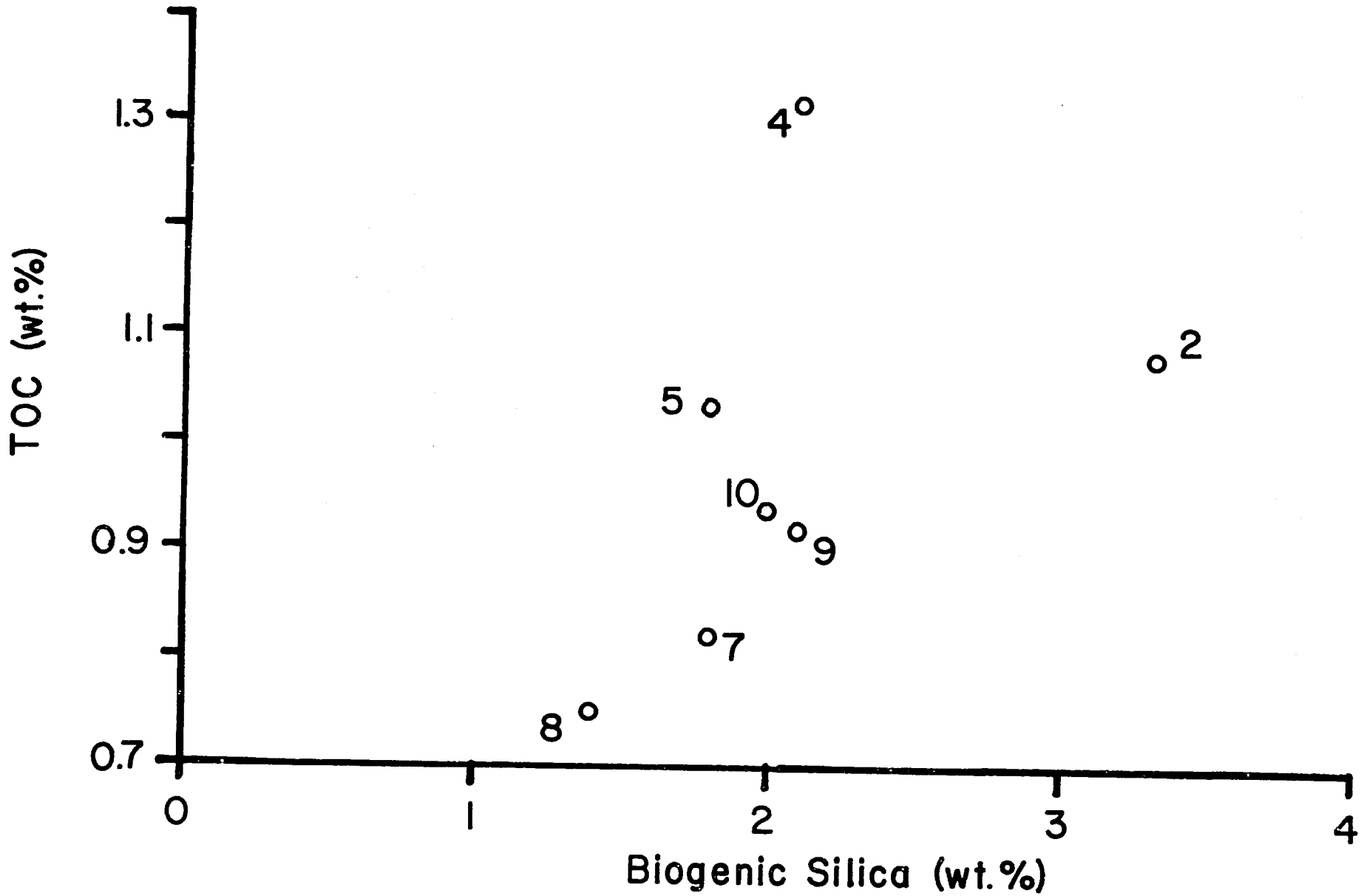

Fig.

Total organic nitrogen (TON) values from sediment samples average 0.14% of the dry weight (Appendix G). The average deviation from the mean of all replicate analyses is 0.006. A number of data points were excluded from LT84-8P, 9P and 10P due to abnormally high TON values, which probably resulted from improperly rinsed sample bottles after nitric acid cleaning.

Carbon to nitrogen (C/N) ratios by weight average 6.9 (Fig. 25) (Appendix G). Mean values for the cores range from 5.7 (LT84-4P) to 7.8 (LT84-10P), and individual values between 4.5 and 14.4. The precision is 0.3 and is estimated from the calculated errors of TOC and TON.

The average C/N ratios for the cores are variable and do not correlate to water depth, core location, TOC, or porosity. The C/N values reveal a noisy down-core trend. However, only C/N values from cores LT84-2P and 5P significantly deviate from the mean core value. In core LT84-2P, high C/N values (7 to 8) occur between 0 and 540 cm and below 1040 cm, whereas, low values (5 to 7) prevail from 540 to 1040 cm. The highest C/N ratios are revealed near the base of core LT84-5P and correlate to higher TOC content at the same depth interval. In core LT84-5P, C/N values steadily increase from 10 to 14 between 1020 and 1170 cm, with a dramatic decline to 8.9 at 1180 cm.

Carbonate

Bulk carbonate values from sediment samples average 10% of the dry weight (Fig. 26) (Appendix H). Mean values for the cores range from 5.2 (LT84-9P) to 19.7% (LT84-4P) and individual analyses from 1.3 to 28.1%. The average of the separate 1 sigma standard deviations from each sub-

Fig. 25. The average carbon (C) to nitrogen (N) ratio of the organic matter by weight vs. depth down core. Note scale change for LT84-5P profile. Map insert shows core locations. The mean value for each profile is indicated after the x.

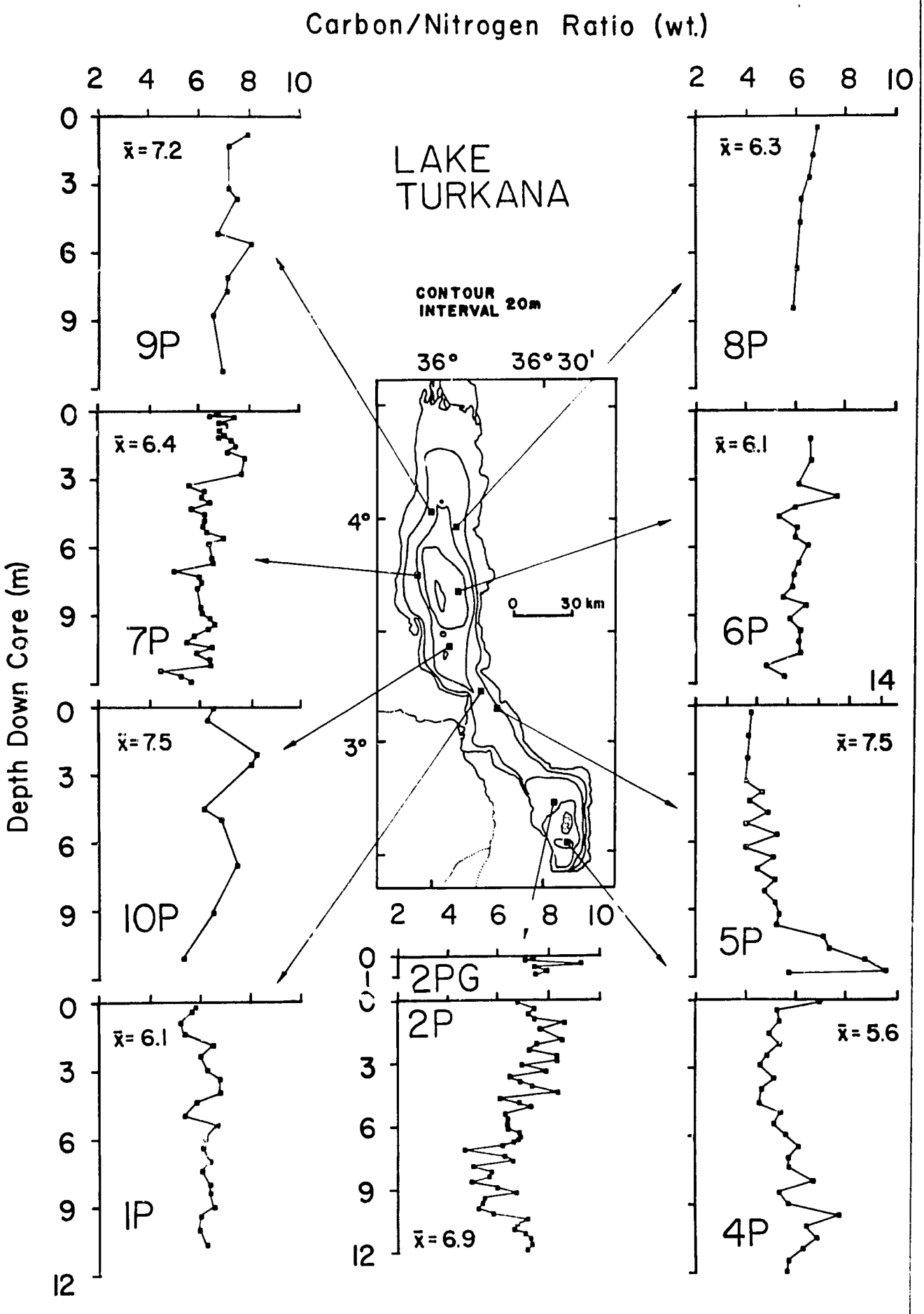
Carbon/Nitrogen Ratio (wt.)
Depth Down Core (m)
LAKE TURKANA
CONTOUR INTERVAL 20m
36°
36° 30'
4°
3°
0 30 km
9P
x̄ = 7.2
8P
x̄ = 6.3
7P
x̄ = 6.4
6P
x̄ = 6.1
10P
x̄ = 7.5
5P
x̄ = 7.5
1P
x̄ = 6.1
2P
x̄ = 6.9
2PG
4P
x̄ = 5.6
14

7SN.

Fig. 26. Weight percent carbonate ($CaCO_3$) of the dry sediment vs. depth down core. The profiles from cores LT84-7P, 8P and 10P were smoothed with a 3 point running average. Map insert shows core locations. The mean value for each profile is indicated after the x. The capital letters "A" and "B" reveal episodes of relatively high carbonate concentrations that were correlated in the north basin.

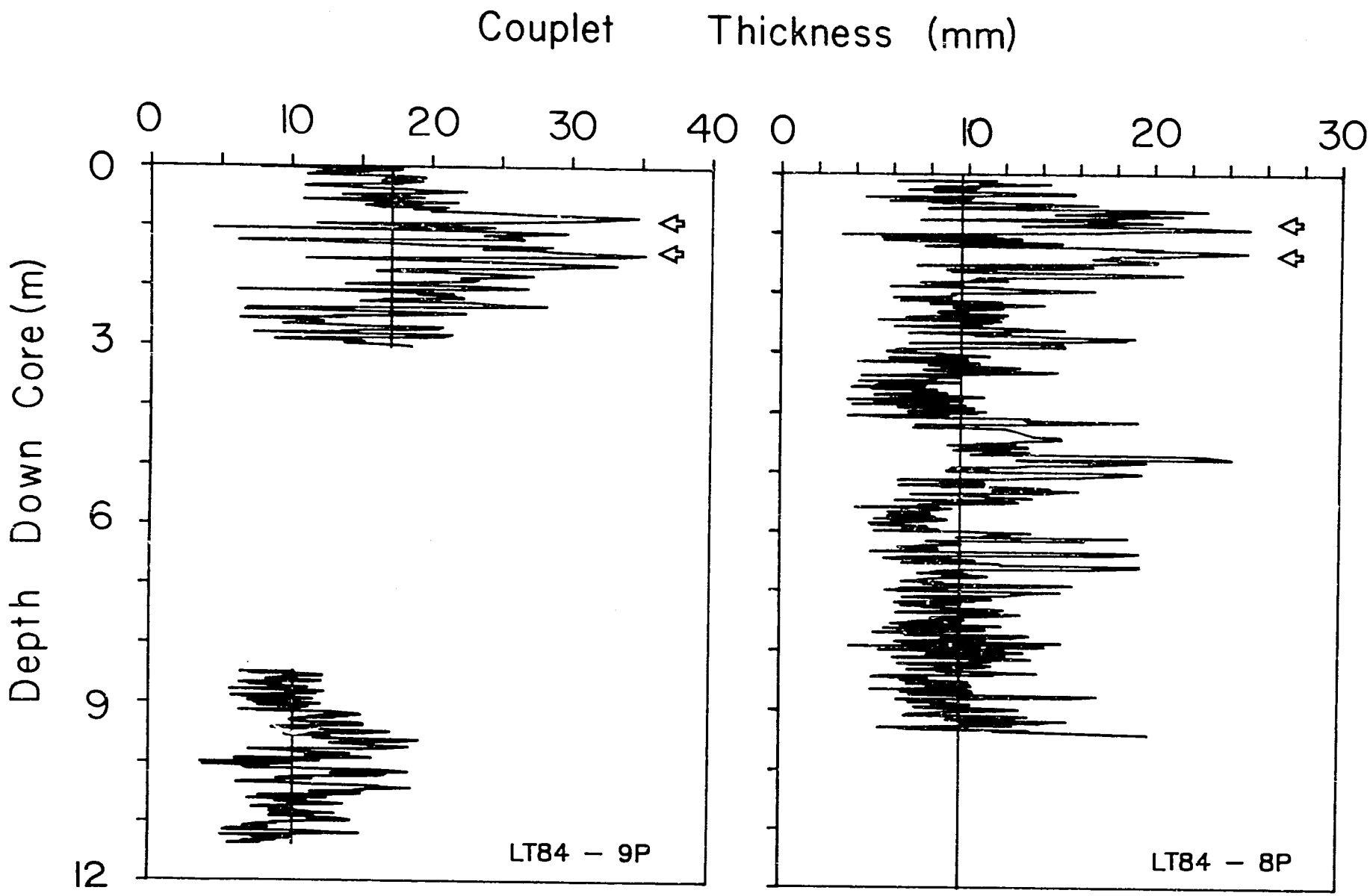
Couplet Thickness (mm)
0
10
20
30
40
0
10
20
30
Depth Down Core (m)
0
3
6
9
12
LT84 – 9P
LT84 – 8P

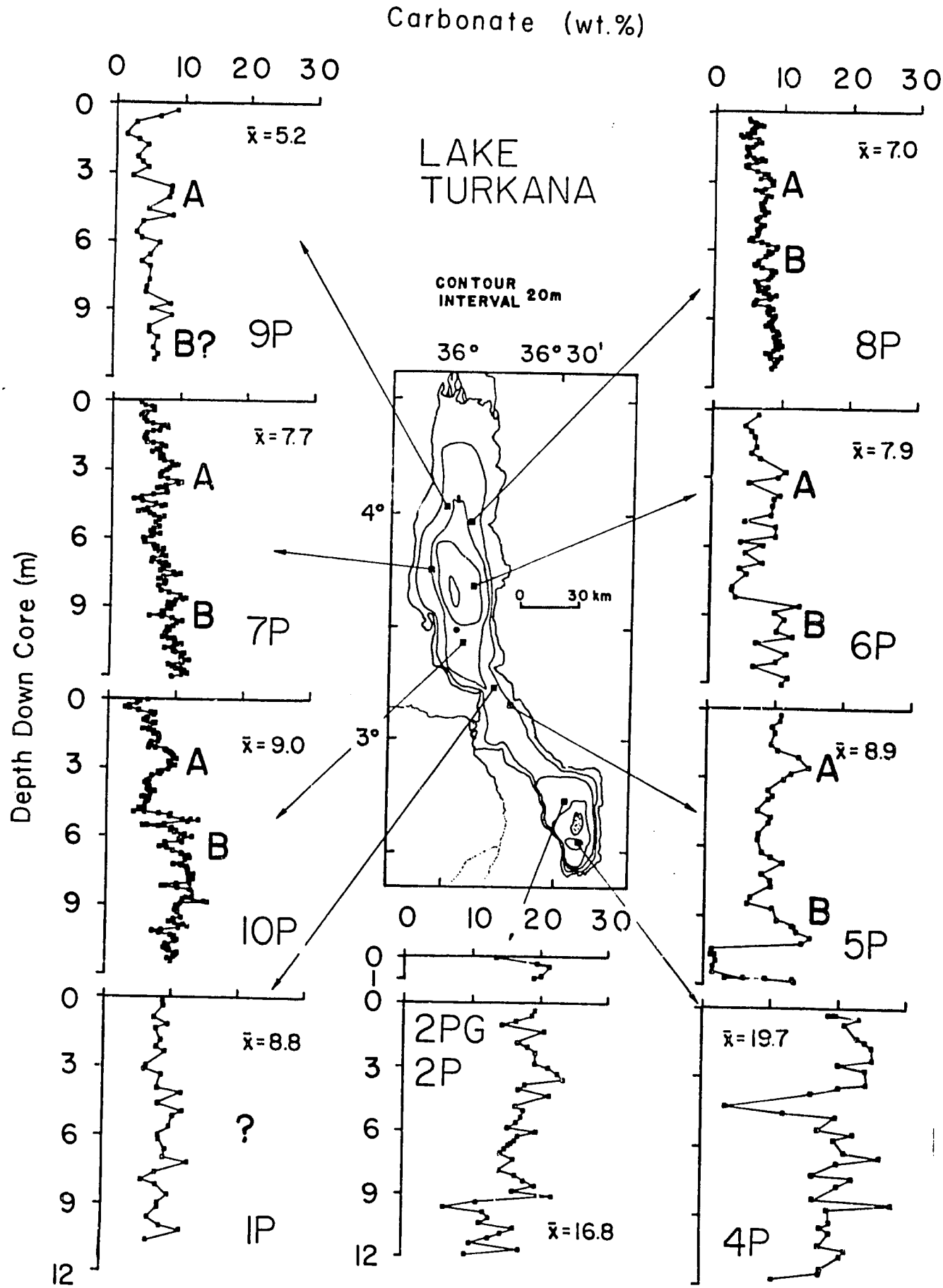
Carbonate (wt.%)
Depth Down Core (m)
LAKE TURKANA
CONTOUR INTERVAL 20m
36°
36°30'
4°
3°
0 30 km
x̄ = 5.2
A
B?
9P
x̄ = 7.0
A
B
8P
x̄ = 7.7
A
B
7P
x̄ = 7.9
A
B
6P
x̄ = 9.0
A
B
10P
x̄ = 8.9
A
B
5P
x̄ = 8.8
?
1P
2PG
2P
x̄ = 16.8
x̄ = 19.7
4P

766

sample is 0.26%, based on at least 6 repetitions of 3 separate sub-samples.

Bulk carbonate values from sediment samples increase with distance from the Omo River. A linear, positive correlation ($r^2 = 0.86$) exists between the mean value for each core and its distance from the Omo River (Fig. 27). Cores LT84-1P and 5P, are slightly depleted in carbonate from this linear trend.

The carbonate profiles reveal a basin-wide, correlative stratigraphy for the cores recovered from the north basin. The general pattern consists of increasing carbonate values with depth down core. Superimposed on this trend are at least 4 major zones of alternating relatively low and high carbonate values with relatively low values at the top of the cores (Fig. 26). The magnitude of the oscillations are larger with distance from the Omo River. The return to higher carbonate values is not obvious at the bottom of core LT84-9P. This core was recovered from a site closest to the Omo River turbid plume, and consequently, faster sedimentation rates can account for the loss of stratigraphic information. An additional oscillation towards lower values is revealed at the lowest 2 meters of core LT84-10P. This core was recovered from an isolated bathymetric high, and consequently, lower sedimentation rates can account for the additional stratigraphic information. The carbonate profiles from cores LT84-7P, 8P and 10P were smoothed with a simple 3 point running average. The smoothed profiles suggest that additional oscillations of slightly smaller amplitude and higher frequency than the major down-core oscillation also are present. For example, the letter B was positioned to coincide with a short

Fig. 27. Weight percent carbonate ($CaCO_3$) vs. distance from the Omo River delta. Each point represents the mean carbonate value from each core and is identified by core number.

wavelength, double oscillation that appears to mark the onset of relatively higher carbonate content down-core.

Statistically, the low frequency oscillations are significant if n-point running averages retain the signal, where n does not exceed the the wavelength of the oscillation in question (R. Strelitz, person. commun.). Cores LT84-7P, 8P and 10P were smoothed with 1-meter interval running averages. Only these cores were smoothed because the sample spacing was at a higher density than the other cores. The smoothed profiles reveal variations in carbonate content (Fig. 28). These fluctuations are greater in magnitude than the precision of the measurements, and can be correlated stratigraphically. For example, relatively lower carbonate concentrations are revealed at 0 to 100 cm and also at 400 to 500 cm down each core, represented by the Roman numerals I and III, respectively. Between zones I and III, relatively higher carbonate concentrations peak at approximately 300 cm, designated by II and correspond to episode A previously mentioned. Below mid-depth, the carbonate profiles steadily increase to the bottom of cores LT84-7P and 8P, and to about 850 cm in core LT84-10P. It is marked by the Roman numeral IV and corresponds to episode B previously mentioned.

The down-core profiles in carbonate in the north basin stratigraphy are not obvious in the central and southern basin cores, with the possible exception of core LT84-5P. The carbonate profile from 5P is similar to the north basin pattern down to a depth of 1045 cm. The profile is anomalous below 1045 cm, where the carbonate content decreases from above 14% to less than 2%. The extremely low values continue down-core to 1170 cm and correspond to depths just above the

Fig. 28. Weight percent carbonate ($CaCO_3$) of the the dry sediment vs. depth down cores LT84-7P, 8P, and 10P. The heavy line is an 1-meter running average of the data. The thin line is a clamped-cubic-spline interpolation through the original data. Roman numerals I and III designate relatively lower carbonate concentrations, and Roman numerals II and IV designate relatively higher carbonate concentrations. These four zones are correlated between the north basin cores.

erosional unconformity. Below the unconformity, the values increase to the bottom of the core.

Trace Element Analysis of Carbonates

Molar ratios of strontium to calcium in adult and juvenile forms of ostracod Sclerocypris clavata from core LT84-2P average 0.005 and 0.007, respectively. The ratio in micrite samples from cores LT84-2P and 7P both average 0.002 (Fig. 29) (Appendix I). Molar ratios of magnesium to calcium in adult and juvenile forms of Sclerocypris clavata from core LT84-2P average 0.014 and 0.016, respectively. The ratios in micrite samples from cores LT84-2P and 7P average 0.2 and 0.3, respectively (Fig. 29) (Appendix I). The standard deviation from multiple analyses of the juvenile form of Sclerocypris clavata is 0.00037 for Sr/Ca and 0.0019 for Mg/Ca ratios. The micrite precision is calculated from at least 5 repetitions of two separate samples. The average of the separate, 1 sigma standard deviations is 0.00035 for Sr/Ca and 0.05 for Mg/Ca ratios. The precision of Mg/Ca analyses is poor and an order of magnitude less in the micrite than in the ostracod analyses. Moverover, the Mg/Ca ratio in the micrite is much higher than would be expected for low-Mg calcite. X-ray diffraction analysis of the micrite confirms Yuretich's (1986) conclusion that it is low-Mg calcite. The anomalously high Mg/Ca ratio indicates that the hydrochloric acid treatment that was used to dissolve the micrite for atomic aborption analysis must have also leached Mg from reactive clay minerals. In retrospect this is not surprising because Yuretich (1986) determined that a major sink for Mg^{2+} as it enters Lake Turkana is diagenetic production of the abundant,

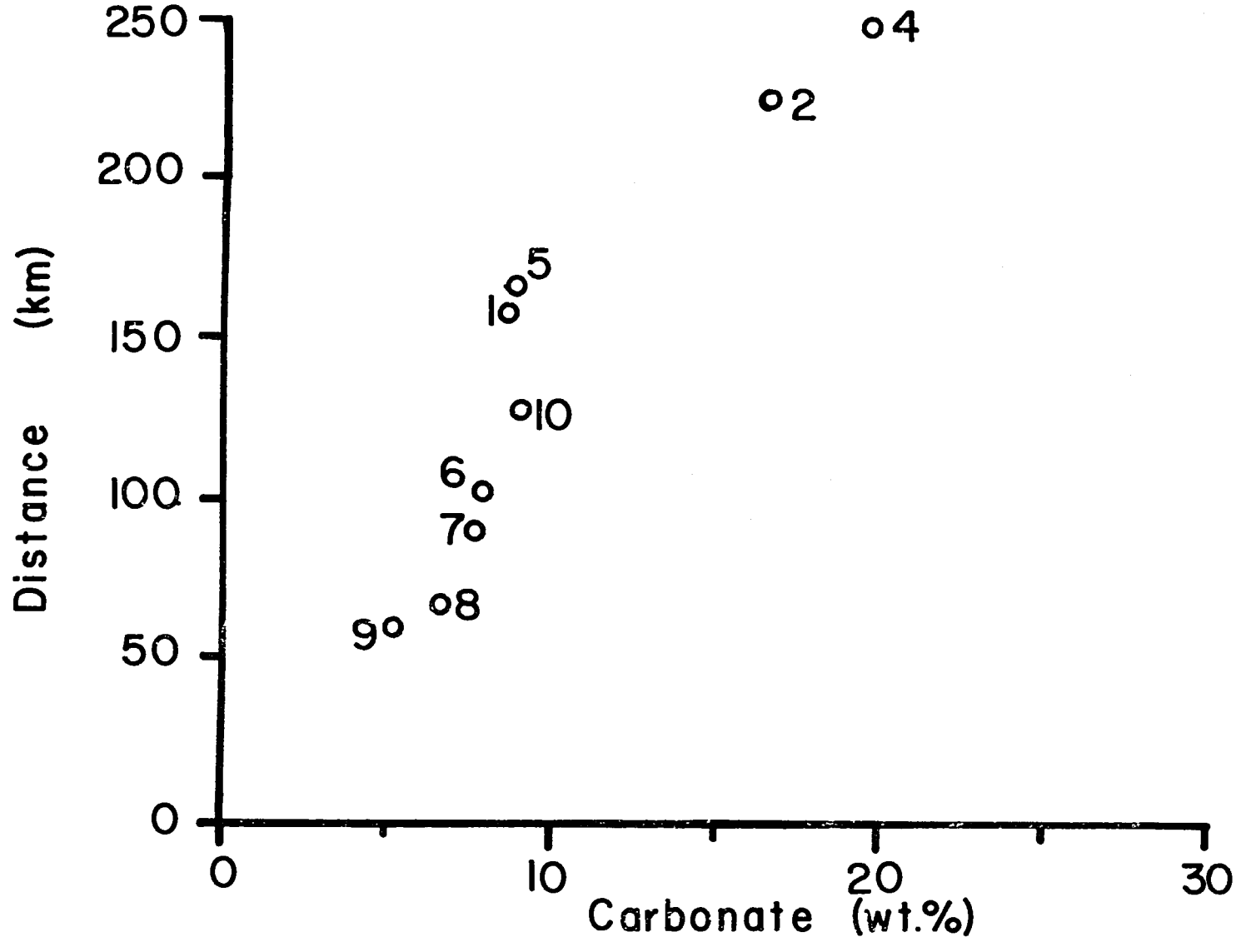
250
200
150
100
50
0
Distance (km)
0
10
20
30
Carbonate (wt.%)
4
2
5
1
10
6
7
8
9

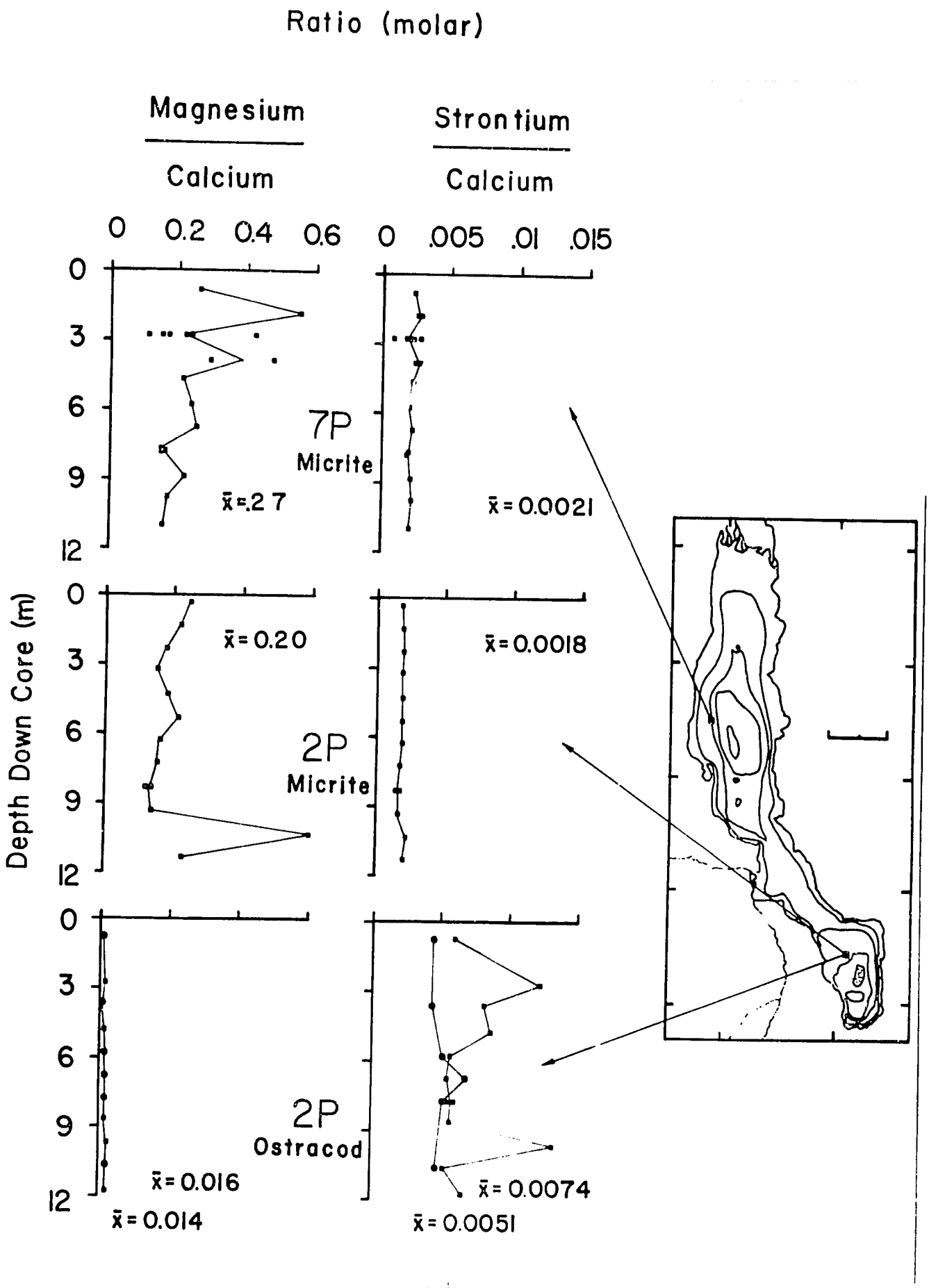
Ratio (molar)
Magnesium
Calcium
Strontium
Calcium
0 0.2 0.4 0.6
0 .005 .01 .015
Depth Down Core (m)
0
3
6
9
12
7P
Micrite
x̄=.27
x̄=0.0021
2P
Micrite
x̄=0.20
x̄=0.0018
2P
Ostracod
x̄=0.016
x̄=0.014
x̄=0.0074
x̄=0.0051

Core: LT84 – 10P

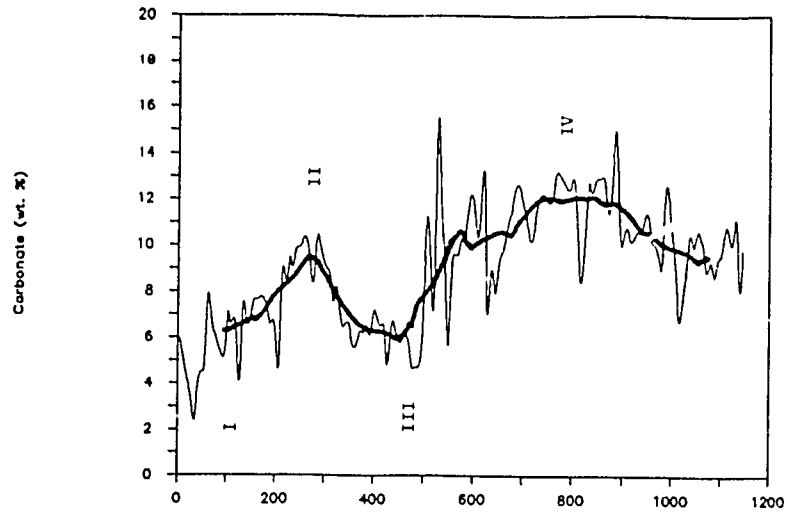

Core: LT84 – 7P

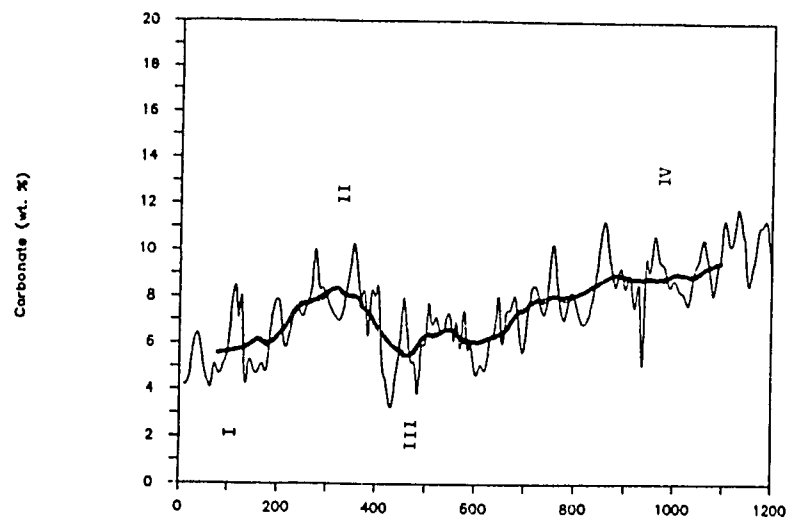

Core: LT84 – 8P

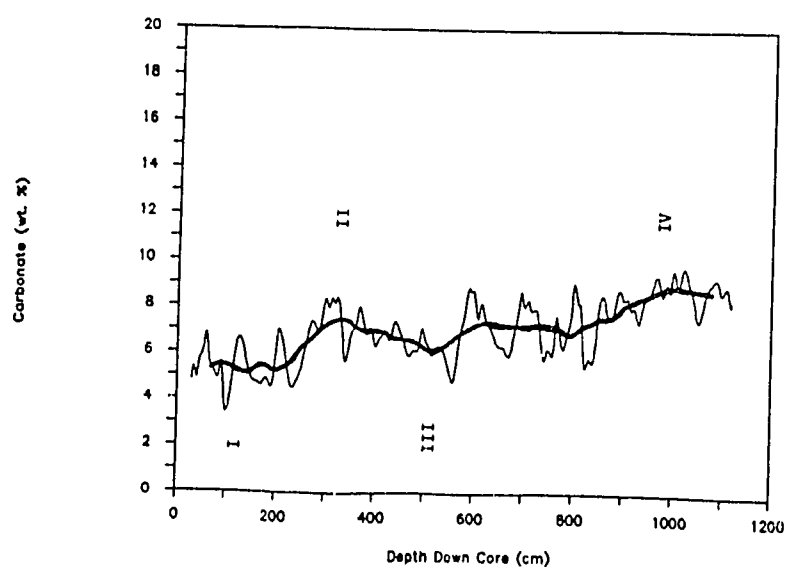

Fig. 29. Magnesium to calcium (left) and strontium to calcium (right) molar ratios vs. depth down cores LT84-2P and 7P. The 2P ostracod (bottom) is the juvenile (squares) and adult (circles) forms of Sclerocypris clavata. The micrite (2P center, 7P top) is all carbonate less than 44 microns in diameter. The mean value for each profile is indicated after the x. Map insert shows core locations.

poorly-crystalline, Mg-rich smectite.

The two forms of ostracods reveal nearly consistent Mg/Ca ratios, but dissimilar Sr/Ca ratios. The juvenile form reveals a variable down-core profile of Sr/Ca ratios with higher values between 274 and 477 cm and at 964 cm, whereas the adult form reveals an uniform profile.

Stable Isotope Analysis of Carbonates

Stable isotope analyses of ostracod Sclerocypris clavata (juvenile form) from core LT84-2P average -0.69°/oo for δC-13 and 3.24°/oo for δO-18 (PDB). The isotope values of micrite samples from core LT84-2P average 0.76°/oo for δC-13 and 1.37°/oo for δO-18 (PDB). The values for core LT84-7P average -0.14°/oo for δC-13 and 0.19°/oo for δO-18 (PDB) (Fig. 30) (Appendix J). Limited ostracod carapaces hampered the estimation of the analytical precision. The average deviation from the mean between the adult and juvenile forms is 0.5°/oo for δC-13 and 0.09°/oo for δO-18. The standard deviation of 3 replicate analyses of the adult form is 0.14°/oo for δC-13 and 0.08°/oo for δO-18. The micrite precision is calculated from at least 4 repetitions of two separate samples. The average of the separate, 1 sigma standard deviations is 0.05°/oo for δC-13 and 0.26°/oo for δO-18. The reproducibility of the ostracod δC-13 and micrite δO-18 analyses is poor and almost an order of magnitude larger than the accuracy of the MAT 251 mass spectrometer (at least 0.03°/oo). The oxygen isotope values from the analysis of the ostracods is within the range of values (3.5 to 5.0°/oo) determined on ostracods from LT84-10P analyszed by G. Lister (pers. commun.) of the Geologisches Institut, ETH, Zurich.

Fig. 30. Oxygen (circle) and carbon (square) isotope values vs. depth down cores LT84-2P and 7P. The 2P ostracod (left) is the juvenile (open symbol) and adult (closed symbol) forms of *Sclerocypris clavata*. The micrite (2P center, 7P right) is all carbonate less than 44 microns. The mean value for each profile is indicated after the x.

The δO-18 profiles from core LT84-2P reveal steadily decreasing (over 1°/oo) and parallel down-core trends for the ostracod and micrite samples. The two δC-13 profiles reveal different down-core trends. The micrite δC-13 profile is parallel to its δO-18 profile. The ostracod δC-13 profile steadily increases down-core to 930 cm, with values below 930 cm returning to the core-top values. The ostracod δO-18 mean value is significantly heavier (2°/oo) than the micrite mean value, whereas the ostracod δC-13 mean value is significantly lighter (1.1°/oo) than the micrite mean value.

The isotope profiles of micrite in LT84-7P are noisy, yet parallel down core. The down-core trends of LT84-7P contain a major deviation towards lighter values at mid-depth (4 to 7 m) and another deviation towards lighter values at 278 cm, although the latter is defined by only one data point. The mean δC-13 value is slightly offset (0.3°/oo) towards lighter values from the mean δO-18 value.

Laminations

The sediments are faintly laminated and consist of alternating light and dark couplets that are 0.1 cm to a few cm thick. The bottom contacts for both the light and dark laminae are typically gradational through a depth interval up to 1 mm thick that is occasionally bioturbated. Occasionally the contact is sharp. Additional sedimentary structures, for example graded bedding, are absent. The light and dark laminae appear identical on the basis of smear slide examination, without distinctive concentrations of any sedimentary component, except that the light layers are possibly finer-grained and more calcareous

than the dark layers. The visual contrast between light and dark laminae varies between basins in the lake and down core. The contrast is greater in cores that were recovered from the north basin, especially closer to the Omo River. The contrast is minimal and sometimes very subtle in cores recovered from the south basin, except for core LT84-3P. The laminae recovered in the north basin cores reveal the greatest contrast in the lowest 3 to 4 m of sediment.

Lamination Thickness

The mean thickness of light/dark couplets is about 10 mm. The mean of LT84-8P, and upper and lower sections of LT84-9P are 9.7, 17.2 and 10.3 mm, respectively (Fig. 31) (Appendix K). The range of individual thicknesses is 1.7 to 45.2 mm. The average of the separate, 1 sigma standard deviations is 0.1 mm, based on three separate measurements of the individual lamination thicknesses for a meter of core.

The profiles of couplet thickness are noisy, yet major and minor oscillations are recognizable (Fig. 31). Laminations in core LT84-8P are thickest at roughly 0.5 to 1.5 m. The thick group is bisected by relatively thin couplets at about 1 m. Another group of thick couplets occurs between 4.0 and 5.7 m. Minor oscillations in couplet thickness are found throughout the profile. The profile from the top section of LT84-9P is stratigraphically consistent with the corresponding profile from the upper 3 meters of 8P with an interval of thicker couplets that occur at about 1 meter depth, which is bisected by a zone of thinner couplets. Both profiles also reveal minor oscillations in couplet thickness through the 3 m interval.

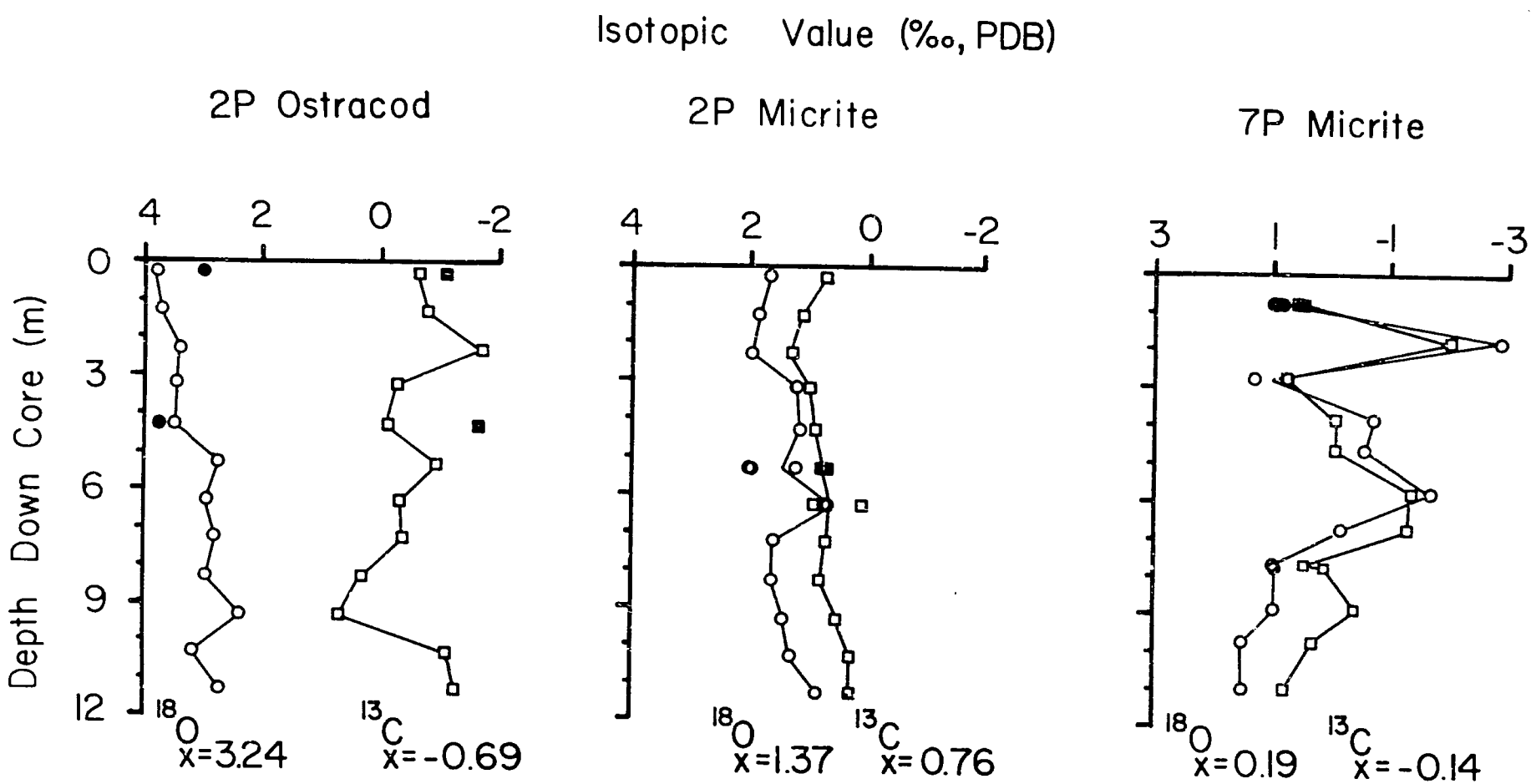
Isotopic Value (‰, PDB)
2P Ostracod
2P Micrite
7P Micrite
Depth Down Core (m)
0
3
6
9
12
4
2
0
-2
3
1
-1
-3
18O
x=3.24
13C
x=-0.69
18O
x=1.37
13C
x=0.76
18O
x=0.19
13C
x=-0.14

Fig.

Fig. 31. Thickness of successive light/dark couplets vs. depth down cores LT84-8P (right) and 9P (left). The profiles were smoothed with a 3 point running average to increase the resolution of the lower frequency information. The vertical line is the mean value for each individual profile. The arrows mark the common double peak thick interval (see text for details).

Lamination Composition

Bulk carbonate, biogenic silica, and grain size (detrital, silt fraction) analyses were performed on subsamples of 56 successive laminae from core LT84-8P (Fig. 32) (Appendix L). TOC and C/N ratios were determined from 21 subsamples, divided into two groups of successive laminae. A separate mean and standard deviation was calculated from the results of the light and dark laminae for each analysis, and are presented in the table below.

Lamination Analysis

Parameter	Light Laminae	Dark Laminae
Carbonate	6.09 ± 1.34	4.85 ± 0.98 %
Median Grain Size	16.1 ± 2.0	15.7 ± 2.0 microns
Biogenic Silica	1.3 ± 0.3	1.3 ± 0.2 %
Total Organic Carbon	0.86 ± 0.05	0.85 ± 0.05 %
C/N Ratios	7.2 ± 0.9	6.9 ± 1.1
*Lamination Thickness	10.1 ± 4.6	8.5 ± 2.9 mm

* from the same interval of core as the geochemical analyses.

The results show that while adjacent light and dark laminations may differ in composition, the difference is not consistent with any of the measured parameters except possibly $CaCO_3$, and even this difference is relatively slight. Clay mineralogy from X-ray diffraction analyses reveal minimal mineralogical changes between successive light and dark laminae. In core LT84-8P, the dark layers may have more montmorillonite than the light layers, but the observation is based on a limited number

Fig. 32. Carbonate ($CaCO_3$, wt.%) median grain size (detrital silt fraction), thickness of individual laminations, biogenic silica (SiO_2, wt. %), total organic carbon (TOC, wt. %), and carbon to nitrogen ratios (C/N ratios) vs. lamination number. The analyses were performed on light, (open squares) and dark (closed circles) successive laminations from core LT84-8P. The mean value for each profile is indicated after the x.

Lamination Analysis

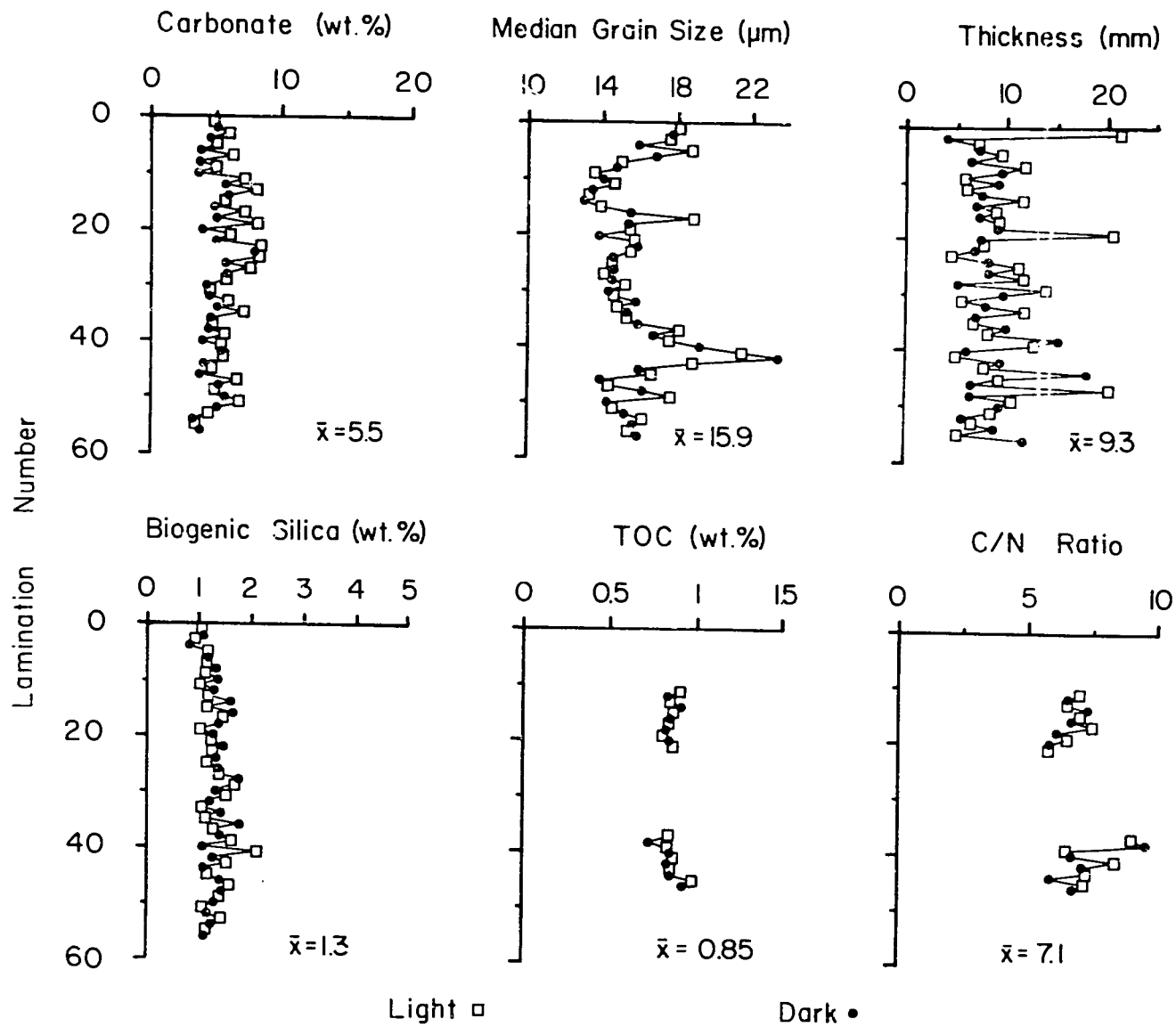

Fig 10

of samples and a consistent trend is not revealed in the other cores.

Down-core trends of these parameters reveal two important observations. Light laminae contain more carbonate than the majority (89%) of the adjacent dark laminae, whereas the other parameters reveal inconsistent inter-lamination trends. Successive laminations with higher carbonate values (for example, the mean carbonate value from 11 to 32 cm is higher than the mean value from 33 to 46 cm, 6.2 vs 5.2%, respectively) correspond to finer median grain sizes (14.9 vs 17.4 microns, respectively) and thinner lamina thicknesses (9.0 vs 10.4 mm, respectively).

Clay Mineralogy

Limited X-ray diffraction analysis of the bulk sediment reveals the dominance (>90%) of clay minerals, especially montmorillonite (Appendix M). The diffraction patterns reveal broad clay peaks, which possibly reflect small crystal size, poor crystallinity or variable composition of the clays. The accessory minerals include illite, kaolinite, low-magnesium calcite, feldspars, quartz, opal and possibly pyrite. Minor differences in their relative abundance occur between localities in the lake. Feldspars and illite are most abundant in LT84-1P. Low-magnesium calcite, pyrite and opal (biogenic silica?) are most abundant in LT84-4P. The limited survey suggests that the relative abundance of different minerals does not change significantly down core. Both low-magnesium calcite and dolomite are found in a LT84-7P micrite sample from 274 cm with low-magnesium calcite the dominant carbonate form.

DISCUSSION

Total Organic Carbon

The TOC values from the profundal sediments reported by this study are similar to values reported by Yuretich (1979). These values are low compared to most other large African lakes. The average TOC values are, for example: Lakes Chad < 1%, Turkana 0.9%, Mobutu Sese Seku 3.5%, Malawi 4.8%, Tanganyika 6.4%, Kivu 6.6%, Victoria 11.3%, and Edward 11.6% (Talbot, 1987). Various factors may influence the TOC content in the sediment including the quantity and source of both the organic and non-organic fractions and in situ anaerobic and aerobic diagenesis.

Primary productivity in Lake Turkana has only been measured at a few sites from 1973 through 1975. The values average 1 $gC/m^2/day$. If they are representative of the whole lake, they are similar in magnitude to other large African lakes (Beadle, 1981). This suggests that primary productivity does not contribute to the low TOC values in the sediments.

The major source of the organic matter can be revealed by its carbon to nitrogen (C/N) ratios. The ratios can differentiate between planktonic (ratios about 6) and non-planktonic (for example terrigenous organic matter with ratios 10 to 70) sources (Wetzel, 1975; Dean, 1981; Meybeck, 1982; Krishnamurthy et al., 1986). The contrast is due to the relative concentration of proteins in the various organisms. C/N ratios of the organic matter in Lake Turkana average less than 7, suggesting that it is dominantly of planktonic origin.

In comparison to Lake Turkana, the source of organic matter in sediments of other large African lakes is a mixture of autochthonous and

allochthonous sources (Talbot, 1987). For example, C/N ratios are greater than 10 and range up to 20 in Lake Malawi (T. Johnson, unpublished data). A number of factors may account for the difference. The quantity of allochthonous organic matter in the Turkana basin is significantly less than the other lakes due to the extreme aridity of the basin. The littoral biomass is limited at Lake Turkana due to the strong winds, except for wave protected shorelines (Cohen, 1984). The lack of allochthonous organic matter may contribute to the low TOC values, yet other factors are also important.

Anaerobic diagenesis of the organic matter is indicated, as stated earlier, by pore water geochemistry. A corresponding decline in the TOC values with depth in the cores is not obvious, however. The impact on the TOC values is therefore assumed minimal.

The mass accumulation rates of organic carbon (MAROC) for cores LT84-2P and 8P are 2 and 0.7 mg $C/cm^2/yr$, respectively. A range of MAROC for the basin is estimated from 0.7 to 3 mg $C/cm^2/yr$, assuming an organic carbon concentration of 1% and a range of sedimentation rates of 0.2 to 0.8 cm/yr, respectively. These values encompass the average MAROC estimated for Lakes Malawi, Tanganyika, and Victoria of 0.9, 2 and 2 mg $C/cm^2/yr$, respectively, based on mean organic concentrations (Talbot, 1987) and mean sedimentation rates (Johnson, 1984) for the respective basins. These rates are similar to rates calculated for Lake Superior, about 1.0 mg $C/cm^2/yr$ (Johnson et al., 1982). The similarity in the MAROC and productivity between these basins suggests that the significantly lower TOC values for Lake Turkana are the result of organic matter being diluted by detrital silicates and not by

differences in the aerobic degradation of the organic matter.

The major difference between these environments is the impact of the Omo River on the sedimentology of Lake Turkana. Although measurements of the detrital loading for various rivers entering the lake are not available, the Omo dominates the hydrology and drains the largest area of the basin. The higher TOC values in the south compared to the north basin, even though productivity may be higher nearer the Omo River, is consistent with the dilution hypothesis. Other autochthonous material, including diatoms, ostracods, biogenic silica and carbonate concentrations, follows a similar trend of higher concentrations in the south than the north basin. The lack of detailed sediment flux and productivity measurements hampers estimates of the relative importance of the factors that limit the TOC concentrations.

Most of the cores (except LT84-1P and 5P) reveal higher TOC values for a one or two meter interval within the first 4 meters of the core (Fig. 23). The higher TOC values correspond roughly to an interval of relatively higher carbonate concentrations (LT84-4P, 6P, 9P) or to the transition from high carbonate to low carbonate concentrations (LT84-2P, 7P, 8P, 10P). The correlation is weak in 4P and 6P where higher TOC values are poorly defined at intervals of higher carbonate content. The correlation is absent at depth in all cores, where another interval of high carbonate usually exists yet lacks the corresponding enrichment in TOC, perhaps due to decomposition of the organic matter.

The fluctuation in the TOC record may result from varying the source of organic matter, productivity, or clastic dilution through time. A change in the abundance of allochthonous to autochthonous organic

material is not revealed by the C/N ratio profiles, which are uniform with depth down core. Lower Omo River discharge, which is assumed to correspond to decreased sediment discharge in the lake, will result in an apparent increase in TOC concentration. During the transition from lower to higher flow, the clastic input may temporarily be trapped in small estuaries (Talbot, 1987) resulting in decreased dilution of the organic matter. Productivity also may increase in the same time interval by temporarily increasing the supply of a limiting nutrient (Wetzel, 1975; Harbott, 1982). Any of these mechanism can create higher TOC concentrations in the sediments. The lack of long term limnologic data from Lake Turkana hampers a decisive conclusion.

Rising and falling lake level, resulting in lateral migration of nearshore and offshore facies, is another mechanism for major variations in TOC content through the sedimentary section. In core LT84-5P, a 2 m interval of higher TOC and C/N values overlies the inferred erosional unconformity (Figs. 23 and 25). The values are the highest found in any of the analyzed cores. The high TOC values may reflect nearshore, muddy deposits, which in the modern lake contain 10 to 100 times more biomass than sandy nearshore and profundal deposits (Cohen, 1984). The high C/N values indicate a mixture of planktonic and littoral or terrestrial organic matter and reflect a more proximal location of the paleo-shoreline (Krishnamurthy et al., 1986). The conclusion supports the hypothesis that the firm, coarse-grained unit at the base of LT84-5P marks an erosional unconformity.

Carbonate

Carbonate is the second most abundant component after the detrital silicate fraction in the sediments in Lake Turkana. The measured carbonate concentrations (wt. % $CaCO_3$) are similar to published values for CaO (Yuretich, 1979, 1986). The positive, linear trend between carbonate concentrations and distance from the Omo River is interpreted to reflect decreasing dilution of the carbonates by clastic material (Fig. 27). Cores LT84-1P and 5P are slightly below the linear trend in Fig. 27, probably because of additional clastic dilution from the Turkwel-Kerio Rivers and abnormal, very low carbonate concentrations just above the erosional unconformity in 5P.

The carbonate fraction of the sediment has two main components, ostracod carapaces and micrite. Other components were identified in only a few samples, and include rare gastropod shells and possibly dolomite. The modern ostracod population in water depths greater than 20 meters is dominated by Sclerocypris clavata, and is limited to less than 10^2 individuals/m^2, whereas, ostracods in vegetated nearshore deposits are dominated by other species and contain approximately 10^5 individuals/m^2 (Cohen, 1982).

The micrite was previously assumed to be biogenic debris (Yuretich, 1979). Isotopic analyses of isolated micrite and species-specific ostracod samples indicate significantly different results. The δO-18 values are approximately $2^o/oo$ lighter and δC-13 values are approximately $1^o/oo$ heavier for the micrite compared to the ostracod tests. These differences suggest that the micrite is not derived from fragmented ostracods.

Various lines of evidence indicates a non-detrital origin for the micrite. SEM analyses showed much of the calcite in the micrite fraction to be euhedral, semi-acicular crystals (Fig. 33). This euhedral character and the lack of an appreciable influx of detrital carbonates to the lake from the drainage basin (Cerling, pers. commun.) suggests that the micrite is not detrital. The increased carbonate concentrations away from the Omo River also supports the non-detrital origin. X-ray diffraction analysis of the fine grained sediment reveals low-Mg calcite. On the basis of the minerology, Yuretich (1986) later hypothesized that the micrite was an authigenic precipitate from the surface waters of the lake. Additional evidence from stable isotope measurements indicates a non-diagenetic formation and reveals additional evidence of authigenic formation for the micrite.

Comparison of the micrite δC-13 values and the corresponding values of the dissolved inorganic bicarbonate (DIC) in the sediment pore waters also reveals significant differences. The δC-13 profiles for the micrite average 0.76 and -0.14^{o}/oo (PDB) for cores LT84-2P and 7P, respectively, with minimal down-core trends. The δC-13 profiles for the DIC reveal increasing values down both cores from 0 to +12°/oo (PDB) (T. Cerling, person. commun.). These differences indicate that the micrite is not a diagenic precipitate, because if it were, its carbon isotope values would resemble the dissolved carbonate values (Irwin et al., 1977; Talbot and Kelts, 1986). SEM examination of the ostracod tests did not reveal overgrowths of calcite, which is typical of diagenetic cements in the marine environment (Bathurst, 1975).

The carbon isotope values for the micrite are heavier (about 1°/oo)

10 μ

10 μ

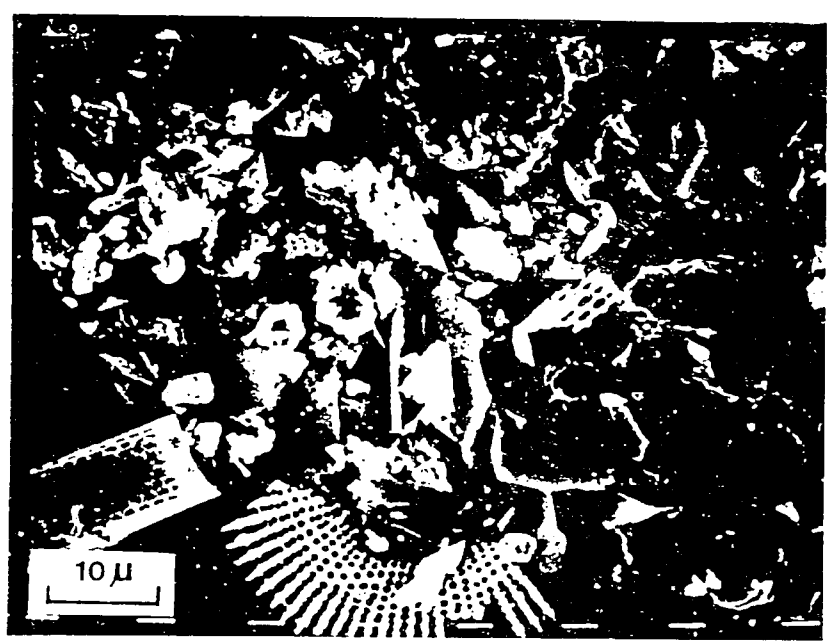
10 μ

2 μ

Fig. 33. Scanning electron microscope photographs of the fine fraction of the sediment. The arrow-shaped particles, most visible in the lower right photo, are euhedral, semi-acicular crystals of low-Mg calcite.

than those for the ostracod tests. This difference is what would be expected after photosynthetic fractionation of the carbon isotopes, where carbon-12 is essentially transferred from the surface waters to the deeper waters by a photosynthetic-respiration pathway. Photosynthetically produced organic matter is enriched in carbon-12 relative to carbon-13, and as it sinks, it oxidizes, releasing carbon-12 encriched CO_2 to the bottom waters. The carbonate retains a carbon-isotopic composition that is characteristic of the water depth (McKenzie, 1985; Lee et al., 1987). The ostracods are epibenthic detritovores (Cohen, 1984). Thus, the carbon isotopic evidence suggests that the micrite forms as an inorganic precipitate in the surface waters, and its formation is enhanced by photosynthesis.

Authigenic carbonates should precipitate at isotopic equilibrium with the water. The equilibrium isotopic fractionation factor for the calcite-water system is:

$$1000 \ln(a) = 2.78 (10^6) \cdot T^{-2} - 2.89$$

assuming:

$$1000 \ln(a) = \delta O\text{-}18_{calcite} - \delta O\text{-}18_{water} \quad (SMOW)$$

where (a) is the isotopic fractionation factor and T is the temperature of the reaction (^oK) (Freidman and O'Neil, 1977). The δO-18 of Lake Turkana has been measured at 5.6^o/oo and the Omo River effluent at -1°/oo (SMOW) (Cerling, limited unpublished data). The micrite with a δO-18 value of 1°/oo (PDB), equivalent to 31.9^o/oo (SMOW), would be in isotopic equilibrium with the lake water if its temperature of formation was 36°C or if the isotopic composition of the water was lowered by 1°/oo. A formation temperature of 36°C is higher than 25.5^{o}C, the mean

temperature of the water column (Ferguson and Harbott, 1982). Water temperatures above 30°C were reported for the surface water (1 m depths) in the open lake and isolated, shallow bays (Ferguson and Harbott, 1982). This may indicate that the crystals precipitate in these warmer surface waters compareed to the rest of the water column, perhaps in the uppermost millimeter on calm days, or in shoreline pools, and are then transported to the deep basin. A second hypothesis concerns the less saline, turbid water mass generated during the flood season of the Omo River. The water mass extends from the Omo River to the central basin. The conductivity of the lake water drops by about 60% north of North Island, and by 10% through the remainder of the north basin during peak flood season. The isotopic mixing of the two water masses would be sufficient to precipitate micrite in equilibrium in the north basin at present water column temperatures, although slightly higher temperatures (28°C) than the mean lake temperatures would be required for the area south of North Island. The mean δO-18 value for micrite samples from LT84-7P is about 1°/oo lower than that from 2P, possibly reflecting the mixing phenomena. This interpretation also is consistent with the carbon isotope argruements presented above because photosynthetic activity peaks during the flood season of the Omo River. A third possibility is that the micrite, that was analyzed, formed during a time when the lake was less saline than today.

The carbonate profiles from the north basin reveal a basin-wide, correlative stratigraphy. The minor differences between the profiles may result from variable sedimentation rates between sites and different sampling densities.

PORE WATER

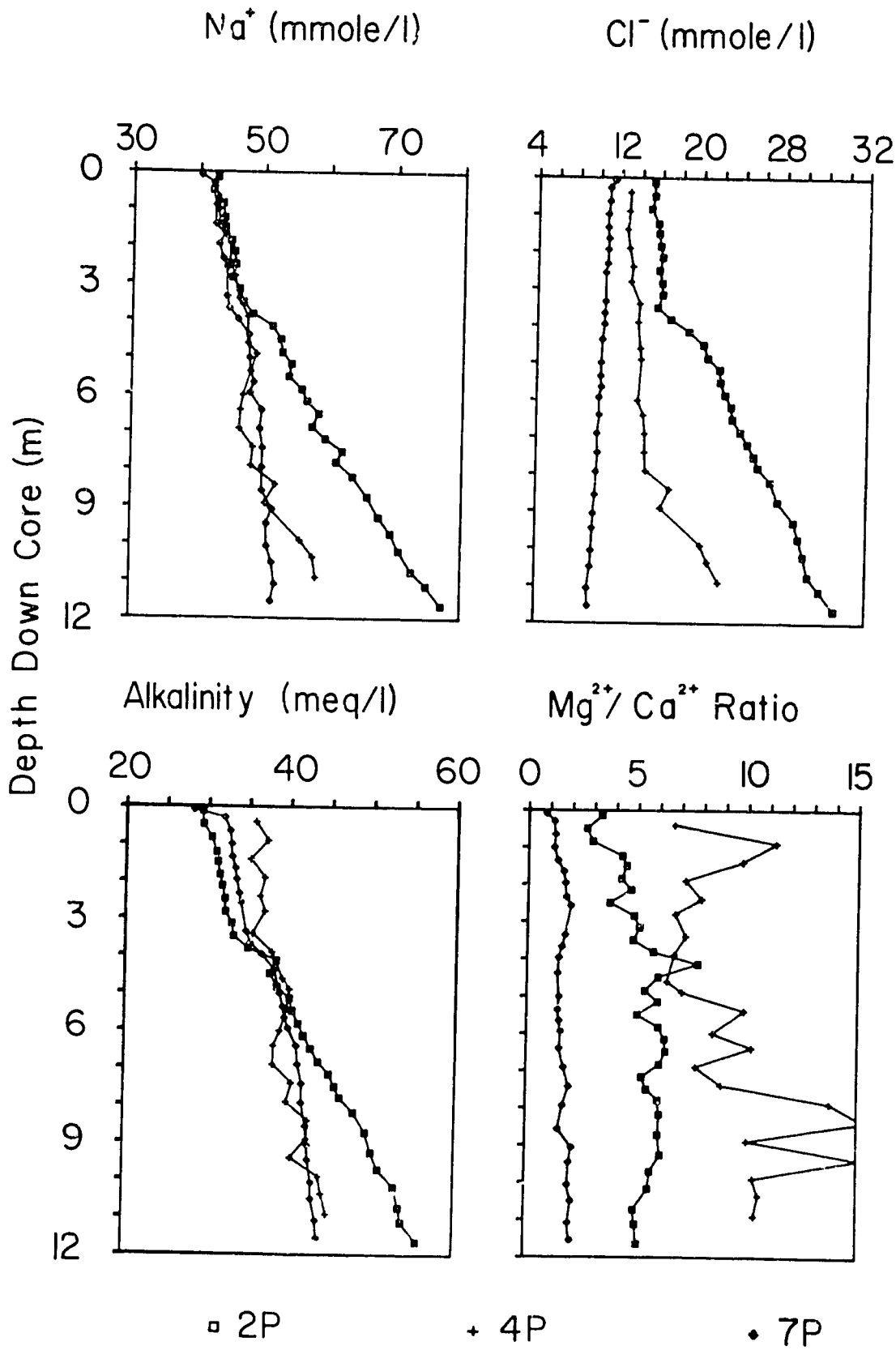
Na+ (mmole/l)
30
50
70
Cl- (mmole/l)
4
12
20
28
32
Depth Down Core (m)
0
3
6
9
12
Alkalinity (meq/l)
20
40
60
Mg2+/ Ca2+ Ratio
0
5
10
15
2P
4P
7P

The carbonate profile from LT84-5P is consistent with the north basin profiles, except for the zero carbonate values located just above the erosional unconformity. The unconformity occurs during the highest carbonate concentrations of the north basin profiles. An age for the oldest sediments just above the unconformity is approximately 4 thousand years, assuming a correlation to the radiocarbon dated core LT84-8P. This age is younger than the minimum estimated age of 10 Ka for the major erosional seismic reflector (Johnson et al., 1987). One explanation for the discrepancy may be multiple occupations of the same erosional unconformity, and it may be resolved by radiocarbon dates from core LT84-5P.

Carbonate profiles from the south basin also may reveal a basin-wide correlation. The apparent inconsistencies between the two profiles are reduced if the correlation of the profile from LT84-2P begins 3 to 4 meters down core LT84-4P (Fig. 26). The magnitude of the offset to correlate the paleosalinity curves interpreted from the diatom data (5 m) (Fig. 20) and significant changes in the trends of the pore water profiles (4 m) (Fig. 34) is not consistent with the carbonate data, however.

The carbonate profiles from the north and south basins are inconsistent. The general trend in the north basin is increasing carbonate values with increasing age, whereas in the south basin, the general trend is decreasing carbonate values with increasing age. This is confirmed by the radiocarbon ages of LT84-2P and 8P (Fig. 35).

The independence of the two basins during the past is also suggested by the pore water profiles (Fig. 34) (Cerling, unpublished data). The

Fig. 34. Pore water chemistry vs. depth down cores LT84-2P (square), 4P (cross) and 7P (diamond). Unpublished data from T. Cerling.

Fig. 35. Weight percent carbonate ($CaCO_3$) vs. age down cores LT84-2P (right) and 8P (left). Age was calculated from the best-fit, linear interpolation of radiocarbon age vs. depth down each respective core.

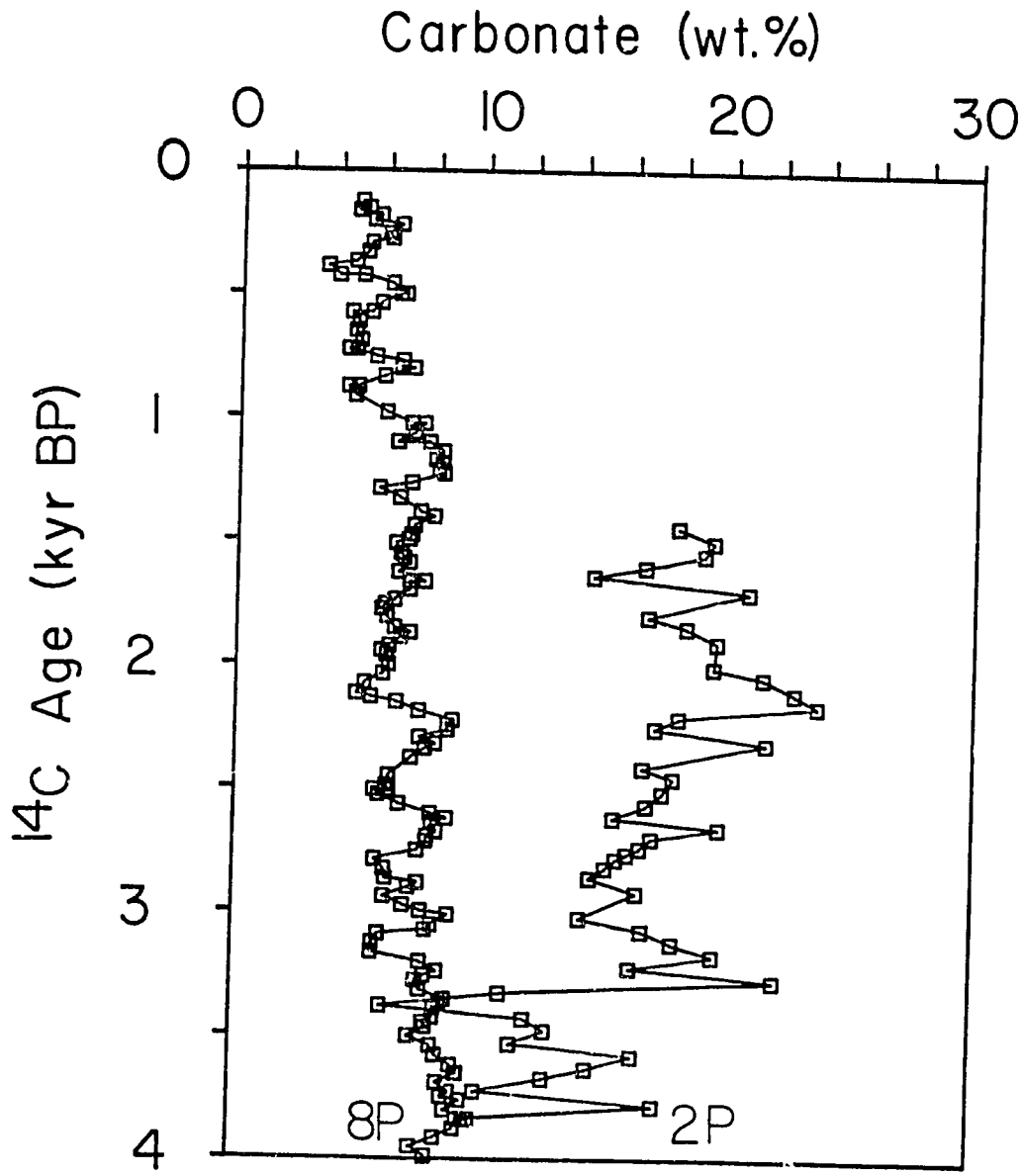

10Ja

pore water profiles from core LT84-7P are representative of the other cores from the north basin. This profile reveals minimal correlation to either core from the south basin. The largest inconsistency between the two basins is revealed by the chloride profiles. The trend in chloride concentrations with increasing depth in the core is decreasing in the north basin and increasing in the south basin. Cerling (1986) attributes the reversal in slope between the basins to the formation of a saline lake in the south basin when lake level was substantially lower and the two basins isolated during the past. He did not estimate the timing of this event.

The down-core fluctuations in carbonate concentrations in the north basin could result from variations in biological productivity, water temperature or Omo River discharge. Photosynthetic uptake of carbon dioxide is faster than the exchange rate of carbon dioxide between the atmosphere and the surface waters, and can thus alter the water chemistry towards supersaturation with respect to calcite (Kelts and Hsü, 1978). Warmer water temperatures decrease the calcite solubility product and decrease the concentration of dissolved CO_2 in the water, and both factors decrease calcite solubility (Brunskill, 1969). Periods of high discharge of the Omo River will decrease the concentrations of dissolved ions in the water column, thus decreasing the probability of carbonate precipitation. The increased discharge, more importantly, will increase the dilution of authigenic carbonates by detrital silicate minerals in the sediments. The long term (millennial) relationship between sediment yield and Omo River discharge, however, may not be constant due to long term changes in climate and corresponding changes

in the basin's vegetation and other factors that influence sediment yield (Blatt et al., 1980).

A weak but statistically questionable correlation is revealed between a paleo-productivity signal (Fig. 36) (biogenic silica or TOC values) and carbonate concentrations (r^2 between 0.05 and 0.3 from each best-fit linear correlation for each core). Both biogenic silica and TOC values may be affected by parameters besides paleo-productivity, however. For example, both $CaCO_3$ and biogenic silica concentrations increase to the south because of distance from the Omo River.

The geographical setting of Lake Turkana results in only small variations in the water temperature throughout the year (Ferguson and Harbott, 1982). The water temperature varied only 2.2°C during a three year study. The long term influence of temperature on the precipitation of carbonates in Lake Turkana probably was constant over the last 4 Ka, because palynological evidence from East Africa suggests constant air temperatures during this period within the resolution of the method (Hamilton, 1982).

A positive correlation exists between oxygen isotope values of both ostracod and micrite samples with carbonate concentrations (Fig. 36) (r^2 between 0.63 and 0.84 from each best-fit linear correlation for cores LT84-2P and 7P). The oxygen isotope values in low latitude, closed-basin lakes such as Lake Turkana are affected more by variation in water composition than in temperature (Abell, 1982). During dry periods when the lake is relatively low and saline, the oxygen isotopic composition of the water and carbonates precipitating in the lake would be relatively heavy. Therefore, relatively higher carbonate concentrations

Fig. 36. Biogenic silica (SiO_2, wt.%) vs. carbonate ($CaCO_3$, wt.%) (above) plotting values from depths which have both analyses. Only values from LT84-2P (square) and 10P (cross) are plotted, although simialar plots from other cores and plots of TOC vs. carbonate from the cores also reveal poor correlations. Oxygen isotope value vs. carbonate ($CaCO_3$, wt.%) (below) plotting values from depths which have both analyses. The ostracod species is Sclerocypris clavata (square). The micrite is all carbonate less than 44 microns in diameter from 2P (cross) and 7P (diamond).

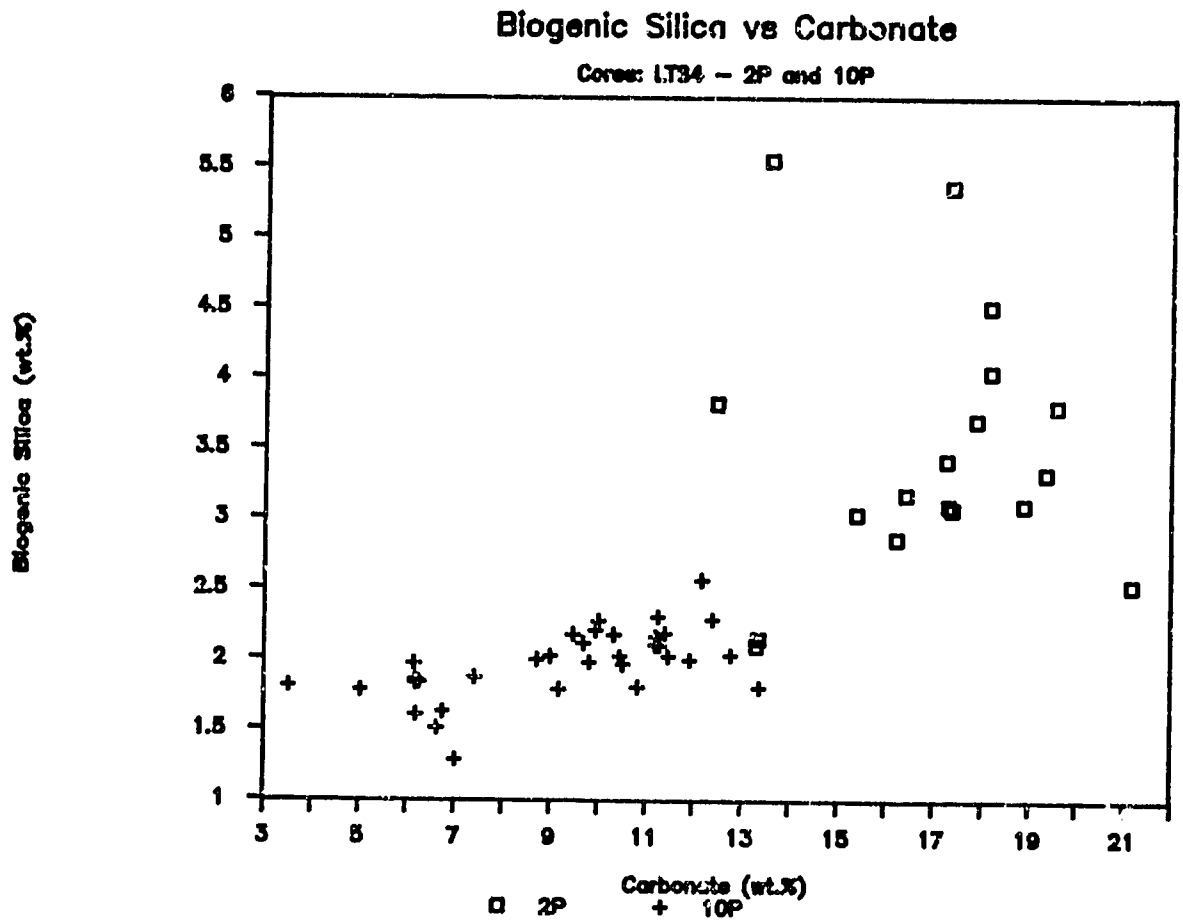
Biogenic Silica vs Carbonate
Cores: LT34 – 2P and 10P
Biogenic Silica (wt.%)
Carbonate (wt.%)
2P
10P

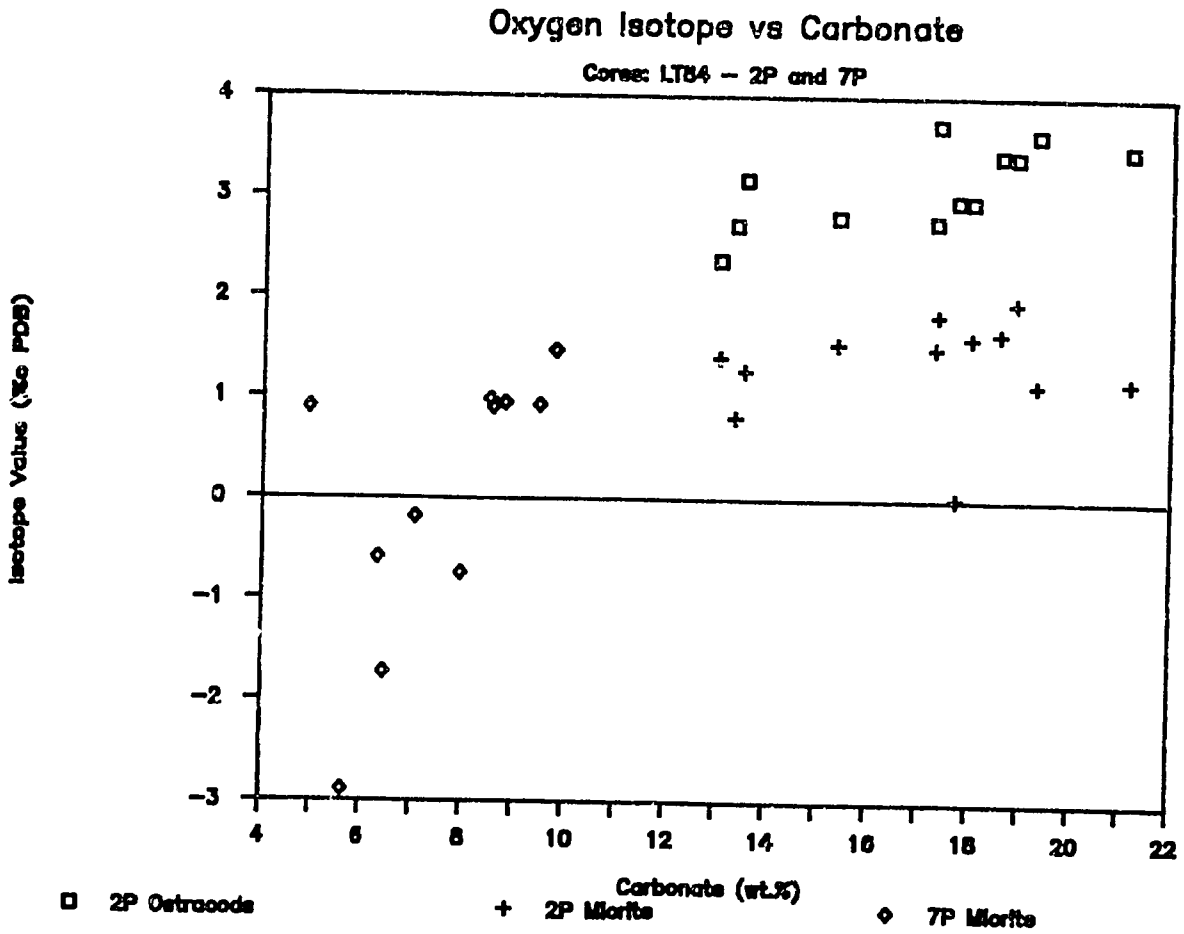
Oxygen Isotope vs Carbonate
Cores: LT84 – 2P and 7P
Isotope Value (‰ PDB)
Carbonate (wt.%)
2P Ostracods
2P Micrite
7P Micrite

correspond to periods of relatively higher salinity or lower lake levels. Another line of evidence in support of the correlation of carbonate with salinity or lake level is that the erosional unconformity in LT84-5P coincides with the horizon of highest carbonate values in the north basin stratigraphy. The paleosalinity interpretations from diatom and trace element analyses also are consistent with the carbonate results.

Three major diatom assemblages are found in the south basin cores. These are dominated by: (1) Thalassiosira and Surirella, (2) Surirella, and (3) Melosira (Fig. 20). The first assemblage reflects more saline waters than the third assemblage, whereas the second assemblage lacks specific salinity affinities (Hecky and Kilham, 1973; Gasse et al., 1983). The modern assemblage is dominated by Surirella species (Harbott, 1982). The interpreted paleo-salinity is greatest between 250 and 425 cm in core LT84-2P. A similar assemblage reflecting the maximum paleo-salinity occurs below 775 cm in core LT84-4P. This suggests a 5 meter offset in the stratigraphy of the two cores. The paleosalinity interpretations between the carbonate profiles and the diatom assemblages are grossly parallel. The timing of the various shifts is slightly offset, though.

Chivas et al. (1985, 1986) have shown that Sr/Ca and Mg/Ca ratios of ostracod carapaces are paleosalinity and paleothermometry indicators. The general trend of Sr/Ca ratios for the juvenile form of Sclerocypris clavata in core LT84-2P is to decrease down core. The interpreted decreasing salinity down core parallels the other paleosalinity interpretations from the core. An estimate for the absolute salinity is

difficult because Chivas et al. (1985, 1986) revealed a species-specific vital effect, which is unknown for the species analyzed in this study. In addition, the juvenile and adult forms revealed different results indicating an intra-species vital effect. Different carbonate assimilation rates may account for the differences between the juvenile and adult forms (R. Forester, pers. commun.).

The concentration of atmospheric CO_2 has changed through geologic time (Delmas et al., 1980; Sundquist and Broecker, 1985), and this has resulted in a variation in carbon isotope values in atmospheric CO_2 (Shackleton et al., 1983; Williams, 1985; Freidli et al., 1986). Light isotope values correspond to increased concentrations of CO_2 in the atmosphere. The changing isotopic composition of the atmosphere should also influence the isotopic composition of the dissolved inorganic carbon (DIC) in lakes, especially high alkalinity lakes (Peng and Broecker, 1980). The isotopic composition of the DIC in Lake Turkana from water samples collected in 1981 is 0.7^{o}/oo (PDB) (Cerling, limited unpublished data), and is slightly enriched over what would be expected if the lakes were in equilibrium with the atmosphere (about 0°/oo). The enrichment of the DIC may be the result of surface water productivity and the preferential uptake of C-12 by phytoplankton.

The profile of carbon isotope values from the micrite fraction of core LT84-7P reveals relatively lighter values at about 0.7 Ka, and about 1.3 to 2.0 Ka (Fig. 30), based on the correlation to the radiocarbon dated core LT84-8P. These intervals nearly coincide with episodes of deficient C-14 as revealed by the comparison of dendrochronologies (tree-ring chronologies) and radiocarbon dating

(Stuiver and Quay, 1981; Klein et al., 1982). The intervals also may correlate with a deep-sea Holocene record of δC-13 (Williams, 1985). Such correlations are interesting but questionable at the present time. The magnitude of the isotopic shifts are different between the various records and, in Lake Turkana, the carbon isotope records in cores LT84-2P and 7P do not match. The possible association of the carbon isotope record in core LT84-7P to other global records needs future research on the subject. The hypothesis can be tested by additional carbon isotope measurements on cores that contain a record of the last few centuries to look for the marked trend in atmospheric isotopic composition since the industrial revolution.

Origin of Laminations and their Climatic Significance

A hypothesis concerning the formation of the faint, alternating light/dark laminations must incorporate the following descriptive and quantitative observations. Visual, smear-slide, SEM, and X-radiograph examination of individual laminations suggest that the only differences between light and dark lamina are the color and possibly carbonate content. The inter-lamina sedimentary uniformity is documented by analyses of 56 successive laminations for biogenic silica, TOC, C/N ratios, and median grain size plus a few clay mineral analyses by X-ray diffraction. The character of the boundary between lamina can be sharp, faint, or gradational through an interval of up to 1 mm with neither layer revealing a consistent type of bottom contact. These data are atypical for seasonal couplets, i.e., varying input of allochthonous and autochthonous material, with a sharp boundary marking the onset of the

allochthonous material (O'Sullivan, 1983). The light layers, however, consistently contain more carbonate (thus the lighter color) than the adjacent dark layers, although a light layer from one section of the core may contain less carbonate than a dark layer in another section of core.

A number of observations suggest that the laminations are responding to variable sediment loading of the Omo River. The contrast between light/dark couplets in the north basin is more distinct than in the south basin suggesting a proximal influence of the Omo River. The mean thickness of the couplets in the upper 3 m of LT84-9P (17 mm) is larger than in the upper 3 m of 8P (10 mm). The difference is consistent with the proximity of the Omo River turbid plume to the LT84-9P site and the more distal location of 8P. The detailed analysis of successive laminae reveals that a general trend exists between higher mean carbonate content, smaller mean grain size and thinner mean couplet thickness. The profile of couplet thickness in the upper 3 m of LT84-9P correlates with the upper 3 m of the profile from core LT84-8P, suggesting that the detailed, high-resolution stratigraphy is a high-resolution analog to the down-core carbonate stratigraphy. The minor discrepancies between the profiles may be attributed to localized variability in deposition and to the different measuring techniques. For example, the glare on the photographs of LT84-9P may have masked some laminations. In summary, the formation of the laminae is interpreted to reflect a high-resolution variation in the mean Omo River discharge, with the light layers corresponding to periods of lower discharge.

The annual flooding of the Omo River is the most important seasonal

signal in the hydrology and limnology of the Turkana basin (Ferguson and Harbott, 1982). The previous hypothesis concerning the origin of the couplets utilized this event coupled with non-flood sedimentation (Yuretich, 1979). The light layers could therefore represent the non-flood depostion and the dark layers could represent the flood deposition.

A number of observations suggest that the correlation is incorrect. Each light/dark couplet in core LT84-8P, represents, on average, a little less than 4 years (3.84), based on the time span represented by the measured section of core (about 3.5 Ka) and the number of couplets (903). If the couplets were annual as previously suggested then the radiocarbon dates would indicate that 75% of the section is missing. There is no independent evidence for hiatuses in the core, however. There are no erosional lag deposits, no graded beds, and high-resolution seismic profiles and echo sounding from the core site show only a pattern of simple basin infilling. In addition, the profile of lamination thickness between the upper 3 m of cores LT84-8P and 9P correlate well, and the detailed lamination analyses are atypical for seasonal couplets. The observations suggest that inter-annual variability controls the pattern of laminations in the lake sediment. An exact 4 year periodicity is not implied. Instead, the recurrence interval may vary, but over a long period, averages about 4 years. It is surprising that this interannual variability can have a greater impact on sediment appearence and composition than does the seasonal variability. It is possible that severe wave activity associated with the strong diurnal winds on Lake Turkana are capable of stirring the

surface sediments to a depth sufficient to homogenize the seasonal record, yet leave the interannual record intact.

An alternative hypothesis is an interannual variability in the frequency, duration or magnitude of wind or storm events. Increased storminess may increase the resuspension of nearshore sediments, that could then be transported offshore to form one of the layers. This process probably would result in major differences in sediment composition and texture between the light and dark layers. The grain size, TOC, C/N ratios of the individual laminations do not reflect any significant differences, however.

Omo River discharge data are not available for a direct test of the hypothesis. Time series analysis of the Nile River flood levels can not statistically reveal cyclicities less than 10 years (Hameed, 1983). A prominent, year-to-year climatic variability exists in the tropics that is attributed to the El Nino-Southern Oscillation (ENSO) (Walker, 1924; Rasmusson and Wallace, 1983). The primary manifestation of the Southern Oscillation is a major shift in atmospheric pressure at sea level between the southeast Pacific subtropical high and the region of low pressure stretching across the Indian Ocean from Africa to northern Australia (Fig. 37). Directly coupled with ENSO events are especially heavy precipitation in the central equatorial Pacific and the coastline of Peru and Ecuador and droughts in Indonesia and eastern Australia. Significant changes in normal oceanic current patterns also occur with the corresponding demise of the Peruvian anchovy fishery. Even beyond these regions, ENSO events have a powerful influence on large-scale temperature and precipitation patterns throughout the tropics (Bradley

Fig. 37. Global pattern of the coefficient of correlation between variations of barometric pressure at Jakarta, Indonesia, and those at other locations throughtout the world. Jakarta pressure is a faithful indicator of the Southern Oscillation. The pattern shown here is based on data in the form of annual averages of sea-level pressure in each of a large number of years (from Berlage, 1967).

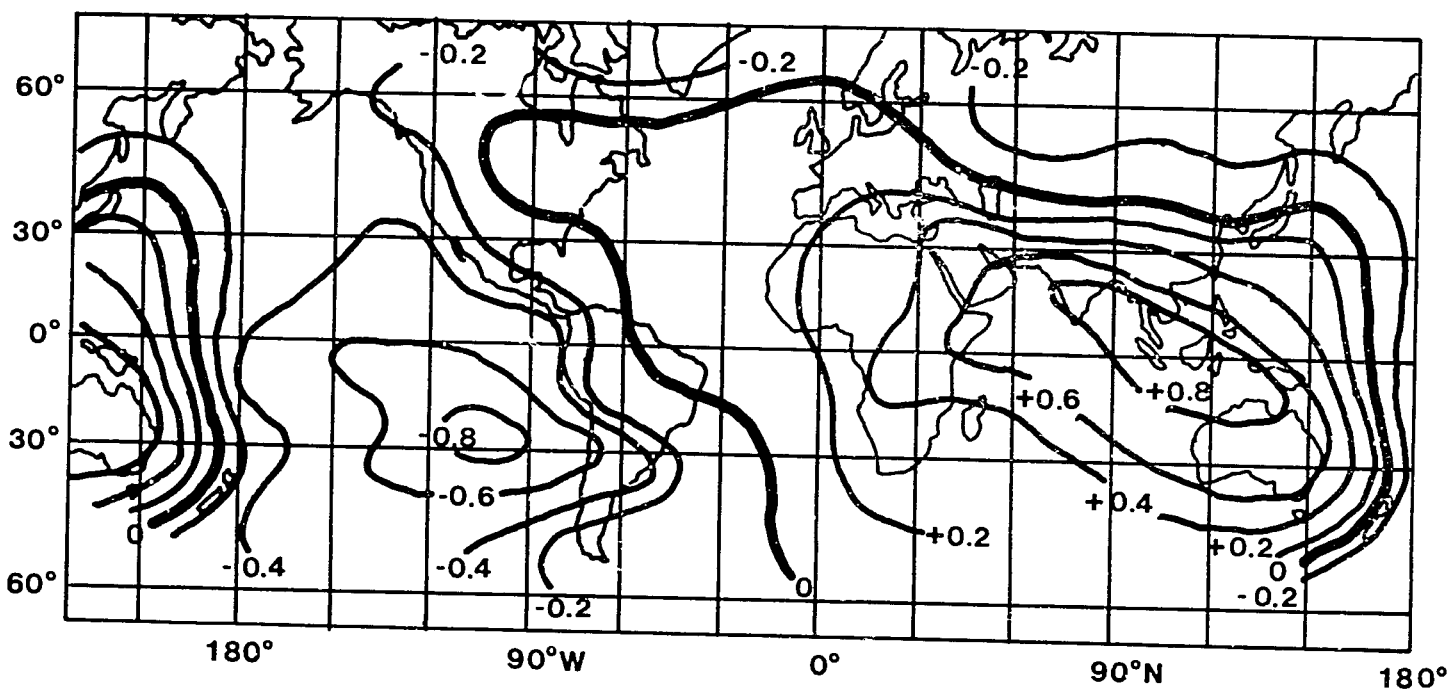
60°
30°
0°
30°
60°
180°
90°W
0°
90°N
180°
-0.2
-0.2
-0.2
-0.8
-0.6
-0.4
-0.4
-0.2
0
0
+0.6
+0.8
+0.4
+0.2
+0.2
0
-0.2

112a

et al., 1987). The monsoon rains in Sri Lanka and India are negatively correlated to ENSO events (Rasmusson and Carpenter, 1983; Rasmusson, 1985). Rainfall in the Sahel is also anomalously low during ENSO years, and is strongly related to nearby sea-surface temperature anomalies (Folland et al., 1986; Palmer, 1986). There is a significant probability that an ENSO event will recur every 3 to 4 years, although the event is quasi-cyclic with the range of the recurrence interval between 2 and 10 years (Quinn et al., 1978). The long term prediction and especially the forcing mechanism of ENSO events is still unknown (Cane et al., 1986).

Records of rainfall in Ethiopia and especially in the Turkana basin are limited in areal distribution and in the length of the records. The only station in the Omo basin with a reasonably long run of rainfall data is at Jima, Ethiopia (Fig. 3). Spectral analysis of the incomplete 33 years of yearly precipitation totals does not reveal significant spectral peaks, probably due to the limited length of the data string. A majority (73%) of the ENSO years, however, have lower recorded rainfall than either the previous or following years (Fig. 38). Addis Ababa, Ethiopia is located in the headwaters of the Blue Nile drainage basin just to the northeast of Jima (Fig. 3). Low rainfall years in the 85-year record are also coupled with a majority (74%) of the ENSO years (Fig. 38). Spectral analysis of this 85-year record reveals a significant (95% confidence level) periodicity at 11 years. An 11-year periodicity is also found in other drought and flood proxy records from around the world (Currie and Fairbridge, 1985). A periodicity at 3.5 years is revealed above background, but not at the 95% confidence level.

Fig. 38. Yearly precipitation records from Jima (above) and Addis Ababa (below), Ethiopia. The solid bars coincide with El Nino years. The circles at the top of each histogram coincide with lunar perigee-syzygy-perihelion alignments. See Fig. 3 for locations of Jima and Addis Ababa.

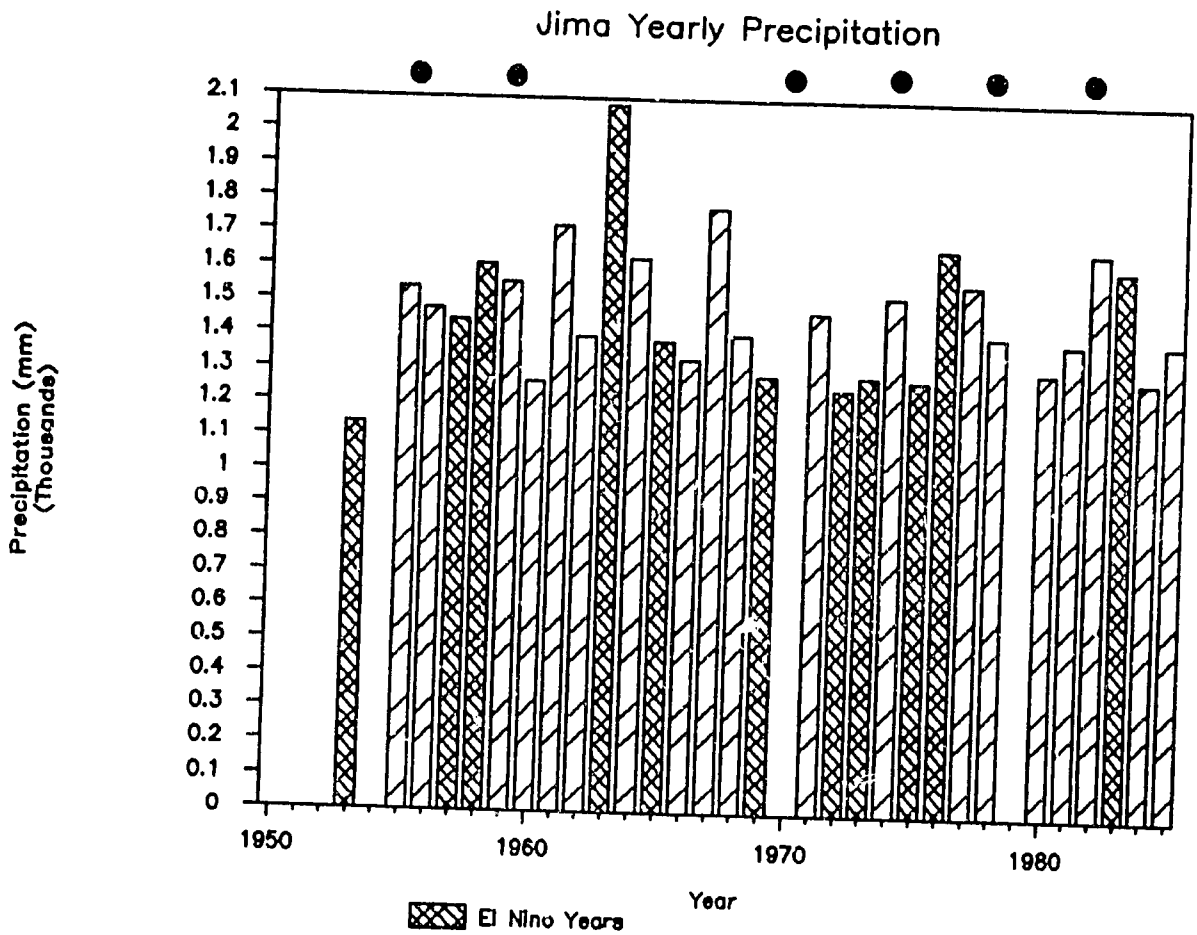
Jima Yearly Precipitation
Precipitation (mm) (Thousands)
2.1
2
1.9
1.8
1.7
1.6
1.5
1.4
1.3
1.2
1.1
1
0.9
0.8
0.7
0.6
0.5
0.4
0.3
0.2
0.1
0
1950
1960
1970
1980
Year
El Nino Years

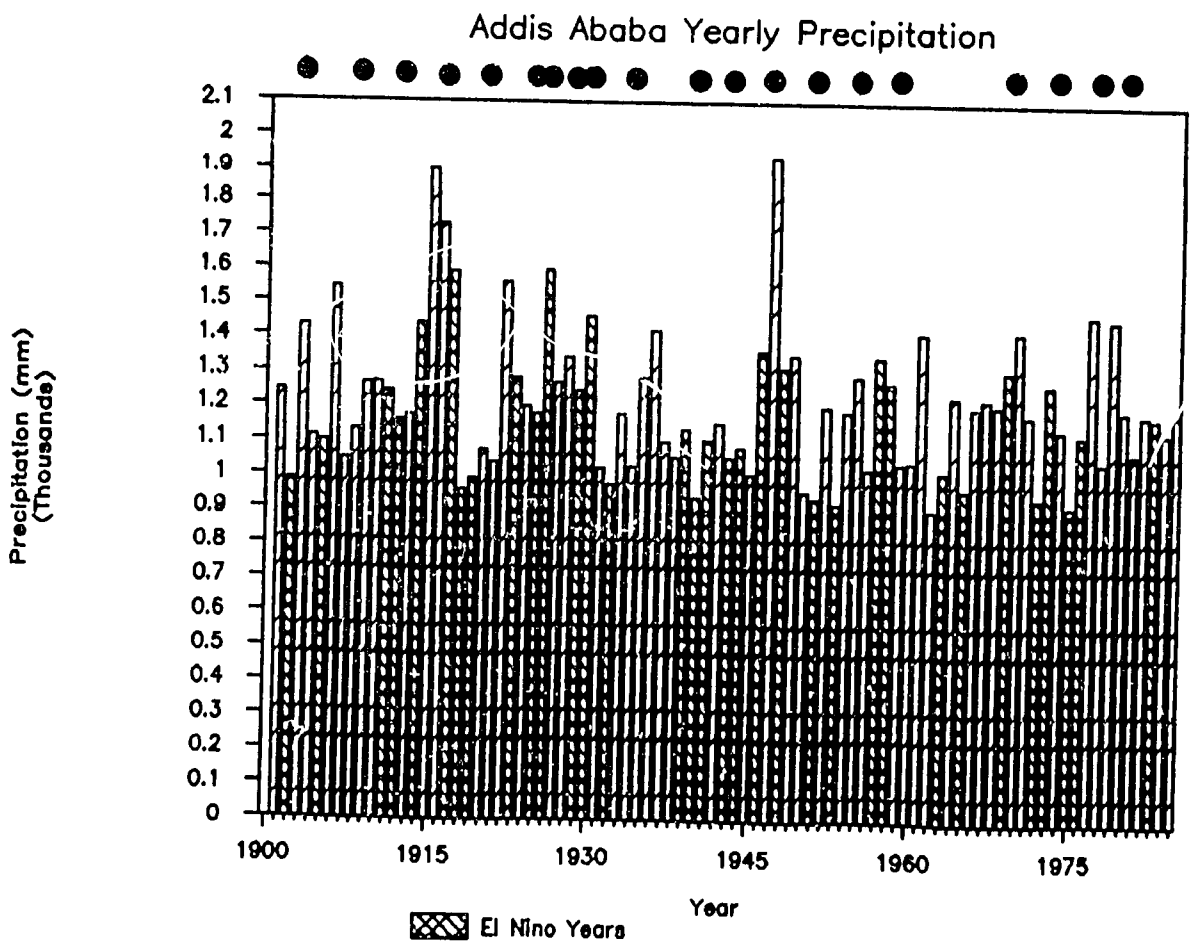
Addis Ababa Yearly Precipitation
Precipitation (mm) (Thousands)
2.1
2
1.9
1.8
1.7
1.6
1.5
1.4
1.3
1.2
1.1
1
0.9
0.8
0.7
0.6
0.5
0.4
0.3
0.2
0.1
0
1900
1915
1930
1945
1960
1975
Year
El Nino Years

Annual rainfall values that were averaged from various districts in Kenya suggests an inter-annual cyclicity near 3.5 years, although peaks near 2 and 5.5 years are also significant (Rodhe and Virji, 1976). The rainfall data suggests that the mean discharge of the Omo River is variable on an inter-annual time scale similar to that of the recurrence of ENSO events. The apparent impact of ENSO on East African climate, coupled with the coincidence of the mean time span represented by the Turkana laminations and ENSO, suggest that the light layers were formed during ENSO events or a closely spaced series of ENSO events. All of our piston cores over-penetrated the lake floor so, at present, there is no direct means of proving this hypothesis by comparison of the uppermost sediment record with historical weather data. A detailed sampling program of filtered water samples, time-series sediment trapping, and 3 m cores to recover the sediment/water interface is planned to further test the hypothesis.

Campbell et al. (1983) calculated that the monsoon rainfall for India responds strongly to 3.85 $\pm$ 0.1 and 20 $\pm$ 2 year periods. The lunar perigee-syzygy-perihelion cycle of about 4.0 years (Wood, 1986) is near the 3.85-year Indian monsoon cycle. The 20-year period is equivalent to the 18.6-year lunar nodal cycle, which is exhibited in other drought and flood proxy records (Currie and Fairbridge, 1985). Campbell et al. (1983) suggested that the advance of the monsoon "front" is modulated by tidal effects of the atmosphere. Wood (1986) has demonstrated the effects of these long term lunar cycles on oceanic tides and corresponding coastal flooding. Campbell et al. (1983) did not attempt to demonstrate the correspondence between the phase of the

lunar cycles and the magnitude of the monsoons. The Ethiopian rainfall data from both Jima and Addis Ababa do not appear to directly correspond to the lunar alignments (Fig. 38).

Calcareous laminations are also found in other modern and ancient lacustrine sediments. The modern examples are similar to the biologically modulated carbonate laminae in Lake Zurich (Kelts and Hsu, 1978) and temperature modulated carbonate laminae in Fayetteville Green Lake (Brunskill, 1969). The seasonal cycle dominates their sedimentation, with additional sources of sediment from, for example, spring runoff or diatom blooms. Ancient sequences of laminae are interpreted as seasonal events or non-glacial varves (e.g., Bradley, 1929; Olsen, 1986) although precise dating for the sections is usually absent. The results from Lake Turkana suggest calcareous laminae may not always result from seasonal processes. The sedimentary record needs closer examination before automatically assuming that laminations are seasonal. Processes influencing the formation of laminations occur on different time scales, and this may be most apparent when comparing laminations in low latitude versus high latitude lakes.

High-Resolution Paleoclimatology

Core LT84-8P was singled out for a detailed, high-resolution analysis for a number of reasons. First, this core contains the longest section of continuous laminations, through the upper 935 cm of the core, that are distinct and could be measured with the aid of a dissecting microscope. Second, the carbonate profile of core LT84-8P correlates well with, and is representative of, carbonate profiles in the other

cores from the north basin (Fig. 26 and 28). Finally, this core is the best dated core with five radiocarbon dates, which reveal a strong correlation in the age-depth relationship.

The carbonate profile is interpreted to reflect the variable discharge of the Omo River. Thus, it indicates a fluctuating lake level about a datum that is at or below the present lake level for most of the last 4,000 years (Fig. 39). The general trend of the profile is one of increasing lake level since 4,000 yr ago to the present day. The down-core fluctuations should be representative of the relative change in climate.

High carbonate zones (inferred low lake levels) occur from about 1.1 to 1.5 and 2.1 to 4.0 Ka assuming the best-fit linear interpolation of radiocarbon age versus depth for the core. The latter correlates to inferred low stands of Lakes Abhe (Gasse, 1977; Gasse and Street, 1978; Fontes et al., 1985) and Ziway-Shala (Gasse, 1980; Gillespie et al., 1983) in Ethiopia, and possibly to records of decreased glacial activity and inferred regional precipitation from a tarn lake on Mt. Kenya (Karlen, 1985) and inferred low stands of lakes in Rajasthan, India (Swain et al., 1983). The 1.1 to 1.5 Ka may correlate to radiocarbon studies of littoral deposits at Lake Abhe and the record from the tarn lake on Mt. Kenya. Minor inconsistencies exist in the exact timing of the lower lake levels from the various proxy records that may be due to either local climatic and hydrologic factors or problems inherent in comparing radiocarbon-dated records.

Two former high stands of lake level for Lake Turkana at 80 m above the 1976 level are well documented and radiocarbon dated (43 dates)

Fig. 39. Weight percent carbonate ($CaCO_3$) (left) and couplet thickness (right) vs. age for core LT84-8P. The age is calculated from the best-fit, linear interpolation of radiocarbon age vs. depth for core LT84-8P. The carbonate data were smoothed by a 3 point running average and cubic spline interpolation. The thickness data were smoothed by a 3 point running average. The vertical line represents the average value for each profile.

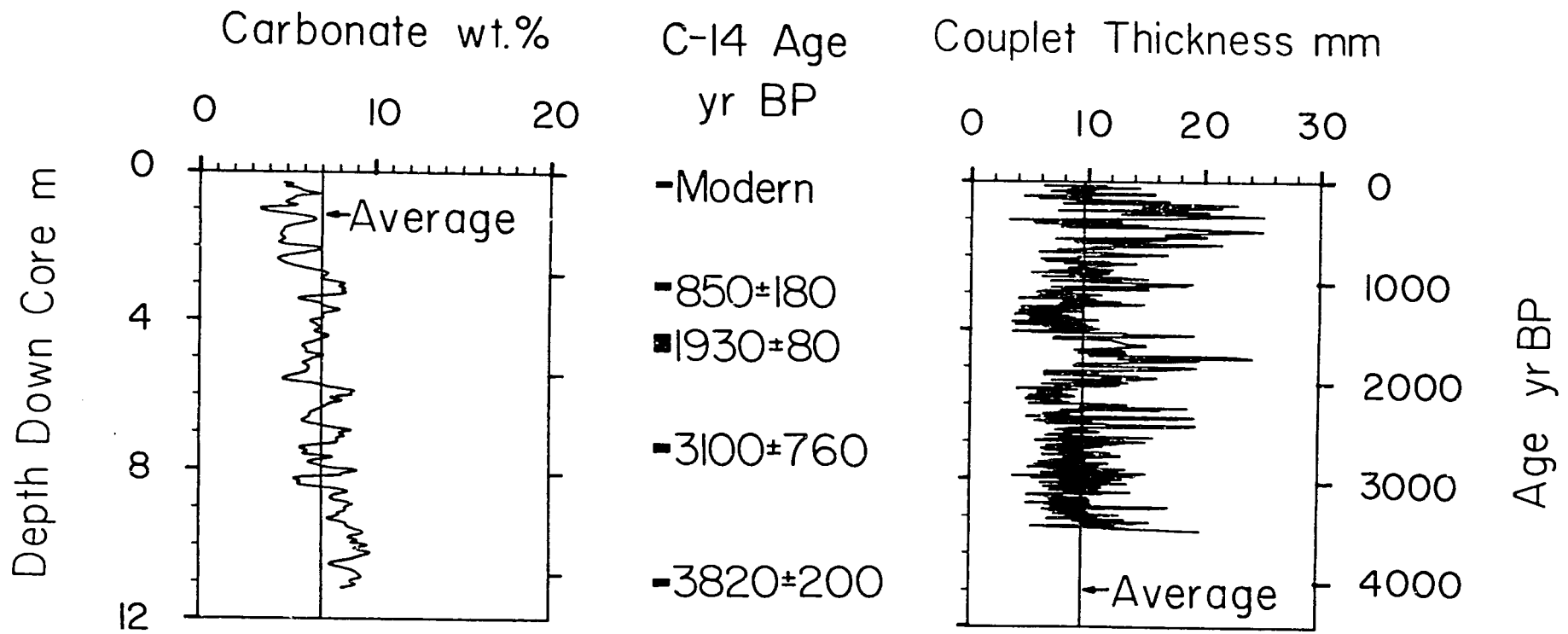
Carbonate wt.%
0
10
20
Average
Depth Down Core m
0
4
8
12
C-14 Age
yr BP
Modern
850±180
1930±80
3100±760
3820±200
Couplet Thickness mm
0
10
20
30
Average
0
1000
2000
3000
4000
Age yr BP

1181

between 10 and 7.5 Ka, and 6.0 and 4.2 Ka with a drop in lake level to 40 m above the 1976 level at approximately 4.0 Ka (Owen et al., 1982). Since then, the lake was at or near its present level based on 9 radiocarbon dates since 3.9 Ka. A previously reported high stand from 3.8 to 3.2 Ka is inconsistent with the results reported here, however, only 3 radiocarbon dates are the basis for this high stand. Butzer (1980) reports that these dates may be unreliable because bone apatite was analyzed from horizons of uncertain elevation. This previously reported high stand may correlate to a high stand in Lake Bogoria, but it was based on a single radiocarbon date from an exposed terrace in the basin, and the authors admit to a strong possibility of hydrothermal replacement of the sample (Tiercelin et al., 1981). The evidence presented here for a low stand starting at about 4.0 Ka is more consistent with the termination of the early Holocene pluvial period for Africa (e.g., Street and Grove, 1976, 1979), detailed records from other lakes in the region (see references above) and with accumulation times for sodium, chloride and total dissolved CO_2 that was calculated for Lake Turkana (Cerling, 1986). The synchronous nature of the inferred lake level record from the carbonate profiles and other proxy records from east Africa indicates a regional climatic change on a millennial time scale.

The down-core profile in couplet thickness in LT84-8P shows a weak negative correlation ($r = -0.51$) with the carbonate profile (Fig. 39). Depth intervals of relatively low concentrations of carbonate match relatively thicker couplets (e.g., 0.5 to 2.9 m and 4.0 to 5.6 m). The relationship is also revealed in the detailed analysis of the 56

laminae. The laminations are too faint to distinguish below 935 cm in the core. This depth corresponds to a period of high carbonate values and the erosional unconformity at LT84-5P. The inferred lower lake level may have allowed wave activity or bioturbation to disturb the laminations.

The possibility of cyclic variability in the fluctuations of both the carbonate and thickness profiles from LT84-8P was analyzed by a Fast Fourier Transformation (FFT) (Davis, 1986). The independent data sets underwent minimal massaging prior to FFT analysis. Both data sets were smoothed with a 3 point running average. A clamped cubic spline routine was used to interpolate a carbonate value for every centimeter down core. The best-fit linear trend was removed from both data sets, and the mean of each series was subtracted from the respective data points. Both data sets were fixed at 1024 points by padding 122 zeros to the end of the thickness data string and truncating 64 points from the end of the carbonate data string. This prepared the data sets for FFT analysis. The FFT of the carbonate data yielded harmonics in terms of depth intervals which were converted to time using the sedimentation rate of 0.27 cm/yr. The FFT of the thickness data yielded harmonics in terms of numbers of lamination couplets which were converted to time using the mean couplet thickness and mean sedimentation rate for the core. The Chi-square test determined the white noise, 95% confidence level for the resulting power spectrum.

Numerous spectral peaks were found to be significant and consistent between both power spectra (Fig. 40). These correspond to about 270, 200, 165 and 100 years. The thickness spectrum has additional peaks at

Fig. 40. Power spectra from Fast Fourier Transformations (FFT) of the LT84-8P carbonate (left) and thickness (right) data sets (see text for analytical details). The vertical line represents the 95% confidence limit. Significant peaks in the spectrum are identified by their periodicity in years.

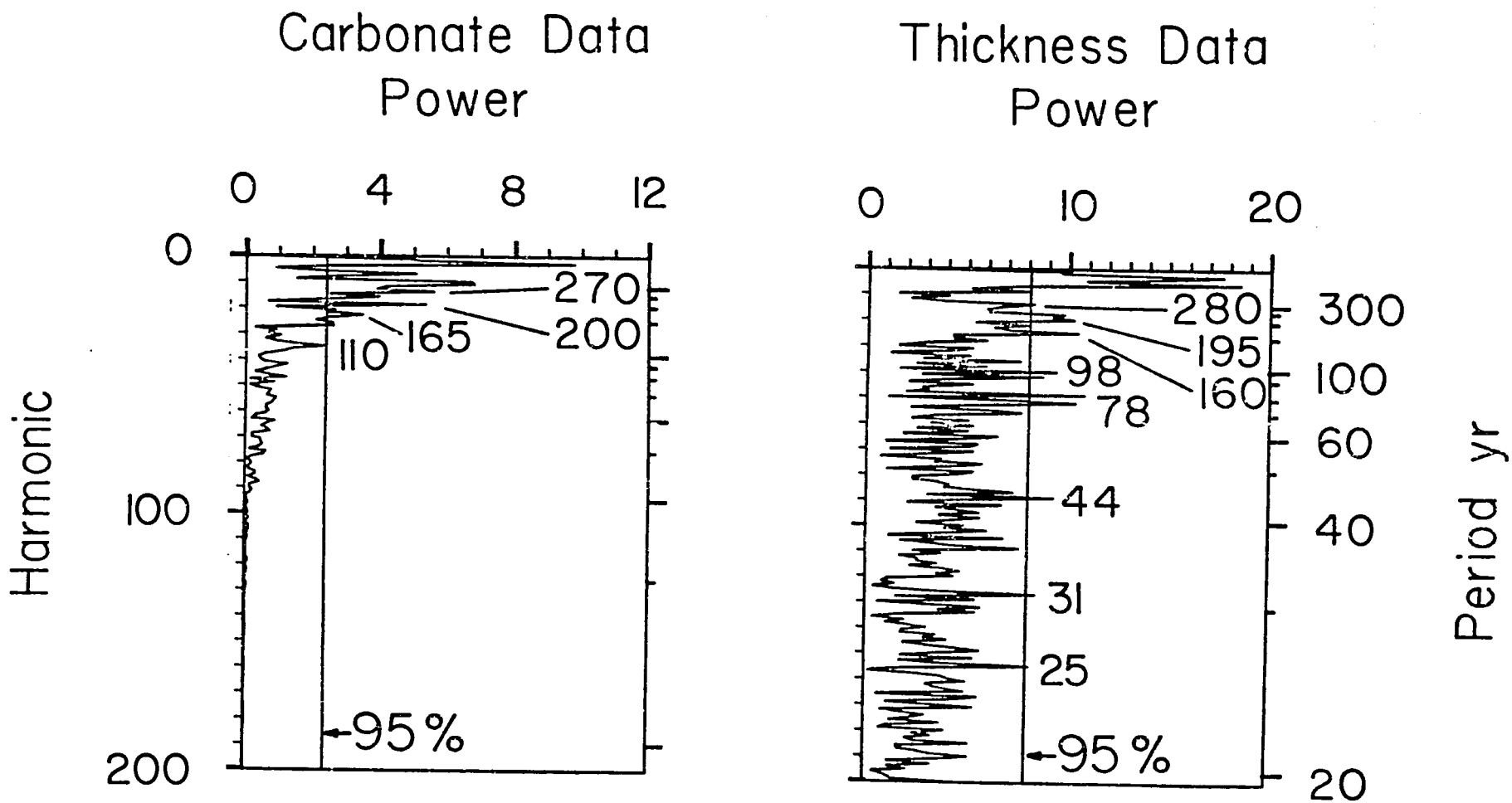
Carbonate Data
Power
0
4
8
12
0
100
200
Harmonic
270
200
165
110
95%
Thickness Data
Power
0
10
20
300
100
60
40
20
Period yr
280
195
160
98
78
44
31
25
95%

121a

78, 44, 31, and 25 years. The resolution of the data sets is not adequate to detect cycles less than approximately 20 years for the thickness data and 50 years for the carbonate data based on sample spacing and down-core averaging. The error associated with the value of these cycles, estimated by calculating the time span in years between successive harmonics, ranges from 1 year for the short cycles progressing logarithmically to 20 years for the longer cycles. In addition, the uncertainty of the sedimentation rate could shift the periods by about 10 percent.

The results indicate cyclic variability in the climate of the Ethiopian Plateau and the Turkana basin on a time scale of decades to centuries. The validity of the decade-to-century variability can be tested by analyzing the phase, persistence and correlation of the cycles. Each of the consistent cycles from the two LT84-8P data sets are in phase, i.e. the difference in phase averages 65° with a range of 50 to 85° (Appendix N). This suggests that each of the major periodicities for both records result from the same forcing mechanism.

FFT analysis of three, 512-point, sub-sets taken from the beginning, middle and end of the 1024-point, filtered and smoothed data sets provided similar spectral features (Appendix N). This suggests that the climatic variability is persistent through the last 4,000 years. Not all of the spectral features that were revealed by the 1024-pt data set were revealed by the analysis of each respective sub-set, however. Some of the lower frequency information was lost due to decreased resolution of the shorter data sets, and some of the higher frequency information was not above the 95% significance level, but was above background noise

and therefore included in the comparison.

Carbonate profiles from LT84-7P and 10P plus two sections of thickness data from 9P were also analyzed by the FFT. The new data sets underwent identical pre-analysis filtering prior to the FFT analysis as the respective carbonate and thickness data sets from LT84-8P, except that the length of the 9P data was set at 256 points. The harmonic axis from the carbonate data was converted to cm/cycle after the depth scales of LT84-7P and 10P were normalized to 8P, based on their carbonate profiles. The harmonic axis from the thickness data was converted to couplets/cycle. The power spectra indicate that many of the periodicities can be matched among the respective data sets of the four cores, suggesting a basin wide response to climatic variability (Fig. 41) (Appendix N). Some of the peaks are not above the 95% confidence limit, but are above background and were included in the comparison. The LT84-9P data sets were too short to reveal the longer periods but did reveal that a smaller period may co-exist in both 9P records at about 5.1 couplets/cycle. This corresponds to a period of approximately 20 years. The LT84-7P and 8P power spectra from the carbonate data indicate that a longer period co-exists in both records at about 93 cm/cycle corresponding to a period of 345 years.

The results from analyzing the sediments of Lake Turkana indicate that variations on a time scale of millennia, based on stratigraphic analysis, to centuries to decades, based on time-series analysis, down to inter-annual events, based on lamination analysis, exist in the paleo-hydrology of the basin and the inferred monsoonal rainfall over the Ethiopian Plateau. Numerous proxy records from throughout the world

Fig. 41. Power spectra from Fast Fourier Transformations (FFT) of LT84 -8P carbonate (left, top) and thickness (right, top) data set as in Fig. 40, in comparison to carbonate spectra of LT84 - 7P and LT84 - 10P and thickness spectra of LT84 - 9P. The horizontal line represents the 95% confidence limit. Spectral peaks are identified by their periodicities in cm/cycle for carbonate data (depth normalized to LT84 - 8P) and couplets/cycle for thickness data.

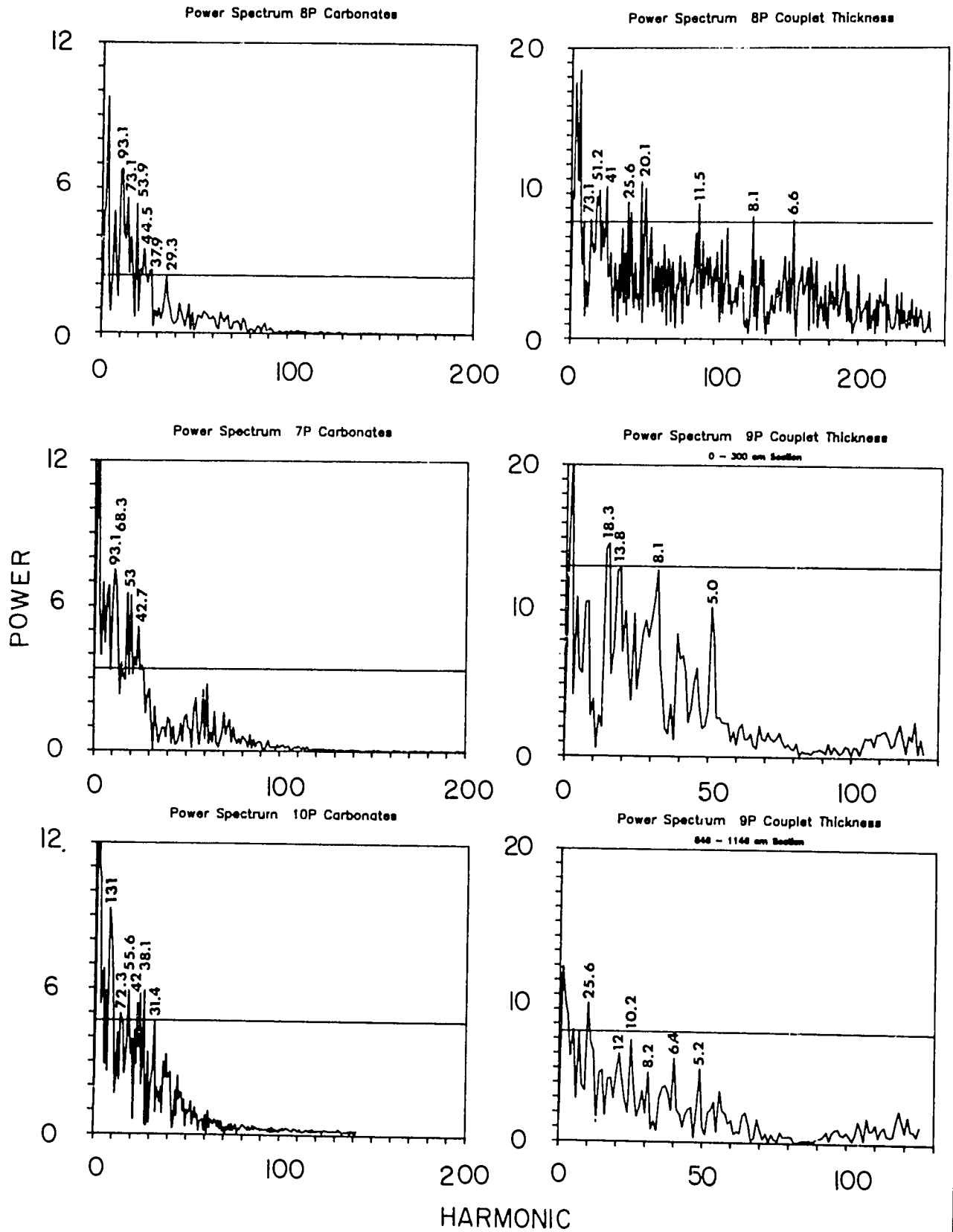
Power Spectrum 8P Carbonates
93.1
73.1
53.9
44.5
37.9
29.3
Power Spectrum 8P Couplet Thickness
73.1
51.2
41
25.6
20.1
11.5
8.1
6.6
Power Spectrum 7P Carbonates
93.1
68.3
53
42.7
Power Spectrum 9P Couplet Thickness
0 – 300 cm Section
18.3
13.8
8.1
5.0
Power Spectrum 10P Carbonates
131
72.3
55.6
42
38.1
31.4
Power Spectrum 9P Couplet Thickness
848 – 1148 cm Section
25.6
12
10.2
8.2
6.4
5.2
POWER
HARMONIC

174a

reveal 11, 18.6, 22 and other short-term periodicities (Quinn et al., 1978; Campbell et al., 1983; Crowley, 1983; Morner and Karlen, 1984; Currie and Fairbridge, 1985). The resolution for the data sets presented here is not adequate to detect these shorter cycles, except for a cycle near 20 years.

Longer periodicities of 31, 45, 78, 181 and 290 years are also observed in various proxy records. For example, the Nile River flood data, compiled since 622 AD, reveals a significant periodicity at 77 years (Hameed, 1984), and an inferred Senegal River discharge record reveals fluctuations on a 31-year average for the past century (Faure and Gac, 1981). The remaining periodicities were observed in proxy records that are not located on the African continent. For example, Holocene Hudson Bay beach ridges reveal a 45-year periodicity (Fairbridge and Hillaire-Marcel, 1977), δO-18 profiles for the last millennium from the Camp Century, Greenland Ice Core reveals periodicities of 78 and 181 years (Johnsen et al., 1970), and the varved Elatina Formation, consisting of about 20,000 varves, in Australia reveals periodicities of 145, 290 and possible 90 years (Williams, 1981). The shorter term (< 25 year) periodicities, that were revealed by these examples, were excluded from this list. All of the records, however, contain just one or two of these cycles, and most are of much shorter duration than the Turkana sediment record. The longer periodicities presented here are rarely detected due to the dearth of continuous and extremely long records that have adequate resolution.

The nature of the forcing mechanism behind the decade-to-century climatic cycles is unknown. Determining the mechanism is beyond the

scope of this dissertation. A unifying mechanism is suggested by Fairbridge (1984). Various orbital and solar parameters match many of the climatic periods reported here: for example the 78-year period may correspond to the 79.4-year "Gleissburg" Solar cycle. The 44-year period may correspond to the 44.48-year "Double-Hale" Solar cycle or the 45.387-year Uranus/Saturn Lap cycle. The 20-year period may correspond to the 22.24-year Heliomagnetic "Hale" Solar cycle, or the 19.857 Jupiter/Saturn Lap cycle, or the 18.6 Lunar Nodal cycle (Fairbridge, 1983; Fairbridge, 1984; Wood, 1986). The 31-year period could be driven by the 31.007-year Lunar Perigee-Syzygy cycle (Wood, 1986) or the 11.065/22.2 sunspot beat (Landscheidt, 1983). The 178-year "King-Hele" Solar cycle (Fairbridge and Hillaire-Marcel, 1977) and 177.92-year Sun/Jupiter Repeat cycle (Fairbridge, 1983) are within the error range of the 170-year period reported here, and similarly the observed 345-year period is in range of the 370.66 Minimum Sunspot cycle (Fairbridge, 1983). Still other correlations can be made, for example the 25-year period and the 270-year period reported here with the 24-year Venus/Jupiter Beat frequency and the 271-year Venus/Moon cycle, respectively (Fairbridge, pers. commun.). Landscheidt (1983) suggests that the solar cycles are due to the planetary stresses applied to the sun. The solar cycles are related to changes in the torque that influence the sun resulting from the sun's oscillatory motion about the center of mass of the solar system. Atmospheric tides may occur due to the planetary motions and hypothetically may induce the cyclic nature of the climate. These correlations are highly speculative at this time, however, and more work is required to determine if these climatic cycles

result from orbital perturbations (Pittock, 1983). Nevertheless, the results show some promise for developing a climatic forecasting capability on a time scale of decades to centuries for sub-Saharan east Africa.

CONCLUSIONS

High-resolution seismic profiles and sediments recovered from Lake Turkana indicate that the lake responds to the overwhelming influence of the Omo River. The predominant pattern of sedimentation is one of simple and rapid basin infilling. The seismic profiles suggest an abundance of gas (probably methane) in the Holocene sediments, which is also indicated by sediment analyses. The highest concentrations of gas are near the major rivers and deepest basins where sedimentation rates are relatively high. A major erosional unconformity revealed in the seismic profiles indicates that lake level was about 60 m lower than the present day, probably just prior to 10 Ka. At this depth, the north and south basins would be isolated lakes.

Sedimentation rates are roughly 0.5 cm/yr, based on the best-fit linear interpolation of the radiocarbon age versus depth in two cores. These rates are at least an order of magnitude larger than the other large lakes of the world, and two to three orders of magnitude larger than the deep sea. The fast sedimentation rates makes Lake Turkana an excellent site for high-resolution paleoclimatic study.

The total organic carbon (TOC) concentrations of the profundal sediments averaged about 1%. The bulk of the organic matter has an autochthonous source. The TOC values are lower than other large East African lakes, however, the mass accumulation rates of carbon are similar for all the basins. The low TOC concentrations in Lake Turkana do not reflect low productivity, but the dilution by non-organic detrital material, and less importantly to aerobic degradation before

burial and the lack of allochthonous organic material. The down-core fluctuations in TOC content coupled with C/N ratios reflect changes in the proximity of the paleo-shoreline, otherwise TOC fluctuations may reflect variable productivity or sedimentation rates within each basin.

The carbonate in the sediments is composed of authigenic low-Mg calcite (micrite) and ostracod tests. Stable isotope geochemistry and other analyses suggest that the micrite is an authigenic precipitate from the surface waters. The increase in the concentration of carbonate in the sediments with increasing distance from the Omo River reflects decreased dilution of the carbonates by detrital input from the Omo River. The carbonate profiles are highly correlatable in the north basin, but the correlation does not match the profiles from the south basin. This suggests that the basins may be sedimentologically independent. The down-core fluctuations in carbonate are interpreted to reflect the paleosalinity of the basin with higher carbonate concentrations corresponding to higher salinities or lower lake levels.

The light/dark couplets in the sediments are interpreted to be a high-resolution analog of the carbonate stratigraphy. The time represented by each couplet is, on average, about 4 years, although the recurrence interval may vary between 2 and 10 years. The laminations are not the result of the seasonal flooding of the Omo River, but are related to the inter-annual variation in sediment discharge. Omo River discharge data are not available for analysis but an inter-annual variability in rainfall is indicated for the Ethiopian highlands. The response of the inter-annual variation may, in part, be associated with the El Nino / Southern Oscillation Event.

The carbonate content and thickness of light/dark couplets fluctuate down core. The fluctuations are interpreted to reflect past variations in sediment discharge with high discharge associated with lower carbonate content and thicker couplets. On a millennial time scale, the down-core profiles in the central and northern parts of the lake provide a consistent history of variable but gradually wetter conditions from 4,000 years ago to the present day. This is consistent with records from many other lakes in East Africa. Time-series analysis reveals a number of significant periodicities that are in phase and consistent between the two independent parameters in core LT84-8P. These correspond to about 270, 200, 165 and 100 years. The thickness spectra indicate additional periodicities at about 75, 44, 31, 25 and possibly 20 years. Many of these are persistent through the last 4,000 years and are observable in other cores in the north basin. The data suggest that the Ethiopian monsoon is variable on a time scale of decades to centuries, and may be driven by cyclic orbital behavior of the solar system.

REFERENCES

Abell, P.I., 1982, Paleoclimates at Lake Turkana, Kenya, from oxygen isotope ratios of gastropod shells. Nature 297:32[illegible]-323.

Adamson, D.A.F., F. Gasse, F.A. Street and M.A.J. Williams, 1980, Late Quaternary history of the Nile. Nature 287:50-55.

Anderson, R.Y., 1964, Varve calibration of stratificaton. Bulletin Kansas State Geological Survey 169:1-24.

Anderson, R.Y., 1986, The varve microcosm: propagator of cyclic bedding. Paleoceanography 1:37[illegible]-382.

Anderson, R.Y. and D.W. Kirkland, 1969, Paleoecology of the Rita Blanca Lake area. Memoirs Geological Society America 113:141-157.

Anderson, R.Y. and L.H. Koopmans, 1963, Harmonic analysis of varve time-series. Journal of Geophysical Research 68: 877-893.

Anthony, R.S., 1977, Iron-rich rhythmically-laminated sediments in Lake of the Clouds, Minnesota. Limnology and Oceanography 22:45-54.

Appleby, P.G. and F. Oldfield, 1978, The calculation of Lead-210 dates assuming a constant rate of supply of unsupported ^{210}Pb to the sediment. Catena 5:1-8.

Arambourg, C., 1933, Mammiferes Miocene du Turkana. Ann. de Paleo. 22:123-146.

Arambourg, C., 1935, 1944, 1948, Mission scientifique de l'Omo (1932 - 1933). Mus. Nat. d'Histoire Naturelle, Paris. Fasc. 1-3. 1-59, 60-230, 231-562.

Arthur, M.A. and R.E. Garrison, 1986, Cyclicity in the Milankovitch band through geologic time: an introduction. Paleoceanography 1:369-372.

Baker, B.H., P.A. Mohr and L.A.J. Williams, 1972, Geology of the Eastern Rift System of Africa. Geological Society of America Special Paper, 136, 67p.

Barton, C.E., D.K. Solomon, J.R. Bowman, T.E. Cerling and M.D. Sayer, 1987, Chloride budjets in transient lakes: Lakes Baringo, Naivasha, and Turkana. Limnology and Oceanography 32:745-751.

Bathurst, R.G.C., 1975, Carbonate sediments and their diagenesis. Elsevier, Amsterdam 658p.

Beadle, L.C., 1981, The inland waters of tropical Africa. Longman, New York 475p.

Behrensmeyer, A.K., 1976, Lothagam, Kanapoi, and Ekora: A general summary of stratigraphy and fauna. In: Y. Coppens et al. (eds.) Earliet man and environments in the Lake Rudolf Basin. Univ Chicago Press, Chicago 163-170.

Berger, A.L., J. Imbrie, J. Hays, G. Kukla and B. Salyzman (eds.) 1984 Milankovitch and Climate. Reidel, Boston. 2 vols.

Berlage, H.P., 1967, The southern oscillation and world weather. K. Ned. Meteorol. Inst. Meded. Verh. 88: 152pp.

Bishop, Walker W. (ed.) 1978, Geological Background to Fossil Man, Scottish Academic Press. Edinburgh.

Blatt, H., G. Middleton and R. Murray, 1980, Origin of sedimentary rocks. Prentice Hall, Englewood Cliffs 782pp.

Bonnifille, R., 1976, Implications of pollen assemblages from the Koobi Fora Formation, East Rudolf, Kenya. Nature 264:403-407.

Bradley, R.S., 1985, Quaternary Paleoclimatology. Allen and Unwin, Boston, 472 p.

Bradley, R.S., H.F. Diaz, G.N. Kiladis and J.K. Eischeid, 1987, ENSO signal in continental temperature and precipitation records. Nature 327:497-501.

Bradley, W.H., 1929, The varves and climate of the Green River Epoc. U.S. Geological Survey Professional Paper 158:87-110.

Brown, F.H., J. Harris, R. Leakey and A. Walker, 1985, Early Homo erectus skeletons from west Lake Turkana, Kenya. Nature 316:788-792.

Brunskill, G.J., 1969, Fayetteville Green Lake, New York. II. Precipitation and sedimentation of calcite in a meromictic lake with laminated sediments. Limnology and Oceanography 14:830-847.

Burgess, C.F., 1985, The structural and stratigraphic evolution of Lake Tanganyika: a case study of continental rifting. M.S. Thesis, Duke University, Durham (unpublished).

Butzer, K.W., 1971a, The lower Omo Basin: Geology, fauna and hominids of the Plio-Pleostocene formations. Naturwissenschaften 58:7-16.

Butzer, K.W., 1971b, Recent history of an Ethiopian Delta. Univ Chicago Press, Geography Dept Research Paper 136, Chicago.

Butzer, K.W., 1976, The Mursi, Nkalabong, and Kibish Formations, lower Omo Basin, Ethiopia. In: Y. Coppens et al. (eds.) Earliet man and environments in the Lake Rudolf Basin. Univ Chicago Press, Chicago

12-23.

Butzer, K.W., 1980, The Holocene lake plain of North Rudolf, East Africa. Physical Geography 1:42-58.

Butzer, K.W., G.L. Isaac, J.L. Richardson and C. Washbourn-Kamau, 1972, Radiocarbon dating of East African Lake Levels. Science 175:1069-1076.

Cambridge Expedition: 1932-1933, 1932, Scientific results of the Cambridge Expedition to the East African Lakes, 1930 - 1931. No. 1 - 14. Journel Linn. Soc. Zool. 38: 99-362.

Campbell, W.H., J.B. Blechman and R.A. Bryson, 1983, Long-period tidal forcing of Indian monsoon rainfall: A hypothesis. Journal of Climate and Applied Meteorology 22:287-296.

Cane, M.A., S.E. Zebiak and S.C. Dolan, 1986, Experimentasl forecasts of El Nino. Nature 321:827-832.

Cerling, T.E., 1979, Paleochemistry of Plio-Pleistocene Lake Turkana, Kenya. Palaeogeography, Palaeoclimatology, Palaeoecology 27:247-286.

Cerling, T.E., 1986, A mass-balance approach to basin sedimentation: Constraints on the recent history of the Turkana Basin. Palaeogeography, Palaeoclimatology, Palaeoecology 43:129-151.

Cerling, T.E., T.C. Johnson, J.D. Halfman and G.S. Lister, 1985, Pore water chemistry of an alkaline rift valley lake: Lake Turkana, Kenya. Geological Society of America, Fall annual meeting abstracts.

Chivas, A.R., P. De Deckker and J.M.G. Shelley, 1985, Strontium content of ostracods indicates lacustrine paleosalinity. Nature 316:251-253.

Chivas, A.R., P. De Deckker and J.M.G. Shelley, 1986, Magnesium content of non-marine ostracods shells: A new palaeosalinometer and palaeothermometer. Palaeogeography, Palaeoclimatology, Palaeoecology 54:43-61.

Cohen, A.S., 1981, Paleolimnological research at Lake Turkana, Kenya. Palaeoecology of Africa 13:61-82.

Cohen, A.S., 1982, Ecological and paleoecological aspects of the rift valley lakes of East Africa. Ph.D. dissertation, U. California, Davis.

Cohen, A.S., 1984, Effect of zoobenthic standing crop on laminae preservation in tropical lake sediment, Lake Turkana, East Africa. Journal of Paleontology 58:499-510.

Cohen, A.S., D.S. Ferguson, P.M. Gram, S.L. Hubler, and K.W. Sims, 1986, The distribution of coarse-grained sediments in modern Lake Turkana, Kenya: Implications for clastic sedimentation models of rift lakes. In: L.E. Frostick et al. (eds.) Sedimentation in the African Rifts. Geological Society of London Special Publication 25:121-133.

Coppens, Y., F.C. Howell, G.L. Isaac, and R.E. Leakey (eds) 1976, Earliest man and environments in the Lake Rudolf Basin. Univ. of Chicago Press, Chicago, 615 pg.

Crossley, R. and R.B. Owen, 1987, Sand turbidites and organic-rich diatomaceous muds from Lake Malawi, Central Africa. In: K. Kelts et al. (eds.) Lacustrine Petroleum Source Rocks. Geological Society of London Special Publication (in press).

Crowley, K.D., C.E. Duchon and J. Rhi, 1986, Climate record in varved sediments of the Eocene Green River Formation. Journal of Geophysical Research 91:8637-8647.

Crowley, T.J., 1983, The geological record of climate change. Reviews of Geophysics and Space Physics 21:828-877.

Currie, R.G. and R.W. Fairbridge, 1985, Periodic 18.6-year and cyclic 11-year induced drought and flood in northeastern China and some global implications. Quaternary Science Reviews 4:109-134.

Curtis, P.K., 1987, The structure and petrology of Central Island, Lake Turkana, Kenya. M.S. Thesis, Duke University, Durham (unpublished).

Curtis, P.K. and J.A. Karson, 1984, Quaternary volcanism and tectonics, Lake Turkana, east African Rift. EOS (American Geophysical Union Transactions) 65:1116.

Damuth, J.E., 1980, Use of high frequency (3.5 - 12 kHz) echograms in the study of near bottom sedimentation processes in the deep-sea: A review. Marine Geology 38:51-75.

Dansgaard, W.S., J. Johnsen, H.B. Clausen, and C.C. Langway, 1971, Climatic record revealed by the Camp Centruy ice core. In: K.K. Turekian (ed.) The Late Cenezoic Ice Ages. Yale Univ. Press, New Haven, 37-56.

Dangaard, W., H.B. Clausen, N. Gundestrup, C.U. Hammer, S.F. Johnsen, P.M. Kristinsdottir and N. Reeh, 1982, A new Greenland deep ice core. Science 218:1273-1277.

Davis, J.C., 1985, Statistics and data analysis in geology. Wiley, New York 646 pg.

de Geer, G., 1912, A geochronology of the last 12,000 years. 11th International Geological Congress (1910), Stockholm 1:241-253.

Dean, W.E., 1981, Carbonate minerals and organic matter in sediments of modern north temperate hard-water lakes. In: F.G. Ethridge and R.M. Flores (eds.) Recent and ancient nonmarine depostional environments: Models for exploration. Society of Economic Paleontologists and Mineralogists 31:213-231.

Dean, W.E., J.P. Bradbury, R.Y. Anderson and C.W. Barnosky, 1984, The variability of Holocene climate change: Evidence from varved lake sediments. Science 226: 1191-1194.

Dean, W.E. and J.V. Gardner, 1986, Milankovitch cycles in Neogene Deep-Sea. Paleoceanography 1:539-554.

Degens, E.T. R.P. von Herzen, H. Wong, W.G. Deuser and H.W. Jannasch, 1973, Lake Kivu: Structure, Chemistry and Biology of an east African Lake. Geol. Rdsch. 61: 245-277.

Delmas, R.J., J.M. Ascencio and M. Legrand, 1980, Polar ice evidenve that atmospheric CO_2 20,000 yr BP was 50% of present. Nature 284:155-157.

DeMaster, D.J., 1979, The marine budgets of silica and Si 2. PhD. Thesis, Yale University. (unpublished).

Dunkelman, T.J., 1986, The structural and stratigraphic evolution of Lake Turkana, Kenya, as deduced from multichannel reflection data. M.S. Thesis, Duke University, Durham (unpublished).

East African Meteorological Department, 1975, Climatological records for East Africa. East Africa Community, Nairobi, 92p.

Edmondson, W.J. and D.E. Allison, 1970, Recording densiometry of X-radiographs for the study of cryptic laminations in the sediment of Lake Washington. Limnology and Oceanography 15:138-144.

Fairbridge, R.W., 1983, The Pleisotocene-Holocene boundary. Quaternary Science Reviews 1:215-244.

Fairbridge, R.W., 1984, Planetary periodicities and terrestrial climate stress. In: N.A. Morner and W. Karlen (eds.) Climatic changes on a yearly to millennial basis. D. Reidel, Boston 509-520.

Fairbridge, R.W. and C. Hillaire-Marcel, 1977, An 8,000-yr palaeoclimatic record of the 'Double-Hale' 45-yr solar cycle. Nature 268:413-416.

Faure, H. and J.Y. Gac, 1981, Will the sahelian drought end in 1985? Nature 291:475-478.

Ferguson, A.J.D. and B.J. Harbott, 1982, Geographical, physical and chemical aspects of Lake Turkana. In: A.J. Hopson (ed.) Lake Turkana: A report on the findings of the Lake Turkana Project, 1972 - 1975. Overseas Development Administration, London. 1-107.

Fisher, A.G., 1986, Climatic rhythms recorded in strata. Annual Review of Earth and Planetary Sciences 14:351-376.

Flohn H. and T. Burkhardt, 1985, Nile Runoff at Aswan and Lake Victoria: A case of discontinuous climate time series. In: Kuhn (ed.) Climate and paleoclimate of lakes, rivers and glaciers. Universitatsverlag Wagner, Innbruck, 125-130.

Folland, C.K., D.E. Parker and F.E. Kates, 1984, World-wide marine temperature fluctuations 1856-1981, Nature 310: 670-673.

Folland, C.K., T.N. Palmer and D.E. Parker, 1986, Sahel rainfall and worldwide sea temperatures, 1901-85. Nature 320:602-607.

Fontes, J.C., F. Gasse, Y. Callot and J.C. Plaziat, 1985, Freshwater to marine like environments from Holocene lakes in northern Sahara. Nature 317:608-610.

Freidli, H., H. Lotscher, H. Oeschger, U. Siegenthaler and B. Stauffer, 1986, Ice core record of the $^{13}C/^{12}C$ ratio of atmosheric CO_2 in the past two centuries. Nature 324:237-238.

Freidman, I. and J.R. O'Neil, 1977, Compilation of stable isotope fractionation factors of geochemical interest. Data of Geochemistry, 6th edition, U.S. Geological Survey Professional Paper 440-KK KK1-KK12.

Fritts, H.C., G.R. Lofgren and G.A. Gordon, 1979, Variations in climate since 1602 as reconstructed from tree rings. Quaternary Research 12:18-46.

Fuchs, V.E., 1934, The geological work of the Cambridge Expedition to the East African Lakes, 1930 - 1931. Geol. Mag. 71:97-112.

Fuchs, V.E., 1935, The Lake Rudolf Rift Valley Expedition, 1934. Geogr. J. 86:114-142.

Fuchs, V.E., 1939, The geologic history of the Lake Rudolf Basin, Kenyan Colony. Phil. Trans. Roy. Soc. 229:219-274.

Gabriel, G.W. and J.L. Aronson, 1987, Chow Bahir rift: A "failed" rift in southern Ethiopia. Geology 15:430-433.

Gasse, F., 1977, Evolution of Lake Abhe (Ethiopia and TFAI), from 70,000 b.p. Nature 265:42-45.

Gasse, F., 1980, Late Quaternary changes in lake levels and diatom

assemblages on the southeastern margin of the Sahara. Palaeoecology of Africa 12:333-350.

Gasse, F. and F.A. Street, 1978, Late Quaternary lake-level fluctuations and environments of the northern Rift Valley and Afar region (Ethiopia and Djibouti). Palaeogeography, Palaeoclimatology, Palaeoecology 24:279-325.

Gasse, F., J.F. Talling and P. Kilham, 1983, Diatom assemblages in East Africa: Classification, distribution and ecology. Rev. Hydrobiol. trop. 16:3-34.

Gillespie, R., F.A. Street-Perrott and R. Switsur, 1983, Post-glacial arid episodes in Ethiopia - implications for climatic prediction. Nature 306:680-683.

Griffiths, J.F., 1972, Climates in Africa, Elsevier, New York, 607p.

Hakanson, L. and M. Jansson, 1983, Principles of lake sedimentology. Springer Verlag, New York, 315pg.

Halfman, J.D., 1982, Textural analysis of lacustrine contourites. Masters Thesis, University of Minnesota. (unpublished).

Hameed, S., 1984, Fourier analysis of Nile flood levels. Geophysical Research Letters 1:843-845.

Hamilton, A.C., 1982, Environmental history of East Africa. Academic Press, New York, 328p.

Hammer, C.U., H.B. Clausen and W. Dansgaard, 1980, Greenland ice sheet evidence of post-glacial volcanism and its climatic impact. Nature 288:230-235.

Harbott, B.J., 1982, Studies on algal dynamics and primary productivity in Lake Turkana. In: A.J. Hopson (ed.) Lake Turkana: A report on the findings of the Lake Turkana Project, 1972 - 1975. Overseas Development Administration, London. 108-161.

Hassan, F., 1981, Historic Nile floods and their implications for climatic change. Science 212:1142-1145.

Hastenrath, S., 1985, A review of Pleistocene to Holocene glacier variations in the tropics. In: M. Kuhn (ed.) Climate and paleoclimate of lakes, rivers and glaciers. Universitatsverlag Wagner, Innsbruck 183-194.

Hay, R., 1976, Geology of the Olduvi Gourge. Univ California Press, Berkeley 203p.

Hays, J.D., J. Imbrie and N.J. Shackleton, 1976, Variations in the earth's orbit: pacemaker of the ice ages. Science 194:1121-1132.

Hecky, R.E. and E.T. Degens, 1973, Late Pleistocene-Holocene chemical stratigraphy and paleolimnology of the rift valley lakes of central Africa. Technical Report, Woods Hole Oceanograpphic Instistute 93p.

Hecky, R.E. and P. Kilham, 1973, Diatoms in alkaline, saline lakes: Ecology and geochemical implications. Limnology and Oceanography 18:53-71.

Hedges, J.I. and J.H. Stern, 1984, Carbon and Nitrogen determinations of carbonate-containing solids. Limnology and Oceanography 29: 657-663.

Herdendorf, C.E., 1982, Large lakes of the world. Journal of Great Lakes Research 8:379-412.

Hopson, A.J. (ed.) 1982, Lake Turkana: A report on the findings of the Lake Turkana Project, 1972 - 1975. 6 vols. Overseas Devopment Adminstration, London. 1616p.

Hopson, A.J. and J. Hopson, 1982, The fishes of Lake Turkana with a description of three new species. In: A.J. Hopson (ed.) Lake Turkana: A report on the findings of the Lake Turkana Project, 1972 - 1975. Overseas Development Administration, London. 280-347.

Imbrie, J., J.D. Hays, D.G. Martinson, A. McIntyre, A.C. Mix, J.J. Morely, N.G. Pisias, W.L. Prell and N.J.Shackleton, 1984, The orbital theory of Pleistocene climate: Support from a revised chronology of the marine ^{18}O record. In: A.L. Berger et al. (eds.) Milankovitch and Climate. Reidel, Boston 269-306.

Irwin, H., C. Curtis and M. Coleman, 1977, Isotopic evidence for source of diagenetic carbonates formed during burial of organic-rich sediments. Nature 269:209-213.

Johnsen, S.J., W. Dansgaard, H.B. Clausen and C.C. Langway, 1970, Climatic oscillations 1200 - 2000 AD. Nature 227:482-483.

Johnson, T.C., 1980, Late-glacial and postglacial sedimentation in Lake Superior based on seismic reflection profiles. Quaternary Research 13:380-391.

Johnson, T.C., 1984, Sedimentation in large lakes. Annual reviews of Earth and Planetary Science 12:179-204.

Johnson, T.C., J.E. Evans and S.J. Eisenreich, 1982, Total organic carbon in Lake Superior sediments: comaprisons with hemipelagic and pelagic marine environments. Limnology and Oceanography 27:481-491.

Johnson, T.C. and J. Fields, 1984, Paleomagnetic dating of post glacial sediments, offshore Lake Superior, Minnesota-Wisconsin, U.S.A.

Chemical Geology 44: 253-265.

Johnson, T.C., J.D. Halfman, W.H. Busch and R.D. Flood, 1984, Effects of bottom currents and fish on sedimentation in a deep-water, lacustrine environment. Geological Society of America, Bulletin 95:1425-1436.

Johnson, T.C., J.D. Halfman, B.R. Rosendahl and G.S. Lister, 1987, Climatic and tectonic effects on sedimentation in a rift valley lake: Evidence from Lake Turkana, Kenya. Geological Society of America, Bulletin 98:439-447.

Jones, G.A. and P. Kaiters, 1983, A vacuum-gasometric technique for rapid and precise analysis of calcium carbonate in sediments and soils. Journal of Sedimentary Petrology 53: 655-660.

Jones, P.D., T.M.L. Wigley and P.B. Wright, 1986, Global temperature variations between 1861 and 1984. Nature 322:430-434.

Karlen, W., 1985, Glacier and climate fluctuations on Mount Kenya, East Africa. In: M. Kuhn (ed.) Climate and paleoclimate of lakes, rivers and glaciers. Universitatsverlag Wagner, Innsbruck 195-201.

Kelts, K. and K.J. Hsu, 1978, Freshwater carbonate sedimentation. In: A. Lerman (ed.) Lakes: Geology, Chemistry, Physics. Springer Verlag, New York 295-323.

Kelts, K., K. Chilardi, R. Hofmann and U. Briegel, 1984, The Limnolgy-ETH Coring System. Technical Report. ETH-Z, Zurich.

Kempe, A.L.W., C.I. Dell and N.S. Harper, 1978, Sedimentation rates and a sediment budget for Lake Superior. Journal of Great Lakes Research 4:276-287.

Kempe, S. and E.T. Degens, 1978, Lake Van varve record: The past 10,420 years. In: E.T. Degens and F. Kurtman (eds.) The Geology of Lake Van. Maden Tetkik ve Arama, Ankara, 169:53-63.

Kendall, R.L., 1969, An ecological history of the Lake Victorian Basin. Ecological Monographs 39:121-176.

Klein, J., J.C. Lerman, P.E. Damon and E.K. Ralph, 1982, Calibration of radiocarbon dates. Radiocarbon 24:103-150.

Krishnamurty, R.V., S.K. Bhattacharya and S. Kusumgar, 1986, Palaeoclimatic changes deduced from $^{13}C/^{12}C$ and C/N ratios of Karewa lake sediments, India. Nature 323:150-152.

Krishnaswawi, S. and D. Lal, 1978, Radionuclide Limnochronology. In: A. Lerman (ed.) Lakes: Chemistry, Geology, Physics. Springer Verlag, New York, 153-178.

Kutzbach, J.E., 1981, Monsoon climate of the Early Holocene: Climate experiment with the earth's orbital parameters for 9,000 years ago. Science 214:59-61.

Kutzbach, J.E. and P.J. Guetter, 1984, The sensitivity of monsoon climates to orbital parameter changes for 9,000 years BP: Experiments with the NCAR general circulation model. In: A.L. Berger et al. (eds.) Milankovitch and Climate. vol. 2, Reidel, Boston 801-820.

Kutzbach, J.E. and F.A. Street-Perrott, 1985, Milankovitch forcing of fluctuations in the level of tropical lakes from 18 to 0 kyrs BP. Nature 317:130-134.

Lamb, H.H., 1977, Climate, present, past and future, Vol. 2, Methuen, London 835 p.

Landscheidt, T., 1983, Solar oscillations, sunspot sycles, and climate change. In: B.M. McCormac (ed.) Weather and Climate responses to solar variations. Colorado Associated University Press, Boulder 293-308.

Leakey, R.E.F., 1970, New Hominid remains and early artefacts from Northern Kenya. Fauna and Artefacts from a new Plio-Pleistocene locality near Lake Rudolf in Kenya. Nature 226:223-224.

Leakey, R.E.F., 1976, Hominids in Africa. American Scientist 64:174-178.

Leakey, R.E.F. and A.C. Walker, 1985, New higher primates from the Early Miocene of Buluk, Kenya. Nature 318:173-175.

Lee, C., J.A. McKenzie and M. Sturm, 1987, Carbon isotope fractionation and changes in the flux and composition of particulate matter resulting from biological activity during a sediment trap experiment in Lake Greifen, Switzerland. Limnology and Oceanography 32:83-96.

Legrand, M. and R.J. Delmas, 1987, A 220-year continuous record of volcanic H_2SO_4 in the Antarctic ice sheet. Nature 327:671-676.

Lerman, A. (ed.) 1978, Lakes: Chemistry, Geology, Physics. Springer Verlag, New York, 363p.

Livingstone, D.A., 1975, Late Quaternary climatic change in Africa. Annual Reviews of Ecology and Systematics 6:249-280.

Livingstone, D.A., 1981, Paleolimnology. In: J.J. Symoens et al. (eds.) The ecology and ultilization of African inland waters. United Nations Environmental Programme, 176-182.

Livingstone, D.A. and R.L. Kendall, 1969, Stratigraphic studies of East African Lakes. Mitt. Internat. Verein. Limnol. 17:147-153.

Lynch, E.L., 1986, Late Quaternary Flucuations of the Western Boundary Undercurrent. Masters Thesis, Duke University. (unpublished).

Maley, J., 1982, Dust clouds, rain types and climatic variations in tropical north Africa. Quaternary Research 18:1-16.

McDougall, I., 1985, K-Ar and $^{40}Ar/^{39}Ar$ dating of the hominid-bearing Pliocene-Pleistocene sequence at Koobi Fora, Lake Turkana, northern Kenya. Geological Society of America, Bulletin 96:159-175.

McKenzie, J.A., 1985, Carbon isotopes and productivity in the lacustrine and marine environment. In: W. Stumm (ed.) Chemical processes in lakes. Wiley, New York 99-118.

Meko, D.M., C.W. Stockton and T.J. Blasing, 1985. Periodicity in tree rings from the corn belt. Science 229:381-384.

Meybeck, M., 1982, Carbon, nitrogen, and phosphorus transport by world rivers. American Journal of Science 282:401-450.

Mitchell, J.M., C.W. Stockton and D.M. Meko, 1979, Evidence of a 22 year rhythm of drought in the western United States related to the Hale Solar Cycle since the 17th century. In: B.M. McCormac and T.A. Seliga (eds.) Solar-terrestrial influences on weather and climate. D. Reidel, Dordrecht, 125-144.

Morner, N.A. and W. Karlen (eds.) 1984, Climate changes on a yearly to millennial basis. D. Reidel, Boston 667p.

Mountian, G.S., 1973, Procedures for description of Woods Hole Oceanographic Institution (WHOI) sediment cores. W.H.O.I. Technical Memorandum 7-73, 25 pp.

Murray-Hughes, R., 1933, Notes on the geological succession, tectonics and economic geology of the western half of Kenya Colony. Report Geological Survey of Kenya. 3, 8p.

Neftel, A., H. Oeschger, J. Schwander, B. Stauffer and R. Zumbrunn, 1982, Ice core samples measurements give atmospheric CO_2 content during the past 40,000 years. Nature 295: 220-223.

Nicholson, S.E., 1978, Climate variations in the Sahel and other African regions during the past five centuries. Journal of Arid Environments 1:3-24.

Nieuwolt, S., 1977, Tropical Climatology, Wiley, New York, 207p.

O'Sullivan, P.E., 1983, Annually-laminated lake sediments and the study of Quaternary environmental changes - A Review. Quaternary Science Reviews 1:245-313.

Olsen, P.E., 1986, A 40-million-year lake record of Early Mesozoic orbital climatic forcing. Science 234:842-848.

Owen, R.B., J.W. Barthelme, R.W. Renaut and A. Vincens, 1982, Palaeolimnology and archaeology of Holocene deposits north-east of Lake Turkana, Kenya. Nature 298:523-529.

Palmer, P.G., 1976, Grass cuticles: A new paleoecological tool for East African lake sediments. Canadian Journal of Botany 54:1725-1734.

Palmer, T.N., 1986, Influence of the Atlantic, Pacific and Indian Oceans on Sahel rainfall. Natue 322:251-253.

Peng, T. and W. Broecker, 1980, Gas exchange rates for three closed-basin lakes. Limnology and Oceanography 25:789-796.

Pittock, A.B., 1983, Solar variability, weather and climate: An update. Quarterly Journal of the Royal Meteorological Society 109:23-55.

Pokras, E.M. and A.C. Mix, 1987, Earth's precession cycle and Quaternary climatic change in tropical Africa. Nature 326:486-487.

Prell, W.L., 1984, Monsoonal climate of the Arabian Sea during the Late Quaternary: A response to changing solar radiation. In: A.L. Berger et al. (eds.) Milankovitch and Climate, Reidel, Boston 349-366.

Prell, W.L. and E. Van Campo, 1986, Coherent response of Arabian Sea upwelling and pollen transport to Late Quaternary monsoonal winds. Nature 323:526-528.

Quinn, W.H., D.O. Zopf, K.S. Short and R.T.W. Kuo Yang, 1978, Historical trends and statistics of the southern oscillation, El Nino, and Indonesian droughts. Fishery Bulletin 76:663-678.

Rasmusson, E.M., 1985, El Nino and variations in climate. American Scientist 73:168-177.

Rasmusson, E.M. and T.H. Carpenter, 1983, The relationship between eastern equatorial Pacific sea surface temperatures and rainfall over India and Sri Lanka. Monthly Weather Review 111:517-528.

Rasmusson, E.M. amd J.M. Wallace, 1983, Meteorological aspects of the El Nino/Southern Oscillation. Science 222:1195-1202.

Reeves, C.V., F.M. Karanja, and I.N. MacLeod, 1987, Geophysical evidence for a failed Jurassic rift and tripple junction in Kenya. Earth and Planetery Sciences Letters 81:299-311.

Reihl, H. and J. Meitin, 1979, Discharge of the Nile River: a barometer of short-period climatic variation. Science 206:1178-1179.

Renberg, I. and U. Segerstrom, 1981, Applications of varved lake

sediments in paleoenvironmental studies. Wahlenbergia 7:125-133.

Reynolds, D.J., 1984, Structural and dimensional repetition in continental rifts. M.S. Thesis, Duke University, Durham (unpublished).

Richardson, J.L. and A.E. Richardson, 1972, History of an African rift lake, and its climatic implictions. Ecological Monographs 42:499-534.

Rodhe, H. and H. Virji, 1976, Trends and periodicities in east African rainfall data. Monthly Weather Review 104:307-315.

Rosendahl, B.R., 1987, Architecture of Continental Rifts with special reference to East Africa. Annual Review of Earth and Planetary Sciences. 15:445-503.

Rosendahl, B.R., D.J. Reynolds, P.M. Lorber, J. McGill, D. Scott, J.J. Lambiase and S.J. Derksen, 1986, Structural expressions in rift basins: Lessons from Lake Tanganyika, East Africa. Geological Society of London Special Publication 25 (in press).

Rossignol-Strick, M., 1983, African monsoons, an immediate climate response to orbital insolation. Nature 304:46-49.

Rossignol-Strick, M., 1985, Mediterranean Quaternary sapropels, an immediate response of the African monsoon to variation of insolation. Palaeogeography, Palaeoclimatology, Palaeoecology 49:237-263.

Sander, S., 1986, The geometry of rifting in Lake Tanganyika, East Africa. M.S. Thesis, Duke University, Durham (unpublished).

Sarnthein, M. and L. Deister-Haass, 1977, Eolian-sand turbidites. Journal of Sedimentary Petrology 47:868-890.

Schwarzacher, W., 1987, The analysis and interpretation of stratification cycles. Paleoceanography 2:79-95.

Shackleton, N.J., M.A. Hall, J. Line and C. Shuxi, 1983, Carbon isotope data in core V19-30 confirm reduced carbon dioxide concentration in the ice age atmosphere. Nature 306:319-322.

Simola, H., 1977, Diatom succession in the formation of annually-laminated sediments in Lovojarvi, a small eutropic lake. Annales Botanici Fenici 14:143-148.

Simola, H., 1983, Limnological effects of peatland drainage and fertilization as reflected in the varved sediments of a deep lake. Hydrobiologia 106:43-57.

Smith, N.D., 1978, Sedimentation processes and patterns in a glacier-fed

lake with low sediment input. Canadian Journal of Earth Sciences 15:741-756.

Specht, T.J., 1987, Architecture of the Malawi rift. M.S. Thesis, Duke University, Durham (unpublished).

Stager, J.C., 1982, The diatom record of Lake Victoria (East Africa): The last 17,000 yrs. In: D.G. Mann (ed.) Proceedings of the 7th International Diatom Symposium 455-476.

Stein, R. and M. Sarnthein, 1984, Late Neogene events of atmospheric and oceanic circulation offshore northwest Africa: High resolution record from deep - sea sediments. Palaeoecology of Africa 16:9-36.

Stockton, C.W., W.R. Boggess and D.M. Meko, 1985, Climate and tree rings. In: A.D. Hecht (ed.) Paleoclimate analysis and modeling, Wiley, New York. 71-150.

Stoffers, P. and R.E. Hecky, 1978, Late Pleistocene-Holocene evolution of the Kivu-Tanganyika Basin. In: A. Matter and M.E. Tucker (eds.) Modern and Ancient Lake Sediments. Special Publication of the International Association of Sedimentologists, Blackwell, Oxford 2:43-55.

Stoffers, P. and A. Singer, 1979, Clay minerals in Lake Mobutu Sese Seko (Lake Albert). Their diagenetic changes as an indicator of the paleoclimate. Geologissche Rundschau 68:1009-1024.

Street, F.A. and A.T. Grove, 1976, Environmental and climatic implications of Late Quaternary lake-level fluctuations in Africa. Nature 261:385-390.

Street, F.A. and A.T. Grove, 1979, Global maps of lake level fluctuations since 30,000 yr BP. Quaternary Research 12:83-119.

Street-Perrott, F.A. and N. Roberts, 1983, Fluctuations in closed-basin lakes as an indicator of past atmospheric circulation patterns. In: F.A. Street-Perrott et al. (eds.) Variations of the Global Water Budget. D. Reidel, Dordrecht, 331-345.

Street-Perrott, F.A. and S.P. Harrison, 1984, Temporal variations in lake levels since 30,000 yr BP - an index of the global hydrological cycle. Geophysical Monograph 29:118-129.

Street-Perrott, F.A. and S.P. Harrison, 1985, Lake levels and climatic reconstruction. In: A.D. Hecht (ed.) Paleocliamte analysis and modeling. Wiley, New York 291-340.

Strickland, J.D.H. and T.R. Parsons, 1968, A handbook of sea water analysis. Fisheries Research Board of Canada, Bulletin 167: 65-70.

Stuiver, M., 1971, Evidence for the formation of atmospheric ^{14}C content

in the Late Quaternary. In: K.K. Turekian (ed.) The Late Cenozoic Glacial Ages, Yale Univ. Press 57-70.

Stuiver, M. and P.D. Quay, 1981, Atmospheric ^{14}C changes resulting from fossil fuel CO_2 release and cosmic ray flux variability. Earth and Planetary Science Letters 53:349-362.

Stuiver, M. and T.F. Brazivnas, 1987, Tree cellulose $^{13}C/^{12}C$ isotope ratios and climatic change. Nature 328:58-60.

Sturm, M., 1979, Origin and composition of clastic varves. In: C. Schluchter (ed.) Moraines and varves. Balkema, Rotterdam. 281-285.

Sudquist, E.T. and W.S. Broecker (eds.) 1985, The carbon cycle and atmospheric CO_2: Natural variations Archean to Present. American Geophysical Union, Geological Monograph 32 627p.

Swain, A.M.. J.E. Kutzbach and S. Hastenrath, 1983, Estimates of Holocene precipitation for Rajasthan, India, based on pollen and lake-level data. Quaternary Research 19:1-17.

Talbot, M.R., 1987, The origin of lacustrine oil source rocks evidence from the lakes of tropical Africa. In: K. Kelts et al. (eds.) Non-marine oil source rocks. Special Publication of the Geological Society of London (in press).

Talbot, M.R. and K. Kelts, 1986, Primary and diagenetic carbonates in the anoxic sediments of Lake Bosumti, Ghana. Geology 14:912-916.

Thompson, L.G. and E. Mosley-Thompson, 1981, Microparticle conuntration variations linked with climatic change: Evidence from polar ice cores. Science 212:812-815.

Thompson, L.G., E. Mosley-Thompson, J.F. Bolzan and B.R. Koci, 1985, A 1,500-yr record of tropical precipation in ice cores from Quelecaya Ice Cap, Peru. Science 229:971-973.

Thompson, L.G., E. Mosley-Thompson, W. Dansgaard and P.M. Grootes, 1986, The little ice age as revealed in the stratigraphy of the tropical Quelecaya Ice Cap. Science 234:361-364.

Tiercelin, J.J., R.W. Renaut, G. Delibrias, J. LeFournier and S. Bieda, 1981, Late Pleistocene and Holocene lake level fluctuations in the Lake Bogoria basin, Northern Kenya rift valley. Palaeoecology of Africa 13:105-120.

Truckle, P.H., 1976, Geology and Late Cainozoic lake sediments of the Suguta Trough, Kenya. Nature 263:380-383.

van Campo, E., J.C. Duplessey and M. Rossignol-Strick, 1982, Climate conditions deduced from a 150 kyr oxygen-isotope - pollen record

from the Arabian Sea. Nature 296:56-59.

Vincent, C.E., T.D. Davies and A.K.C. Beresford, 1979, Recent changes in the level of Lake Naivasha, Kenya, as an indicator of equatorial westerlies over East Africa. Climatic Change 2:175-189.

von Hohnel, L.R., 1894, Discovery of Lakes Rudolf and Stefanie. 2 vols. Bell, London.

Vondra, C.F. and B.E. Bowen, 1978, Stratigraphy, sedimentary facies and paleoenvironments, East Lake Turkana, Kenya. In: W.W. Bishop (ed.) Geological Background to fossil man. Scottish Academic Press, Edinburg 395-414.

Walker, G.T., 1924, Correlation in seasonal variatins in weather, no. 9: A further study of world weather. Memoirs of the Indian Meteorological Department 24:275-332.

Wetzel, R.G., 1975, Limnology. Sanders College Publishing, Philadelphia 743p.

Williams, D.F., 1985, Carbon isotope variations in surface waters of the Gulf of Mexico on time scales of 10,000, 30,000, 150,000, and 2 million years. In: E.T. Sundquist and W.S. Broecker (eds.) The carbon cycle and atmospheric CO_2: Natural variations Archean to Present. American Geophysical Union, Geological Monograph 32:329-341.

Williams, G.E., 1981, Sunspot periods in the late Precambrian glacial climate and solar-planetary relations. Nature 291:624-628.

Williams, G.E. and C.P. Sonett, 1985, Solar signiture in sedimentary cycles from the Late Precambrian Elatina Formation, Autralia. Nature 318:523-527.

Williams, M.A.J., 1975, Late Pleistocene tropical aridity synchronous in both hemispheres? Nature 253:617-618.

Williams, M.A.J. and D.A.F. Adamson, 1982, A land between two Niles. Balkema, Rotterdam 246p.

Williamson, P.G., 1978, Evidence for the major features and development of rift paleolakes in the Neogene of East Africa from certain aspects of lacustrine mollusc assemblages. In: W.W. Bishop (ed.) Geological background to fossil man. Scottish Academic Press, Edinburg 507-527.

Williamson, P.G., 1986, A Late Mesozoic transform fault system in the southeast Turkana Depression, North Kenya: Implications for early development of the African Rift. Nature in press.

Williamson, P.G., G.G. Raynolds, R.J.G. Savage and R.J. O'Connell, 1986,

Early rift sedimentation in the Turkana Basin, North Kenya. Geological Society of London Special Paper 25 (in press).

Wood, F.J., 1986, Tidal dynamics: Coastal flooding and cycles of gravitational force. D. Reidel, Boston 558p.

Yuretich, R.F., 1979, Modern sediments and sedimentary processes in Lake Rudolf (Lake Turkana), Eastern Rift Valley, Kenya. Sedimentology 26:313-331.

Yuretich, R.F., 1986, Controls on the composition of modern sediments, Lake Turkana, Kenya. In: L.E. Frostich et al. (eds.) Sedimentation in the African Rifts. Geological Society of LOndon Special Publication 25 (in press).

Yuretich, R.F. and T.E. Cerling, 1983, Hydrogeochemistry of Lake Turkana, Kenya: Mass balance and mineral reactions in an alkaline lake. Geochimica et Cosmochimica Acta 47:1099-1109.

APPENDIX

Contents

		Page
A.	Core Data Sheet	149
B.	Carbon-14 and Lead-210 Dating	150
C.	Porosity	151
D.	Diatom Abundances	155
E.	Biogenic Silica	157
F.	Median Grain Size of Silt Sized Fraction	159
G.	Total Organic Carbon, Total Organic Nitrogen, Carbon/Nitrogen Ratio	161
H.	Carbonate	170
I.	Strontium and Magnesium Molar Ratios	175
J.	Carbon and Oxygen Stable Isotopes	177
K.	Thickness of Light/Dark Laminae Couplets	178
L.	Lamination Analysis	183
M.	X-Ray Diffraction Minerology	185
N.	Periodicity Analysis	186

Core Data Sheet

Core	Water Depth (m)	Latitude	Longitude	Core Length (cm)
LT84 - 1G	30	3°33.2'N	35°59.0'E	62
LT84 - 2G	4	3°33.5'N	35°55.8'E	106
LT84 - 1P	29	3°12.4'N	36°13.7'E	1086
LT84 - 2P	57	2°43.0'N	36°32.2'E	1200
LT84 - 2PG	(Trigger core of LT84 - 2P)			107
LT84 - 3P*	48	2°32.2'N	36°40.9'E	347
LT84 - 4P	95	2°33.2'N	36°36.0'E	1214
LT84 - 5P*	22	3°09.8'N	36°17.3'E	1190
LT84 - 6P*	70	3°40.8'N	36°07.0'E	1237
LT84 - 7P	40	3°45.9'N	35°55.6'E	1228
LT84 - 8P	29	3°56.2'N	36°06.8'E	1131
LT84 - 9P*	27	4°01.3'N	35°59.5'E	1146
LT84 - 10P*	53	3°26.3'N	36°04.5'E	1160

Note: * represents cores at ETH, Zurich.

Carbon-14 and Lead-210 Dating

Average Linear Sedimentation Rates:

LT84 - 2P: 0.49 cm/yr (C-14)
LT84 - 8P: 0.27 cm/yr (C-14)
Others not determined

Carbon-14 C-14 Age in years B.P. Depth in centimeters.

Core: **LT84 - 2P**

Depth	C-14 Age	Beta #
15 ± 10	1400 ± 160	16446
332 ± 10	2220 ± 80	16447
735 ± 10	2820 ± 190	16448
1178 ± 10	3840 ± 220	16449

Core: **LT84 - 8P**

Depth	C-14 Age	Beta #
20 ± 10	116.4 ± 2.7% Modern	16451
290 ± 10	850 ± 180	16450
447.5 ± 27.5	1930 ± 80	19457
488 ± 20	90 ± 180	18360
615 ± 20	107.2 ± 2.2% Modern	18361
725 ± 10	3110 ± 760	16452
1090 ± 10	3820 ± 200	16453

Core: **LT84 - 4P**

Depth	C-14 Age	Beta #
665 ± 15	100.7 ± 1.2% Modern	18356

Core: **LT84 - 7P**

Depth	C-14 Age	Beta #
338 ± 20	118.3 ± 1.7% Modern	18357
767 ± 20	123.6 ± 1.3% Modern	18358
1076 ± 20	510 ± 120	18359

Shipment Dates

Shipment	Beta #	Date Reported
1	16446-16453	Jun 1986
2	18356-18361	Nov 1986
3	19457	Jan 1987

Lead-210 Lead-210 Activity in dmg. Depth in centimeters.

Core	Depth	Activity
LT84 - 2PG	7 ± 4	0.82
"	16 ± 4	1.805 ± 0.074
"	30 ± 2	1.349 ± 0.068
"	50.5 ± 3.5	1.71
"	57 ± 2	1.265 ± 0.066
"	65.5 ± 2.5	1.11
"	78 ± 2	1.369 ± 0.059
"	95 ± 2	1.501 ± 0.069
LT84 - 1P	2 ± 2	1.658 ± 0.065
LT84 - 2P	2 ± 2	1.553 ± 0.068
LT84 - 4P	33 ± 2	1.334 ± 0.067
LT84 - 7P	20 ± 2	1.637 ± 0.091
LT84 - 8P	5 ± 2	1.542 ± 0.076

Porosity

All Cores: Minimum = 0.84 Maximum = 0.99 Average = 0.91

Core: **LT84 - 1P** Minimum = 0.86 Maximum = 0.92 Average = 0.89

Depth	Porosity	Depth	Porosity	Depth	Porosity	Depth	Porosity
70	0.89	90	0.90	220	0.92	240	0.91
300	0.92	315	0.89	340	0.89	365	0.90
400	0.90	420	0.90	440	0.89	465	0.89
500	0.89	520	0.90	540	0.90	565	0.89
600	0.90	620	0.90	640	0.91	665	0.91
700	0.89	720	0.89	740	0.89	765	0.88
800	0.86	820	0.88	840	0.88	865	0.88
900	0.88	920	0.89	940	0.88	965	0.87
1000	0.88	1020	0.88	1040	0.87	1065	0.87

Core: **LT84 - 2PG** Minimum = 0.95 Maximum = 0.96 Average = 0.95

Depth	Porosity	Depth	Porosity	Depth	Porosity	Depth	Porosity
5	0.96	10	0.95	20	0.95	35	0.95
50	0.96	70	0.95	90	0.95	100	0.95

Core: **LT84 - 2P** Minimum = 0.89 Maximum = 0.95 Average = 0.92

Depth	Porosity	Depth	Porosity	Depth	Porosity	Depth	Porosity
10	0.94	40	0.94	65	0.94	90	0.95
108	0.92	140	0.94	189	0.94	210	0.94
240	0.94	265	0.94	290	0.95	310	0.94
340	0.94	365	0.92	390	0.93	410	0.93
440	0.92	465	0.93	490	0.92	510	0.92
540	0.92	565	0.92	590	0.92	610	0.92
630	0.92	650	0.92	662	0.91	672	0.92
690	0.92	710	0.90	740	0.91	765	0.91
790	0.91	815	0.90	840	0.90	865	0.90
890	0.90	915	0.90	940	0.91	965	0.92
990	0.91	1015	0.90	1040	0.90	1065	0.90
1090	0.89	1110	0.90	1135	0.89	1165	0.90
1190	0.90						

Core: **LT84 - 4P** Minimum = 0.91 Maximum = 0.94 Average = 0.92

Depth	Porosity	Depth	Porosity	Depth	Porosity	Depth	Porosity
10	0.94	28	0.91	45	0.92	70	0.93
95	0.92	130	0.91	145	0.93	170	0.92
195	0.93	225	0.92	245	0.92	270	0.92
285	0.92	330	0.91	345	0.92	370	0.91
395	0.93	425	0.94	455	0.94	470	0.93
525	0.93	570	0.93	625	0.92	670	0.92
695	0.92	720	0.92	735	0.91	770	0.91
795	0.91	895	0.91	925	0.92	945	0.93
970	0.92	995	0.91	1045	0.91	1070	0.92
1095	0.92	1125	0.92	1145	0.92	1170	0.92
1195	0.92						

Core: **LT84 - 5P** Minimum = 0.84 Maximum = 0.90 Average = 0.87

Depth	Porosity	Depth	Porosity	Depth	Porosity	Depth	Porosity
10.5	0.90	30	0.90	55	0.89	80	0.89
105	0.90	130	0.89	155	0.89	180	0.90
210	0.88	230	0.88	255	0.88	281	0.89
305	0.88	330	0.84	355	0.90	380	0.88
395	0.87	420	0.84	445	0.88	470	0.87
495	0.86	520	0.86	545	0.87	570	0.87
600	0.85	625	0.85	645	0.87	670	0.87
695	0.86	720	0.84	745	0.87	770	0.86
797	0.87	820	0.88	845	0.87	870	0.88
895	0.88	920	0.88	945	0.86	970	0.86
995	0.85	1021	0.85	1045	0.87	1070	0.87
1095	0.87	1120	0.85	1145	0.86	1170	0.85
1180	0.85						

Core: **LT84 - 6P** Minimum = 0.91 Maximum = 0.95 Average = 0.93

Depth	Porosity	Depth	Porosity	Depth	Porosity	Depth	Porosity
5	0.95	30	0.95	50	0.94	75	0.94
100	0.94	125	0.93	145	0.92	170	0.93
195	0.94	220	0.94	250	0.94	275	0.94
300	0.94	325	0.94	345	0.93	380	0.93
395	0.93	425	0.93	440	0.93	466	0.92
493	0.92	516	0.92	538	0.92	558	0.93
582	0.93	595	0.93	630	0.94	648	0.93
673	0.93	698	0.93	723	0.94	744	0.94

779	0.93	792	0.92	825	0.93	835	0.92
860	0.92	888	0.92	919	0.91	947	0.91
970	0.92	995	0.92	1021	0.92	1043	0.92
1069	0.92	1103	0.92	1124	0.92	1147	0.92
1172	0.93	1200	0.92	1227	0.92		

Core: **LT84 - 7P** Minimum = 0.86 Maximum = 0.99 Average 0.91

Depth	Porosity	Depth	Porosity	Depth	Porosity	Depth	Porosity
0	0.93	23	0.92	28	0.93	37	0.93
52	0.93	66	0.93	87	0.93	107	0.93
116	0.93	129	0.92	158	0.93	183	0.92
208	0.99	227	0.93	249	0.93	278	0.93
305	0.92	328	0.91	355	0.92	381	0.91
406	0.92	430	0.91	455	0.91	482	0.91
507	0.92	533	0.90	558	0.92	583	0.91
608	0.91	628	0.91	648	0.91	673	0.88
705	0.89	730	0.91	755	0.91	780	0.90
808	0.90	840	0.89	864	0.88	890	0.91
914	0.91	938	0.90	960	0.90	990	0.91
1017	0.89	1040	0.91	1065	0.92	1095	0.90
1120	0.91	1143	0.86	1166	0.88	1190	0.90
1211	0.89						

Core: **LT84 - 8P** Minimum = 0.88 Maximum = 0.94 Average = 0.91

Depth	Porosity	Depth	Porosity	Depth	Porosity	Depth	Porosity
10	0.93	30	0.92	50	0.92	70	0.91
130	0.93	150	0.93	170	0.93	190	0.93
210	0.92	230	0.93	250	0.93	270	0.94
290	0.93	320	0.92	345	0.88	365	0.91
395	0.91	415	0.91	445	0.92	465	0.91
495	0.91	515	0.91	545	0.91	565	0.90
595	0.91	615	0.90	645	0.91	665	0.90
695	0.89	715	0.90	745	0.91	765	0.91
815	0.91	845	0.91	865	0.91	895	0.91
915	0.91	945	0.92	970	0.91	995	0.91
1020	0.90	1050	0.90	1070	0.91	1095	0.90
1115	0.91						

Core: **LT84 - 9P** Minimum = 0.85 Maximum = 0.94 Average = 0.89

Depth	Porosity	Depth	Porosity	Depth	Porosity	Depth	Porosity
5.5	0.93	31	0.94	56	0.92	81	0.90
108	0.89	133	0.89	155	0.90	180	0.92
205	0.91	233	0.87	255	0.87	280	0.88
315	0.91	338	0.89	363	0.92	388	0.92
413	0.92	442	0.89	463	0.88	491	0.91
516	0.89	541	0.88	563	0.85	588	0.88
609	0.89	638	0.87	663	0.87	693	0.88
713	0.90	751	0.90	773	0.88	804	0.88
828	0.88	854	0.89	879	0.89	901	0.88
929	0.89	954	0.87	980	0.87	1003	0.86
1026	0.86	1051	0.88	1073	0.88	1104	0.89
1126	0.90						

Core: **LT84 - 10P** Minimum = 0.90 Maximum = 0.94 Average = 0.92

Depth	Porosity	Depth	Porosity	Depth	Porosity	Depth	Porosity
10	0.94	36	0.93	60	0.93	82	0.94
105	0.94	130	0.94	155	0.94	180	0.94
210	0.94	230	0.94	255	0.94	280	0.93
316	0.93	351	0.92	376	0.92	400	0.93
425	0.93	450	0.93	475	0.91	500	0.93
525	0.92	550	0.91	575	0.92	600	0.92
625	0.92	650	0.92	675	0.92	700	0.92
725	0.92	760	0.91	785	0.92	810	0.91
835	0.92	860	0.91	885	0.91	910	0.92
935	0.92	960	0.92	985	0.91	1010	0.92
1035	0.92	1060	0.91	1088	0.92	1110	0.91
1135	0.90						

Note: Depth down core in centimeters.
Porosity determined by water loss.

Diatom Abundances

Appendix D

Core: **LT84 – 2P**

Code	Diatom Species or Group
1	Surirella sp.
2	Stephanodiscus astrea
3	Thalassiosira rudolfi
4	Anomoeoneis spheaerophora
5	Melosira nyassensis
6	Others: Rhopalodia, Gomphocymbella, Cocconeis and Cymbella sp.

Depth	1	2	3	4	5	Depth	1	2	3	4	5
25	43.2	27.1	28.8	0.9	–	50	41.2	23.7	30.4	1.6	–
75*	17.0	72.0	–	11.0	–	100*	52.0	40.0	4.0	4.0	–
125	57.6	15.9	19.1	3.3	1.8	150	44.3	34.0	1.0	5.7	10.3
175	48.4	31.4	8.4	1.4	8.9	200	80.3	11.1	3.6	–	0.6
225	63.7	23.9	8.6	0.3	3.5	250	28.6	48.9	15.4	11.5	6.0
275	19.3	48.0	3.4	11.0	16.9	300	16.5	12.2	60.3	4.3	4.9
325	33.7	13.3	25.1	3.5	8.7	350	42.3	27.3	14.5	3.4	11.1
375	21.9	45.9	12.5	3.7	15.3	400	46.2	32.1	8.6	1.3	11.6
425	42.8	29.0	13.7	1.5	12.0	450	28.3	48.0	5.3	1.3	16.4
475	36.2	41.0	2.9	0.8	19.0	500	62.4	25.7	3.0	–	8.9
525	38.1	43.0	0.2	3.1	14.0	550	51.8	34.3	0.4	1.5	11.5
575	25.7	54.6	–	–	19.5	600	58.7	32.8	–	0.8	7.8
625	53.2	35.2	–	0.6	11.0	650	21.0	60.7	–	0.5	17.8
675	36.1	46.5	–	–	17.0	700	59.4	26.4	–	1.0	13.1
725	49.0	34.2	–	0.3	15.6	750	52.2	28.7	–	0.3	18.4
775	13.5	10.5	0.2	0.2	75.5	800	–	–	–	–	100.0
825	4.7	2.7	–	0.2	92.2	850	–	–	–	–	100.0
875	16.4	7.1	–	–	76.5	900	10.3	26.2	–	0.5	61.4
925*	51.7	43.1	–	3.4	1.7	950	26.5	14.7	–	0.2	58.2
975	0.5	51.2	–	0.2	48.1	1000	1.6	34.1	–	0.5	63.6
1025	8.9	44.3	–	–	46.9	1050	.3	86.0	–	–	13.8
1075	.2	73.5	–	–	26.3	1100	.2	22.8	–	–	77.0
1125	–	20.7	–	–	79.3	1150	.5	4.5	–	–	95.1
1175	–	5.3	–	–	94.7	1200	–	61.8	–	–	38.2

Core: **LT84 - 4P**

Code	Diatom Species or Group
1	Surirella sp.
2	Stephanodiscus astrea
3	Thalassiosira rudolfi
4	Anomoeoneis spheaerophora
5	Melosira nyassensis
6	Others: Rhopalodia, Gomphocymbella, Cocconeis and Cymbella sp.

Depth	1	2	3	4	5	Depth	1	2	3	4	5
25	80.7	12.4	0.6	0.6	1.9	50	86.4	7.5	-	0.8	1.1
75	81.9	8.6	0.5	1.3	3.4	100	71.9	19.5	-	-	6.2
125	57.8	15.4	-	2.7	15.1	150*	81.3	11.4	-	1.0	1.0
175	87.7	7.2	-	-	1.4	200*	46.8	25.9	-	1.9	3.7
225	97.0	0.7	-	0.5	0.7	250	69.9	3.4	-	1.7	2.8
275	76.5	15.6	2.9	1.0	1.0	300	83.5	8.2	-	0.8	1.7
325	83.7	6.6	0.4	0.4	1.7	350*	34.0	61.2	-	-	2.4
375	95.6	1.9	-	0.7	0.5	400	100.0	-	-	-	-
425*	96.6	-	-	-	-	450	92.4	2.7	1.3	1.3	1.3
475	84.7	3.2	3.5	1.5	1.2	500	89.0	-	0.9	0.6	0.9
525	75.2	5.1	2.6	0.9	0.9	550*	77.6	9.0	7.5	1.5	1.5
575	68.6	14.0	6.0	3.3	3.3	600	67.3	9.3	6.5	3.7	1.9
625	64.1	3.9	2.6	3.9	5.3	650	67.6	7.3	-	2.0	1.6
675	70.1	4.8	1.2	2.0	1.6	700	79.0	6.2	4.0	2.2	1.8
725	79.6	7.9	0.5	1.4	8.8	750	75.3	8.7	3.0	0.2	4.3
775	97.2	1.2	0.5	-	0.2	800	82.7	0.6	1.4	0.2	0.8
825	42.1	5.1	45.9	1.3	2.6	850	57.6	6.8	26.1	1.6	3.8
875	4.2	2.9	90.5	0.4	1.4	900	63.0	2.6	33.2	0.4	0.6
925	31.4	1.4	63.3	0.2	1.1	950	40.1	0.4	58.9	-	0.2
975	52.6	9.3	32.9	-	1.2	1000*	37.5	6.3	47.9	2.0	2.0
1025	29.1	0.7	68.4	0.2	0.4	1050	71.6	28.0	-	-	0.2
1075	46.2	6.2	40.5	1.8	1.6	1100	26.9	32.8	31.1	1.7	4.7
1125	79.7	0.7	19.4	-	0.2	1150	33.5	3.3	60.5	0.2	1.7
1175*	10.3	20.7	50.0	-	15.5	1200	16.0	2.4	77.8	0.7	2.8

Note: Depth down core in centimeters.
Numbers represent percent abundance at specific depth.
- Represents particular species or group not found in specific count.

* represents slide with less than 100 valves on a smear slide.

Data collected and compiled by K. Hahn.

Biogenic Silica Appendix E

All Cores Minimum = 0.61 Maximum = 7.40 Average = 2.09

Core: **LT84 - 2P** Minimum = 2.06 Maximum = 7.40 Average = 3.39

Depth	SiO_4	Depth	SiO_4	Depth	SiO_4	Depth	SiO_4	Depth	SiO_4
10	3.51	10*	3.13	65	4.50	108	3.26	108*	2.91
140	5.35	210	4.26	210*	3.81	310	2.66	310*	2.39
390	3.80	410	3.08	410*	3.10	490	2.92	510	2.99
510*	3.83	610	3.08	610*	3.04	710	2.46	710*	3.59
815	3.02	815*	2.68	865	3.70	915	2.74	915*	3.59
1040	7.40	1040*	3.68	1110	4.17	1110*	3.45	1135	2.14
1190	2.06	1190*	2.11						

Core: **LT84 - 4P** Minimum = 1.50 Maximum = 3.02 Average = 2.08

Depth	SiO_4	Depth	SiO_4	Depth	SiO_4	Depth	SiO_4	Depth	SiO_4
225	1.56	425	1.99	845	1.50	870	3.02	1070	2.32

Core: **LT84 - 5P** Minimum = 0.61 Maximum = 2.51 Average = 1.80

Depth	SiO_4	Depth	SiO_4	Depth	SiO_4	Depth	SiO_4	Depth	SiO_4
10.5	2.51	105	2.10	210	2.26	305	2.25	395	2.30
495	1.60	600	2.33	695	1.98	797	2.23	895	1.97
943	2.05	995	1.73	996	2.00	1068	1.19	1095	1.49
1096	0.92	1096*	0.61	1146	0.80	1171	1.09	1173	2.13
1173*	1.98	1188	1.76	1188*	2.20				

Core: **LT84 - 7P** Minimum = 1.53 Maximum = 2.00 Average = 1.75

Depth	SiO_4	Depth	SiO_4	Depth	SiO_4	Depth	SiO_4	Depth	SiO_4
23	1.69	87	1.64	158	2.00	328	1.56	430	1.60
533	1.59	673	1.82	780	1.53	864	1.90	1017	1.98
1166	1.86								

Core: **LT84 - 8P** Minimum = 0.81 Maximum = 2.41 Average = 1.56

Depth	SiO_4	Depth	SiO_4	Depth	SiO_4	Depth	SiO_4	Depth	SiO_4
10	0.89	10*	0.83	90	1.43	90*	1.04	170	1.12
170*	0.81	250	0.90	250*	1.27	320	1.61	345	1.26
345*	1.11	445	1.91	445*	2.36	545	1.72	545*	1.84
645	2.41	645*	1.58	745	2.14	745*	1.34	845	1.67
845*	1.62	945	1.84	945*	2.15	995	1.97	1050	1.99
1050*	1.72								

Core: **LT84 - 9P** Minimum = 1.49 Maximum = 2.54 Average = 2.10

Depth	SiO_4	Depth	SiO_4	Depth	SiO_4	Depth	SiO_4	Depth	SiO_4
31	2.17	233	1.49	363	2.44	563	2.54	773	1.85

Core: **LT84 - 10P** Minimum = 1.27 Maximum = 2.56 Average = 1.96

Depth	SiO_4	Depth	SiO_4	Depth	SiO_4	Depth	SiO_4	Depth	SiO_4
36	1.80	79	1.85	99	1.60	130	1.83	179	1.87
199	1.62	230	2.17	279	2.11	333	1.27	376	1.82
394	1.50	424	1.96	475	1.77	502	1.99	524	2.09
575	2.17	590	2.10	623	2.01	675	2.01	692	1.99
721	2.16	721*	2.30	785	2.02	795	2.56	833	2.18
885	1.80	892	2.28	944	1.96	985	1.80	1000	2.20
1033	2.01	1088	1.78	1100	1.97	1134	2.27		

Notes: Depth down core in centimeters.
SiO_4 is weight percent biogenic silica as SiO_4.

* represents duplicate analysis for that interval.

Median Grain Size of Silt Sized Fraction Appendix F

All Cores: Minimum = 11.90 Maximum = 22.43 Average = 15.77

Core: **LT84 - 2P** Minimum = 14.03 Maximum = 20.15 Average = 16.20

Depth	Median	Depth	Median	Depth	Median	Depth	Median	Depth	Median
10	17.59	10*	17.79	65	16.19	108	18.32	108*	18.43
140	14.77	210	15.31	210*	15.34	310	14.98	310*	14.48
390	18.26	410	15.84	410*	16.64	490	17.01	510	15.37
510*	15.62	610	15.68	610*	15.69	710	16.86	710*	17.23
815	14.50	815*	14.03	865	14.68	915	14.13	915*	14.11
1040	14.82	1110	16.30	1135	16.27	1190	19.69	1190*	20.15

Core: **LT84 - 4P** Minimum = 14.01 Maximum = 16.93 Average = 15.45

Depth	Median	Depth	Median	Depth	Median	Depth	Median	Depth	Median
225	14.01	425	16.93	845	13.64	870	16.04	1070	16.62

Core: **LT84 - 5P** Minimum = 13.24 Maximum = 20.23 Average = 17.11

Depth	Median	Depth	Median	Depth	Median	Depth	Median	Depth	Median
10.5	20.23	105	18.99	210	18.11	305	19.61	395	19.02
495	18.57	695	17.85	797	16.56	895	14.99	943	14.55
995	14.96	996	15.67	1068	18.59	1095	16.29	1096	17.19
1096*	17.24	1100	18.95	1146	13.24	1171	15.06	1173	16.66
1173*	16.66	1188	17.40						

Core: **LT84 - 7P** Minimum = 12.29 Maximum = 15.03 Average = 13.69

Depth	Median	Depth	Median	Depth	Median	Depth	Median	Depth	Median
23	13.[illegible]	87	13.92	158	14.00	328	13.25	430	15.03
533	14.[illegible]	673	13.32	780	14.31	864	13.41	1017	12.29
1166	12.90								

Core: **LT84 - 8P** Minimum = 14.49 Maximum = 18.08 Average = 15.94

Depth	Median	Depth	Median	Depth	Median	Depth	Median	Depth	Median
10	14.49	10*	14.70	90	14.65	90*	15.02	170	14.86
170*	14.51	250	15.63	250*	15.75	320	14.90	345	16.43
345*	16.38	445	17.51	445*	16.28	545	17.05	545*	17.47
645	15.26	645*	15.09	745	16.79	745*	17.48	845	15.35
845*	15.47	945	16.60	945*	16.68	995	14.97	1050	17.08
1050*	18.08								

Core: **LT84 - 9P** Minimum = 11.90 Maximum = 17.66 Average = 14.58

Depth	Median	Depth	Median	Depth	Median	Depth	Median	Depth	Median
31	17.66	233	11.90	363	13.88	563	13.93	773	15.52

Core: **LT84 - 10P** Minimum = 14.21 Maximum = 22.43 Average = 17.41

Depth	Median	Depth	Median	Depth	Median	Depth	Median	Depth	Median
36	14.99	79	16.86	99	16.24	130	16.45	179	16.43
199	15.34	279	16.40	333	15.47	376	22.43	394	18.74
424	19.68	475	15.82	502	18.32	524	18.73	575	20.65
590	14.41	623	19.48	675	16.88	692	15.20	721	16.37
721*	19.87	721*	19.87	785	17.12	795	16.14	833	18.03
885	19.39	892	19.12	944	16.89	1000	17.30	1033	16.93
1088	14.89	1100	14.21	1134	19.88				

Note: Depth down core in centimeters.
Median grain size of silt-sized fraction in microns.

* represents duplicate analysis from same interval.

Total Organic Carbon, Total Organic Nitrogen, Carbon/Nitrogen Ratio

All Cores: Carbon: Minimum = 0.41 Maximum = 4.31 Average = 0.93
Nitrogen: Minimum = 0.07 Maximum = 0.30 Average = 0.14
C/N Ratio: Minimum = 4.45 Maximum = 14.4 Average = 6.87

Core: **LT84 - 1P** Carbon: Minimum = 0.62 Maximum = 0.88 Average = 0.77
Nitrogen: Minimum = 0.11 Maximum = 0.14 Average = 0.12
C/N Ratio: Minimum = 5.19 Maximum = 6.80 Average = 6.11

Depth	TOC #1	TOC #2	TON #1	TON #2	Avg TOC	Avg TON	C/N Ratio
20	0.68	0.73	0.12	0.12	0.71	0.12	5.79
40	0.82	0.73	0.14	0.14	0.78	0.14	5.66
90	0.68	0.69	0.13	0.13	0.69	0.13	5.19
140	0.67	0.66	0.13	0.12	0.67	0.12	5.35
190	0.84	0.92	0.13	0.14	0.88	0.14	6.51
240	0.82	0.78	0.13	0.14	0.80	0.13	5.97
300	0.80	0.74	0.12	0.12	0.77	0.12	6.26
340	0.95	0.73	0.11	0.11	0.79	0.11	6.76
340*	0.73	0.74	0.11	0.12			
400	0.75	0.85	0.12	0.12	0.80	0.12	6.80
440	0.67	0.64	0.11	0.11	0.65	0.11	5.83
500	0.64	0.60	0.12	0.11	0.62	0.12	5.38
540	1.45	0.67	0.13	0.12	0.85	0.12	6.65
540*	0.64	0.65	0.10	0.12			
600	0.76	1.15	0.11	0.11	0.88	0.13	6.16
600*	0.94	0.68	0.18	0.12			
640	0.77	0.77	0.13	0.12	0.77	0.13	6.12
700	1.10	0.72	0.12	0.12	0.81	0.12	6.37
700*	0.72	0.71	0.12	0.12			
740	0.72	0.74	0.12	0.12	0.73	0.12	6.05
800	0.70	0.69	0.11	0.11	0.70	0.11	6.39
840	0.74	0.75	0.11	0.13	0.75	0.12	6.40
900	0.77	0.83	0.13	0.12	0.80	0.12	6.53
940	0.76	0.74	0.13	0.12	0.75	0.12	6.01
1000	0.71	0.74	0.12	0.12	0.73	0.12	5.95
1065	0.72	0.72	0.12	0.11	0.72	0.12	6.26

Core: **LT84 - 2PG** Carbon: Minimum = 1.05 Maximum = 1.87 Average = 1.27
Nitrogen: Minimum = 0.14 Maximum = 0.20 Average = 0.16
C/N Ratio: Minimum = 7.05 Maximum = 9.26 Average = 7.75

Depth	TOC #1	TOC #2	TON #1	TON #2	Avg TOC	Avg TON	C/N Ratio
5	1.38	1.35	0.19	0.18	1.37	0.18	7.45
10	1.05	1.05	0.14	0.14	1.05	0.14	7.36
20	1.21	1.24	0.17	0.17	1.23	0.17	7.05
35	1.87	1.86	0.20	0.20	1.87	0.20	9.26

50	1.21	1.11	0.15	0.15	1.16	0.15	7.43
50*	1.19	1.13	0.16	0.16			
70	1.40	1.35	0.18	0.16	1.38	0.17	7.92
90	1.05	1.48	0.15	0.15	1.17	0.16	7.52
90*	1.08	1.05	0.16	0.15			
100	1.12	1.22	0.14	0 15	1.17	0.15	8.03

++

Core: LT84 - 2P Carbon: Minimum = 0.71 Maximum = 1.38 Average = 1.04
Nitrogen: Minimum = 0.10 Maximum = 0.21 Average = 0.16
C/N Ratio: Minimum = 4.65 Maximum = 8.60 Average = 6.73

Depth	TOC #1	TOC #2	TON #1	TON #2	Avg TOC	Avg TON	C/N Ratio
10	0.99	1.05	0.14	0.16	1.02	0.15	6.73
40	1.04	1.10	0.14	0.15	1.07	0.14	7.41
65	1.07	1.06	0.14	0.15	1.06	0.15	7.18
90	1.11	1.15	0.15	0.15	1.13	0.15	7.39
108	0.88	0.85	0.10	0.10	0.86	0.10	8.60
140	1.32	1.30	0.17	0.18	1.31	0.17	7.64
189	1.39	1.37	0.16	0.17	1.38	0.16	8.53
210	0.87	0.93	0.12	0.12	0.90	0.12	7.51
240	1.14	1.14	0.16	0.16	1.14	0.16	7.22
265	1.21	1.18	0.15	0.14	1.19	0.14	8.30
290	1.28	1.34	0.15	0.16	1.31	0.16	8.31
310	1.36	1.27	0.19	0.19	1.32	0.19	6.93
340	1.19	1.25	0.16	0.15	1.22	0.15	7.89
365	0.85	0.85	0.13	0.13	0.85	0.13	6.45
390	1.22	1.21	0.18	0.18	1.21	0.18	6.84
410	1.02	0.98	0.14	0.13	1.00	0.14	7.32
440	0.90	0.91	0.11	0.11	0.91	0.11	8.32
465	0.94	0.92	0.15	0.15	0.93	0.15	6.06
490	1.02	0.97	0.15	0.14	0.99	0.15	6.82
510	0.95	0.96	0.13	0.13	0.96	0.13	7.27
540	1.04	1.02	0.17	0.16	1.03	0.16	6.25
565	1.11	1.06	0.18	0.16	1.08	0.17	6.38
590	0.90	0.90	0.14	0.14	0.93	0.15	6.36
590*	0.86	0.87	0.11	0.13			
590*	0.99	1.01	0.15	0.15			
590*	0.95	0.94	0.18	0.17			
610	1.13	1.06	0.17	0.17	1.09	0.17	6.39
630	1.01	1.06	0.15	0.15	1.04	0.15	6.82
650	1.04	1.02	0.15	0.15	1.03	0.15	6.87
662	1.20	1.25	0.18	0.18	1.22	0.18	6.77
672	1.05	1.00	0.15	0.16	1.03	0.16	6.58
690	0.87	0.89	0.14	0.15	0.87	0.14	6.16
690*	0.86	0.85	0.14	0.14			
710	0.81	0.80	0.18	0.17	0.80	0.17	4.65
740	1.09	1.19	0.17	0.16	1.09	0.17	6.24
740*	1.04	1.03	0.18	0.19			

765	0.99	0.94	0.15	0.15	0.97	0.15	6.56
790	0.94	0.90	0.19	0.18	0.92	0.19	4.98
815	0.90	1.15	0.15	0.16	0.94	0.17	5.72
815*	0.83	0.90	0.17	0.18			
840	1.02	1.07	0.19	0.18	1.04	0.18	5.66
865	0.93	0.92	0.19	0.18	0.92	0.19	4.92
890	1.10	0.96	0.16	0.16	1.01	0.17	5.97
890*	0.96	1.00	0.17	0.18			
915	1.01	1.02	0.15	0.15	1.01	0.15	6.71
940	1.15	1.14	0.21	0.21	1.15	0.21	5.44
965	1.01	1.01	0.18	0.19	1.01	0.19	5.38
990	1.00	0.97	0.19	0.19	0.99	0.19	5.23
1015	0.98	1.02	0.17	0.17	1.00	0.17	5.79
1040	0.71	0.72	0.10	0.10	0.71	0.10	7.15
1065	0.91	0.95	0.13	0.15	0.93	0.14	6.71
1090	1.09	1.09	0.16	0.17	1.09	0.16	6.62
1110	1.11	1.25	0.15	0.17	1.20	0.17	7.06
1110*	1.19	1.24	0.18	0.18			
1135	1.17	1.14	0.16	0.16	1.15	0.16	7.26
1165	1.17	1.20	0.16	0.16	1.19	0.16	7.32
1190	1.01	1.00	0.13	0.12	0.99	0.14	7.13
1190*	0.97	1.00	0.15	0.15			

++

Core: **LT84 - 4P** Carbon: Minimum = 1.06 Maximum = 1.80 Average = 1.31
Nitrogen: Minimum = 0.16 Maximum = 0.29 Average = 0.24
C/N Ratio: Minimum = 4.55 Maximum = 7.66 Average = 5.65

Depth	TOC #1	TOC #2	TON #1	TON #2	Avg TOC	Avg TON	C/N Ratio
10	1.76	1.73	0.24	0.26	1.74	0.25	6.95
45	1.28	1.37	0.24	0.26	1.32	0.25	5.26
95	1.29	1.31	0.25	0.24	1.30	0.24	5.35
145	1.32	1.30	0.27	0.27	1.31	0.27	4.94
195	1.60	1.26	0.26	0.25	1.34	0.25	5.35
195*	1.24	1.26	0.24	0.26			
245	1.14	1.16	0.24	0.24	1.15	0.24	4.84
285	1.10	1.13	0.24	0.25	1.11	0.24	4.56
345	1.23	1.27	0.24	0.25	1.25	0.24	5.13
395	1.12	1.17	0.24	0.25	1.14	0.25	4.64
455	1.21	1.03	0.22	0.23	1.06	0.23	4.55
455*	1.00	0.98	0.24	0.23			
495	1.20	1.17	0.22	0.22	1.18	0.22	5.37
545	1.32	1.32	0.26	0.25	1.32	0.26	5.13
595	1.48	1.37	0.26	0.25	1.43	0.26	5.58
645	1.77	1.73	0.28	0.29	1.75	0.29	6.08
695	1.59	1.60	0.27	0.29	1.60	0.28	5.68
735	1.42	1.34	0.24	0.24	1.38	0.24	5.71
795	1.79	1.81	0.27	0.27	1.80	0.27	6.68
845	1.18	1.31	0.23	0.23	1.24	0.23	5.31

895	1.14	1.14	0.20	0.20	1.14	0.20	5.68
945	1.25	1.19	0.16	0.16	1.22	0.16	7.66
995	1.08	1.07	0.17	0.17	1.08	0.17	6.40
1045	1.12	1.16	0.17	0.17	1.14	0.17	6.81
1095	1.30	1.31	0.19	0.22	1.30	0.21	6.26
1145	1.39	1.40	0.24	0.25	1.39	0.24	5.70
1195	1.36	1.39	0.24	0.24	1.38	0.24	5.67

Core: **LT84 - 5P** Carbon: Minimum = 0.46 Maximum = 4.31 Average = 0.98
Nitrogen: Minimum = 0.07 Maximum = 0.30 Average = 0.12
C/N Ratio: Minimum = 5.23 Maximum = 14.4 Average = 7.48

Depth	TOC #1	TOC #2	TON #1	TON #2	Avg TOC	Avg TON	C/N Ratio
30	0.55	0.54	0.09	0.10	0.56	0.10	5.59
30*	0.57	0.57	0.10	0.10			
80	0.62	0.62	0.07	0.07	0.62	0.07	8.86
130	0.53	0.55	0.10	0.10	0.54	0.10	5.42
180	0.69	0.68	0.07	0.08	0.68	0.07	9.16
230	0.50	0.48	0.09	0.09	0.49	0.09	5.40
281	0.55	0.53	0.08	0.08	0.54	0.08	6.93
330	0.46	0.47	0.09	0.09	0.46	0.09	5.27
380	0.56	0.54	0.09	0.09	0.55	0.09	6.32
420	0.48	0.48	0.09	0.09	0.48	0.09	5.52
470	0.61	0.60	0.09	0.09	0.61	0.09	6.74
520	0.52	0.53	0.10	0.10	0.53	0.10	5.29
570	0.80	0.81	0.11	0.11	0.80	0.11	7.34
625	0.50	0.48	0.09	0.09	0.49	0.09	5.23
670	0.67	0.67	0.09	0.10	0.67	0.09	7.08
720	0.56	0.59	0.10	0.10	0.58	0.10	5.96
770	0.76	0.73	0.11	0.10	0.75	0.10	7.18
820	0.78	0.78	0.12	0.12	0.78	0.12	6.47
870	0.89	0.88	0.12	0.12	0.89	0.12	7.20
920	1.02	1.03	0.14	0.14	1.03	0.14	7.47
970	1.65	1.18	0.29	0.13	1.28	0.18	7.28
970*	1.11	1.19	0.14	0.15			
1021	2.09	1.98	0.20	0.19	2.03	0.20	10.31
1070	2.54	2.63	0.22	0.23	2.24	0.21	10.68
1070*	1.80	1.99	0.19	0.20			
1120	3.33	3.23	0.25	0.25	3.32	0.26	12.93
1120*	3.33	3.40	0.26	0.27			
1170	4.38	4.23	0.30	0.30	4.31	0.30	14.35
1180	0.95	0.91	0.11	0.10	0.93	0.10	8.91
1180*	0.87	0.82	0.12	0.11			

Core: **LT84 - 6P** Carbon: Minimum = 0.64 Maximum = 1.36 Average = 0.88
Nitrogen: Minimum = 0.13 Maximum = 0.18 Average = 0.15
C/N Ratio: Minimum = 4.78 Maximum = 7.71 Average = 6.07

Depth	TOC #1	TOC #2	TON #1	TON #2	Avg TOC	Avg TON	C/N Ratio
30	0.84	0.83					
75	0.82	0.83					
125	0.83	0.84	0.12	0.13	0.84	0.13	6.61
170	0.84	0.81					
220	0.83	0.90	0.13	0.13	0.87	0.13	6.65
275	0.80	0.81					
325	0.84	0.81	0.14	0.15	0.82	0.13	6.12
325*	0.81	0.83	0.13	0.12			
380	1.36	1.36	0.17	0.18	1.36	0.18	7.71
425	0.82	0.85	0.14	0.14	0.84	0.14	6.01
466	0.79	0.79	0.15	0.15	0.79	0.15	5.35
516	0.93	0.93	0.16	0.15	0.93	0.15	6.08
558	0.88	0.89	0.15	0.15	0.88	0.15	6.00
595	1.07	1.09	0.17	0.16	1.08	0.17	6.49
673	0.94	0.92	0.15	0.15	0.93	0.15	6.12
723	0.92	0.92	0.15	0.16	0.92	0.16	5.92
779	0.82	0.82	0.14	0.14	0.82	0.14	5.87
825	0.77	0.75	0.14	0.14	0.76	0.14	5.48
860	1.10	1.09	0.17	0.17	1.09	0.17	6.42
919	0.76	0.74	0.13	0.13	0.75	0.13	5.76
970	0.88	0.92	0.14	0.15	0.90	0.15	6.19
1021	0.84	0.85	0.14	0.14	0.85	0.14	6.13
1069	1.08	1.08	0.17	0.18	1.08	0.18	6.18
1124	0.64	0.65	0.13	0.14	0.64	0.13	4.78
1172	0.83	0.82	0.15	0.15	0.82	0.15	5.54

Core: **LT84 - 7P** Carbon: Minimum = 0.52 Maximum = 1.45 Average = 0.82
Nitrogen: Minimum = 0.10 Maximum = 0.19 Average = 0.13
C/N Ratio: Minimum = 4.51 Maximum = 7.80 Average = 6.39

Depth	TOC #1	TOC #2	TON #1	TON #2	Avg TOC	Avg TON	C/N Ratio
9	0.80	0.75	0.12	0.11	0.78	0.11	6.79
23	0.85	0.78	0.13	0.13	0.82	0.13	6.44
28	0.86	0.88	0.11	0.12	0.87	0.12	7.46
52	0.80	0.78	0.13	0.11	0.79	0.12	6.82
66	0.71	0.70	0.10	0.10	0.71	0.10	7.08
87	0.80	0.81	0.11	0.13	0.81	0.12	6.81
107	0.71	0.76	0.10	0.11	0.73	0.10	7.04
116	0.88	1.01	0.13	0.15	0.95	0.14	6.83
129	0.77	0.87	0.11	0.11	0.82	0.11	7.27
158	1.02	1.02	0.14	0.13	1.02	0.14	7.45
183	0.86	0.88	0.12	0.12	0.87	0.12	7.16

208	1.42	1.48	0.18	0.19	1.45	0.19	7.80
278	1.28	1.24	0.16	0.16	1.26	0.16	7.72
328	0.78	0.75	0.14	0.13	0.77	0.14	5.61
355	0.90	0.89	0.14	0.15	0.89	0.14	6.23
381	0.71	0.70	0.11	0.12	0.70	0.11	6.13
406	0.80	0.80	0.12	0.13	0.80	0.12	6.45
430	0.64	0.68	0.12	0.11	0.66	0.12	5.71
455	0.89	0.86	0.14	0.14	0.87	0.14	6.25
482	0.77	0.78	0.12	0.12	0.77	0.12	6.26
507	0.85	0.84	0.14	0.14	0.85	0.14	6.18
533	0.73	0.73	0.11	0.12	0.73	0.12	6.33
558	1.05	1.04	0.15	0.15	1.05	0.15	6.99
583	0.86	0.81	0.13	0.13	0.83	0.13	6.41
648	0.90	0.92	0.14	0.14	0.91	0.14	6.53
673	0.68	0.71	0.11	0.10	0.69	0.11	6.60
705	0.62	0.62	0.12	0.13	0.62	0.12	5.01
730	0.86	0.78	0.15	0.13	0.82	0.14	5.99
755	0.79	0.77	0.13	0.13	0.78	0.13	6.12
780	0.81	0.79	0.13	0.14	0.80	0.13	5.94
864	0.69	0.73	0.12	0.12	0.71	0.12	6.08
890	0.65	0.61	0.10	0.10	0.63	0.10	6.15
914	0.86	0.88	0.13	0.13	0.87	0.13	6.49
938	0.82	0.86	0.13	0.13	0.84	0.13	6.66
960	0.84	0.86	0.13	0.13	0.85	0.13	6.36
990	0.74	0.75	0.13	0.13	0.75	0.13	5.83
1017	0.72	0.72	0.14	0.12	0.72	0.13	5.52
1040	0.81	0.84	0.12	0.13	0.82	0.13	6.55
1065	0.78	0.78	0.13	0.13	0.78	0.13	5.90
1095	0.86	0.83	0.13	0.13	0.85	0.13	6.44
1120	0.93	0.92	0.14	0.14	0.93	0.14	6.48
1143	0.47	0.58	0.11	0.12	0.52	0.12	4.51
1166	0.58	0.63	0.10	0.12	0.61	0.11	5.32
1190	0.67	0.64	0.11	0.11	0.66	0.11	5.74
1211	0.75	0.76	0.13	0.11	0.75	0.12	6.31

Core: **LT84 - 8P** Carbon: Minimum = 0.41 Maximum = 1.05 Average = 0.77
Nitrogen: Minimum = 0.08 Maximum = 0.17 Average = 0.13
C/N Ratio: Minimum = 4.45 Maximum = 7.39 Average = 5.65

Depth	TOC #1	TOC #2	TON #1	TON #2	Avg TOC	Avg TON	C/N Ratio
10	0.78	0.79	0.12	0.11	0.79	0.12	6.69
30	0.69	0.68	0.10	0.11	0.69	0.10	6.57
50	0.65	0.71	0.12	0.13	0.68	0.12	5.46
50*	0.75	0.75	0.11	0.10			
70	0.75	0.72	0.10	0.10	0.74	0.10	7.39
70*	0.74	0.73	0.10	0.10			
90	0.83	0.78	0.14	0.14	0.81	0.14	5.68
90*	0.85	0.86	0.11	0.10			

110	0.81	0.81	0.12	0.12	0.81	0.12	6.94
110*	0.82	0.85	0.12	0.13			
130	0.83	0.83	0.17	0.17	0.83	0.17	4.86
130*	1.05	0.88	0.14	0.13			
150	0.77	0.78	0.11	0.11	0.77	0.11	6.83
150*	0.88	0.86	0.12	0.12			
170	0.77	0.75	0.16	0.16	0.76	0.16	4.78
170*	1.00	0.94	0.14	0.14			
190	0.89	0.91	0.13	0.14	0.90	0.13	6.92
190*	0.84	0.84	0.11	0.10			
210	0.92	0.88	0.17	0.17	0.90	0.17	5.38
210*	0.97	0.96	0.12	0.13			
230	0.88	1.06	0.12	0.16	0.97	0.14	6.92
230*	0.90	0.93	0.14	0.12			
250	0.70	0.75	0.16	0.16	0.73	0.16	4.59
250*	0.70	0.72	0.11	0.09			
270	0.94	0.92	0.14	0.12	0.93	0.13	7.38
270*	0.88	0.89	0.10	0.11			
290	1.03	1.07	0.16	0.17	1.05	0.16	6.51
320	0.99	0.93	0.14	0.13	0.96	0.13	7.09
345	0.77	0.77	0.13	0.13	0.77	0.13	6.06
365	0.79	0.77	0.13	0.13	0.78	0.13	6.01
395	0.65	0.65	0.12	0.11	0.65	0.11	5.63
415	0.79	0.80	0.14	0.14	0.79	0.14	5.73
445	0.75	0.79	0.17	0.16	0.77	0.16	4.65
465	0.69	0.70	0.13	0.13	0.69	0.13	5.34
495	0.72	0.74	0.16	0.16	0.73	0.16	4.62
515	0.79	0.80	0.16	0.16	0.80	0.16	5.10
545	0.61	0.66	0.14	0.15	0.64	0.14	4.51
565	0.66	0.68	0.13	0.13	0.67	0.13	5.04
595	0.65	0.64	0.14	0.14	0.64	0.14	4.53
615	0.69	0.73	0.14	0.15	0.71	0.14	4.98
645	0.58	0.62	0.13	0.14	0.60	0.13	4.45
665	0.68	0.69	0.14	0.14	0.69	0.14	4.92
695	0.63	0.69	0.13	0.13	0.66	0.13	5.01
715	0.72	0.71	0.15	0.14	0.71	0.15	4.91
745	0.84	0.75	0.14	0.15	0.81	0.14	5.62
745*	0.84	0.83	0.14	0.15			
765	0.80	0.80	0.16	0.16	0.80	0.16	5.04
795	0.83	0.78	0.16	0.15	0.80	0.15	5.26
815	0.76	0.81	0.14	0.15	0.79	0.14	5.46
845	0.71	0.68	0.13	0.13	0.69	0.13	5.21
865	0.85	0.85	0.16	0.16	0.85	0.16	5.36
895	0.71	0.75	0.14	0.14	0.73	0.14	5.21
915	0.78	0.75	0.15	0.15	0.77	0.15	5.05
945	0.70	0.73	0.14	0.14	0.71	0.14	5.16
970	0.66	0.64	0.12	0.12	0.65	0.12	5.39
995	0.61	0.61	0.13	0.14	0.61	0.14	4.51
1020	0.65	0.66	0.12	0.12	0.66	0.12	5.30
1050	0.41	0.41	0.08	0.08	0.41	0.08	5.19
1070	0.64	0.64	0.13	0.13	0.64	0.13	5.06

1095	0.66	0.63	0.13	0.12	0.64	0.13	5.13
1115	0.59	0.63	0.12	0.13	0.61	0.12	4.94

++

Core: **LT84 - 9P** Carbon: Minimum = 0.81 Maximum = 1.26 Average = 0.92
Nitrogen: Minimum = 0.09 Maximum = 0.16 Average = 0.12
C/N Ratio: Minimum = 7.15 Maximum = 8.54 Average = 7.96

Depth	TOC #1	TOC #2	TON #1	TON #2	Avg TOC	Avg TON	C/N Ratio
31	0.94	0.90			0.92		
81	0.85	0.84			0.84		
133	0.81	0.82	0.10	0.10	0.81	0.09	8.54
133	0.80	0.81					
180	0.88	0.93			0.90		
233	0.95	0.97	0.11	0.12	0.96	0.11	8.40
280	0.94	0.93			0.94		
315	0.80	0.82			0.81		
363	1.12	1.12	0.16	0.16	1.12	0.16	7.15
413	1.27	1.25			1.26		
463	1.02	0.96	0.13	0.13	0.99	0.13	7.67
516	0.82	0.83			0.83		
563	0.96	0.96	0.11	0.11	0.96	0.11	8.44
609	0.94	0.94			0.94		
663	0.84	0.83	0.11	0.11	0.83	0.11	7.68
713	0.98	0.98			0.98		
773	0.97	0.96	0.13	0.12	0.97	0.12	7.84
828	0.97	0.94			0.95		
879	0.79	0.82			0.81		
929	0.87	0.88			0.87		
980	0.83	0.81			0.82		
1026	0.90	0.89			0.90		
1073	0.84	0.83			0.83		
1126	0.90	0.91			0.92		
1126	0.92	0.96					

++

Core: **LT84 - 10P** Carbon: Minimum = 0.66 Maximum = 1.48 Average = 0.92
Nitrogen: Minimum = 0.08 Maximum = 0.17 Average = 0.13
C/N Ratio: Minimum = 5.14 Maximum = 10.1 Average = 7.77

Depth	TOC #1	TOC #2	TON #1	TON #2	Avg TOC	Avg TON	C/N Ratio
10	0.79	0.75	0.08	0.08	0.77	0.08	10.00
60	0.86	0.86	0.13	0.13	0.86	0.13	6.56
105	0.91	0.99			0.95		
155	0.84	0.85			0.84		
210	1.36	1.42	0.12	0.15	1.39	0.14	10.08
225	1.50	1.46	0.16	0.18	1.48	0.17	8.51

316	0.95	0.91			0.93		
351	0.89	0.89			0.89		
400	0.92	0.97			0.94		
450	0.83	0.90	0.13	0.13	0.87	0.13	6.65
500	0.91	0.92	0.09	0.10	0.92	0.09	9.89
550	0.77	0.73			0.75		
600	0.93	0.96			0.95		
650	0.97	0.86			0.92		
700	0.98	0.95	0.14	0.13	0.97	0.14	7.03
760	0.76	0.75			0.75		
810	1.00	0.77			0.77		
810	0.67	0.65			0.66		
860	0.89	0.81			0.85		
910	0.86	0.92	0.15	0.15	0.89	0.15	6.05
960	0.98	1.06			1.02		
1010	0.92	0.95			0.94		
1060	0.80	0.77			0.78		
1110	0.78	0.82	0.16	0.16	0.80	0.16	5.14

Notes: Depth down core in centimeters.
TOC is weight percent total organic carbon as C.
TON is weight percent total organic nitrogen as N.
C/N is ratio of TOC to TON.

* represents duplicate analysis from given depth.

Carbonate

All Cores: Minimum = 1.27 Maximum = 28.08 Average = 10.04

Core: **LT84 - 1P** Minimum = 5.87 Maximum = 12.75 Average = 8.78

Depth	$CaCO_3$	Depth	$CaCO_3$	Depth	$CaCO_3$	Depth	$CaCO_3$	Depth	$CaCO_3$
20	8.84	40	8.93	90	7.53	120	9.56	140	7.88
190	8.56	220	7.98	240	9.22	300	6.47	315	6.21
340	8.69	400	8.16	420	11.69	465	8.28	500	11.85
520	10.47	565	10.01	600	8.32	620	8.49	665	9.45
700	9.15	720	12.75	765	7.98	800	5.87	820	8.18
865	9.79	900	8.47	920	8.35	965	6.81	1000	8.66
1020	11.62	1065	6.78						

Core: **LT84 - 2PG** Minimum = 13.48 Maximum = 21.26 Average = 18.67

Depth	$CaCO_3$	Depth	$CaCO_3$	Depth	$CaCO_3$	Depth	$CaCO_3$	Depth	$CaCO_3$
5	13.48	35	19.48	50	21.26	90	20.07	100	19.09

Core: **LT84 - 2P** Minimum = 6.15 Maximum = 23.63 Average = 16.55

Depth	$CaCO_3$	Depth	$CaCO_3$	Depth	$CaCO_3$	Depth	$CaCO_3$	Depth	$CaCO_3$
10	17.88	40	19.33	65	18.97	90	16.58	108	14.53
140	20.76	189	16.72	210	18.26	240	19.52	290	19.41
310	21.41	340	22.69	365	23.63	390	17.99	410	17.05
440	21.56	490	16.59	510	17.80	540	17.37	565	16.73
590	15.46	610	19.68	630	16.98	650	16.52	662	16.02
672	15.58	690	15.16	710	14.55	740	16.42	790	14.15
815	16.66	840	17.86	865	19.53	890	16.22	915	22.01
940	10.98	965	6.15	990	11.98	1015	12.82	1040	11.46
1065	16.36	1090	14.55	1110	12.79	1135	10.05	1165	17.24
1190	9.37								

Core: **LT84 - 4P** Minimum = 3.52 Maximum = 28.08 Average = 19.67

Depth	$CaCO_3$	Depth	$CaCO_3$	Depth	$CaCO_3$	Depth	$CaCO_3$	Depth	$CaCO_3$
28	19.82	28*	18.54	28*	19.18	45	23.06	70	21.09
130	22.88	145	24.01	170	25.05	225	25.11	245	20.13
270	24.08	330	24.24	345	20.20	370	16.11	425	3.52
455	12.05	470	19.79	525	17.15	545	22.32	570	19.57
625	21.04	645	26.27	670	19.99	720	16.43	735	22.17
770	20.06	825	16.58	845	28.05	870	18.67	925	18.97
945	17.58	970	18.97	1025	17.35	1045	21.20	1070	20.54
1125	17.60	1145	17.43	1170	10.60				

Core: **LT84 - 5P** Minimum = 1.27 Maximum = 15.70 Average = 8.94

Depth	$CaCO_3$	Depth	$CaCO_3$	Depth	$CaCO_3$	Depth	$CaCO_3$	Depth	$CaCO_3$
30	10.89	55	10.84	80	9.68	105	10.07	155	9.51
180	10.47	210	13.76	255	15.14	281	12.55	305	11.42
355	9.17	380	9.82	395	9.20	445	7.62	470	9.56
495	9.24	545	7.91	570	7.74	625	8.40	645	9.65
670	11.47	720	8.35	745	9.61	770	9.78	820	6.80
845	6.38	870	10.04	920	10.76	943	13.08	945	13.31
970	13.68	996	15.71	1021	14.51	1045	1.31	1068	1.63
1070	1.28	1096	1.82	1120	1.56	1145	1.51	1146	1.72
1170	6.06	1171	3.27	1173	9.32	1180	13.29	1188	13.53

Core: **LT84 - 6P** Minimum = 3.22 Maximum = 13.30 Average = 7.87

Depth	$CaCO_3$	Depth	$CaCO_3$	Depth	$CaCO_3$	Depth	$CaCO_3$	Depth	$CaCO_3$
30	6.57	75	4.72	100	5.52	125	6.14	170	6.33
195	5.70	220	6.94	275	10.78	300	9.72	325	5.39
380	9.92	395	9.11	425	8.87	466	8.68	493	4.92
516	9.46	558	9.38	582	4.36	595	7.72	630	5.11
673	7.65	698	4.30	723	5.39	779	3.31	792	3.23
825	3.81	860	13.37	888	9.65	919	11.20	970	9.89
995	12.46	1021	6.99	1069	11.65	1103	9.97	1124	6.73
1172	11.7	1200	10.98	1227	11.65				

Core: **LT84 - 7P** Minimum = 2.62 Maximum = 15.39 Average = 7.65

Depth	$CaCO_3$	Depth	$CaCO_3$	Depth	$CaCO_3$	Depth	$CaCO_3$	Depth	$CaCO_3$
9	5.67	22	2.78	28	6.02	32	8.54	42	4.04
52	5.90	52*	5.02	60	2.89	66	4.91	70	4.76
80	4.99	90	4.41	100	5.60	107	7.56	110	9.14
116	7.45	120	8.01	129	5.78	130	7.05	140	5.28
150	2.89	160	6.54	170	4.94	180	3.77	183	6.78
190	7.45	200	7.45	208	8.81	210	4.88	220	5.96
230	7.01	240	8.20	250	7.39	260	5.85	270	9.92
278	10.56	280	8.92	290	7.98	300	8.28	310	7.70
320	6.34	330	7.20	340	7.77	350	9.55	355	11.47
360	9.81	370	7.79	380	6.27	381	7.86	390	6.27
400	9.98	406	8.06	410	6.61	420	3.70	430	3.01
440	3.11	450	7.41	455	8.97	460	7.30	470	5.79
480	2.62	482	5.40	490	3.89	500	7.55	507	7.26
510	8.44	520	5.75	530	7.18	540	6.59	550	6.81
558	7.84	560	4.21	570	8.27	580	5.06	583	8.29
590	4.99	600	4.65	610	4.54	620	6.14	630	4.04
640	8.56	648	8.03	651	6.64	660	4.69	670	9.96
680	7.82	690	6.37	700	4.38	705	7.30	710	9.78
720	6.91	730	8.89	730*	6.[illegible]3	740	7.95	750	7.23
755	12.61	760	11.04	770	5.3[illegible]	780	6.67	790	9.23
800	8.47	810	6.22	830	6.66	840	9.31	850	9.82
860	11.86	864	2.00	870	7.97	882	8.92	890	8.84
890*	10.98	900	7.29	910	7.06	920	12.48	930	3.35
938	8.18	940	5.84	950	9.29	960	12.23	960*	10.57
970	9.05	982	9.57	990	9.28	990*	6.94	1000	9.10
1010	10.25	1020	5.65	1030	8.51	1040	9.08	1040*	8.65
1050	10.75	1060	9.47	1065	11.40	1070	9.11	1080	7.97
1090	7.37	1095	12.80	1100	9.05	1110	11.34	1120	11.51
113[illegible]	8.70	1140	15.39	1143	8.12	1150	8.18	1160	9.94
1166	9.86	1170	9.61	1180	12.43	1190	11.26	1190*	11.41
1200	9.61	1210	7.04	1220	8.12				

Core: **LT84 - 8P** Minimum = 2.28 Maximum = 11.09 Average = 6.62

Depth	$CaCO_3$	Depth	$CaCO_3$	Depth	$CaCO_3$	Depth	$CaCO_3$	Depth	$CaCO_3$
30	4.81	50	4.90	70	6.00	110	4.37	110*	5.14
119	5.26	130	7.95	130*	6.14	140	5.92	150	4.97
150*	4.99	160	3.42	170	5.79	180	4.68	190	4.10
190*	4.34	198	5.61	202	6.57	210	7.61	210*	6.95
219	5.07	230	5.57	230*	3.67	240	3.92	258	6.41
270	7.60	270*	8.57	280	4.83	290	8.00	290*	6.60
300	8.68	309	9.66	312	5.69	320	9.53	324	9.22
334	6.34	340	5.55	350	5.35	365	8.84	370	8.12
380	6.99	390	6.49	395	7.75	399	6.68	410	4.98

415	8.36	420	7.04	430	5.65	440	7.06	440*	8.45
449	7.43	460	5.25	465	6.62	470	6.28	478	4.82
490	7.28	495	7.24	500	6.72	510	6.10	515	5.88
520	5.80	530	6.70	540	6.20	550	5.11	561	4.41
565	5.25	570	6.91	580	7.56	590	7.95	595	11.09
600	6.96	608	8.00	615	7.64	620	8.86	630	6.76
650	5.98	660	6.16	665	6.49	665*	6.29	670	4.35
680	7.04	690	8.85	695	8.18	700	9.01	710	7.10
715	8.71	720	7.89	730	6.99	740	7.65	750	2.74
760	8.19	765	7.89	770	6.56	780	7.12	789	4.93
795	8.92	799	9.23	810	8.28	815	6.90	820	8.55
830	2.56	840	6.19	850	8.42	860	8.54	865	8.28
870	6.84	880	7.60	890	8.76	895	9.87	900	7.08
910	8.01	915	9.73	920	5.93	930	8.30	940	7.72
950	8.65	961	8.90	970	9.63	970*	9.28	980	9.04
990	7.23	995	10.74	999	8.15	1010	9.48	1020	8.91
1020*	11.09	1030	8.79	1040	7.81	1050	8.76	1060	5.81
1070	9.72	1070*	8.94	1080	10.14	1090	8.40	1095	8.91
1100	8.81	1110*	8.26	1115	9.48	1118	7.10		

Core: **LT84 - 9P** Minimum = 1.34 Maximum = 8.86 Average = 5.23

Depth	$CaCO_3$	Depth	$CaCO_3$	Depth	$CaCO_3$	Depth	$CaCO_3$	Depth	$CaCO_3$
31	8.86	56	6.32	81	2.76	133	1.34	155	3.17
180	4.53	233	2.98	255	3.70	280	4.63	315	2.27
363	8.11	388	8.04	413	7.61	463	4.74	491	8.22
516	3.88	563	2.92	588	3.75	609	6.34	663	5.00
693	3.71	713	5.03	773	4.97	804	4.55	828	4.44
879	8.06	901	5.29	929	8.23	980	4.98	1003	5.03
1026	6.27	1073	5.69	1104	6.36	1126	5.96		

Core: **LT84 - 10P** Minimum = 1.91 Maximum = 21.55 Average = 9.01

Depth	$CaCO_3$	Depth	$CaCO_3$	Depth	$CaCO_3$	Depth	$CaCO_3$	Depth	$CaCO_3$
3	6.98	10	4.91	10*	5.47	19	3.83	29	3.38
36	2.21	39	1.91	49	5.53	59	6.00	60	7.48
69	7.50	79	5.62	82	4.93	89	6.63	99	4.39
103	6.84	105	10.12	119	3.59	129	4.78	130	7.27
139	6.07	149	7.40	155	7.27	159	8.09	169	7.59
179	7.56	180	7.56	189	7.39	199	4.79	209	6.68
210	7.03	219	7.75	225	10.90	229	8.08	230	9.35
239	10.41	249	9.34	259	10.13	269	11.60	279	5.86
280	9.93	289	12.89	303	7.69	313	6.50	316	10.67
323	5.70	333	8.24	351	6.42	354	4.64	364	6.90
374	5.53	376	6.42	384	6.64	394	6.44	400	5.54

404	9.43	414	6.27	424	3.82	425	6.70	434	5.05
444	7.31	450	6.42	470	3.69	475	6.91	482	3.91
492	3.35	492*	5.02	500	8.69	502	9.58	513	10.28
524	8.00	525	15.68	525*	14.02	534	11.38	544	10.99
550	3.30	550*	3.81	554	8.93	561	10.74	570	9.14
575	9.25	580	12.47	590	9.01	600	13.78	600*	9.98
612	14.57	623	7.87	625	11.29	634	6.92	644	8.07
650	8.98	661	10.20	672	10.61	675	12.84	682	10.73
692	13.27	700	13.63	702	8.43	721	12.74	721*	9.20
725	11.21	731	13.86	741	11.01	760	11.79	766	14.03
775	13.44	785	11.55	785*	13.96	795	11.54	805	12.04
810	13.96	815	5.46	815*	6.79	825	12.94	833	12.10
835	13.11	844	12.11	854	13.09	860	13.56	866	12.15
872	10.31	882	11.90	885	21.55	885*	12.03	892	10.33
902	10.88	910	10.15	912	10.96	923	10.25	933	9.82
935	11.79	954	10.08	960	11.52	963	8.90	974	9.93
983	9.54	985	11.18	993	13.81	1000	11.60	1010	6.93
1014	6.27	1024	7.69	1033	10.27	1035	11.08	1044	9.37
1054	9.47	1060	13.11	1062	8.12	1070	9.36	1080	9.44
1088	9.07	1092	7.64	1100	11.08	1110	9.98	1114	11.27
1124	10.92	1134	8.30	1135	10.82	1144	8.78		

Note: Depth cown core in centimeters.
$CaCO_3$ is weight percent bulk carbonate as $CaCO_3$.

* represents duplicate analysis for the interval.

Strontium and Magnesium Molar Ratios

Appendix I

Core: **LT84 - 1G** Ostracod Sclerocyris clavata juvenile form

Depth	Sr/Ca (10^{-3})	Mg/Ca (10^{-2})	Depth	Sr/Ca (10^{-3})	Mg/Ca (10^{-2})
34	4.71	1.54	34*	5.07	1.86
34*	5.38	2.01	34*	5.43	1.81
34*	4.75	1.67	34*	5.80	1.91
34*	4.90	1.60	34*	5.02	1.79
34*	5.57	2.13	34*	4.86	1.59

Core: **LT84 -- 2P & 2PG** Ostracod Sclerocyris clavata juvenile form

Depth	Sr/Ca (10^{-3})	Mg/Ca (10^{-2})	Depth	Sr/Ca (10^{-3})	Mg/Ca (10^{-2})
74 (2PG)	5.92	1.35	74	5.96	0.95
274	12.2	1.43	362	8.15	0.69
477	8.65	1.23	576	5.77	1.60
672	5.52	1.69	772	6.06	1.75
772*	5.50	1.60	862	5.73	1.48
964	13.2	2.31	1060	5.32	2.01
1174	6.61	2.00			

Core: **LT84 - 2P** Ostracod Sclerocyris clavata adult form

Depth	Sr/Ca (10^{-3})	Mg/Ca (10^{-2})	Depth	Sr/Ca (10^{-3})	Mg/Ca (10^{-2})
74	4.44	0.10	74*	4.50	0.09
362	4.41	0.10	576	5.25	1.30
672	6.88	1.87	772	5.22	1.65
1060	4.77	2.08			

Core: **LT84 - 2P** Micrite

Depth	Sr/Ca (10^{-3})	Mg/Ca (10^{-1})	Depth	Sr/Ca (10^{-3})	Mg/Ca (10^{-1})
29	1.82	2.44	129	1.90	2.19
229	1.95	1.76	319	1.91	1.51
429	1.93	1.82	529	1.90	2.13
625	1.89	1.59	723	1.71	1.54
829	1.56	1.35	829*	1.46	1.18
829*	1.56	1.19	829*	1.50	1.29
829*	1.72	1.26	930	1.63	1.39
1030	2.22	6.19	1129	2.03	2.28

Core: **LT84 - 7P** Micrite

Depth	Sr/Ca (10^{-3})	Mg/Ca (10^{-1})	Depth	Sr/Ca (10^{-3})	Mg/Ca (10^{-1})
78	2.29	2.60	178	2.53	5.52
178	2.80	7.37	274	1.77	2.36
274*	1.71	1.69	274*	0.81	1.09
274*	2.77	4.24	274*	2.03	1.52
274*	2.25	2.18	382	2.36	2.92
382*	2.70	4.78	462	2.23	2.11
572	1.96	2.37	670	2.22	2.55
765	1.96	1.51	772	1.89	1.61
772*	1.91	1.52	882	2.10	2.19
974	2.20	1.71	1096	2.04	1.57

Note: Depth down core in centimeters.
Ostracod and micrite samples from same sub-sample of sediment.
Ratios are molar of individual element Sr, Mg, Ca, respectively.
Sr is strontium. Mg is Magnesium. Ca is calcium.
(10^{-3}) represents exponetial factor.
Micrite is <44 micron bulk carbonate sample.
* represents duplicate analysis for that interval.

Carbon and Oxygen Stable Isotopes

Core: **LT84 - 1G** Ostracod Sclerocypris clavata

Depth	C-13	O-18	Depth	C-13	O-18	Depth	C-13	O-18
30	-0.147	3.320	30*	0.133	3.354	30*	0.015	3.483

Core: **LT84 - 2P** Ostracod Sclerocypris clavata

Depth	C-13	O-18	Depth	C-13	O-18	Depth	C-13	O-18
29**	-1.108	3.004	29	-0.625	3.831	129	-0.778	3.723
229	-1.693	3.402	319	-0.267	3.475	429	-0.127	3.493
429**	-1.628	3.761	529	-0.922	2.752	625	-0.319	2.964
723	-0.363	2.802	829	0.317	2.956	930	0.698	2.365
1030	-1.106	3.17	1129	-1.238	2.715			

Core: **LT84 - 2P** Micrite

Depth	C-13	O-18	Depth	C-13	O-18	Depth	C-13	O-18
29	0.741	1.647	129	1.121	1.834	229	1.304	1.955
319	0.986	1.179	429	0.879	1.143	529	0.702	1.924
529*	0.794	1.185	529*	0.751	1.971	529*	0.784	0.621
625	0.917	0.786	625	0.089	0.971	625	0.897	0.019
723	0.695	1.548	829	0.779	1.608	930	0.513	1.406
1030	0.277	1.275	1129	0.269	0.809			

Core: **LT84 - 7P** Micrite

Depth	C-13	O-18	Depth	C-13	O-18	Depth	C-13	O-18
78	0.503	0.784	78*	0.572	0.937	78*	0.607	0.984
78*	0.453	0.922	78*	0.514	0.881	178	-2.032	-2.89
274	0.756	1.309	274*	0.742	0.658	382	-0.098	-0.738
462	-0.098	-0.589	572	-1.396	-1.725	670	-1.327	-0.183
765	0.416	0.951	772	0.081	0.908	882	-0.435	0.931
974	0.268	1.475	1096	0.76	1.47			

Note: Isotope values are relative to PDB (°/oo).
Depth down core in centimeters.
Micrite is <44 micron bulk carbonate sample.
* represents duplicate analysis for that interval.
** represents adult form of the ostracod.

Thickness of Light/Dark Laminae Couplets Appendix K

Core: **LT84 - 8P** Top 9 meters. ¯Average = 9.7

#	Thickness	#	Thickness	#	Thickness	#	Thickness	#	Thickness	#	Thickness
1	16.5	2	11.0	3	7.0	4	5.9	5	5.7	6	8.1
7	18.7	8	5.6	9	9.6	10	16.7	11	17.0	12	6.5
13	7.3	14	11.7	15	5.6	16	13.4	17	12.6	18	4.7
19	3.3	20	12.4	21	11.6	22	6.5	23	8.5	24	9.5
25	12.6	26	19.5	27	15.1	28	12.5	29	6.5	30	8.6
31	3.2	32	4.7	33	5.7	34	15.6	35	9.5	36	5.1
37	4.5	38	11.6	39	6.2	40	2.6	41	8.6	42	12.8
43	2.8	44	18.6	45	4.6	46	20.5	47	13.5	48	16.9
49	9.1	50	10.7	51	7.4	52	9.0	53	7.3	54	23.2
55	27.1	56	18.3	57	5.4	58	25.2	59	13.4	60	25.8
61	17.8	62	10.3	63	7.8	64	7.6	65	7.0	66	27.6
67	14.6	68	19.0	69	20.3	70	7.4	71	11.0	72	32.7
73	23.0	74	19.6	75	16.8	76	17.2	77	17.2	78	3.9
79	2.4	80	3.5	81	11.8	82	12.1	83	10.5	84	4.8
85	5.7	86	5.7	87	18.1	88	14.3	89	6.3	90	5.3
91	4.9	92	10.9	93	5.8	94	10.6	95	15.7	96	17.5
97	12.2	98	4.8	99	7.0	100	11.4	101	6.8	102	29.5
103	15.2	104	16.8	105	25.0	106	27.5	107	22.5	108	17.9
109	21.8	110	13.3	111	19.5	112	17.3	113	20.6	114	22.8
115	17.2	116	10.7	117	4.3	118	6.9	119	10.7	120	27.6
121	11.9	122	4.9	123	9.8	124	11.9	125	9.2	126	11.4
127	6.9	128	14.3	129	19.0	130	21.2	131	24.5	132	10.9
133	11.1	134	9.4	135	10.8	136	10.5	137	15.3	138	4.8
139	6.9	140	10.7	141	10.5	142	6.8	143	7.8	144	13.6
145	7.8	146	5.3	147	4.4	148	13.1	149	11.3	150	11.2
151	11.0	152	17.2	153	13.8	154	19.5	155	11.5	156	4.6
157	11.3	158	12.3	159	3.5	160	7.0	161	7.6	162	12.9
163	6.6	164	7.7	165	8.8	166	4.5	167	5.9	168	14.3
169	8.7	170	12.6	171	5.4	172	6.9	173	11.7	174	16.5
175	14.2	176	7.3	177	7.9	178	12.6	179	12.4	180	10.8
181	9.0	182	8.8	183	12.1	184	4.5	185	11.1	186	9.7
187	7.5	188	9.5	189	14.3	190	12.7	191	6.5	192	4.5
193	9.2	194	13.7	195	12.8	196	5.3	197	5.8	198	4.6
199	10.9	200	10.5	201	14.1	202	8.4	203	11.6	204	9.1
205	11.0	206	12.0	207	4.0	208	7.7	209	6.5	210	10.2
211	12.6	212	12.1	213	15.3	214	10.3	215	20.1	216	7.3
217	8.3	218	6.8	219	5.5	220	14.8	221	10.4	222	11.9
223	9.0	224	20.0	225	13.9	226	23.2	227	18.1	228	14.3
229	7.0	230	6.0	231	7.8	232	24.9	233	12.8	234	8.1
235	10.8	236	8.3	237	5.5	238	4.8	239	9.1	240	7.8
241	3.4	242	5.8	243	8.0	244	6.1	245	5.8	246	6.2
247	9.4	248	9.7	249	7.2	250	8.4	251	12.6	252	8.8
253	12.3	254	5.6	255	6.0	256	5.8	257	9.2	258	8.2
259	9.2	260	12.6	261	5.5	262	4.2	263	4.3	264	4.0
265	8.1	266	10.4	267	10.6	268	11.0	269	4.7	270	11.0
271	8.2	272	8.5	273	9.2	274	12.1	275	14.0	276	12.5

277	5.6	278	6.3	279	11.1	280	6.7	281	10.4	282	17.8
283	16.5	284	8.4	285	6.5	286	9.7	287	5.0	288	3.0
289	5.9	290	4.1	291	11.8	292	6.2	293	10.9	294	7.7
295	6.6	296	10.0	297	2.4	298	2.7	299	7.6	300	3.0
301	11.0	302	6.2	303	11.5	304	5.9	305	5.1	306	8.1
307	2.8	308	4.2	309	13.8	310	5.3	311	4.0	312	3.3
313	4.5	314	3.7	315	5.9	316	7.2	317	4.9	318	6.3
319	3.5	320	5.1	321	8.2	322	8.6	323	8.4	324	4.3
325	11.4	326	7.3	327	4.1	328	11.0	329	7.3	330	8.6
331	4.5	332	4.0	333	6.7	334	4.6	335	8.9	336	6.8
337	12.7	338	11.5	339	8.7	340	7.5	341	4.0	342	4.1
343	4.4	344	2.3	345	7.7	346	9.3	347	10.9	348	9.2
349	5.6	350	5.4	351	7.7	352	2.0	353	9.4	354	6.3
355	1.7	356	3.7	357	11.6	358	8.1	359	10.2	360	7.0
361	8.8	362	3.2	363	8.5	364	15.0	365	7.7	366	5.1
367	12.0	368	6.1	369	8.1	370	6.4	371	18.7	372	5.4
373	7.7	374	10.0	375	9.5	376	3.9	377	2.0	378	5.5
379	3.4	380	8.5	381	3.8	382	4.9	383	7.4	384	8.2
385	12.0	386	19.9	387	7.4	388	12.4	389	20.4	390	24.9
391	4.8	392	6.9	393	10.0	394	9.7	395	9.7	396	7.3
397	6.7	398	7.4	399	10.6	400	13.3	401	12.3	402	15.2
403	17.5	404	12.6	405	13.2	406	12.3	407	11.7	408	14.0
409	6.0	410	10.9	411	10.0	412	8.6	413	17.0	414	14.2
415	8.8	416	6.2	417	13.5	418	8.3	419	13.2	420	12.8
421	14.1	422	10.0	423	10.0	424	10.7	425	45.2	426	12.8
427	14.7	428	10.5	429	15.0	430	23.4	431	20.7	432	9.7
433	19.3	434	11.0	435	7.9	436	8.6	437	15.5	438	6.6
439	11.6	440	8.6	441	8.6	442	9.7	443	18.0	444	26.4
445	13.8	446	13.5	447	21.0	448	5.2	449	9.5	450	4.7
451	4.8	452	15.7	453	7.1	454	9.3	455	12.6	456	11.0
457	9.4	458	3.8	459	6.6	460	8.8	461	10.3	462	7.7
463	8.1	464	18.7	465	12.7	466	12.2	467	12.2	468	9.9
469	26.0	470	9.8	471	7.5	472	7.7	473	5.8	474	11.2
475	11.3	476	7.5	477	14.9	478	10.9	479	8.4	480	21.3
481	6.1	482	7.1	483	5.3	484	12.3	485	7.1	486	17.4
487	14.0	488	4.8	489	9.1	490	8.4	491	7.1	492	9.3
493	9.1	494	6.4	495	3.7	496	3.4	497	5.0	498	7.0
499	7.7	500	10.8	501	9.1	502	5.2	503	11.3	504	7.1
505	5.3	506	6.1	507	6.0	508	6.2	509	6.4	510	9.9
511	8.0	512	5.3	513	6.5	514	7.6	515	3.3	516	10.4
517	6.9	518	7.7	519	9.4	520	5.0	521	6.7	522	5.3
523	3.2	524	10.2	525	12.8	526	3.9	527	8.6	528	7.0
529	7.6	530	6.6	531	5.5	532	5.2	533	3.7	534	5.8
535	5.3	536	5.2	537	5.6	538	3.9	539	6.6	540	4.8
541	7.0	542	8.8	543	7.9	544	7.1	545	8.6	546	5.2
547	7.5	548	7.1	549	7.9	550	10.7	551	4.3	552	6.2
553	4.7	554	12.4	555	12.8	556	9.3	557	18.4	558	8.4
559	10.2	560	16.8	561	5.8	562	14.6	563	8.0	564	33.5
565	7.2	566	8.3	567	8.1	568	11.4	569	8.9	570	8.5
571	9.9	572	10.9	573	8.1	574	6.1	575	9.3	576	7.1
577	6.9	578	5.1	579	7.4	580	7.4	581	7.0	582	10.7

583	7.9	584	5.3	585	9.4	586	7.4	587	4.3	588	3.9
589	6.4	590	7.5	591	14.7	592	31.2	593	11.9	594	9.5
595	5.7	596	6.0	597	8.0	598	7.5	599	4.6	600	4.7
601	9.1	602	4.3	603	10.8	604	10.2	605	10.4	606	10.9
607	6.2	608	6.6	609	6.9	610	10.7	611	16.0	612	8.8
613	11.0	614	15.9	615	31.4	616	10.3	617	8.4	618	11.2
619	8.1	620	6.1	621	14.0	622	4.3	623	9.9	624	8.0
625	12.4	626	8.4	627	8.6	628	9.4	629	14.6	630	9.5
631	7.7	632	8.5	633	9.3	634	6.0	635	8.0	636	8.5
637	8.0	638	3.8	639	7.9	640	8.6	641	7.4	642	10.4
643	7.6	644	7.4	645	8.3	646	13.7	647	19.1	648	14.5
649	5.8	650	6.1	651	7.5	652	9.9	653	5.6	654	5.5
655	6.0	656	6.7	657	6.7	658	5.7	659	12.4	660	13.7
661	19.2	662	7.1	663	10.2	664	5.2	665	6.7	666	7.9
667	10.5	668	14.9	669	5.8	670	13.6	671	9.5	672	8.5
673	4.8	674	6.6	675	7.1	676	6.0	677	9.3	678	13.2
679	6.9	680	5.1	681	7.7	682	7.6	683	8.5	684	7.0
685	13.6	686	12.7	687	9.9	688	10.0	689	5.0	690	5.2
691	8.6	692	10.4	693	13.1	694	11.7	695	14.1	696	10.5
697	7.9	698	7.4	699	10.3	700	6.7	701	8.5	702	10.5
703	6.7	704	12.6	705	7.7	706	3.9	707	9.3	708	12.7
709	7.4	710	4.6	711	6.9	712	6.5	713	8.9	714	5.1
715	5.6	716	13.1	717	11.3	718	11.4	719	5.5	720	3.9
721	7.4	722	7.1	723	13.5	724	8.8	725	11.0	726	10.7
727	5.8	728	5.2	729	4.1	730	6.7	731	9.7	732	6.9
733	7.7	734	7.4	735	5.3	736	9.7	737	23.9	738	6.7
739	7.0	740	12.4	741	9.4	742	11.4	743	5.5	744	5.1
745	8.1	746	7.1	747	4.6	748	10.4	749	19.8	750	15.2
751	4.7	752	3.0	753	3.4	754	15.2	755	9.3	756	18.3
757	5.6	758	7.0	759	3.4	760	11.9	761	7.6	762	16.8
763	8.9	764	13.7	765	5.5	766	6.5	767	11.8	768	17.1
769	7.5	770	7.7	771	5.5	772	5.1	773	8.6	774	14.5
775	9.5	776	16.6	777	6.6	778	7.7	779	19.8	780	5.2
781	5.3	782	8.6	783	6.7	784	6.1	785	12.6	786	8.3
787	13.3	788	10.2	789	9.7	790	9.5	791	5.8	792	8.1
793	6.7	794	12.4	795	8.1	796	5.1	797	14.1	798	13.6
799	8.0	800	20.1	801	5.7	802	8.8	803	3.2	804	4.3
805	8.3	806	2.5	807	6.1	808	6.2	809	5.8	810	9.9
811	5.2	812	8.9	813	5.6	814	7.6	815	6.5	816	6.7
817	7.4	818	9.8	819	8.8	820	11.9	821	6.9	822	6.6
823	7.2	824	11.3	825	7.5	826	12.1	827	10.5	828	8.4
829	5.7	830	9.7	831	11.8	832	5.6	833	3.8	834	5.3
835	16.4	836	8.0	837	6.7	838	7.2	839	5.7	840	15.2
841	10.3	842	5.1	843	8.4	844	7.6	845	11.4	846	10.2
847	22.0	848	19.2	849	5.7	850	5.7	851	7.5	852	6.7
853	12.2	854	5.8	855	8.8	856	7.1	857	5.1	858	14.6
859	6.2	860	8.4	861	10.2	862	12.3	863	7.2	864	8.1
865	6.4	866	9.7	867	9.7	868	17.8	869	11.3	870	6.2
871	9.0	872	10.2	873	7.2	874	5.5	875	7.9	876	8.5
877	6.1	878	5.6	879	15.2	880	15.2	881	9.7	882	9.8
883	12.2	884	5.0	885	14.0	886	10.5	887	22.0	888	10.8

889	9.4	890	9.3	891	16.1	892	11.8	893	9.7	894	4.1
895	7.7	896	4.2	897	9.0	898	6.2	899	5.1	900	9.5
901	9.0	902	11.6	903	19.8						

++

Core: **LT84 - 9P** Top 3 meters. Average = 17.2

#	Thickness	#	Thickness	#	Thickness	#	Thickness	#	Thickness	#	Thickness
1	8.3	2	11.0	3	4.2	4	18.1	5	13.9	6	21.6
7	10.1	8	14.7	9	10.3	10	11.7	11	12.9	12	8.6
13	19.7	14	26.2	15	12.7	16	15.2	17	22.0	18	12.2
19	23.9	20	17.1	21	12.5	22	8.1	23	13.7	24	11.0
25	12.2	26	19.6	27	15.0	28	21.0	29	21.3	30	25.1
31	12.2	32	13.9	33	14.7	34	18.5	35	19.0	36	20.8
37	3.6	38	8.1	39	25.3	40	19.0	41	21.4	42	16.5
43	8.0	44	22.5	45	18.7	46	22.4	47	15.1	48	25.1
49	19.7	50	27.7	51	36.4	52	40.2	53	20.0	54	31.9
55	25.6	56	5.1	57	4.7	58	26.5	59	29.5	60	17.6
61	3.8	62	3.7	63	5.8	64	20.9	65	37.3	66	31.1
67	10.1	68	30.1	69	38.4	70	11.4	71	6.9	72	7.8
73	4.4	74	6.4	75	13.3	76	17.5	77	12.3	78	23.3
79	23.6	80	39.1	81	8.5	82	34.4	83	43.5	84	28.0
85	29.9	86	8.2	87	13.3	88	11.6	89	23.4	90	31.9
91	28.4	92	39.6	93	19.8	94	21.9	95	10.8	96	19.5
97	17.9	98	25.1	99	31.3	100	25.5	101	16.4	102	24.4
103	29.3	104	15.1	105	16.7	106	16.1	107	8.7	108	23.4
109	37.3	110	20.2	111	9.8	112	3.8	113	4.8	114	27.2
115	21.8	116	15.7	117	19.6	118	27.7	119	19.0	120	20.4
121	10.1	122	19.7	123	15.0	124	33.7	125	24.6	126	26.6
127	10.1	128	5.8	129	4.7	130	14.8	131	3.7	132	4.8
133	11.5	134	20.4	135	21.7	136	25.4	137	9.9	138	15.4
139	13.7	140	12.5	141	5.1	142	5.4	143	8.5	144	9.3
145	14.4	146	10.3	147	12.3	148	9.0	149	9.9	150	11.9
151	6.2	152	15.0	153	18.2	154	12.7	155	31.7	156	17.1
157	5.1	158	23.6	159	12.0	160	5.3	161	4.7	162	15.0
163	16.8	164	32.8	165	13.4	166	12.9	167	10.5	168	5.5
169	10.5	170	15.0	171	17.6	172	13.2	173	12.4	174	15.9
175	18.8	176	18.5								

++

Core: **LT84 - 9P** Bottom 3 meters. Average = 10.3 Appendix K

#	Thickness	#	Thickness	#	Thickness	#	Thickness	#	Thickness	#	Thickness
1	13.1	2	9.6	3	8.4	4	11.1	5	4.8	6	5.7
7	13.1	8	15.3	9	8.9	10	12.5	11	8.5	12	10.6
13	8.7	14	8.0	15	8.4	16	8.7	17	9.2	18	19.1
19	8.6	20	6.5	21	7.0	22	5.9	23	15.6	24	5.5
25	7.0	26	9.1	27	9.3	28	9.2	29	10.7	30	8.3
31	15.1	32	9.1	33	7.2	34	5.2	35	5.0	36	12.5
37	12.3	38	12.8	39	5.3	40	17.8	41	6.7	42	11.5
43	8.9	44	7.4	45	4.4	46	5.9	47	9.6	48	4.6
49	6.8	50	15.8	51	11.2	52	8.2	53	7.1	54	8.6
55	5.6	56	13.7	57	6.5	58	5.4	59	10.8	60	17.2
61	8.9	62	4.6	63	9.9	64	9.5	65	8.7	66	16.1
67	8.1	68	7.6	69	15.9	70	6.8	71	7.1	72	5.5
73	10.6	74	7.2	75	20.3	76	14.8	77	9.9	78	20.8
79	5.4	80	16.6	81	12.3	82	11.1	83	8.9	84	12.6
85	8.8	86	10.8	87	11.2	88	10.8	89	13.4	90	21.5
91	11.1	92	13.3	93	11.9	94	7.4	95	9.9	96	9.1
97	11.5	98	11.0	99	14.5	100	15.1	101	22.3	102	10.7
103	11.1	104	8.0	105	10.1	106	11.5	107	14.9	108	12.5
109	9.8	110	13.3	111	18.3	112	26.4	113	9.4	114	13.7
115	15.8	116	14.3	117	18.2	118	15.1	119	22.5	120	13.5
121	9.9	122	5.3	123	6.4	124	13.4	125	9.7	126	8.7
127	13.3	128	13.4	129	16.5	130	10.3	131	7.0	132	18.4
133	16.7	134	12.8	135	4.1	136	4.9	137	9.5	138	12.4
139	6.4	140	17.9	141	3.0	142	4.4	143	3.6	144	6.2
145	8.7	146	7.2	147	14.6	148	5.2	149	3.2	150	3.2
151	10.5	152	9.5	153	5.8	154	7.3	155	7.3	156	7.5
157	7.5	158	6.0	159	21.5	160	23.3	161	11.0	162	10.5
163	17.7	164	22.8	165	9.0	166	15.1	167	10.3	168	5.6
169	14.7	170	7.1	171	13.4	172	8.5	173	7.3	174	12.0
175	9.4	176	3.4	177	7.5	178	8.1	179	7.7	180	14.9
181	10.0	182	12.2	183	27.4	184	10.4	185	18.6	186	17.9
187	8.0	188	20.2	189	6.5	190	16.6	191	17.0	192	12.0
193	10.4	194	8.5	195	4.7	196	21.9	197	7.6	198	8.8
199	6.3	200	6.1	201	12.4	202	12.0	203	9.5	204	12.3
205	5.4	206	11.6	207	19.7	208	10.6	209	8.9	210	12.8
211	8.1	212	7.0	213	7.2	214	8.0	215	9.3	216	10.3
217	8.3	218	10.8	219	12.0	220	8.8	221	5.2	222	19.1
223	10.8	224	10.2	225	5.5	226	13.8	227	7.0	228	8.6
229	10.4	230	16.6	231	7.1	232	15.2	233	19.0	234	9.1
235	14.4	236	10.2	237	6.2	238	10.5	239	9.6	240	7.5
241	5.9	242	9.9	243	6.1	244	7.8	245	6.5	246	7.0
247	9.7	248	6.0	249	10.0	250	6.4	251	4.0	252	6.4
253	6.6	254	4.1	255	7.0	256	4.9	257	6.5	258	5.7
259	21.4	260	12.5	261	11.4	262	13.3	263	6.0	264	3.0
265	6.5	266	10.4	267	5.7	268	8.2	269	8.3	270	10.7
271	6.3	272	13.5	273	4.3	274	8.5	275	9.9	276	9.0
277	6.0	278	5.1	279	9.0	280	10.0	281	5.0	282	6.4

Appendix K

Note: Lamination couplet thickness in mm, average of all measurements.
corresponds to location of couplet in specific sequence.

++
++

Lamination Analysis

Appendix L

Lamination	Color	Thickness	$CaCO_3$	Median	SiO_4	TOC	C/N
1	Light	213	4.81	18.15	1.06		
2	Dark	42	5.13	17.79	1.09		
3	Light	72	6.03	17.61	0.93		
4	Dark	74	4.64	15.94	0.80		
5	Light	95	5.04	18.79	1.17		
6	Dark	66	3.93	16.91	1.18		
7	Light	118	6.38	15.07	1.16		
8	Dark	96	3.77	14.79	1.32		
9	Light	59	5.05	13.62	1.13		
10	Dark	93	3.65	14.09	1.37		
11	Light	61	7.22	14.61	1.05	0.91	6.97
12	Dark	77	5.73	13.47	1.29	0.84	6.59
13	Light	116	8.17	13.29	1.19	0.85	6.53
14	Dark	71	5.97	13.01	1.60	0.92	7.33
15	Light	90	5.67	13.91	1.17	0.87	7.04
16	Dark	74	4.90	15.54	1.66	0.85	6.69
17	Light	93	7.17	18.85	1.45	0.84	7.49
18	Dark	93	5.10	15.42	1.37	0.83	6.14
19	Light	206	8.22	15.50	1.03	0.80	6.51
20	Dark	76	4.00	13.86	1.28	0.84	5.87
21	Light	79	6.14	15.71	1.25	0.87	5.77
22	Dark	70	5.04	15.91	1.47		
23	Light	45	8.50	15.51	1.27		
24	Dark	83	8.02	14.65	1.32		
25	Light	113	8.32	14.57	1.15		
26	Dark	84	5.80	14.64	1.36		
27	Light	118	7.66	14.12	1.39		
28	Dark	53	5.89	14.57	1.76		
29	Light	140	5.80	15.24	1.69		
30	Dark	99	4.35	14.37	1.34		
31	Light	57	4.56	14.69	1.53		
32	Dark	81	4.57	15.83	1.20		
33	Light	119	6.00	14.83	1.06		
34	Dark	71	5.15	15.32	1.42		
35	Light	69	7.18	15.30	1.14		
36	Dark	101	4.69	15.96	1.76		
37	Light	83	4.77	18.10	1.29	0.84	9.04
38	Dark	153	4.48	16.76	1.40	0.73	9.60
39	Light	129	5.65	17.60	1.63	0.83	6.51
40	Dark	62	4.03	19.26	1.07	0.85	6.72
41	Light	51	5.49	21.46	2.13	0.87	8.39

42	Dark	95	5.54	23.47	1.27	0.84	7.15
43	Light	80	5.53	18.86	1.54	0.85	7.26
44	Dark	182	4.13	16.03	1.10	0.86	5.89
45	Light	95	4.72	16.63	1.18	0.98	7.15
46	Dark	66	3.82	14.01	1.41	0.93	6.78
47	Light	205	6.59	14.36	1.59		
48	Dark	66	5.26	16.25	1.44		
49	Light	107	4.93	17.65	1.41		
50	Dark	94	5.78	14.32	1.31		
51	Light	86	6.89	14.59	1.09		
52	Dark	57	5.15	15.22	1.17		
53	Light	67	4.49	16.15	1.43		
54	Dark	89	3.32	15.67	1.22		
55	Light	53	3.48	15.39	1.15		
56	Dark	119	3.88	15.93	1.11		

Note: Color is relative compared to laminae above and below.
Thickness is lamina thickness (tens of mm), and average value for each lamina.
$CaCO_3$ is weight percent carbonate as $CaCO_3$.
SiO_4 is weight percent biogenic silica as SiO_4.
TOC is weight percent total organic carbon as C.
C/N is ratio of TOC to weight percent total organic nitrogen as N.

X-Ray Diffraction Minerology

Core: **LT84 - 1P**

Depth	Color	Montmorillinite	Illite	Kaolinite	Calcite	Feldspars	Others
39	Light	70	18	3	2	7	-
40	Dark	73	16	5	< 1	6	-
929	Dark	68	22	4	1	5	-
930	Light	70	16	3	2	9	-

Core: **LT84 - 4P**

Depth	Color	Montmorillinite	Illite	Kaolinite	Calcite	Feldspars	Others
62	Light	73	12	4	7	4	Py,Op
63	Dark	66	12	6	10	6	Py,Op
1151	Dark	88	7	3	1	1	Py,Op
1153	Light	80	12	3	3	2	Py,Op
1153	White	72	12	6	7	3	Py,Op

Core: **LT84 - 8P**

Depth	Color	Montmorillinite	Illite	Kaolinite	Calcite	Feldspars	Others
46	Dark	90	< 1	5	< 1	3	-
47	Light	80	11	4	2	3	-
293	Dark	80	8	6	2	4	Py
294	Light	70	14	7	3	6	Py
552	Dark	84	8	3	1	4	Py,Qtz
553	Light	86	9	2	1	2	-
823	Light	76	14	3	2	4	-
824	Dark	84	10	3	< 1	3	Qtz

Note: Depth down core in centimeters.
Numbers represent relative abundance from peak heights with standard crystallinity corrections.
Color is relative compared to adjacent lamination.
Others catagory: Py, Pyrite; Op, Opal; Qtz, Quartz; - non present. The pyrite peak is barely above background.

Data collected and compiled by M. Bishop.

Periodicity Analysis

Phase Comparisons: LT84 - 8P Carbonate vs. Thickness FFT data.

Carbonate Data Period (yr)	Phase (°)	Thickness Data Period (yr)	Phase (°)
270	180	280	115
200	220	195	280
165	210	160	160
110	300	98	25
		78	275
		44	270
		31	60
		25	10

Periodicity Comparisons: LT84 - 8P data vs. LT84 -7P, 9P and 10P.

Carbonate Data Comparisons

LT84 - 8P (cm/cycle)*	LT84 - 7P*	LT84 - 10P*
? (480 yr)		131 ± 13
93.1 (345 yr)	93.1 ± 9	
73.1 (270 yr)	68.3 ± 5	72.3 ± 4
53.9 (200 yr)	53 ± 3	55.6 ± 3
44.5 (165 yr)	42.7 ± 2	42 ± 2
37.9 (116 yr)		38.1 ± 2
29.3 (110 yr)		31.4 ± 1 (or 27.3 ± 0.8 **)

Thickness Data Comparisons

LT84 - 8P (couplet/cycle)	LT84 - 9P top	LT84 - 9P bottom
73.1 (280 yr)		
51.2 (195 yr)		
41.0 (160 yr)		
25.6 (98 yr)		25.6 ± 2.8
20.1 (78 yr)	18.3 ± 1.5	
11.5 (44 yr)	13.5 ± 0.4 **	12.1 ± 0.6 **
8.1 (31 yr)	8.1 ± 0.3 **	8.26 ± 0.3 **
6.6 (26 yr)		6.4 ± 0.3 **
? (19.6 yr)	5.0 ± 0.1 **	5.2 ± 0.1 **

Note: * Depths of carbonate profiles were normalized to LT84 - 8P, based on carbonate stratigraphy.

** Periods are prominent but not significant at the 95% level.

Persistence Comparisons: First, Middle and Last 512-pt sections of LT84-8P data sets.

Carbonate Data Comparisons

LT84 - 8P (cm/cycle) (1024-pts)	First (0-512)	Middle (340-852)	Last (512-1024)
93.1 (345 yr)			
73.1 (270 yr)	73.1 ± 12	85.3 ± 18	85.3 ± 18
53.9 (200 yr)			51.2 ± 6
44.5 (165 yr)	46.5 ± 5	46.5 ± 5	
37.9 (116 yr)	39.4 ± 3	39.4 ± 3	
29.3 (110 yr)	30.1 ± 2		28.4 ± 2

Thickness Data Comparisons

LT84 - 8P (couplet/cycle) (1024-pts)	First (0-512)	Middle (300-812)	Last (512-902)
73.1 (280 yr)			
51.2 (195 yr)	51.2 ± 5.6	46.5 ± 3.7	46.5 ± 3.7
41.0 (160 yr)			
25.6 (98 yr)	24.3 ± 1.3 **		25.6 ± 1.3 **
20.1 (78 yr)	19.7 ± 0.8	19.7 ± 0.8	18.3 ± 0.8
11.5 (44 yr)	11.6 ± 0.3	11.4 ± 0.3 **	11.3 ± 0.3
8.1 (31 yr)	8.1 ± 0.1 **	8.0 ± 0.1 **	8.0 ± 0.1 **
6.6 (25 yr)	6.6 ± 0.1 **	6.1 ± 0.1 **	6.3 ± 0.1 **
- (19.6 yr)	5.4 ± 0.1 **		

Note: ** Periods are prominent but not significant at the 95% level.

BIOGRAPHY

John David Halfman

Born: November 9, 1956
Concord, Massachusetts.

Education:
B.S. Geology Department, Univerity of Miami, FL., 1978.
M.S. Geology and Geophysics Department, University of Minnesota, MN., 1982.
Ph.D. Geology Department, Duke University, NC., 1987.

Honors and Positions Held:

Magna Cum Laude, University of Miami, FL., 1978.
Research Associate, Geology Department, University of Miami, FL., 1979 - 1980.
Research Assistant, Geology and Geophysics Department, University of Minnesota, MN., 1980 - 1983.
Lecturer, Mathematical Sciences Department, University of Minnesota, MN., 1983.
Research and Teaching Assisitant, Geology Department and Marine Laboratory, Duke University, NC., 1984 - 1987.

Publications:

Halfman, J.D. and T.C. Johnson, 1984, The sediment texture of contourites in Lake Superior. In: D.A.V. Stow and D.J.W. Piper (eds.) Fine-grained sediments: Deep-water processes and facies. p 293-307.

Halfman, J.D. and T.C. Johnson, 1984, Enhanced atmospheric circulation over North America during the Early Holocene. Science 224:61-63.

Johnson, T.C., J.D. Halfman, W.H. Busch and R.D. Flood, 1984, Effects of bottom currents and fish on sedimentation in a deep-water, lacustrine environment. Geological Society of America, Bulletin 95:1425-1436.

Johnson, T.C., J.D. Halfman, B.R. Rosendahl and G.S. Lister, 1987, Climatic and tectonic effects on sedimentation in a rift-valley lake: Evidence from high-resolution seismic profiles, Lake Turkana, Kenya. Geological Society of America, Bulletin 98:439-447.

Society Memberships:

Geological Society of America
American Society of Limnology and Oceanography